REACTION CALORIMETRY IN SUPERCRITICAL FLUIDS A STUDY OF THE DISPERSION POLYMERIZATION OF METHYL METHACRYLATE IN SUPERCRITICAL CARBON DIOXIDE

THÈSE N^{O} 3472 (2006)

PRÉSENTÉE LE 24 MARS 2006
À LA FACULTÉ SCIENCES DE BASE

Groupe des procédés macromoléculaires

SECTION DE CHIMIE ET GÉNIE CHIMIQUE

ÉCOLE POLYTECHNIQUE FÉDÉRALE DE LAUSANNE

POUR L'OBTENTION DU GRADE DE DOCTEUR ÈS SCIENCES

PAR

Sophie FORTINI

ingénieure chimiste diplômée EPF
de nationalité suisse et italienne et originaire de Monthey (VS)

acceptée sur proposition du jury:

Prof. P. Vogel, président du jury
Dr Th. Meyer, directeur de thèse
Prof. M. Kemmere, rapporteur
Prof. F. Stoessel, rapporteur
Prof. G. Storti, rapporteur

ÉCOLE POLYTECHNIQUE
FÉDÉRALE DE LAUSANNE

Lausanne, EPFL
2006

Remerciements

Cette thèse a été réalisée entre avril 2002 et février 2006 au sein du laboratoire du génie de la réaction de polymérisation, récemment renommé groupe des procédés macromoléculaires, dirigé par le MER Dr. Thierry Meyer. Je tiens à lui présenter ma gratitude pour m'avoir proposé ce travail de thèse original, intéressant et exaltant. Ce projet m'a donné l'opportunité de relever des challenges variés qui m'ont conduite à un épanouissement personnel et professionnel important. Je tiens également à lui adresser ma profonde reconnaissance pour toutes les opportunités professionnelles qui m'ont été offertes, telles que les voyages à l'étranger à l'occasion de congrès, les collaborations scientifiques avec le groupe du Prof. Keurentjes et de la Prof. Kemmere (Université de Eindhoven) et du Prof. Morbidelli (ETHZ)… pour ne citer qu'eux…

Je remercie tous mes collègues directs pour les moments de riche partage intellectuel et de camaraderie:

- *Merci à Frédéric Lavanchy pour nos discussions enrichissantes et notre soutien mutuel dans le cadre du développement de la calorimétrie de réaction appliquée aux fluides surcritiques*

- *Merci à Charalampos Mantelis, qui reprend le flambeau de ce projet, pour avoir lu et relu avec grande dévotion ce manuscrit. Je lui souhaite beaucoup de succès pour son projet de thèse*

- *Merci à Raphaël Barbey, qui a travaillé durant plus d'une année avec moi en tant que stagiaire à la suite de son travail de diplôme, pour son amitié et la qualité de son travail. Je lui souhaite beaucoup de succès pour son projet de thèse*

- *Merci à Philip Nising pour son soutien conséquent en tant que responsable informatique et de divers appareils analytiques en plus de la charge de sa thèse*

Ce projet de thèse n'aurait jamais pu éclore en sa forme actuelle et me procurer la satisfaction que j'en tire sans l'appui de tout le personnel de l'atelier mécanique tel que André Fattet, Jean-Claude Rapit et particulièrement Gérard Bovard dit Bobo pour les intimes. Je les remercie d'avoir toujours été disponibles, même lors de mes entrées en scène à l'atelier à 7h00 du matin! Je souhaite une heureuse retraite à qui de droit et un bel avenir à qui de droit. Je tiens également à remercier le personnel de l'atelier électronique, Gabriel Roch, Gérard Ferini et Olivier Noverraz qui s'est particulièrement dévoué lors de l'installation du matériel informatique afin que je réalise ma défense de thèse dans les meilleures conditions. Je n'oublie pas le personnel de l'institut de microscopie de l'EPFL (CIME) dont particulièrement Fabienne Bobard et Brian Senior pour leur disponibilité et leur excellent travail. On peut largement admirer leurs œuvres tout au long de ce manuscrit. J'adresse ma reconnaissance à Paul Bowen et à Cristina Soare pour m'avoir généreusement formée sur l'utilisation d'appareils dans le cadre de mesures liées à la technologie des poudres.

J'adresse ma reconnaissance à l'entreprise Mettler-Toledo pour son soutien financier et son implication dans ce projet. Je remercie Urs Groth , Bernie Kloetzli et Herbert Briggeler pour leur soutien technique et scientifique dans le cadre du développement du calorimètre de réaction.

Je remercie avec grand enthousiasme les membres de mon jury, par ordre alphabétique, Prof. Maartje Kemmere, Prof. Francis Stoessel, Prof. Giuseppe Storti ainsi que le président du jury Prof. Pierre Vogel pour avoir accepté de partager ce travail avec moi et consacré de leur précieux temps à son expertise.

Evidemment, sont inclus dans ces années de thèse des moments de joie, de pleure, de rire, des soirées festives, des soirées nanas, partagés avec mes amis de la K-fet: ma Béa (correction de ma thèse en live depuis San Francisco), Chrystèle, Ilaria, Pétra, Justyna, Pascal, Bastien, Ralf, Thomas, Eric, Benoît. A ceux qui se reconnaîtront, je les remercie de m'avoir donné généreusement leur amitié profonde et connaissent l'émotion que j'ai éprouvée de les quitter pour prendre un nouvel envol.

Je garde une place toute particulière à deux amies d'études avec qui j'ai fait les 400 coups et ai vécu des moments intenses de solidarité et d'amitié: Sabrina Laus et Isabelle Querbach.

Il ne faut pas cacher qu'un travail de thèse demande beaucoup d'investissement et que certains passages peuvent être soumis au doute. Je garde une place toute particulière au fond de mon cœur à mes amis chablaisiens et lausannois qui m'ont soutenue, ont manifesté leur confiance en moi et leur amitié inconditionnelle, et cela, depuis plus de 15 ans!

C'est avec beaucoup d'émotion que j'écris ces quelques lignes en pensant à la reconnaissance infinie et à l'importance de l'amour, porteur de confiance, que m'ont donné sans compter ma maman, Graziella Raspa, mon papa, Filiberto Fortini, mon frère, Patrice, et mon âme sœur, justement ma sœur, Ane Jinpa. Merci également à mon beau-papa et ma belle-maman, Philippe et Elisabeth Ritter. Je n'oublie pas Jocelyne.

Je dédie cette thèse, sans hésitation, à mon fiancé et mon compagnon de toujours (presque), Ludovic Ritter. Il a été ma source de motivation, mon exutoire, un pilier de mon équilibre… toujours présent pour me soutenir dans les moments difficiles et partager les beaux moments de cette riche période.

Summary

This thesis is devoted to the study of the dispersion polymerization of methyl methacrylate in supercritical carbon dioxide ($scCO_2$), using a poly(dimethylsiloxane) macromonomer (PDMS macromonomer) as stabilizer. Supercritical fluids (SCF) and SCF mixtures are characterized by a temperature and a pressure above their critical point(s), which is the last point on the vaporization line of a pure component. This means that these fluids operate from moderate to high pressure. They can be used in various processes ranging from extractions, nanoparticle formation for controlled drug release, chemical reactions and polymer processing. Nowadays, the best candidate for SCF processing is carbon dioxide. The fundamental motivation of using $scCO_2$ as a solvent is based on its potential to replace harmful chemical organic volatile compounds (VOCs) in order to develop more sustainable and environmentally friendly chemical processes. At this point, the crucial role of CO_2 in the development of the so-called "green chemistry" comes on the stage. CO_2 is a natural abundant compound with low toxicity exhibiting no inflammability. This last property is very advantageous considering the cost investments spent by the chemical industry to control the safety of the chemical processes using highly flammable compounds like VOC solvents. As expected, environmental arguments are not sufficient to motivate the development of new chemical process routes. Therefore, additional arguments to use SCFs have to be found, and they do exist. As supercritical fluids are compressible fluids they can exhibit liquid-like and gas-like properties, which can be tuned easily by varying the operating conditions, like pressure and temperature. This fundamental behavior of SCF is their main asset and demonstrates their superiority to develop more flexible processes.

The polymer industry is one of the industries that uses the largest volumes of organic solvents and sometimes halogenated ones, well known to destroy the ozone layer. The use of $scCO_2$ gives to chemists and engineers the opportunity to develop more sustainable polymer processes, considering the numerous chemical and physical advantages of carbon dioxide. The processing of $scCO_2$ for polymer production is no more than fifteen years-old. This means that a certain quantity of knowledge has been acquired but still a lot of unknowns hinder their promotion at industrial level. This work is inserted in this context and finds there its main motivations.

This thesis is composed of two different but intrinsically connected approaches of the dispersion polymerization of the methyl methacrylate (MMA) in $scCO_2$. A part of this thesis is devoted to the development of techniques allowing the on-line monitoring of polymerizations in $scCO_2$ at "larger" scale, conducted from an engineering approach. The intrinsically connected part is devoted to the understanding of the fundamental phenomena that govern the dispersion polymerization of MMA in $scCO_2$, its kinetic features and the product characteristics of the polymer produced, being conducted from a chemical approach of the subject. Up to now, most of the studies dealing with polymerization reactions in $scCO_2$ are realized in small autoclaves between 2 and 60 ml allowing pertinent fundamental analysis but with poor similarities with an industrial reactor. A keystone of this work is the development of a supercritical reaction calorimeter composed of a 1.3 liters high pressure reactor allowing the kinetic study of the

dispersion polymerization, which in turn gives a direct insight into the parameters that control the dispersion polymerization stability, efficiency and mechanism. Based on an adapted heat balance, the calorimeter can give the profile of monomer conversion (thermal conversion). Furthermore, the volume of the reactor allows inserting on-line sensors inside the reactor. This possibility led to the development of an ultrasonic sensor to monitor the polymerization process. The combination between the calorimetric information and the sensor signal shows the potential of these sensors to monitor polymerization reactions in $scCO_2$. By measuring the speed of sound evolution during the course of the polymerization, it is possible to calculate the composition of the medium and thus evaluate the monomer conversion.

The analysis of the effects of temperature, stirring speed and impeller types demonstrate that the dispersion polymerization of MMA can be effective under a wide range of operating conditions using the PDMS macromonomer as stabilizer. The experiments point out that the stability of the dispersion polymerization and in turn the rate of polymerization, the polymerization loci[1] and the polymer quality depend strongly on the stabilizer concentration but more fundamentally on its degree of solubility in the carbon dioxide. Phase behavior measurements demonstrate that the 5'000 g/mol PDMS macromonomer exhibits a relative good solubility in carbon dioxide and that this solubility can be greatly improved by the presence of the monomer in the mixture. In fact, the monomer acts as a cosolvent for the PDMS macromonomer improving the solvency of the $scCO_2$ (polarity, density). This study demonstrates that the concentration of the monomer in the reacting medium is a key parameter to control the stability of the dispersion throughout the polymerization process.

A dispersion polymerization is characterized by polymer-rich particles dispersed in a continuous phase, i.e. the CO_2-rich continuous phase. The results give evidence of the fact that the polymerization can take place in both phases depending on the concentration of stabilizer and its solubility in the reacting medium. In this case, bimodal molecular weight distributions and intermediate rate of polymerization are observed. When only one reaction locus is active, monomodal molecular weight distributions are obtained. Furthermore, the locus of the polymerization influences directly the rate at which the polymer is produced and the degree of polymerization.

In order to complete the study, a model has been developed demonstrating that diffusion limitations are operative in the dispersion polymerization of MMA in $scCO_2$. A gel effect is present in the polymer-rich phase that leads to the increase of the molecular weight of the polymer produced, as observed also experimentally. Moreover, the presence of this gel effect occurring inside the polymer-rich particles explains the auto-acceleration of the polymerization rate as the conversion increases. The model demonstrates that in the case of an effective dispersion polymerization of the methyl methacrylate in $scCO_2$ the main reaction loci are the polymer-rich particles.

Key words: supercritical carbon dioxide, dispersion polymerization, reaction calorimetry, on-line monitoring, phase equilibrium, kinetics, modeling free radical polymerization reactions.

[1] *A dispersion polymerization is composed of polymer-rich particles dispersed in the CO_2-rich continuous phase. The polymerization locus is referred to the phase into which the polymerization can take place.*

Version abrégée

Cette thèse traite de l'étude de la polymérisation par dispersion du méthacrylate de méthyle dans le dioxyde de carbone surcritique (CO_2sc) pour laquelle un composé polymérique, le poly(diméthylsiloxane) macromonomère (PDMS macromonomère), est utilisé comme stabilisant. Les fluides surcritiques (FSCs) et les mélanges surcritiques sont caractérisés par une température et une pression au-dessus de leur point(s) critique(s), lequel correspond au dernier point sur la courbe de vaporisation d'un composé pur. Cela signifie que ces fluides opèrent à des pressions modérées ou élevées. Les FSCs peuvent être utilisés dans des procédés divers allant de l'extraction, à la formation de nanoparticules pour la production de médicament à libération contrôlée, en passant par les réactions chimiques et les procédés de production de polymères. Le meilleur candidat pour les procédés surcritiques est le dioxyde de carbone. La motivation fondamentale d'utiliser le CO_2sc comme solvant est basée sur son potentiel de pouvoir remplacer les composés organiques volatiles (VOCs) toxiques et de permettre le développement durable de procédés chimiques en harmonie avec notre environnement. Le CO_2 est un composé naturel, abondant dans la nature, non inflammable et caractérisé par une faible toxicité. Le fait qu'il soit non inflammable offre un énorme avantage si l'on considère les coûts d'investissement supportaient pas les entreprises chimiques dans la sécurités des procédés utilisant des solvants très inflammables tels que les VOCs. Sans surprise, les arguments environnementaux sont insuffisants pour motiver le développement de nouvelles voies de procédé chimique. Ainsi, il doit exister des arguments supplémentaires pour utiliser les FSCs. Et ils existent. Etant donné que les fluides surcritiques sont par nature compressible, ils ont à la fois des propriétés caractéristiques des liquides et des gaz, qui peuvent être modulées en changeant les conditions de pression et de température. Ce comportement fondamental des FSCs est probablement leur principal « atout » et démontre leur supériorité pour développer des procédés plus flexibles.

L'industrie des polymères est une des industries qui consomment les plus larges volumes de solvants organiques et parfois halogénés, très connus pour détruire la couche d'ozone. L'utilisation du CO_2sc donne aux chimistes et aux ingénieurs une opportunité de développer des procédés durables de fabrication de polymère si l'on tient également compte des nombreux avantages chimiques et physiques du CO_2sc. Les premières découvertes de voie de synthèse de polymères basée sur l'utilisation du CO_2sc ne datent que de quinze ans. Cela signifie qu'un certain savoir a été acquis, mais de nombreuses inconnues demeurent, qui empêchent leur utilisation à l'échelle industrielle. Ce travail s'insère dans ce contexte et c'est là qu'il y trouve sa principale motivation.

Cette thèse se compose de deux approches différentes mais intrinsèquement liées de l'étude de la polymérisation par dispersion du méthacrylate de méthyle dans le CO_2sc. Une partie de cette thèse, conduite par le regard de l'ingénieur, est dévouée au développement de techniques permettant le contrôle en ligne des réactions de polymérisation dans le CO_2 à l'échelle du réacteur de laboratoire. La deuxième partie, conduite par le regard du chimiste, est dévouée à la compréhension des phénomènes fondamentaux qui gouvernent la polymérisation par dispersion du MMA dans le CO_2sc. Jusqu'à maintenant, la plupart des études traitant des réactions de polymérisation dans le CO_2sc ont été réalisées dans de petits réacteurs de l'ordre de 2 à 60 ml

permettant des analyses fondamentales pertinentes mais ayant très peu de similarités avec un réacteur industriel. Un pivot de ce travail fut le développement d'un calorimètre de réaction composé d'un réacteur haute pression de 1.3 litres qui permet d'étudier la cinétique des polymérisations et qui, en retour, permet d'identifier les paramètres qui contrôlent la stabilité de la polymérisation par dispersion, son rendement et son mécanisme. Basé sur un bilan de chaleur adapté, le calorimètre permet d'accéder au profile de conversion du monomère (conversion thermique). De plus, le volume du réacteur permet l'introduction de sondes dans l'autoclave. Cette possibilité nous a conduit à développer une sonde ultrason qui permet le contrôle en ligne du procédé de polymérisation. La combinaison entre les informations calorimétriques et le signal de la sonde montre le potentiel de ces sondes pour contrôler les réactions de polymérisation dans le CO_2sc. A partir de la mesure de l'évolution de la vitesse du son au cours de la polymérisation, il est possible de calculer la composition du milieu et donc d'évaluer la conversion du monomère.

L'analyse des effets de la température, de la vitesse d'agitation et du type d'agitateur démontre que la polymérisation par dispersion du MMA dans le CO_2sc donne des rendements élevés sur une gamme étendue de conditions opératoires en utilisant le PDMS macromonomère comme stabilisant. Les expériences mettent en évidence que la stabilité de la dispersion et donc la vitesse de polymérisation, les lieux de la polymérisation[1] et la qualité du polymère dépendent de la concentration en stabilisant et de manière plus fondamentale de sa solubilité dans le milieu. Des mesures d'équilibre de phase montrent que la solubilité du stabilisant dans le CO_2 peut être accrue par la présence du monomère dans le mélange réactionnel. En fait, le monomère agit comme un cosolvant pour le PDMS améliorant les qualités de solvant du CO_2 (densité, polarité).

Une polymérisation par dispersion est caractérisée par des particules riches en polymère dispersées dans une phase continue, i.e. la phase riche en CO_2. Les résultats montrent que la polymérisation peut avoir lieu dans les deux phases en fonction de la concentration en stabilisant utilisée et de sa solubilité. Dans ce cas, le polymère est produit à des vitesses de réaction intermédiaires et est caractérisé par une distribution de masse moléculaire bimodale. Lorsque seulement un lieu de polymérisation est actif, des distributions monomodales de masse moléculaires sont obtenues. Le lieu de la polymérisation influence directement la vitesse à laquelle le polymère est produit et le degré de polymérisation. Afin de compléter l'étude, un modèle a été développé et démontre que la polymérisation qui a lieu dans les particules riches en polymère est contrôlée par des phénomènes de diffusion. L'effet gel, ainsi appelé, conduit à une augmentation de la masse moléculaire du polymère produit, comme observé expérimentalement. La présence de cet effet gel explique également l'auto-accélération de la vitesse de polymérisation lorsque la conversion augmente. Le modèle prouve que dans le cas d'une polymérisation par dispersion dans des conditions optimales les particules riches en polymère sont le principal lieu de la polymérisation.

Mots-clés: dioxyde de carbone surcritique, polymérisation par dispersion, calorimétrie de réaction, contrôle en ligne, équilibre de phase, cinétique, modélisation des polymérisations radicalaires.

[1]Une polymérisation par dispersion est composée de particules riches en polymère dispersées dans une phase continue riche en CO_2. Le lieu de la polymérisation se réfère à la phase dans laquelle la polymérisation a lieu.

Symbols and Abbreviations

Symbols

A	surface	$[m^2]$
c_v	isochoric specific heat capacity	[J/kg/K] or [J/mol/K]
c_p	isobaric specific heat capacity	[J/kg/K] or [J/mol/K]
c	velocity of sound	[m/s]
D	diffusion coefficient	$[m^2/s]$
d_s	stirrer diameter	[m]
d_r	reactor inner diameter	[m]
e	reactor wall thickness	[m]
ΔG	Gibbs free energy	[J] or [J/mol]
h	heat transfer coefficient	$[W/m^2/K]$
$\Delta_{rx}H$	enthalpy of a reaction	[J/kg] or [J/mol]
K	Boltzsmann's constant	$1.3807 \cdot 10^{-23}$ [J/K]
k_d	rate constant of decomposition	[1/s]]
k_p	rate constant of propagation	[l/mol/s]
k_t	rate constant of termination	[l/mol/s]
$k_l a$	mass transport coefficient	[1/s]
m	mass	[kg]
M	molar mass	[kg/mol]
N_A	Avogadro's number	$6.022 \cdot 10^{23}$ [1/mol]
n	rotation speed	[1/s]
Ne	Newton number (power number)	[-]
Nu	Nusselt number	[-]
P	pressure	[Pa] or [bar]
P_c	critical pressure	[Pa] or [bar]
Q	thermal power	[W]
R	universal gas constant	8.3144 [J/K/mol]
Re	Reynolds number	[-]
R_p	polymerization rate	[kg/l/s] or [mol/l/s]
r	radius of interaction	[m]
ΔS	variation of the entropy	[J/K] or [J/mol/K]
T	temperature	[°C] or [K]
T_c	critical temperature	[°C] or [K]
t	time	[s]

U	overall heat transfer coefficient	[W/m^2/K]
U	internal energy	[J] or [J/mol]
V_r	reactor volume	[m^3]
w	mass fraction	[-]

Greek

β	isentropic compressibility	[1/Pa]
ϕ	volumic fraction	[-]
η	dynamic viscosity	[Pa s]
κ	isothermal compressibility	[1/Pa]
λ	thermal conductivity	[W/m/K]
ρ	density	[kg/m^3]
ω	mass fraction	[-]

Subscripts

acc	refers to an accumulation term
c	refers to a critical value
cal	refers to a calibration term
dos	refers to a dosing term
j	refers to the jacket
M	refers to the monomer
P	refers to the polymer
r	refers to the reactants or reactor
rx	refers to a reaction term
S	refers to the solvent
w	refers to the reactor wall
s	refers to the stirrer
stir	refers to stirring
1	refers to the CO_2-rich phase
2	refers to the polymer-rich phase

Abbreviations

AIBN	azobis(isobutyronitrile)
LCST/UCST	lower critical solution temperature/upper critical solution temperature
MMA	methyl methacryalte
PDMS-mMA	poly(dimethylsiloxane) monomethacrylate
PMMA	poly(dimethyl methacrylate)

Forward

In 1985, the discovery of a “hole” in the ozone layer above the Antarctic spread the commotion in the international community. The same year, the Vienna convention recognized officially and for the first time the harmful effect of certain substances and in particular that of the chlorofluorocarbon compounds (CFC) on the ozone layer, which protects the earth against the ultraviolet radiation of the sun. This Vienna convention led finally the ratification in 1987 of the Montréal protocol. The latter obliges the signatory countries to decrease drastically the use of various substances such as the CFCs

The polymer industry becomes particularly concerned by this problem due to the fact that many polymers are produced using organic compounds as solvents and sometimes even halogenated ones, due mainly to their high solvent power. From that moment, solvent-free polymerization processes and new routes of polymer processing started to attract more and more the interest of both the industry and academia. One of the possible alternatives is the use of supercritical fluids.

Polymer-supercritical fluid mixtures are complex mixtures. Despite the fact that supercritical fluids have been studied extensively for the past two decades, still an important work has to be made to gain accurate and detailed knowledge of their fundamental properties. Such knowledge is essential to the utilization and optimization of supercritical fluid technology in materials preparation and processing.

This thesis is focused on the development of two technologies, allowing the on-line monitoring of polymerization reactions in supercritical fluids at larger scale, namely the reaction calorimetry and the ultrasound technology. They are already used to monitor polymerizations in common solvent. As supercritical fluids are pressurized fluids, the challenge is to adapt the existing methodology to high pressure conditions and to the supercritical fluid properties. The final aim of this project is to understand the mechanism and the parameters that control the dispersion polymerization of methyl methacrylate in $scCO_2$ through both experimental work and the development of a comprehensive mathematical model.

Content

1 Introduction

1.1 Supercritical fluids as alternative solvents

The use of carbon dioxide as a solvent and raw material has been investigated continuously in academia and/or industry since 1950. Interest in supercritical fluids (SCF) actually started with research in extraction techniques. A major technical breakthrough came with the development of natural product extraction by Kurt Zosel at the Max-Planck-Institute for coal research in the early 1960s.[1] Based on his work, the first application of supercritical carbon dioxide ($scCO_2$) was the extraction of caffeine from green coffee at industrial scale between 1975 and 1985. The combined properties of supercritical carbon dioxide were realized in a cost competitive and environmentally superior process. The main argument for the development of the SCF process was the elimination of residual solvents in the product, especially methylene chloride, which had been used previously to decaffeinate the coffee. From that point, supercritical carbon dioxide properties have been applied to a range of separations and extractions allowing to obtain specific compounds from natural products such as tea, hops and spices, including extractions of metals from aqueous solution.[2-12]

The two most popular supercritical fluids are carbon dioxide and water. Since they are nontoxic and non-flammable they are essentially environmentally benign solvents that can be used even for food processing, without significant regulation. In addition they are two of the most inexpensive solvents commercially available and the most accessible ones. The crucial advantage of CO_2 over H_2O is its low critical temperature close to near-ambient temperature compared to the critical temperature of water being 375°C. The drawback of using CO_2 is its poor solvating power particularly for polar compounds and high molecular weight compounds. This disadvantage can be overcome by adding a co-solvent to change the polarity of carbon dioxide. The use of supercritical water is currently focused mainly in waste water treatment; conversion of poorly biodegradable substances to less toxic or non toxic end products with reduction of the final volume of wastes. Supercritical water (scH_2O) oxidation (SCWO) has extensively demonstrated to be one of the most effective methods to purify complex industrial wastes by oxidation of the hazardous compounds. Nevertheless, scaling and corrosion remain two major technical challenges that need to be solved before this technology can be put to widespread use. Cocero *et al.* have designed a reactor capable of operating effectively under industrial requirements.[13] scH_2O is also a potential medium for chemical synthesis and a mean of polymer recycling.[14, 15 16, 17]

Pollution prevention and waste management represent two of the most important challenges of the 21st century. Billions of kilograms of solvent wastes are annually emitted in the environment, either as volatile emissions or with aqueous discharge streams. Many of these solvents are known to upset our ecosystems by depleting the ozone layer and participating in the reactions that form tropospheric smog. In addition, some of them are known to be carcinogenic, and neurotoxic and may cause sterility in those individuals frequently exposed to them.[18] The proliferation of the use of organic solvents, halogenated solvents and precious water in manufacturing and processing industries, such as electronics, dyes and coatings, has created the right environment for the creation and the development of environmentally responsible and energy efficient processes. The Montreal Protocol, ratified in 1988, banned the use of chlorofluorocarbons (CFCs), carbon tetrachloride and others because of their deteriorating effect on the earth's ozone layer.[19] This clearly motivates the research for the development of alternative solvents with less environmental impact and ideally no impact on health. By far the most widely used SCF is carbon dioxide. A special interest has been devoted to the use of carbon dioxide to create greener processes and products, with focus on research and commercialization since 1995.[20] Carbon dioxide is a natural solvent that could replace water and many other solvents in a variety of applications. As highlighted previously, CO_2 is inexpensive, nonflammable, exhibits a relatively low toxicity and is naturally abundant. Actually, CO_2 is readily available from natural reservoirs and is a by-product from the productions of ammonia, ethanol, hydrogen and natural gases.[21] In addition to environmental benefits, CO_2 based processes can also be more energy efficient than those based on water or conventional solvents. For example, the low heat of vaporization of CO_2 significantly reduces the energy costs that are associated with water intensive processing industries and also eliminates the inevitable contamination problems associated with the pollution of water effluents. Obviously, this is related to the fact that carbon dioxide is a gas at ambient pressure and temperature and thus can be completely and easily removed from products simply by venting the carbon dioxide or depressurizing the system.

In the ecological balance, one has to consider that carbon dioxide is a "greenhouse gas", even if it is a naturally abundant material. If CO_2 can be withdrawn from the environment, used in a process, then rejected to the environment clean, no environmental detriments accrue. While CO_2 could be in theory extracted from the atmosphere (distillation of air), most CO_2 used in processes today is collected from the effluent of ammonia plants or derived from naturally occurring deposits (tertiary oil recovery) leading to the so-called feedstock strategy.[22] Actually, if CO_2 can be isolated within a process one could consider this as a form of sequestration. Therefore, it is essential to consider the source of CO_2 in order to adequately judge the reliability of the process.

Many polymer productions and processing applications involve an excessive use of organic solvents, either as a reaction medium or as a processing medium for extraction, impregnation or viscosity reduction. Thus, in the polymer industry, SCFs are currently the subject of intense research and commercial interest. They can be used in a variety of processes, for example as solvents in polymer synthesis, as plasticizing agents or for chemical recycling. In subchapters 1.4 and 1.5 the processing and synthesis of polymers using $scCO_2$ are extensively discussed, in regard to the study of the dispersion polymerization of methyl methacrylate in $scCO_2$ performed in the presented work.

1.2 Physical and chemical properties of supercritical fluids

A supercritical fluid is defined as:

A state of a compound, mixture or element above its critical pressure, P_c, and critical temperature, T_c, but below the pressure required to condense it into a solid:[14]

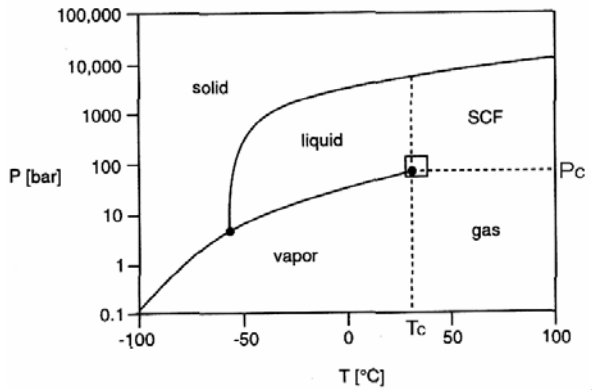

Figure 1.1: Phase diagram of carbon dioxide [14].

Figure 1.1 shows the phase diagram of carbon dioxide. The IUPAC definition omits the clause concerning condensation of the SCF into a solid. The melting curve extending over the supercritical region is often neglected even though the pressure on this curve is not always impractically high. For example, the pressure required to solidify CO_2 at its critical temperature is only 5'700 bar, while 140'000 bar are required for water.

The properties of supercritical fluids are frequently described as having values between those of a gas and a liquid.

*Table 1.1: Characteristic magnitudes of thermophysical properties of fluids, ρ for the density, η for the viscosity, D for the diffusion coefficient, * at ambient temperature.*[17]

	Liquid	**Supercritical**	**Gas**
ρ [kg m^{-3}]	1000	100-800	1*
η [Pa S]	10^{-3}	10^{-5}-10^{-4}	10^{-5}
D [m^2 s^{-1}]	10^{-9}	10^{-8}	10^{-5}

Table 1.1 shows the unusual properties of a SCF: for example a viscosity the same as a gas, a density the same as a liquid and a diffusion coefficient that lies between that of a gas and a liquid. This means that a SCF will have the gaseous property of being able to penetrate porous and fibrous solids and the liquid property to dissolve materials. Moreover, it does not possess any surface tension and hence no capillary forces will appear during extraction.

Table 1.2: Physical properties of common supercritical fluids, α is the polarizability, μ is the dipole moment and Q is the quadrupole moment.[14, 23, 24]

Solvent		T_c [°C]	P_c [bar]	ρ_c [kg m^{-3}]	α x10^{25} [cm^3]	μ [D]	Q x10^{26} [erg$^{1/2}$ cm$^{5/2}$]	Cost [CHF/kg]
Ar	Argon	-122.5	48.6	531	16.3	0		7.5
CO_2	Carbon dioxide	31.1	73.8	466	26.5	0	-4.3	2.8
H_2O	Water	374	220.6	322	15.9	1.85	-3.0	0.13
NH_3	Ammonia	132.4	113.2	235	22.6	1.47	-1.0	2.8
N_2O	Nitrous oxide	36.4	72.5	453	n.a.	0.17	-3.0	11.1
SF_6	Sulfur hexafluoride	45.5	37.6	737	54.6	0		16
Xe	Xenon	16.6	58.3	1099	1099	0		12.8
CH_4O	methanol	239.5	80.8	273	32.3	1.7		-
C_2H_4	Ethene	9.2	50.4	214	50.4	0	+1.5	14.7
C_2H_6	Ethane	32.2	48.7	207	45.0	0	-0.65	23.1
C_3H_8	Propane	96.7	42.5	220	62.9	0.09		3.6
C_4H_{10}	n-butane	152.0	38.0	228	n.a.	0.05		19.4
CF_4	Tetrafluoro-methane	-45.7	37.5	630	28.6	0		83.3

A particular focus is devoted to the use of SCF in the near-critical or supercritical state, due to the interesting physico-chemical properties under these conditions.[25] As substances approach their critical point, certain physical properties such as surface tension, refractive index, viscosity, dielectric constant, heat capacity, diffusivity and solvent strength become discontinuous and exhibit a strong temperature and pressure dependence, as shown in Figure 1.2 for pure carbon dioxide.

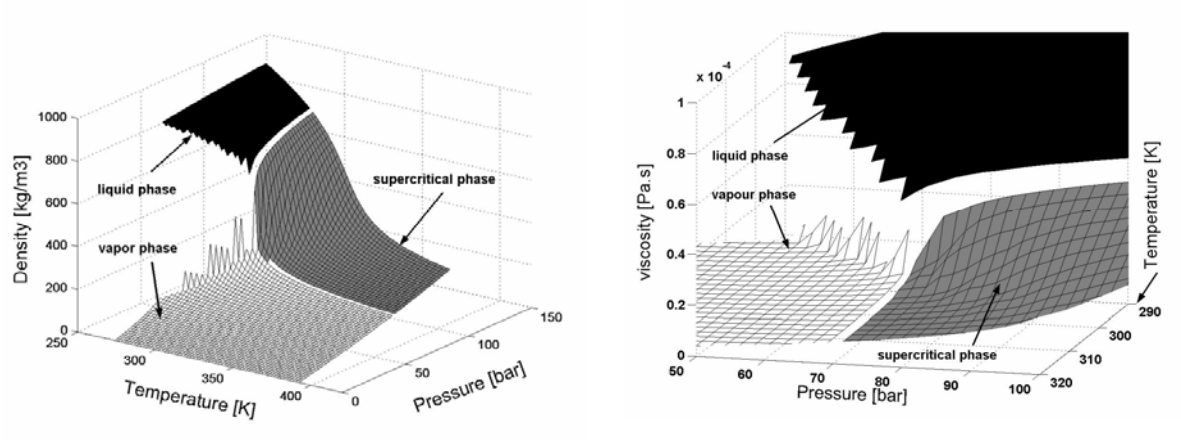

a b

Figure 1.2: 3D plot a) of the density and b) of the viscosity of pure carbon dioxide versus pressure and temperature.[26, 27]

Figure 1.2 shows that it is possible to tune the properties of SCF from gas-like through liquid-like by simply varying the pressure and/or the temperature.[28] The main reason for this is related to the fact that SCFs are highly compressible materials. Therefore, it is possible to understand the enormous benefit of a pressure tunable dissolving power in physical or chemical processes allowed by the use of SCFs. This provides the opportunity to develop processes for extracting, purifying and recrystallizing substances and produce new products that at present cannot be obtained by conventional processing technologies.[29] Moreover, regarding to their low viscosity (Figure 1.2 b), SCFs give also the possibility to enhance mass and heat transport.

The density of a SCF can be directly correlated to its solvent power as expressed by the Hildebrand parameter:

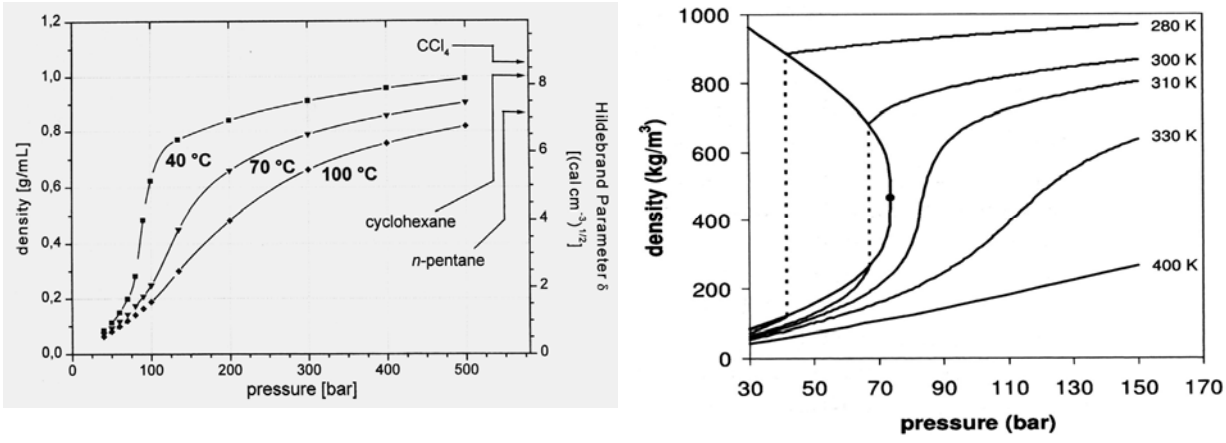

a b

Figure 1.3: a) Density and solvent power of $scCO_2$ as a function of pressure and temperature[14] *and b) Projection of the phase diagram in the density-pressure plane*[30-32].

In order to exploit as much as possible the benefits of those tunable properties, industrial operations with supercritical fluids are usually performed near the region enclosed by $T/T_c \approx 1\text{-}1.1$ and $P/P_c \approx 1\text{-}2$ where the changes in density and solubility are the largest.[33, 34] In counterpart, it should be kept in mind that it can be difficult to maintain operating conditions close to critical point since small changes in pressure and/or temperature will lead to drastic changes in the fluid properties and instabilities in the process.

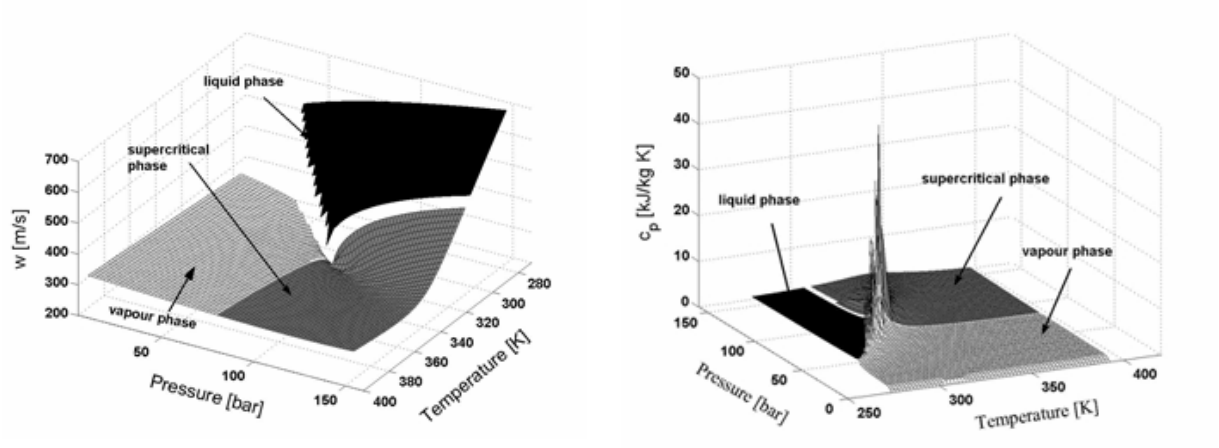

a b

Figure 1.4: 3D plot a) of the speed of sound (w) and b) of the isobaric heat capacity of pure carbon dioxide versus pressure and temperature. [26, 27]

Figure 1.4 b represents the evolution of the isobaric specific heat capacity, c_p, of pure carbon dioxide with respect to temperature and pressure. The isobaric heat capacity, C_p, and the isochoric heat capacity, C_v, are characterized by a critical enhancement related to the divergence of the enthalpy and the internal energy, respectively, at the critical point:

$$C_p = \left(\frac{\partial H}{\partial T}\right)_P \quad \text{and} \quad C_V = \left(\frac{\partial U}{\partial T}\right)_V \tag{1.1}$$

As the enthalpy and the internal energy of the liquid and the gas phase converge at the critical point, their corresponding derivatives with respect to temperature diverge, meaning that the resulting properties will theoretically tend to infinity.

These thermodynamic properties allow the introduction of another property which they are linked to and that will be used in this work, i.e. the speed of sound, c:

$$c = \sqrt{\left(\frac{\partial P}{\partial \rho}\right)_S} = \sqrt{\frac{c_P}{c_V} \cdot \left(\frac{\partial P}{\partial \rho}\right)_T} = \sqrt{\frac{1}{\rho} \cdot \frac{c_P}{c_V \cdot \kappa}} = \sqrt{\frac{1}{\rho \cdot \beta}} \tag{1.2}$$

where $\beta = \frac{1}{\rho} \cdot \left(\frac{\partial \rho}{\partial P} \right)_S$ and $\kappa = \frac{c_P}{c_V} \cdot \beta$ 1.3

Equations 1.2 and 1.3 show that the magnitude of speed of sound is directly related to the medium properties, such as the density (ρ), the isothermal compressibility (κ) or the isentropic compressibility (β). The fact that the compressibility becomes exceptionally high in the vicinity of the critical point means that a corresponding decrease in the velocity of sound has to be observed in this domain. As shown in figure 1.4 a, the speed of sound reaches a minimum as the critical point is approached. Therefore, this means that this characteristic of the speed of sound can be used to localize critical points of fluids and fluid mixtures.[35-38]

As pointed out previously, carbon dioxide is the most commonly used supercritical fluid because of its accessible critical state (T_c = 31.8 °C, P_c=73.8 bar) particularly its low critical temperature, low toxicity and high purity at low cost. CO_2 has a high TLV (threshold limit value of exposure) of 5'000 ppm, rendering it less toxic than many organic solvents, by comparison with the TLV of acetone of 750 ppm, of pentane of 600 ppm, of chloroform of 10 ppm. Moreover, carbon dioxide is relatively inert towards organic compounds; byproducts owing to side reactions are relatively rare with CO_2. Thus, carbon dioxide can provide not only environmentally advantages, but also chemical advantages when applied strategically:[20]

- CO_2 is the result of complete oxidation of organic compounds; it is therefore particularly useful as a solvent in oxidation reactions.[39]
- CO_2 is an aprotic solvent and can be used without penalty in cases where labile protons could interfere with the reaction.
- CO_2 is inert towards polymer-based free radicals, because it does not support chain transfer to solvent during free radically initiated polymerization.[40]
- CO_2 is highly miscible with gases. Liquid CO_2 can absorb much higher quantities of H_2 and O_2 than typical organic solvents and water.[41]
- CO_2 is miscible with a variety of low molecular weight organic liquids as well as many fluorous and silicone compounds.
- CO_2 exhibits a liquid viscosity only of 1/10 compared to water. Transport properties are thus improved, meaning that CO_2 can wet and penetrate complex geometries better than simple liquids. Solutes will diffuse faster than in analogous system using conventional liquids. Therefore, heat transfer in a CO_2 mixture can be improved.

Meanwhile, CO_2 also presents some chemical disadvantages:

- CO_2 exhibits a critical pressure requiring high pressure specialized equipment meaning higher capital cost processes.
- $scCO_2$ exhibits a dielectric constant generally between 1.1 and 1.5 depending upon the density. A low dielectric constant suggests a poor solvent power and hence solubility in CO_2 can require much higher pressure for certain class of solutes than more polar compressible fluids.
- CO_2 is a Lewis acid and can react with bases (amines, phospohines, alkyl anions) leading to undesired decrease in the rate of reaction (formation of carbamate) and in the solubility of the substrates.[42] The reactivity of CO_2 with amines can be an advantage as well as a disadvantage. Actually, researchers have employed CO_2 as a protecting group for amines.[43]
- CO_2 can poison noble metal catalyst used in hydrogenation reactions, depending on the metal used (platinum) and on the operating conditions (palladium).[20]
- CO_2 is a rather weak solvent having a low polarizability per unit volume and low cohesive energy density. This is perhaps the greatest drawback of CO_2, inhibiting to a certain extent its commercial use.
- CO_2 poisons Ziegler-type polymerization catalysts and thus it will terminate olefin polymerizations that employ classical Ziegler catalysts (titanium halide).

In summary, the advantages of using supercritical fluids are the following:

- SCFs can have similar solvating powers to liquid organic solvents, but their higher diffusivities, lower viscosity and lower surface tension make them more effective in many case.
- Since their density is pressure tunable, separation is easy to achieve.
- The ability to add modifiers to a SCF, for example to change the polarity, gives them more selective separation power.
- Little harm is done to the environment in terms of residues from processes using SCFs compared to volatile organic compounds (VOCs) and ozone depleting substances (ODSs).

1.3 Phase equilibria in SCFs

To form a stable polymer-SCF solvent solution at a given temperature and pressure, the Gibbs free energy must be negative and at a minimum:

$$\Delta G_m = \Delta H_m - T \cdot \Delta S_m \qquad 1.4$$

Enthalpic interactions depend predominately on solution density and on polymer segment-segment, solvent-solvent and polymer segment-solvent interaction energies. The entropy of mixing depends on both the combinatorial entropy of mixing and the noncombinatorial entropy of mixing associated with the volume change on mixing.[44] The thermodynamic properties of pure substances and mixtures are governed by the intermolecular forces acting between the molecules or the polymer-segment.[32] The most commonly occurring interactions are dispersion, dipole-dipole, dipole-quadrupole and quadrupole-quadrupole.[32]

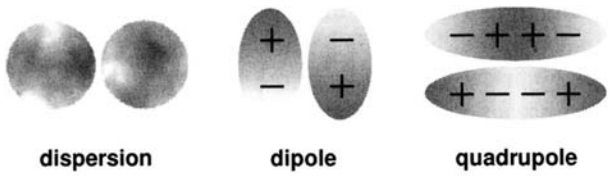

Figure 1.5: Charge distribution for different types of interaction. [32]

An approximate form of the attractive part of the intermolecular potential energy, $\Gamma_{ij}(r,T)$, is:[24]

$$\Gamma_{ij}(r,T) \approx -\left[C_1 \frac{\alpha_i \alpha_j}{r^6} + C_2 \frac{\mu_i^2 \mu_j^2}{r^6 kT} + C_3 \frac{\mu_i^2 Q_j^2}{r^8 kT} + C_4 \frac{\mu_j^2 Q_i^2}{r^8 kT} + C_5 \frac{Q_i^2 Q_j^2}{r^{10} kT} + SI \right] \qquad 1.5$$

where α is the polarizability, μ is the dipole moment, Q is the quadrupole moment, and $C_{1\text{-}5}$ are constants.[24] SI represents specific interactions such as complex formation or hydrogen bonding.

Nonpolar dispersion interactions, first right-hand term in equation 1.5, depend only on the polarizability of the components and not on the temperature. Therefore, the pressure needed to dissolve a nonpolar polymer in a nonpolar SCF solvent should decrease as the polarizability of the solvent increases.[45] SCFs consisting of heteroatoms have bond dipoles that result in the appearance of dipole moments or higher order ones, such as quadrupole moments. The potential energy of dipolar and quadrupolar interactions are inversely proportional to temperature meaning that at elevated temperature the configurational alignment of directional interactions, such as

dipoles or quadrupoles, is disrupted by the thermal energy, leading to a nonpolar behavior.[45] Thus, it may be possible to dissolve a nonpolar polymer in a polar SCF solvent. However, to obtain a sufficient density to dissolve the solutes at those elevated temperatures, substantially higher pressures need to be applied. Specific interactions such as complex formation or hydrogen bonding can also contribute to increase the solvent strength of the supercritical fluid. These interactions are also highly temperature-sensitive.

Polymers present special problems regarding to dissolution in any solvent. The very low entropy of mixing in polymer/solvent binaries due to the long chains of the polymer requires a very favorable enthalpic interaction between polymer segments and solvent to ensure dissolution of substantial polymer concentration.[45] Therefore, homogeneous processes are possible for polymers exhibiting high solubility in CO_2, otherwise heterogeneous processes, such as dispersion polymerizations, have to be considered for those polymers which are insoluble (see subchapter 1.5).

In order to understand the results discussed in the chapter treating the phase equilibria in the case of the dispersion polymerization of methyl methacrylate in $scCO_2$, it is necessary to build up the theoretical bases of mixtures phase behavior and their classification. Apparently not all scientists working on the domain of phase equilibria agree with each other with respect to the classification of mixtures behavior and their corresponding definitions. The classification presented in this work is based on the work of McHugh and Krukonis.[25]

The first argument to conceive the use of CO_2 as a solvent for polymerization reactions is based on the fact that it exhibits good solubility for small molecules and thus for most of the monomers. In terms of phase behavior, this means that in most cases monomer-CO_2 mixtures exhibit a Type I phase behavior, corresponding to the simplest case: [25]

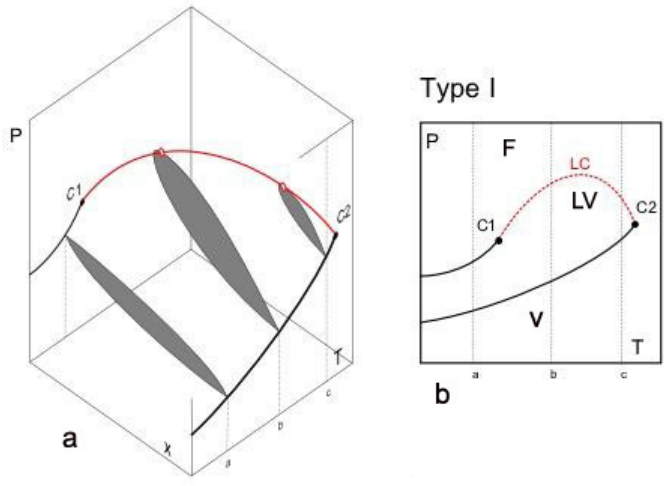

Figure 1.6: a) P-T-x phase diagram and b) P-T projection for a binary mixture of Type I [25].

In Figure 1.6, the two pure component critical points are labeled C_1 and C_2, where component 1 represents the more volatile component and component 2 represents the less volatile component or heavy component. In Type I binary mixture, the fluid domain is homogeneous and continuous, meaning that the compounds are miscible in all proportions and there is no liquid-liquid immiscibility region. A continuous critical curve (LC) connects the critical points, C1 and C2, of the pure substances.

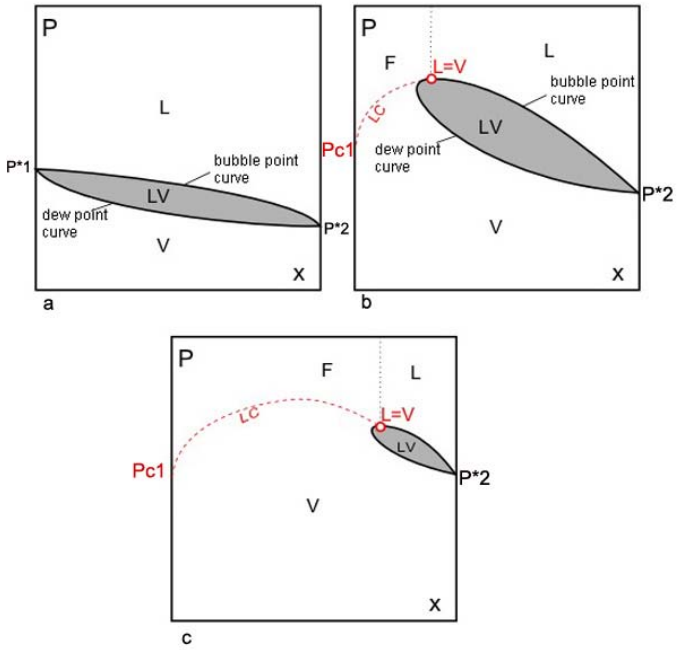

Figure 1.7: Isotherms for a binary mixture of Type I a) T lower than T_{c1} and T_{c2} and b-c) for temperatures between T_{c1} and T_{c2}..[25]

In Figure 1.7 the x-axis corresponds to the composition of the heavy compound. When the temperature is higher than the critical temperature of the most volatile compound, T_{c1}, but below the critical temperature of the heavy compound, T_{c2}, the dew and the bubble curves start normally at P_2*, but they do not reach the P-T plan of the volatile compound because the vapor pressure does not exist anymore, Figure 1.7 b and c. In this case, the dew and the bubble curves meet at the critical point of the mixture when x>0. The critical point of the mixture is situated at the maximum of the corresponding loop. The liquid in equilibrium with the gas phase will be enriched suddenly with the heavy product, 2, when the pressure gets very close to the critical pressure. When consecutive isotherms between T_{c1} and T_{c2} are observed the loop gets smaller and smaller and the critical point will move toward the critical point of the heavy compound. The loci of these intermediate critical points between C1 and C2 form the continuous critical curve LC. Figure 1.7 a shows the isotherm for a case where the temperature of the system is below the

critical temperature of both components. The phase behavior discussed here is encountered in the case of methyl methacrylate-CO_2 mixtures.

Once the monomer-CO_2 phase equilibrium is known, the second step is to establish the polymer-CO_2 mixture phase behavior in order to plan adequate operating conditions. The importance of the low density polyethylene (LDPE) production by free radical polymerization at high pressure, between 1500 and 3000 bar, and temperatures between 150 and 300°C led the scientists to better understand the transitions occurring in polymer-solvent systems at high pressure.[46] Although a polymer-solvent system is a mixture of multiple compounds because of the polymer polydispersity, it has been demonstrated that polymers can be considered as a pseudo-simple compound.[47, 48] This means that the behavior of polymer-solvent systems can be derived from Type III and IV for small molecules.

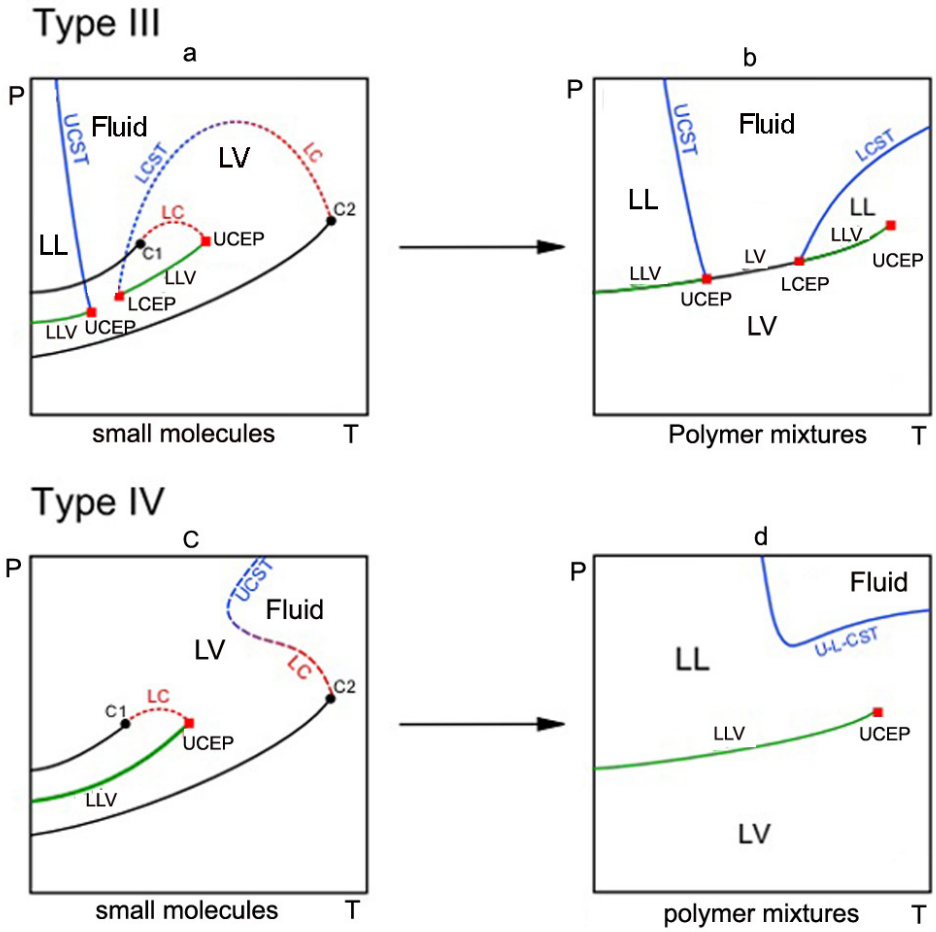

Figure 1.8: Characteristic projection on the P-T plan for polymer-solvent systems (b and d) derived from state diagram for simple systems of Type III and IV (a and c).[25]

Figure 1.8 a shows a generalized P-T phase behavior of Type III for binary mixtures of small molecules. These mixtures are characterized by two immiscibility domains in the liquid phase delimited by the liquid-liquid-vapor equilibrium (LLV) curves. Two critical lines are observed (dashed line): one starting from the critical point C1 and reaching the immiscibility curve LLV at its highest temperature extremity, UCEP point (upper critical end point), the other starting from the critical point of the heavy compound and reaching the same LLV at its lowest temperature extremity, LCEP point (lower critical end point). The upper critical solution temperature curve (UCST curve) has a negative slope at low temperatures and describes the pressure dependency of a liquid-liquid (LL) → fluid transition as the temperature is isobarically increased. Enthalpic interactions between the two components in solution typically govern the location of the UCST curve.[49] Because the temperatures are fairly low and the compounds considered are dense liquids, the UCST curve is expected to be relatively insensitive to pressure, i.e. smooth negative slope. The dashed curve starting from the critical point of the heavy compound or less volatile component, C_2, is called the lower critical solution temperature curve (LCST curve) which should describe the pressure dependency of a liquid-vapor (LV) → fluid transition when referred to Figure 1.8 a. But the transitions experimentally observed along this LCST curve at conditions near the critical point of the more volatile component are more characteristic of liquid-liquid→ fluid transition. So this portion of the curve is termed LCST curve, as the two phases coalesce into a single phase when temperature is lowered isobarically. The location of the LCST curve is generally controlled by the free volume difference between each component in solution. As the temperature increases, one of the components exhibits a much greater volume expansion than the other component leading to a large negative entropy of mixing that eventually induces the solution to phase separate. Both UCST and LCST branches of the critical mixture curve are often referred as cloud point curves.[50-54] For polymer-solvent systems, the pressure or temperature interval for a clear to totally opaque fluid → liquid + liquid transition along the UCST or LCST curves can be much greater than the interval for small molecules. This is due to the polydispersity of the polymers, which are characterized by a distribution of molecules having different molecular weights. Therefore, this means that the molecules will not precipitate at the same value of pressure and temperature leading to a higher transition interval. Generally, the transition is not very distinct, because the mixture just gets cloudier and cloudier; hence the name cloud point. In practice the cloud point pressure transition is usually of the order of 5-7 bar as long as the polymer has a molecular weight polydispersity less than 3.0.

The phase behavior shown in figure 1.8 a is typical for small molecule mixtures in which there is significant size difference between the two species or when the intermolecular potential functions of the two species differ considerably.[45] Figure 1.8 b shows the extrapolated behavior expected for a polymer-solvent mixture. As highlighted previously, it is important to realize that

the binary polymer-solvent diagram represents a multicomponent phase behavior since all polymers have a molecular weight distribution characterized by the polydispersity, which depends on the technique used to make the polymer. At high temperatures, the LCST curve does not reach a distinct end point since polymers do not have critical points. Moreover, the LLV lines of a polymer-solvent mixture is essentially superposed onto the vapor pressure curve of the solvent, because polymers have a negligible vapor pressure. The location of the LCST curve in polymer-SCF mixture of Type III can be greatly influenced by the quality of the solvent and the pressure applied. Increased hydrostatic pressure (compressible fluid) and higher polarity of the solvent lead to a decrease in the molar volume of the solvent and a reduction of the free volume difference between the solvent and the polymer. This means that lower pressure and temperature are required to obtain a fluid phase.

When the two components in solution differ considerably with respect to their molecular size and/or intermolecular potentials, the UCST curve shifts to higher temperature and merges with the LCST curve to give Type IV phase behavior shown in Figure 1.8 c. For the polymer-solvent system, Figure 1.8 d, the LCST curve no longer intersects an LLV line. The pressures of the cloud point curve are relatively constant at high temperatures, and rise sharply with decreasing temperature. In other words, the Type IV phase behavior is observed for mixtures for which the enthalpic contributions (weak interaction between molecules) and the entropic contributions (important difference between the sizes of the molecules) are so weak that elevated pressure and temperature are required to force the molecules to interact. Many polymer-solvent mixtures exhibit this type of behavior especially if one of the two components is nonpolar and the other one is polar. Because at high temperatures polar and quadrupolar interactions are broken by the thermal energy, the polar compound starts to behave as a nonpolar one.

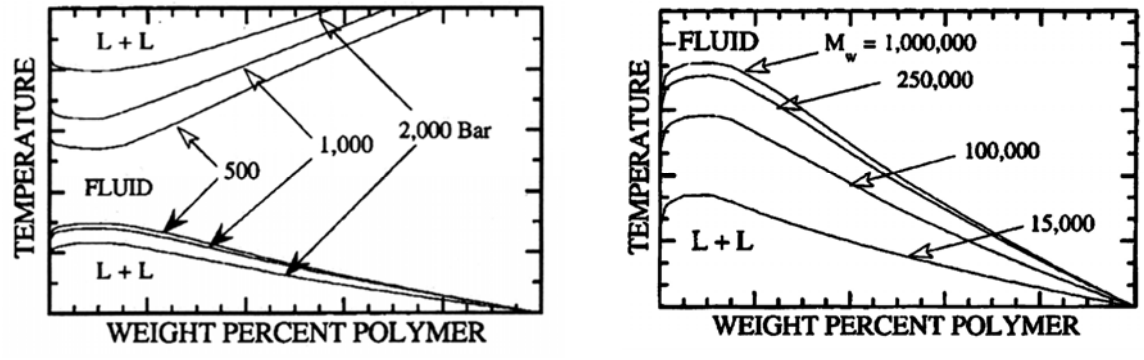

a b

Figure 1.9: a) Schematic representation of the impact of the pressure on the UCST (maximum) and LCST (minimum) temperature for a polymer-solvent mixture. b) Schematic representation of the influence of polymer molecular weight on the phase behavior of a polymer-SCF mixture at an arbitrary pressure. The same type of behavior is expected if pressure is substituted for the temperature axis.[45]

Figure 1.9 a shows that the maximum/minimum temperature of the temperature-composition loop for a polymer-SCF solution is relatively insensitive to composition in the range of 3-15 wt% polymer. Figure 1.9 a shows that also the pressure maximum/minimum of a pressure-composition (P-x) loop is insensitive to composition in this domain. This means that a single cloud point curve in the composition range of 3-15wt% polymer defines the maximum pressure of the P-T trace in the P-x loop and cloud point curves essentially superpose.[45] However, Figure 1.9 b shows that the molecular weight of the polymer will also greatly influence the temperature required to obtain a homogeneous mixture. This means that the maximum of the P-x loop for a given isotherm shifts to lower concentration with increasing molecular weight.

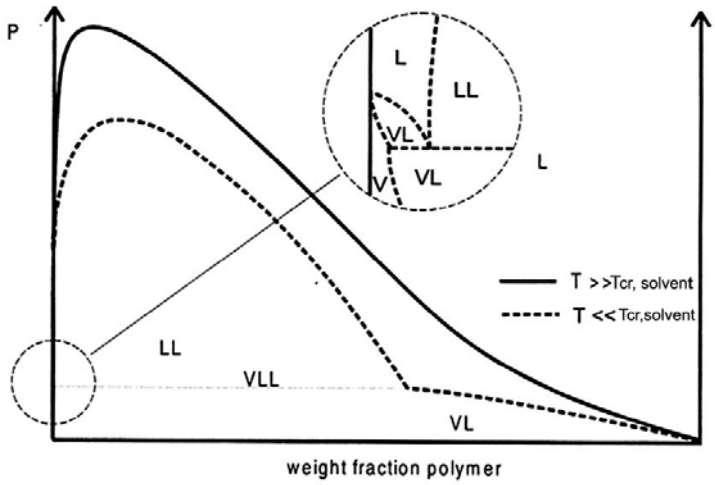

Figure 1.10: Qualitative P-x diagram of a polymer-CO_2 binary mixture both above and below the critical temperature of the solvent [55]. The figure includes liquid-liquid (LL), vapor-liquid (VL) and three-phase vapor-liquid-liquid (VLL) types of phase envelopes.

Figure 1.10 shows a schematic P-x loop of a polymer-SCF mixture. The observed asymmetry, as the one observed in the isobaric plan, due to the large disparity in size between polymer and solvent has a very important impact on polymer processing with SCF. Figure 1.10 allows understanding that solubilization of low concentrations of polymer in a solvent will require the highest pressures. On the contrary, swelling the polymer by the solvent, i.e. solubilize the solvent in the polymer, requires significantly lower pressures. The relatively low pressures required to elicit high degree of swelling may be one reason why applications where CO_2 is the minor component have been successfully commercialized, while those employing dilutes solutions have not.

Phase behavior is a fundamental aspect of supercritical fluids. In the case of dispersion polymerizations in $scCO_2$, the reaction mixture is initially homogeneous. At the earliest stages of the polymerization, initiation and propagation occur in the solution phase and oligomers are formed, which are soluble in the reaction mixture. As the growing chains become too large to remain solubilized, the chains nucleate from the solution to form particles. The use of a stabilizer (polymeric structure) is required to stabilize the growing particles and avoid the flocculation of the produced polymer. Therefore, the knowledge of phase behavior is needed to evaluate the initial state of the mixture, to develop efficient stabilizer and to control the polymerization at each step of the process. This means also that in the case of polymerization reactions at least ternary mixture phase behaviors have to be considered, i.e. monomer-solvent-polymer or monomer-solvent-stabilizer mixtures. In fact, it can be expected that the addition of a third compound in a mixture can influence the solubility of the compound already present in the mixture. Generally, the presence of the monomer on a CO_2-polymer mixture acts as a cosolvent allowing the extension of the miscibility region. The unreacted liquid monomer increases the density of the CO_2-solvent phase and reduces the free-volume difference between the polymer and the solvent, leading to enhanced polymer solubility. Because the monomer has the same physicochemical properties as the repeat units of the polymer, it energetically favors solvent-polymer interactions allowing the expansion of the single phase region. For example, it has been shown that the addition of methyl methacrylate (MMA) in carbon dioxide results in a reduction of phase separation in the system MMA-CO_2-PMMA lowering the corresponding pressure and temperature of the mixture cloud point.[56] Johnston *et al.* have shown that the addition of methyl methacrylate in a mixture of CO_2 and polydimethylsiloxane, the latter being used as stabilizer in dispersion polymerization, results in a reduction in the phase separation pressure of 6 bars per percent of monomer added in the mixture, indicating that MMA is a cosolvent for PDMS.[57] Furthermore, this suggests that during the course of the polymerization reaction the phase behavior will change as the conversion of monomer increases leading to change in composition of the phases in equilibrium.

1.4 Process design using supercritical fluids

Although extensive R&D investigations have been made, only few supercritical fluids' industrial applications have been developed. Most companies consider that supercritical fluid technology is too expensive because of the very high investment costs in comparison with classical low pressure-equipments and that it should be restricted to high-added-value products. This is not true when large volumes of materials are treated as shown in the case of the extraction of the caffeine from the coffee beans. Hydroformilation operates at 200-300 bar at large scale and low density polyethylene is produced at over 2000 bar. Several authors have reviewed the aspects of process design and costing for supercritical fluid industrial applications.[58-60] For

example, Kemmere *et al.* have shown that the removal of residual monomer from latex products using CO_2 is technically and economically viable.[61] Continuous reactors for SCF applications have advantages over batch reactors; they do not require depressurization to feed in the reactants and recover the products.[28] The idea here is to avoid the energy costs related to the compression of the gas. This remark is pertinent if it is considered that most of the polymerizations conducted in $scCO_2$ have been realized up to now in batch processes. Continuous mode also allows for "easier" choices for high pressure systems such as loop reactors. On the other hand, the advantage of a batch process is that depressurization up to ambient pressure allows the complete separation of the products from the CO_2 and permits to spare the costs of highly energetic and complicated separation units.

It appears also that the main obstacle that hinders the promotion of supercritical processes at industrial scale is the lack of thermodynamic models for the mixtures (mixing behavior) and kinetics data or reaction data (rate constant, heat of reaction, arrhenius constant). Those are fundamental parameters necessary to develop a process and point out the advantages of using SCFs.

At present time, the most important markets are related to natural product processing for applications in food and neutraceutical/pharmaceutical/cosmetic industries. Most of the current plants use CO_2 to process food (extraction, fractionation). The recrystallization of materials by supercritical fluid processing enables the manufacture of special structured products of significant high quality and function that simply cannot be produced with conventional methods. This is due to the versatile operating conditions that are possible with SCFs and their mixtures and that provide the flexibility in controlling the size of the particles (from microns to nanometers). Two methods have been developed to produce ultrafine particles and several reviews are available on polymer particles processing using supercritical fluids:[62-68]

- Rapid expansion of supercritical fluid solutions, RESS process
- Supercritical anti-solvent precipitation, SASP process

The coating or encapsulation of nanoparticles finds particular interest for the controlled release of drugs, genes and other bioactives agents. For example, the production of polymeric microspheres for controlled drug delivery is an area where RESS process is used. This process allows the production of thin film coatings, polymer fibers, and fine particles of a submicrometer size. The RESS process is unique, as RESS products are generated "dry", meaning little or no residual solvent. The process works by exploiting the property changes brought about by density changes. In this process, materials are dissolved in a suitable supercritical fluid. The mixture is then sprayed through a heated nozzle (see Figure 1.11 a). This rapid expansion of the homogeneous supercritical solution is accompanied by a temperature and a pressure drop leading

to phase separation. The nozzle diameter and length are among the parameters that influence the particle size generated.

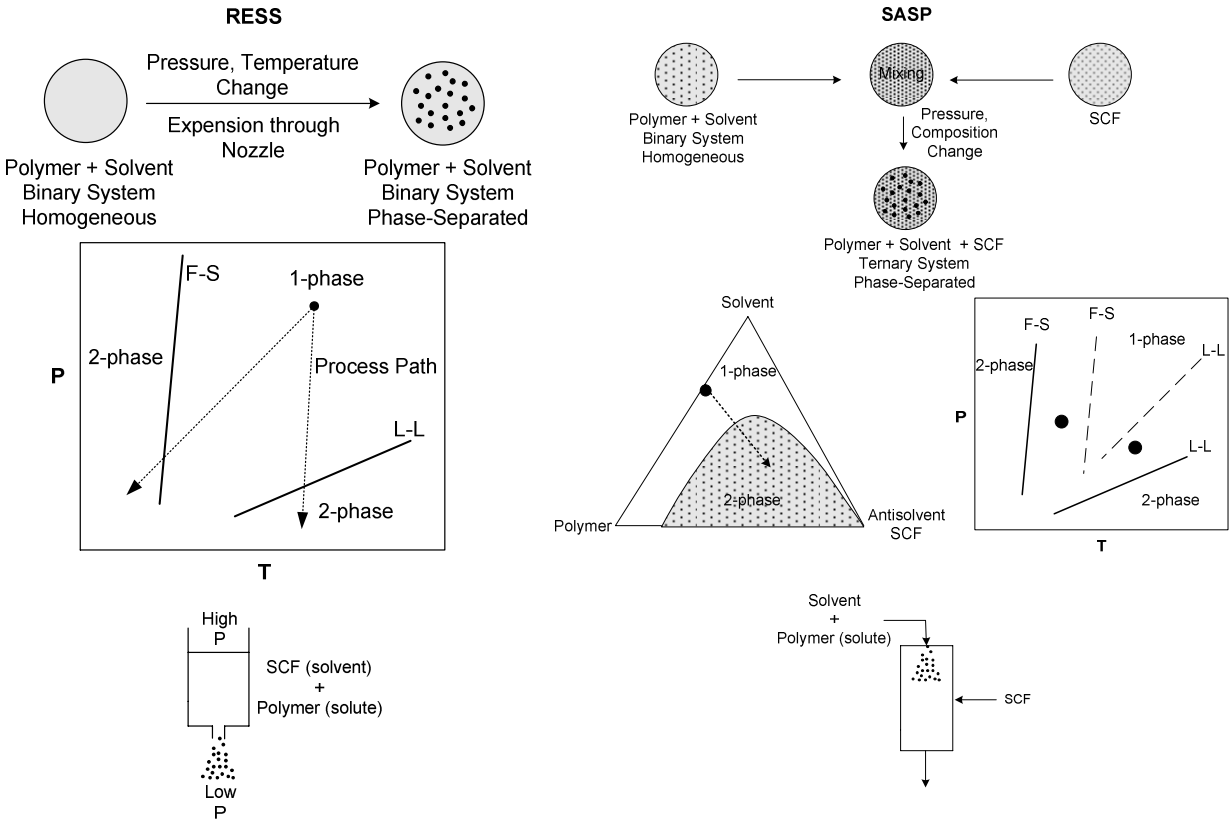

a b

Figure 1.11: Schematic representation a) of the RESS process and b) of the SASP process [62].

The SASP process involves the mixing of a polymer solution with a supercritical fluid that functions as an antisolvent, i.e. the polymeric compound is not soluble in the supercritical phase. This process is also known as precipitation of a compressed fluid anti-solvent. The material is first dissolved in a suitable solvent. Then the mixture is sprayed into supercritical carbon dioxide, contained in a high pressure chamber (see Figure 1.11 b). Droplets are formed and the original solvent dissolves in the carbon dioxide, leaving the insoluble material in powder form. Like RESS this technique is currently used in the pharmaceutical industry.[67]

Polymers require far more post-synthesis processing than do small molecules. Although the solubility of most polymers in CO_2 is extremely low, the solubility of CO_2 in many polymers is substantial. The sorption of carbon dioxide by polymers and the resulting swelling of the polymer induce changes in the mechanical and physical properties of the polymer. The most

important effect is the plasticization of the polymer and is characterized by changes in the polymer system such as:

- A lowering of the glass transition, T_g, of glassy polymer.
- An increase of the melting temperature.
- A lower rigidity at room temperature.
- Increased elongation and flexibility of individual chains of the polymer.
- Increased toughness.

Swelling a polymer with CO_2 drops its viscosity significantly and allows for a number of CO_2-enhanced processes where the diffusivity of the solutes in the polymer matrix is the key parameter, i.e. rapid extraction and impregnation processes. Extraction applications include removal of residual monomer,[61] of solvents and catalysts.[69] The dying of textiles and fibers have been extensively examined,[70-72] motivated by the reduction in energy required for mixing, as well as elimination of the aqueous waste stream commonly associated with dying operation. Howdle *et al.* have shown the use of $scCO_2$ to swell an aliphatic polyester and to incorpore an enzyme in the polymer matrix with no loss of the enzyme activity.[73] Such a process allows the blending of temperature sensitive compounds with polymer without the need of additional solvent-based processing. Another application of the solubility of carbon dioxide in polymers is the production of foams.[74] Moreover, due to its vanishing low interfacial tension, $scCO_2$ is able to successfully wet and penetrate very small features of a component or structure. This leads to the use of $scCO_2$ as cleaning agents, including precision cleaning of surfaces.[75] For example, in the microelectronics industry, half of the hundreds of individual process steps involve washing.

As highlighted previously, carbon dioxide has also a series of chemical advantages. For example, because it does not support chain transfer to solvent during free radical polymerization, it is an ideal solvent for use in such polymerization.[40] The most important industrial application of supercritical carbon dioxide for polymer synthesis is the one realized by Dupont. In fact, Dupont has announced in 2001 the build up of a $275 million dollar manufacturing plant to produce Teflon® (PTFE, poly(tetrafluoroethylene)) and other fluoropolymers in supercritical carbon dioxide. Most of the polymerization currently conducted by Dupont in its semi-works facilities are precipitation polymerizations, where the improved control of the molecular weight and the enhanced safety is inherent to the use of TFE (tetrafluoroethylene)/CO_2 mixtures. Conventional routes to fluoropolymers typically employ aqueous or chlorofluorocarbon (CFC) based solvent systems leading to premature chain termination.

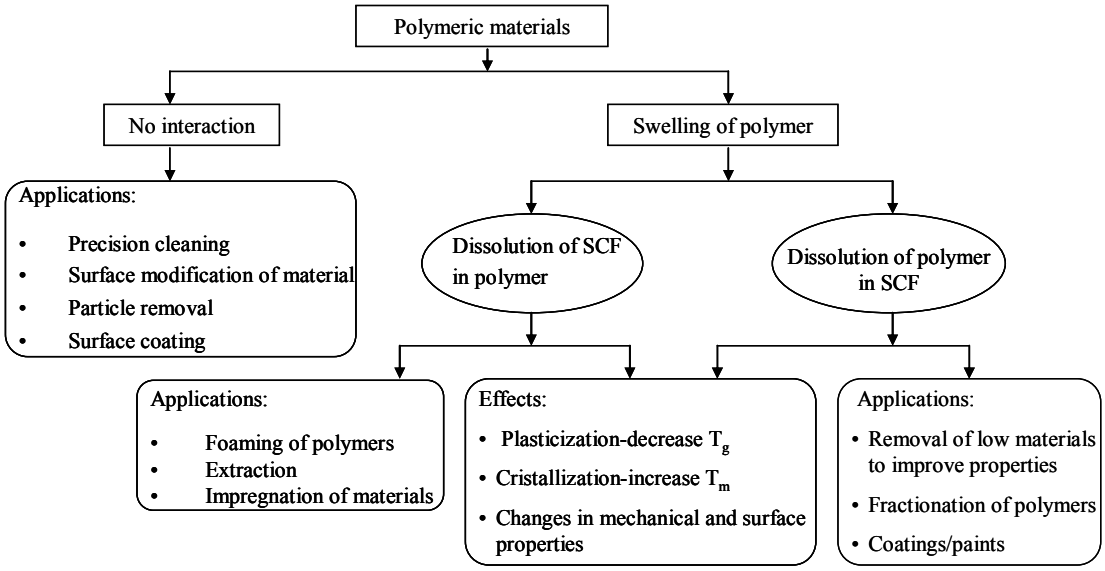

Figure 1.12 Flow diagram of the interaction of carbon dioxide with polymers [76].

1.5 Polymerization reactions in supercritical carbon dioxide

In the following subchapters the main features of the different types of polymerization reactions realized in $scCO_2$ are discussed. There are several reviews treating this subject used as references. [40, 77-81]

1.5.1 Homogeneous polymerization

Only two classes of polymers have shown significant solubility in CO_2 under practical conditions; amorphous (and low melting) fluoropolymers and silicones. Amorphous fluoropolymers are important in a range of technologically demanding applications, but the synthesis and processing of these materials can be difficult due to their poor solubility in most common organic solvents. The use of chlorofluorocarbon (CFC) solvents has been common for this purpose. However strict limitations are now imposed on CFCs due to environmental issues. DeSimone *et al.* have shown that amorphous fluoropolymers can be synthesized by homogeneous solution polymerization in supercritical carbon dioxide using thermal free-radical initiation.[82] Fluorinated acrylate and methacrylate monomers as 1H,1H-perfluorooctyl acrylate (FOA) were polymerized in CO_2 using 2,2'-azobis(isobutyronitrile) (AIBN) as initiator (59.4 °C, 207 bar, 48h). The solution properties of PFOA in $scCO_2$ were investigated by small angle neutron scattering (SANS), and the second virial coefficient for the polymer was found to be positive, confirming that CO_2 is a good solvent for PFOA.[83, 84] Such polymers were subsequently used as stabilizers in dispersion polymerizations (subchapter 1.5.4) in $scCO_2$.

Beuermann *et al.* have described the free-radical polymerization of styrene in supercritical carbon dioxide under homogeneous conditions at high pressures and temperatures (80°C, 200-1500 bar) in the presence of a chain transfer agent (CBr_4).[85] These reactions remain homogeneous due to a combination of high pressure conditions, relatively low molecular weight of the products (caused by chain transfer) and low monomer conversions (7.1-36.2%). In fact, the residual monomer in the medium acts as a cosolvent and contributes to maintain the solubility of the produced polymer in the medium.

In addition to homogeneous free-radical polymerization, CO_2 has also been used as a medium for the homogeneous cationic polymerization of fluorinated vinyl monomers and cyclic ethers using Lewis acid initiator ($EtAlCl_2$ or BF_3).[86] The fluorinated polymers were obtained with good yields and have molecular weight similar to that of materials synthesized using Freon-113 as solvent.

Thus, CO_2 can be used as a solvent alternative to replace CFCs for the homogeneous processing of fluoropolymer processing. But, it has to be emphasized that in many cases fluoromonomer poylmerizations are still precipitation polymerizations, when using $scCO_2$ as solvent. In fact, McHugh *et al*. have shown that many fluoropolymers are insoluble in CO_2.[87]

The lack of solubility of common polymers in carbon dioxide is sometimes described as a major disadvantage to its use as a polymerization medium. However, it should be reminded that the insolubility of the polymer in the continuous phase is actually a prerequisite for processes such as suspension, emulsion, dispersion polymerization, and that these heterogeneous polymerization techniques are the methods of choice for the synthesis of many materials.

1.5.2 Precipitation polymerization

Carbon dioxide is a rather poor solvent for most high molecular weight polymers. In the absence of a stabilizing agent, polymers precipitate rapidly from the CO_2 solution as they are formed. However, heterogeneous polymerization of CO_2-soluble hydrophilic and lipophilic monomers in liquid or supercritical CO_2 have proved to be very successful.[80] DeSimone *et al.* have shown that in the precipitation polymerization of acrylic acid in $scCO_2$ the very fast propagation rate allowed the synthesis of high molecular weight polymer, even though it precipitates from the solution.[88] The continuous precipitation poylmerization of vinylidene fluoride has also been studied. The main characteristic of this synthesis is that bimodal molecular weight distributions are obtained.[89] Another example is the copolymerization of tetrafluoroethylene with hexafluoropropene leading to a heterogeneous process when high

molecular weight copolymers are formed.[90] The fluorinated copolymer produced in CO_2 exhibits superior performance during extrusion, owing to fewer gels and tighter composition distribution. A primary advantage of the use of CO_2 in this process is that the solvent contains no abstractable protons and hence the fluoroolefin monomers do not chain transfer to solvent. In certain systems such as these, particularly where the polymer is insoluble in its corresponding monomer, precipitation polymerizations can be quite efficient and can give high molar mass products with good yields. However, amorphous polymer precipitation often leads to undefined morphologies and, in many cases, low degrees of polymerization.[91] The important advantage of using CO_2 as the continuous phase is that the products can be isolated directly from the reactor as a dried, solvent-free powder after depressurization or venting of the carbon dioxide.

1.5.3 Emulsion polymerization

In emulsion and suspension polymerization, neither the monomer nor the polymer is soluble in the continuous phase. Moreover, in emulsion polymerization, high quantity of soluble surfactant (polymeric material) is required to form the micelles and to stabilize the monomer droplets. In literature, only the inverse emulsion polymerization of acrylamide has been published.[92] The explanation may be that it is difficult to find monomers that are not soluble in carbon dioxide and surfactants that are, keeping in mind that CO_2 is a good solvent for small molecules and a poor solvent for high molecular weight polymers. No matter how, emulsion polymerization of water soluble monomers in $scCO_2$ could be a viable target in the context of green chemistry, given that the commercial route employs an organic continuous phase and also requires significant energy input to separate product from emulsion following polymerization.

1.5.4 Dispersion polymerization

Dispersion polymerization,[93] where the monomer is soluble in the continuous phase while the polymer is not, has been extensively studied. Thus, a dispersion polymerization begins as a homogeneous solution where both monomer and initiator are soluble in the reaction medium. As the reaction proceeds, oligomers are produced through solution-phase polymerization. Once oligomers reach a critical size, they begin to precipitate from the solution. At this point surfactants are needed to stabilize the precipitated particles in order to prevent flocculation and aggregation. The polymerization continues in the stabilized polymer colloids. Johnston *et al.* have made an exhaustive study on the particle growth regime and the particle formation regime in the case of the dispersion polymerization of methyl methacrylate (MMA) in $scCO_2$.[57, 94] They have shown that the nucleation occurs at the very early stage of the polymerization corresponding to less than 5% monomer conversion. Only few minutes at 65°C are needed to reach the final particles number that remains constant throughout the polymerization. After this

step, the average particle diameter will increase either by precipitation of the polymer chains onto the particle surface or by the polymerization occurring inside the particles.[95]

Stabilizers for dispersion polymerizations are specifically designed surfactants that contain a CO_2-phobic and a CO_2-philic region. The conventional methods used to prevent coagulation and flocculation of the polymer particles in a colloidal dispersion include electrostatic, electrosteric, and steric stabilization.[93] Steric stabilization offers several advantages over the other two mechanisms, such as the effectiveness of polymer stabilizers in solvent with low dielectric constant. For this reason, steric stabilization provides the stabilization mechanism of choice for CO_2 systems. In this case, the stabilizer is a macromolecule which preferentially exists at the polymer-solvent interface and prevents aggregation of the particles by coating the surface of each particle and imparting long range repulsion between them. Thus, the CO_2-phobic region acts as an anchor to the growing polymer, either by physical adsorption or by chemical grafting. And the CO_2-philic region sterically stabilizes the growing polymer particles, preventing flocculation and precipitation. Therefore, the key requirement to successful dispersion polymerization is finding a suitable stabilizer. Because most commercially available surfactants designed for use in aqueous systems are completely insoluble in $scCO_2$,[77] an important field of investigation is the design of surfactants for CO_2 applications.

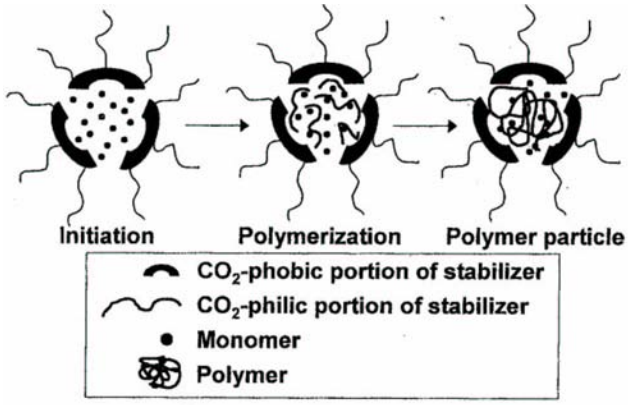

Figure 1.13 : Dispersion polymerization in CO_2 using a CO_2-philic stabilizer.[33]

Most of the vinyl monomers are miscible with CO_2 at relatively moderate pressures, while high molecular weight polymers are notoriously insoluble. Thus, the dispersion polymerization of vinyl polymers appears to be the method of choice to process those polymers in carbon dioxide. Despite the fact that stabilizers are quite expensive, the processing of polymers through dispersion polymerization in $scCO_2$ has several important advantages. The separation of the produced polymer from the CO_2 phase does not require drying or devolatilization process and thus allows potentially energy savings. Moreover, a dispersion

polymerization produces stable latex that could form the basis for coating formulations that could be sprayed without VOC (volatile organic compound) release.

DeSimone and coworkers[96], as pioneers, have published the results of the dispersion polymerization of methyl methacrylate (MMA) in supercritical CO_2 (204 bar and 65 °C) using the polymer poly(FOA) as stabilizer:[96]

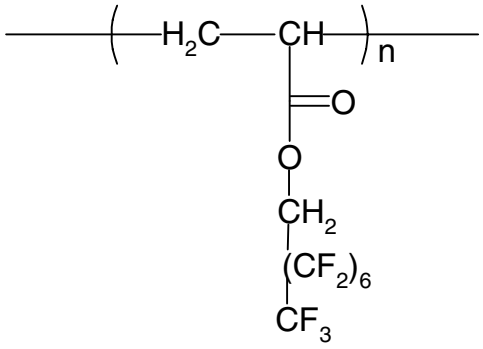

Figure 1.14 : Structure of poly(FOA), polyperfluorooctyl acrylate.

Two polymeric stabilizers of different molecular weight ($1.1 \cdot 10^4$ g/mol and $2.0 \cdot 10^5$ g/mol) were tested. Without added stabilizer, the PMMA precipitated and the reaction proceeded to low conversion (<40%) leading to the production of a low molecular weight polymer. When stabilizers were used, high yields (>90%) and high molecular weight polymers (>$3.0 \cdot 10^3$ g/mol) were obtained. By increasing the concentration of stabilizer, smaller and more uniform particles were created. At identical stabilizer concentrations, the use of the low molecular weight stabilizer led to the production of more particles with smaller diameter. Johnston *et al.* have demonstrated that the stabilization of the particles by the poly(FOA) is mainly due to the effective solvation by CO_2 of the fluorinated blocks (CO_2-philic blocks).[97, 98]

Hsiao *et al.* have shown that with a higher molecular weight poly(FOA) ($1.0 \cdot 10^6$ g/mol) lower concentration of stabilizer is required to stabilize the PMMA particles.[99] They have observed that the particle size decreases (from 2.86 to 1.55 μm) as the stabilizer concentration increases (from 0.24 to 16 wt%). According to the theory emitted by Barrett,[93] the influence of the stabilizer concentration on the size of the particles can be interpreted in the following way. The number of particles formed, given a reasonable constant rate of precipitation, will depend on the rate at which the stabilizer adsorbs at the surface of the particles. In turn, the rate of adsorption depends directly on the concentration of the stabilizer and on the strength of anchorage. Hsiao *et al*. have also shown, as already observed in dispersion polymerization in organic solvent,[93] that higher concentration of stabilizer leads to the formation of a second

population of smaller particles increasing the polydispersity of the particle size distribution. This means that it exits an optimum of stabilizer concentration defined for each process. Actually, excess of stabilizer present at any stage of the polymerization can cause further nucleation to occur, whilst a deficiency of stabilizer leads either to flocculation or to particle coalescence depending on the nature of the dispersed particle.[93]

Another type of fluorinated copolymer stabilizer, such as the poly(methyl methacrylate-*co*-hydroxyethyl methacrylate)-*g*-poly(perfluoropropylene oxide) (PMMA-HEMA-PFPO), has been used in the dispersion polymerization of MMA by Beckman *et al.*[100] These comb-type copolymers are composed by an acrylate backbone (PMMA-HEMA) acting as the anchor, and fluoroether side chains (PFPO), acting as the soluble components:

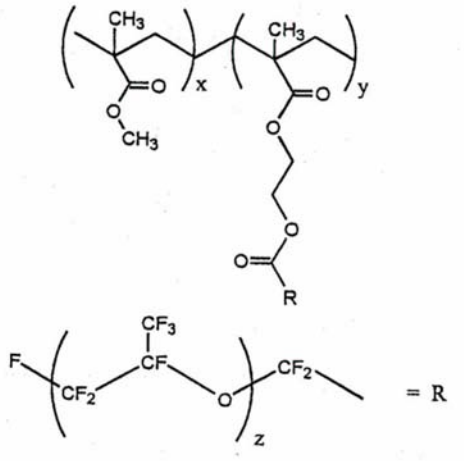

Figure 1.15 : Structure of PMMA-HEMA-PFPO graft copolymer.[100]

In their study, they have shown that the length of the backbone is the most important factor in determining the polymerization rate, the particle size, and the particle size distribution. Once the backbone was above a certain chain length, monodisperse, micron size particles were rapidly formed. This can be explained by the fact that an increase in the length of the backbone leads to a better anchorage and higher surface coverage of the growing polymer particles. The extent of the soluble component is also important to ensure enough solubilization of the stabilizer in the continuous phase. In fact, they have observed that an increase in the number of grafts per backbone leads to an increase of the rate of polymerization until a limit is reached. They have also demonstrated that the rate of polymerization is a function of the stabilizer concentration. When this concentration is too high, a decrease in the polymerization rate is observed due to a decrease of the rate of diffusion of the monomer into the growing particles.

Howdle *et al.* have published the use of a very simple fluoroether carboxylic acid as stabilizer for MMA polymerizations, the so-called Krytox 157 FSL. In their study, they have demonstrated that the hydrogen bonding between the acid and MMA's carbonyl group can provide sufficient anchoring to stabilize the dispersion and hence form small PMMA particles.[101, 102] The main advantage of this weak interaction is its reversibility; no residual stabilizer is detected in the final polymer after depressurization. Moreover, the Krytox™ 157 FSL is a commercially available stabilizer. This is another advantage considering that only few stabilizers for supercritical CO_2 application are available on the market.

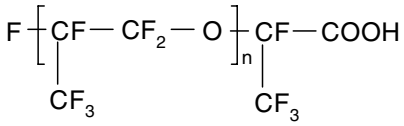

Figure 1.16: Structure of Krytox™ 157 FSL.

Morbidelli *et al.* have analyzed the effect of the reactor mixing in a 500 ml reactor volume using the same stabilizer.[103] In their study, they have shown that the pseudo-graft stabilizer can be effective to produce high yields of polymer but only under specific conditions. Indeed, they observe that the dispersion polymerization is destabilized under efficient stirring (400 rpm) leading to an important coagulation of the particles induced, as they have demonstrated, by shear forces. Very low stirring speeds (25 rpm) are needed to avoid the formation of a tacky solid or coagulate powder.

Silicone polymers can also be used as stabilizers in dispersion polymerizations. DeSimone *et al.* have published the results of the dispersion polymerization of methyl methacrylate using a poly(dimethylsiloxane) macromonomer (PDMS macromonomer) as stabilizer:[104]

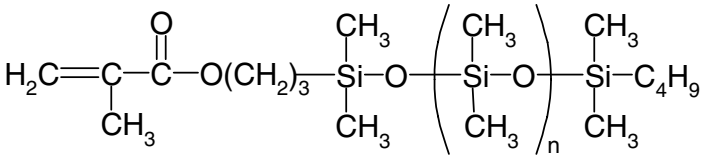

Figure 1.17 : Structure of a PDMS macromonomer , PDMS-monomethacrylate.

Macromonomers are polymers with a polymerizable terminal functional group. Certain silicone macromonomers are also commercially available but they are, as fluorinated stabilizers, very expensive. They are commonly used for the formation of graft copolymers. The disadvantage of such molecules is that they are chemically incorporated in the final polymer.

DeSimone *et al*. have shown that at least 3.5 wt% of macromonomer with respect to monomer are necessary to obtain monodispersed polymer particles at high yield. In their study, they have observed that the PDMS homopolymer, which lacks the reactive MA functional group, is less effective in stabilizing the polymerization, because a much greater concentration of the homopolymer is needed to achieve the same results obtained with the macromonomer. Purifications of the PMMA have shown that only a small fraction of the macromonomer is incorporated into the polymer.

Johnston *et al.* have shown that in the case of the dispersion polymerization of MMA using a 10'000 g/mol PDMS macromonomer at least a pressure of 207 bar is required to solubilize the PDMS in the $scCO_2$.[57, 94] In their study of the particle formation and the particle growth regime, they have pointed out the importance of the solubility of the stabilizer in the medium and the parameters that can influence it. For example, for pressure below the threshold pressure of 207 bar, the PDMS is poorly solvated by the continuous phase and is unable to stabilize the growing polymer particles. Moreover, they have shown that the extraction of the monomer from the latex produced at low conversion leads to particles flocculation, indicating that MMA is a cosolvent for PDMS and plays an important role in the stabilization of the dispersion.

Howdle *et al.* have reported that the dispersion polymerization of MMA using a PDMS macromoner can also be sensitive to stirring effect.[105] They have shown that improved yield and molecular weight are obtained in the case of the absence of stirring. They have attributed this phenomenon to the quenching of the propagating radicals at the metal surface of the vessel, introducing additional termination mechanism that leads to the production of lower molecular weight polymers at low conversion when stirring is used. They have suggested that the deposition of a protective passivating film is hindered by efficient agitation.

The use of reactive silicones has shown that their performance is in many cases less satisfying than that of the various fluorinated stabilizers, because higher concentrations and higher molecular weight stabilizers are necessary. Today's stabilizers are expensive and the challenge to find less costly alternatives to promote dispersion polymerization in $scCO_2$ is important. The challenge is to find surfactants less complex than polymers. Moreover, although micron-size particles of PMMA are produced, latex stability is relatively poor. This means that when the particles produced are recovered and dried, it becomes difficult to redisperse the product again in CO_2 or in water for applications in coating formulation. Johnston *et al.* have investigated the mechanism of particles redispersion and the design of surfactants that would allow both polymerization and redispersion.[106] The idea is to use a single surfactant than can both sterically stabilize the particles produced during the dispersion polymerization in $scCO_2$ and

to electrostatically stabilize the particles when transferred to water for example. If the cost of stabilizers could be lowered and the stability of the latex improved, a CO_2-based dispersion could form the basis of a coating system without volatile organic compound release.

1.6 Monitoring reactions in SC media

In this subchapter, a focus is made on the monitoring techniques available that can be or have been applied to reactions in supercritical fluids.[107] The on-line monitoring of reactions, i.e. the ability to follow the conversion of reactants into products, is essential to:

- Find the best operating conditions of a process leading to the obtaining of a high product quality at high conversion and selectivity.
- Analyze the effects of the experimental parameters (temperature, pressure concentrations) on the rate of reactions and on product properties in order to adapt the synthesis to specific requirements that can be governed by the specification of the products or by the process routes.
- Understand the fundamental chemical and physical aspects that control the chemical reactions.
- Develop safe processes characterized by equilibrium between product requirements and safe operating conditions.

Different methods are available to monitor chemical reactions. A technique can be to extract samples from the reactor during the course of the reaction and analyze the sample composition at different steps of time (i.e. conversion). But, sampling methods are tedious and time consuming. Moreover, they are invasive methods that can perturb the evolution of the reactions. Furthermore, it can be easily understood that it is rather difficult to develop such methods for supercritical fluid applications, because the system works under pressure. This means that at each sample extraction a decrease in pressure inside the reactor can occur. But smart design of the sampling unit (e.g. a HPLC valve) and the sampling procedure can avoid this problem encountered with off line sampling in high pressure systems. Hence, whatever the chemical process, on-line methods based on a noninvasive measurement procedure are mostly preferred. For those reasons, sensors than can be directly introduced into the reactor and that are sensitive to composition change are developed to monitor reactions. The necessity to obtain a better understanding of the chemical reactions under supercritical conditions has led many scientists to adapt the existing technologies for high pressure applications.

Spectroscopic methods are often used as in-line sensors, because they are characterized by a high sensitivity to the product chemistry and concentration that defines the frequency of the

absorption bands and the intensity of the bands, respectively. For example, FT-IR (Fourier Transform Infrared Spectroscopy) sensors can measure the concentration of a component in a mixture at the level of the ppm. Olesik *et al.* have reported the direct monitoring of the decomposition of isopropylamine oxide in CO_2 using FTIR spectroscopy.[108] With this technique, they are able to point out the solvation-density effects of $scCO_2$ on the rate of reaction. Another spectroscopic method applied to supercritical fluid chemical reactions is the vibrational spectroscopy like Raman and IR spectroscopy.[109] An advantage of this type of spectroscopy is related to the fact that the spectrum of the analyzed compound is greatly influenced by the solvent properties. Kessler *et al.* have reported the use of in situ Raman spectroscopy for the investigation of the fast decomposition rate of the tertiary butyl peroxypivalate at a pressure of 2000 bar.[110] This compound is a standard initiator used in the radical polymerization of olefins at high pressure.

Several groups have used UV-Vis cells to analyze the evolution of the turbidity occurring at the early stage of the dispersion polymerizations in $scCO_2$.[57, 94, 95, 111] By this technique, they are able to point out and analyze the mechanism of the particles formation and growth in dispersed systems using $scCO_2$ as solvent. This method that can be applied only at low conversion is based on the fact that dispersion polymerizations start in a homogeneous medium that allows the transmission of light. As soon as the polymer chains are insoluble in the solvent and nucleate to form the primary particles, the turbidity in the medium increases leading to a decrease in intensity of the light transmitted. This technique has allowed demonstrating that the dispersion polymerization of MMA starts in the continuous CO_2-rich phase. When larger particles are present and when the concentration of the monomer in the continuous phase has decreased significantly, polymerization can take place in a competitive way inside the particles.[100]

It has been shown in the subchapter 1.2 that the velocity of propagation of sound waves depends directly on the properties of the medium, such as the density and compressibility. This means that if during a chemical reaction those properties change significantly it is possible to use this characteristic for the development of on-line sensors. Actually, Hauptmann *et al.* have shown the numerous advantages and applications of ultrasonic sensors (between 20 kHz and 100 MHz) in the process industry.[112] Such sensors allow non-invasive and in-line measurement with a rapid response at low cost and low power consumption offering long term stability, high resolution and accuracy. Because polymerization reactions can be characterized by drastic changes of the physico–chemical properties during the course of the reaction, they are the natural candidates to apply ultrasonic methods for their monitoring. Morbidelli *et al.* have used this acoustic method with success to measure the evolution of the conversion in homopolymerizations and copolymerizations in dispersed systems, such as the methyl

methacrylate emulsion polymerization in water and copolymerization of styrene and butyl acrylate.[113] The same methodology has been applied to bulk and solution polymerizations by Renken *at al.*[114, 115] and Meyer *et al.*[116] for monitoring the high solid content polymerization of styrene and methyl methacrylate, respectively. This work will show the first application of the speed of sound measurement to the monitoring of the dispersion polymerization of MMA in $scCO_2$. The use of this technique allows calculating from the on-line measurement of the speed of sound the composition of the medium at each step of time (i.e. conversion).

Because most chemical processes are accompanied by temperature changes of the reaction mixture due to the release or consumption of heat during the course of the reaction, calorimetric methods can be applied for the in-line monitoring of chemical reactions. Howdle *et al.* have developed a power compensation calorimeter for the monitoring of the dispersion polymerization of MMA[117] and the precipitation polymerization of vinylidene fluoride[118] in $scCO_2$. The measurement is based on fact that an internal heater will deliver a varying power, which is controlled externally, to maintain a constant temperature between the autoclave and the outside environment. In fact, the power required to maintain this fixed temperature difference will depend on the thermal events occurring in the system and on the rate at which they occur. Their preliminary experimental results demonstrate the feasibility of this technique to monitor the polymerizations in $scCO_2$ and to identify the endothermic and exothermic events occurring in the system.

Nowadays, most of the techniques developed for the monitoring of chemical reactions in SCFs are applied to small reactor volume. The advantages are that small amounts of reactants are needed and that the apparatus can be built up with lower investment costs. The important disadvantage is that such systems do not have real similarities with industrial reactors. Reaction calorimetry, a well known technology developed several decades ago, permits to overcome this disadvantage. This technique is based on the use of higher reactor volume, between 1-2 liters, that allows performing all the standard operations found in an industrial chemical process, i.e. heating, cooling, dosing, introduction of sensors. The establishment of a heat balance that includes all the heat contributions and their balance at each step of time allows isolating the heat contribution of the reaction. Subsequently, it is possible to calculate the profile of the monomer conversion (thermal conversion) from the heat generation rate of the reaction. It has to be highlighted that the reaction calorimetry technology was initially developed to offer to the chemist an engineering approach of the chemical reactions in order to develop safe processes and to analyze the effects of parameters such as the mixing and the heat transfer in a system with geometry close to the one of industrial reactor. The first application of this high potential and accurate technology for the monitoring of the dispersion polymerization of MMA in $scCO_2$ is exhaustively discussed throughout this work.

1.7 Outline of the thesis

This chapter has treated the very interesting properties of supercritical fluids and particularly the potential of carbon dioxide to replace common organic solvents. Although carbon dioxide gives the opportunity to improve polymer processing and to replace halogenated solvents, only few industrial applications at the moment use the supercritical fluid technology. In order to promote this technology at industrial scale, an important work is being made and has to be made to develop a better understanding of the fundamental aspects of SCF-polymer systems in terms of kinetics, phase behavior and mixture properties. Because most studies devoted to dispersion polymerizations in $scCO_2$ are performed in small reactor volumes providing little engineering information, this has led us to develop a 1.3 liters high pressure reaction calorimeter. This supercritical reaction calorimeter was designed for the on-line monitoring of the dispersion polymerization of MMA in $scCO_2$. This polymerization is realized using a poly(dimethylsiloxane) macromonomer as stabilizer. Market availability was a governing factor in the choice of the stabilizer, as very few commercially available stabilizers can be used with CO_2.

The calorimetric tool developed in this project allows analyzing the effects of the operating parameters, such as temperature, stirring, impeller type and stabilizer concentration, on the rate of polymerization and on the polymer properties. In the light of the experimental results obtained, an exhaustive theoretical study has been possible and permits to point out the fundamental aspects that govern the stability of the dispersion, the polymerization loci and hence the characteristics of the produced PMMA. A particular focus is made on the analysis of the molecular weight distribution, the particles morphology and their size distribution for polymer produced in each batch reaction. Having the scope to investigate the dispersion polymerization of MMA in $scCO_2$ at each level, a study of the phase behavior of the ternary system monomer-CO_2-stabilizer has been realized. This analysis allows the understanding of the fundamental parameters that need to be considered for the development of an effective and stable dispersion polymerization.

As highlighted previously, the work presented in this thesis is also devoted to the development of methods capable to monitor the monomer conversion during the course of the polymerization process. In order to reach this goal, the calorimetric information have been coupled to measurements of the speed of the sound. The ability of the ultrasonic sensor to follow the change in composition in the reacting medium and to give a precise estimate of the monomer conversion will be discussed.

In order to complete the study, a kinetic model, implemented in the software Predici®, has been developed. This model will help to understand the kinetic mechanisms occurring during the dispersion polymerization and their effect on the rate of polymerization and on the polymer molecular weight distribution.

2 Reaction calorimetry

Reaction calorimetry is a well known technology which has been used since several decades in process optimization and in process safety assessment. Hence, the potential of this technology is not only exploited in academical research for fundamental calorimetric analysis but also by the chemical industry for kinetic and thermodynamic studies. A key parameter in the study and control of chemical reactions is related to the conversion of the reactants into products. Conversion monitoring permits to control the reproducibility of the reaction conditions and to have direct information of the effect of operating variables on the course of the reactions. Because most chemical reactions are accompanied by release or consumption of heat, heat evolution is a fingerprint of the course of the reaction and therefore, a directly measurable characteristic of a chemical reaction. Consequently, with an adapted heat balance around the reactor, it is possible to obtain the profile of reactants conversion based on thermal analysis.

Because polymerization reactions are accompanied by strong exothermicity and auto acceleration kinetics, temperature changes can occur inside the reactor. Those temperature profiles have a considerable influence on the final mechanical and processing properties of polymers, as well as on the safety of operations.[119] Therefore, temperature control is crucial in the design of industrial reactors.[119] This leads to the necessity to identify the different sources of heat in a process and their magnitude in order to establish an equilibrated heat balance for process safety and control. For this purpose, different calorimetric techniques are available allowing the determination of thermodynamic parameters (enthalpy of reaction, heat capacity) as well as engineering parameters (heat transfer, stirring effect) under a wide range of operating conditions.

As a consequence of the previous remarks, it appears to be crucial to be able to develop apparatuses allowing process control and thermal analysis of supercritical fluid reactions in order to promote this technology at industrial scale. The originality of the presented work, which becomes integrated to this goal, is the adaptation of the heat flow reaction calorimetry to supercritical fluid applications, allowing in the precise case the kinetic study of the dispersion polymerization of methyl methacrylate in $scCO_2$. The development of the supercritical reaction calorimeter was carried out in close collaboration with Mettler-Toledo, the supplier of the RC1 model of calorimeters.

This chapter treats the different calorimetric techniques, their applications and characteristics in order to point out the advantages and the disadvantages of each method and to situate the reaction calorimetry field respect to the other methods. The particular features of heat

flow reaction calorimetry applied to the on-line monitoring of dispersion polymerizations in supercritical carbon dioxide are discussed.

2.1 Introduction to calorimetric methods

Calorimetry is a science by itself. There are a lot of different calorimeters available on the market. The choice of a type of calorimeter depends on two main parameters:[120]

- The specific case studied: necessity to have representative conditions of the industrial process, analysis of extreme conditions to study a thermal runaway or the thermal stability, measurement of fundamental data like heat capacity.
- The quantity of the sample needed to do the calorimetric measurement, parameter closely linked to the specific required analysis.

Table 2.1: Classification of most known calorimetric techniques taking into account the principle of measurement, the application and the characteristic size of the sample. [120]

Method	Measurement principles	Application domain	Sample size	Temperature domain	Typical Sensitivity [W/kg]
Differential scanning calorimetry (DSC)	Differential, ideal or isoperibolic flow	Screening, Decomposition, Reaction kinetics	1-50 mg	-50 - 500°C	2-10
Accelerating rate calorimeter (ARC)	Ideal accumulation	Decomposition	0.3-5 g	30-400 °C	0.5
Calvet calorimeter	Differential, ideal flow	Reactions kinetics, decomposition	0.5-3 g	30-300 °C	0.1
Dewar	Ideal accumulation	Reactions and thermal stability	100-1000 g	30-250 °C	-
Reaction calorimetry (RC)	Ideal flow	Reactions	300-2000 g	-40-250 °C	1

In the case of polymerization reactions, the two most used calorimeters are the differential scanning calorimeter (DSC) and the reaction calorimeter (RC). The particular advantages of using DSC are the small sample quantity needed, the ability to study highly exothermic reactions, the absence of stirring usually adopted in order to homogenize the reaction mass. Therefore, this technique is particularly adapted to study highly viscous systems, such as bulk polymerizations and reactions with solids. Serious objections are made as for the use of microcalorimetric results. Indeed, microcalorimeters generally operate under specific conditions, not representative of industrial processes (particularly regarding to stirring effects, heat transfer and operation modes). The use of reaction calorimetry can overcome those disadvantages of the

DSC method. As, shown in Table 2.1, the main advantages of operating with reaction calorimetry are related to the size of the rector itself, being between 1 and 2 liters. The system geometry permits the insertion of sensors into the reactor and the realization of standard industrial operations like stirring, dosing, cooling and heating, leading to a system representative of an industrial one. This powerful tool allows the chemist to set on an engineering oriented approach for the development of chemical processes.[121] Moreover, it must be emphasized that until now the majority of research groups have carried out polymerization reactions in $scCO_2$ in small reactor volumes around 2-60 ml, achieving excellent fundamental analysis but giving poor engineering information. Many authors have already reported the particular advantages of reaction calorimetry applied to polymerization reactions.[122-141]

The supercritical reaction calorimeter developed in this project gives us the opportunity to monitor on-line reactions in $scCO_2$ following the heat generation rate. Moreover, a sensor, measuring the speed of sound during the course of the dispersion polymerization of methyl methacrylate in $scCO_2$, has been coupled to the thermal information. With both techniques, it is possible to obtain a direct profile of monomer conversion without any perturbation of the system by sampling.

2.2 Reaction calorimetry

A reaction calorimeter (RC) consists of a stirred tank reactor with a surrounding jacket where circulating fluid promotes the heat transfer from and to the reactor. The following list gives the specific data that RC technology delivers and the corresponding applications in process design:[133]

- Thermodynamic data such as heat capacities, changes of enthalpy during phase transition, adsorption and chemical reactions.
- Instantaneous measurement of heat flow and heat transfer coefficient for reactor design.
- Determination of kinetic constants, overall reaction rate constants, overall activation energy allowing the selection of kinetic models for quantitative description of chemical processes and their optimization.
- Establishment of safety limits for batch, semi-batch and continuous chemical reactions.
- Development of advanced control strategies in order to optimize selectivity and capacity.

Reaction calorimeters can be classified according to their measurement and control principles into four categories:[142] heat flow reaction calorimeters, power compensation reaction calorimeters, heat balance reaction calorimeters and Peltier calorimeters.

Howdle *et al.* have published results of the development and application of power compensation calorimetry to the dispersion polymerization of MMA in $scCO_2$. Reactions were performed in a small autoclave of 60 ml. This technique allows the on-line monitoring of the dispersion polymerization but as noticed by the author, the technique cannot be qualified as a high precision and sensitive one.[117, 118]

In the particular case of polymerization reactions, the two main reaction calorimeters used are the heat flow calorimeters and the heat balance calorimeters:[126]

- In the heat flow calorimetry the calculation of the heat balance is based on the conductive heat flow through the reactor wall. The temperature of the reactor-content, T_r, is measured and controlled by varying the temperature of the coolant, T_j. In this system, in order to convert the temperature signal into a heat flow signal, an overall heat transfer coefficient, U, has to be determined.
- In heat balance calorimetry, the calculation of the heat balance is based on the convective heat flow through the jacket loop. The temperature of the reactor-content, T_r, is also controlled by varying the temperature of the coolant, T_j. Here, the heat flow rate from the reactor-content through the reactor wall into the cooling liquid is determined by measuring the difference between the jacket inlet, $T_{j,0}$, and outlet temperature, T_j, and the mass flow of the cooling liquid.

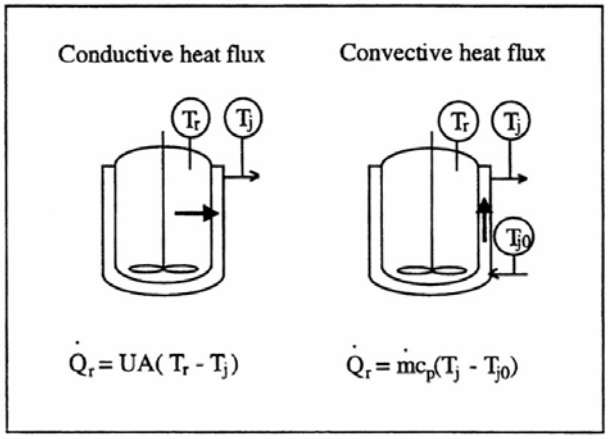

Figure 2.1: Schematic presentation of the operating principle of a heat flow calorimeter (conductive heat flow) and a heat balance calorimeter (convective heat flow).[126]

During polymerization reactions and particularly in bulk polymerizations, the viscosity of the reaction mass can increase drastically and fouling at the reactor wall can occur. These typical features of many polymerizations affect the heat transfer. Since in heat balance calorimetry the heat flow measured is independent of the changes in heat transfer properties during the reaction, this technique presents some advantages to study polymerization reactions. On the contrary, heat flow calorimetry requires the determination of the overall heat transfer coefficient, U, the latter being a function of the properties of the reaction mass, in order to evaluate a correct heat balance. In heat flow calorimetry, because of the high flow rate of the coolant inside the jacket, the difference in jacket temperature between the inlet and the outlet can be neglected. In heat balance calorimetry, the inlet and outlet jacket temperatures need to be known, leading the use of reasonably small flow rate through the jacket in order to obtain a measurable difference T_j-$T_{j,0}$. This feature is in contradiction with the fact that to obtain fast reactor temperature control the flow rate through the jacket should be high. Therefore, the advantage of heat flow calorimeters is a better reactor dynamic, keeping in mind that additional parameters evaluation are required (U). Most of the heat flow calorimeters commercially available nowadays are based on the pioneer work of Regeneass.[143-149]

Table 2.2: Advantages and disadvantages of the adiabatic, isoperibolic and isothermal mode.[133]

Calorimetric method	Heat balance	Advantages	Disadvantages
Adiabatic	Heat exchange = 0	Change in temperature is proportional to conversion Monitoring of fast reactions	Change in temperature affects reaction Temperature and concentration effects on reaction kinetics can only be separated by mathematical modeling Dangerous with strongly exothermic reactions Not possible for endothermic reactions
Isoperibolic	T_{jacket} =constant	Very simple practical system	Reactions kinetics are influenced by temperature changes and mathematical modeling is needed for their determination
Isothermal	T_r = constant	Reaction rate is proportional to heat flow Reaction conditions and operation mode correspond with pilot and large scale reactors Heat transfer coefficients are detectable	Reaction temperature must be measured with high resolution Heat transfer coefficients must be determined by calibration The calorimetric system is complex

Once the type of reaction calorimeter is chosen, the second step is to define the pertinent operation mode (i.e. adiabatic, isoperibolic and isothermal see Table 2.2), which depends on the scopes of the analysis itself and the studied reaction. As the main goals of the presented project are to analyze the kinetic of dispersion polymerizations in $scCO_2$ using heat flow measurements and to determine the effect of the operating conditions on the reaction rate and on the molecular properties of the produced polymers, the isothermal mode is the most effective method.[142]

2.2.1 Heat balance for supercritical heat flow reaction calorimetry

The development of an adapted heat balance taking into account the heat transfer through the reactor wall requires particular attention when working with supercritical fluids.[26, 150-152] The main reason is that the supercritical phase occupies all the available volume like a gas phase would do. This means that all the reactor elements are in direct contact with the reaction mass (cover and flange see Figure 2.2) and have to be thermally perfectly controlled. Therefore, the heat transfer is not limited to the transfer of heat between the reaction mass and the jacket as it is the case of reaction occurring in a liquid. In fact, in classical systems the gas phase in equilibrium with the liquid phase is neglected in the heat balance because of its negligible mass and poor heat transfer. Precautions can be used to avoid heat losses in closing the reactor but the gas phase is rarely introduced in standard reaction kinetic studies.

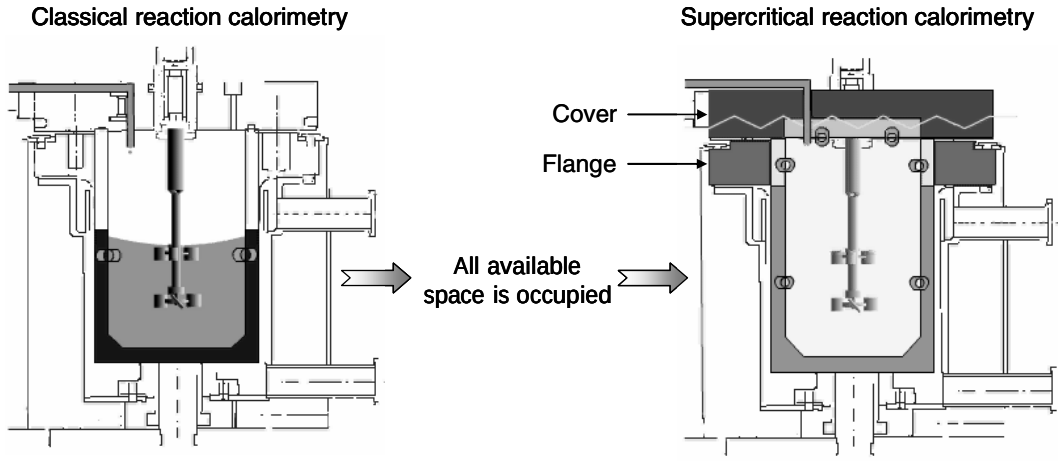

Figure 2.2 : Schematic comparison between classical and supercritical reaction calorimetry.[23]

The most fundamental assumptions behind all the equations presented in this section are that the reactor, T_r, and the jacket, T_j, temperatures are homogeneous, meaning that the reaction system is perfectly mixed. The reactor temperature homogeneity will depend on the mixing efficiency. The jacket temperature homogeneity is guaranteed by the high flow rate of the coolant.

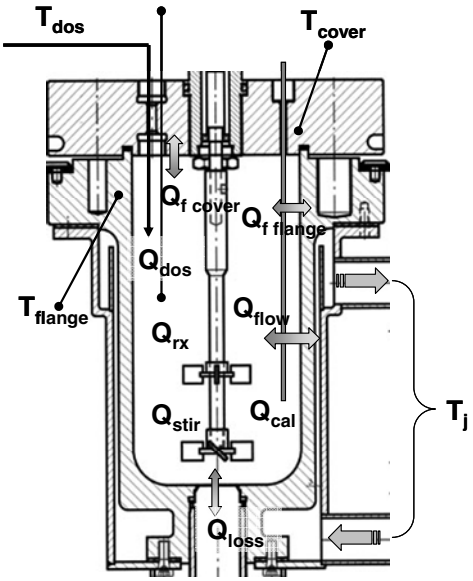

Figure 2.3: Representation of the different terms included in the heat balance established mainly on temperature measurements.[23]

The general heat balance for a semi-batch process is given in the following equation where the terms are expressed as heat release or thermal power:

$$Q_{acc} = Q_{rx} + Q_{dos} + Q_{cal} + Q_{stir} - (Q_{flow} + Q_{f\,cover} + Q_{f\,flange} + Q_{loss}) \qquad 2.1$$

where Q_{acc} is the accumulation term; Q_{rx} is the heat production rate of the reaction; Q_{dos} is the amount of heat due to the addition of reactants; Q_{cal} is the heat delivered by the calibration probe; Q_{stir} corresponds to the mechanical energy of the stirrer which is converted into viscous friction and finally into thermal energy; Q_{flow} is the heat exchange across the reactor wall by forced convection; $Q_{f\,cover}$ is the heat exchange occurring between the reactor content and the cover; $Q_{f\,flange}$ is the heat exchange between the reactor content and the flange; Q_{loss} is the heat losses to the surroundings due to radiation and/or natural convection.

$$Q_{acc} = \left(m_r \cdot c_{vr} + \sum m_i \cdot c_{pi}\right) \cdot \frac{dT_r}{dt} \qquad 2.2$$

Because SCFs occupy all the available volume, the reactor has to be considered as an isochoric system. Therefore, for the reaction mass the isochoric heat capacity, c_{vr}, should be used in the accumulation term. In the case of an isochoric system, an increase in temperature will result in an increase in pressure, explaining why the isobaric heat capacity, c_p, should not be used for the reaction mass. For an open liquid system, a change in temperature will result in a liquid volume expansion (thermal expansion) and the overall pressure will stay constant at

ambient pressure. The second term in the parenthesis represents the isobaric heat capacity of all the inserts (sensor, stirrer…) into the reactor and in contact with the reacting system. For those metallic inserts, the temperature and pressure dependencies can be neglected and therefore it is possible to use isobaric heat capacity invariant with P and T. In equation 2.2, one should remark that surprisingly the heat capacity of the reactor is not included in the expression. In fact, the heat capacity of the reactor in equation 2.1 is taken into account implicitly in the evaluation of the heat flow term Q_{flow} (see equation 2.7). In the heat flow evaluation, a so-called apparent jacket temperature, T_a, is calculated from the real jacket temperature, T_j. This correction takes into account that part of the heat flow through the reactor wall is used to heat or cool the reactor wall and thus is not transferred from the wall to the reactor content. The conversion of the physical value T_j into a theoretical value T_a is based on a model copyrighted by Mettler-Toledo. Because the dispersion polymerizations are run in isothermal mode, i.e. with no significant variation of T_r, the term Q_{acc} is small and even negligible.

As highlighted in Table 2.2, one advantage of working in isothermal mode is that the heat release by the reaction, Q_{rx}, is directly proportional to the measured heat flow which is in turn directly proportional to the reaction rate considering the relationship given in equation 2.3:

$$Q_{rx} = R_p \cdot \left(-\Delta_{rx}H\right) \cdot V_r \qquad 2.3$$

where R_p is the global rate of polymerisation; $\Delta_{rx}H$ is the heat of polymerization of the monomer; V_r is the total volume of the reactor for a supercritical reaction.

It must be noted that when several parallel reactions occur, like in polymerization reactions, the heat signal represents the sum of all the heat contributions. Therefore, the heat effects cannot be separated and distinguished.

The reaction enthalpy can be determined by integrating the peak of the heat generation rate, Q_{rx}:

$$\Delta_{rx}H = \frac{\int_{t0}^{tf} \left(Q_{rx} - Q_{base}\right) \cdot dt}{m_{r0} \cdot X} \qquad 2.4$$

where Q_{base} is the baseline; m_{r0} is the initial amount of monomer; X is the monomer conversion at time t_f.

A major quantity calculated during this study is the thermal conversion, X_{th}:

$$X_{th}(t) = \frac{\int_{t0}^{t} (Q_{rx} - Q_{base}) \cdot dt}{\int_{t0}^{tf} (Q_{rx} - Q_{base}) \cdot dt} \qquad 2.5$$

The conversion at time t is calculated from the integral of the heat generation rate, Q_{rx}, and normalized to 100%. The numerator of equation 2.5 represents the integration of the heat from the initial time, t_0, to time t. The denominator represents the integration of Q_{rx} over the entire reaction time.

If a feed stream to a reactor is at a different temperature, T_{dos}, from the reactor content temperature, T_r, there is an amount of convective heat transport to the reactor. The first right term in equation 2.6 represents the feed rate, $\dot{m}$, of the dosed reactants:

$$Q_{dos} = \frac{dm_{dos}}{dt} \cdot c_{p,dos} \cdot (T_{dos} - T_r) \qquad 2.6$$

When the temperature difference between reactor and feed is small and/or when the feed rate is small this term can be neglected.

Q_{cal} in equation 2.1 is the amount of heat delivered by a calibration probe, measured on-line and delivering a known amount of heat of approximately 25 W. This calibration probe is used to measure the overall heat transfer coefficient, U, a necessary parameter to evaluate the heat exchange between the reaction mass and the jacket coolant:

$$Q_{flow} = UA \cdot (T_r - T_a) \qquad 2.7$$

where A is the heat exchange area corresponding to the maximum geometric surface of the jacket in the case of SCF applications; T_a is the modified jacket temperature.

As highlighted previously, the measurement of the overall heat transfer coefficient is crucial for obtaining an accurate heat balance in heat flow calorimetry. The following paragraphs are dedicated to its evaluation method.

The calibration procedure lasts 1 hour, during which the internal temperature, T_r, is kept constant (i.e. isothermal mode) and the following equation applies:

$$Q_{acc} = Q_{cal} + Q_{stir} - (Q_{flow} + Q_{f\,cover} + Q_{f\,flange} + Q_{loss}) \qquad 2.8$$

In fact during a calibration procedure, the calorimeter cannot really keep constant the reactor temperature and small variations in T_r are observed. Experimentally, since the heat input is symmetrical, this leads to symmetrical accumulation curves, dT_r / dt:

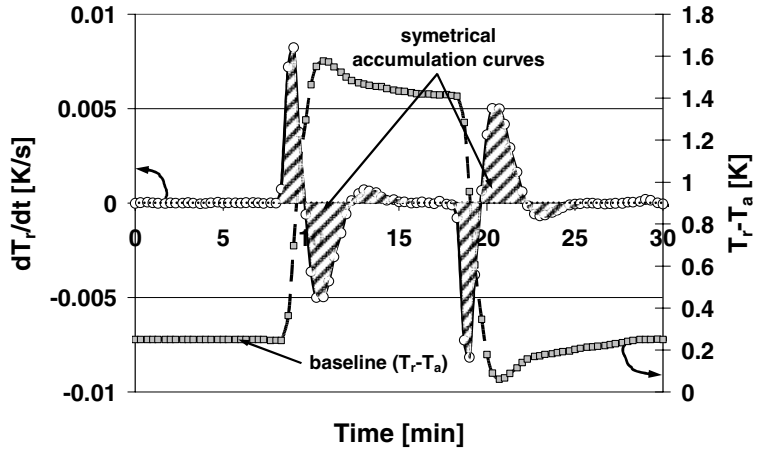

Figure 2.4: Typical shape of the reactor accumulation and the corresponding baseline during a calibration procedure.[23]

Because the accumulation is symmetrical over the experiment (Figure 2.4), this term can be set to zero allowing the evaluation of UA using the simplified equation 2.11.

Equations 2.1 and 2.8 and Figure 2.3 show that, in the case of supercritical reaction calorimetry, not only the heat flow through the reactor wall has to be considered, but all the heat transfers that occur between the reaction mass and an element at a different temperature:

$$Q_{f\,cover/\,f\,flange} = U_{cover/\,flange} \cdot A_{cover/\,flange} \cdot \left(T_r - T_{cover/\,flange}\right) \qquad 2.9$$

where $U_{cover/\,flange}$ is the heat transfer coefficient between the reaction mass and the cover or flange; $A_{cover/\,flange}$ is the heat exchange surface of the cover or the flange in contact with the reaction mass.

In the case of the developed reaction calorimeter, the cover and the flange temperatures are set to the reactor temperature, i.e. identical temperature for all those elements. Therefore, their contribution can be neglected when solving equation 2.8.

In order to solve equations 2.8 and 2.1, the last terms that need to be evaluated are the heat input by stirring, Q_{stir}, and the heat losses to the surroundings, Q_{loss}. Because these terms are not directly measurable, a way to take them into account is to define an appropriate baseline, Q_{base}, avoiding the necessity to know their absolute value:

$$Q_{base} = Q_{stir} - Q_{loss} = UA \cdot (T_r - T_a)\big|_{base} \qquad 2.10$$

The evaluation of the baseline, which depends on the precision of the evaluation of the overall heat transfer coefficient, is crucial because it determines the accuracy of the calculation of the heat generation rate and thus of the thermal conversion, the key property used in this study.

Combining equations 2.7, 2.8 and 2.10, the overall heat transfer coefficient is determined through the parameter, UA, calculated by the following equation:

$$UA = \frac{\int_{t1}^{t2} (Q_{cal} - Q_{base}) \cdot dt}{\int_{t1}^{t2} (T_r - T_a) \cdot dt} \qquad 2.11$$

where A is the maximal geometric inner surface of the jacket.

The equipment used in this study gives only the possibility to evaluate the overall heat transfer coefficient at the beginning and at the end of a reaction. The limitation is related to the fact that only one equation is available for the heat balance evaluation. Therefore, it is mathematically impossible to find a particular solution for two unknowns (infinite solutions), namely UA and Q_{rx}. For that reason, the absolute value of the baseline using equation 2.10 is only known for the initial and final state of the system.

The first question is: Is this evaluation sufficient or not? The answer is yes if the baseline is constant throughout the reaction, i.e. independent of the medium properties. On the contrary, the answer is no, if the baseline is dependent on the medium properties that could change during the course of the reaction.

This leads to the second question: Do the change of the properties of the reacting medium influence the value of the overall heat transfer coefficient U and hence of the baseline?

The heat transfer coefficient, U, is related the physico-chemical properties of the reacting medium by the following equations:

$$\frac{1}{U} = \frac{1}{h_r} + \frac{e}{\lambda_w} + \frac{1}{h_e} \qquad 2.12$$

$$Nu = \frac{h_r \cdot d_r}{\lambda} = C \cdot \mathrm{Re}^{2/3} \cdot Nu^{1/3} = C \cdot \left(\frac{n \cdot d_s^2 \cdot \rho}{\eta} \right)^{2/3} \cdot \left(\frac{c_p \cdot \eta}{\lambda} \right)^{1/3} \qquad 2.13$$

In equation 2.12, the overall heat transfer coefficient is expressed as the sum of three heat transfer resistances in series. $1/h_r$ is the internal film resistance and depends on the physico-chemical properties of the reacting medium as shown by the Nusselt number (Nu) relationship (equation 2.13). e/λ_w is the reactor wall heat transfer resistance, which depends on the thickness, e, and on the thermal conductivity of the reactor wall, λ_w, $1/h_e$ is the external heat transfer resistance and depends on the physico-chemical properties of the coolant circulating inside the jacket.

Equation 2.13 gives the answer to the previous question and allows understanding the dependency of the overall heat transfer coefficient on the properties of the mixture, such as the density (ρ), the heat capacity (c_p) and the viscosity (η). Therefore, it is expected that the value of the baseline can vary during the course of a reaction, for which the measurement of U could account for.

The third question is: Is it expected that the heat contributions (Q_{stir} and Q_{loss}), to which the baseline account for, are influenced by the change of the properties of the reacting medium?

On one hand, for the heat losses to the surroundings, the answer is no. Moreover, this term can be considered as constant throughout the reaction, because the temperature difference between the jacket and the environment is expected to be almost constant. On the other hand, the answer is yes for the heat input into the reacting medium due to mechanical stirring:

$$Q_{stir} = Ne \cdot \rho_M \cdot n^3 \cdot d_S^5 \qquad 2.14$$

where Ne is the Newton number, ρ the density of the mixture, n the stirring speed or revolution frequency of the agitator and d_S the diameter of the agitator.

The equation 2.14 shows that the heat input by the stirrer is a function of the density of the medium and of the so-called Newton number (Ne), which in turn is a function of the medium viscosity. In fact, the evaluation of the Newton number can be made using the so-called Newton plots where Ne is plotted as a function of the Reynolds number:

$$\mathrm{Re} = \frac{\rho \cdot n \cdot d_S{}^2}{\eta} \qquad 2.15$$

where η is the dynamic viscosity of the mixture.

Newton plots have been established for a variety of different types of stirrers operating with newtonian fluids.[153, 154] The main idea behind these considerations is to point out that the higher the viscosity of the medium, the lower the Reynolds number and the higher the Newton number, keeping in mind that the real relationship is more complex.

Finally, it is therefore possible to understand that a significant change in density and in viscosity of the medium during the course of the reaction influences the magnitude of the heat input by the stirrer. In turn, this means that the value of the baseline is not constant and can significantly change during the course of reaction. This can be the case for polymerization reactions because the viscosity can change significantly throughout the process, depending on the type of polymerization and on the polymer concentration.

In result, if it would be possible to evaluate U during the course of the reaction, it would be in turn possible to take into account the changes of the heat contributions included in the baseline. Because the used procedure is limited to an evaluation in absence of reaction, one has to find a mean to approximate the shape (value) of the baseline during the interval of time when the reaction occurs. For the calculation of Q_{rx} (solving equation 2.1) realized by the use of the software WinRc®, it is possible to choose a baseline proportional to the thermal conversion allowing taking into account the non-linear changes in the heat transfer coefficient and hence of the baseline. This means that the software calculates by the mean of iteration a baseline from the shape of the thermal conversion defined by the equation 2.5.

The chapter 4 treats the thermal analysis of the dispersion polymerization of MMA in $scCO_2$ using practical examples in order to explain exhaustively the procedure, clarify the evaluation of the baseline and expose the arguments that have motivated the choice of this methodology.

3 Modeling dispersion polymerization of MMA in $scCO_2$

This chapter deals with the kinetics modelling of the dispersion polymerization of MMA in $scCO_2$. The model is implemented in the software PREDICI®. PREDICI (Polyreaction Distributions by Countable System Integration) is a simulation package for the treatment of kinetic equations for polyreactions. Basically, it allows the computation of chain length distribution of macromolecules generated in polymerization processes, combined with the simulation of additional reaction components and reactor variables.

3.1 Theoretical considerations of existing models

Two comprehensive mathematical models for quantitative prediction of the time evolution of monomer conversion and molecular weight distribution have been published by Kiparissides and his coworkers[155](first author Chatzidoukas) and by Morbidelli and his coworkers[156, 157](first author Müller), dealing with the dispersion polymerization of MMA in $scCO_2$.

The similarities of these models are the following:

- Two reaction loci are considered: the polymer-rich dispersed phase and the CO_2-rich continuous phase. All the elementary reactions (i.e initiation, propagation, chain transfer and termination), characteristic of radical polymerization, can occur in both phases.
- At high monomer conversion, it is well known that almost all reactions can become diffusion-controlled. Specifically, the initiation, the propagation and the termination are related to the phenomena of cage, gel and glass effect, respectively. Diffusion-controlled phenomena are considered when describing the propagation and the termination in the polymer-rich phase. Elementary reactions occurring in the continuous CO_2 –rich phase are not considered to be diffusion-limited.
- Monomer, initiator and solvent are assumed to undergo very fast transport between the phases and to be at equilibrium concentrations. Those equilibrium concentrations are calculated using the Sanchez-Lacombe equation of state:[158]

$$\tilde{P} = \tilde{T} \cdot \left[\left(\frac{1}{r} - 1 \right) \cdot \tilde{\rho} - \ln\left(1 - \tilde{\rho}\right) \right] - \tilde{\rho}^2 \qquad 3.1$$

where $\tilde{P}$, $\tilde{T}$, $\tilde{\rho}$ are the reduced pressure, temperature and density of a pure substance, respectively. r is the number of sites (mers) occupied by a molecule in the lattice and is proportional to the molecular weight of the pure component.
The Sanchez-Lacombe equation of state (EOS) allows describing the PVT behavior and the phase partitioning of a multicomponent system at equilibrium conditions (equality of the chemical potential).The difficulty in calculating the equilibrium concentrations is to determine the numerical values of the pertinent parameters appearing in the EOS.

- The mechanism of nucleation process is not included. This means that the authors consider a number of particles constant throughout the process and present in the system from the beginning.

The differences between both models are the following:

- Chatzidoukas *et al.* consider that up to a conversion, X_c, the polymerization occurs only in the continuous phase and for conversion higher than X_c polymerization continues only in the polymer-rich phase.[155]

- Chatzidoukas *et al.* consider also that the polymer undergoes fast transport between phases and is at interphase equilibrium, with concentrations evaluated using the Sanchez-Lacombe EOS.[155]

- Müller *et al.* introduce in their evaluation of the population balance equations, which describes the concentration of active and dead chains as a function of time in each phase, a parameter related to the rate of mass transport of these species between phases.[156, 157] Thus, the polymer species are not considered to be at interphase equilibrium. Their concentrations depend on the rate at which they are transferred from one phase to another. The overall mass transport is determined for each chain length. Therefore, the concentrations of high molecular weight species in both phases depend strongly on their chain length.

- Müller *et al.* consider a diffusion-controlled initiator efficiency in the polymer-rich phase.[156, 157]

3.2 Assumptions

In order to understand the developed model for the dispersion polymerizations of MMA in $scCO_2$, it is necessary to point out the assumptions on which the model is based.

1. The system is composed by two phases: a polymer-rich phase (or dispersed phase) and a CO_2-rich continuous phase which does not contain any dead chains.
2. Initiation occurs only in the continuous phase and is not diffusion-limited.
3. Propagation occurs only in the polymer-rich phase. Initiator radicals diffuse in the polymer-rich phase, where propagation is considered to be diffusion-limited.
4. Termination occurs only in the polymer-rich phase and is considered to be diffusion-limited.
5. Monomer undergoes transport between the continuous and the dispersed phase until the equilibrium concentrations are reached.
6. CO_2 is considered to be at a constant concentration in the continuous phase and in the dispersed phase.
7. Particles formation is not accounted for. As a consequence, the effect of stabilizer is not considered both in terms of contribution to particle formation and stabilization.
8. The dispersed phase or polymer-rich phase is considered to be a whole unique phase, i.e. no population balance equation needs to be used.

Beside this model, a simple model for solution polymerization in supercritical carbon dioxide has been developed, in which the initiation, the propagation and the termination rate constant are evaluated for the CO_2 phase. The comparison of the molecular weight distribution and the rate of polymerization predicted for both models will help to understand the experimental results.

Rindfleisch *et al*. have demonstrated that high molecular weight PMMA does not dissolve in pure CO_2 at temperature less than 250°C and pressures below 2500 bar.[159] Lora *et al.* have shown that a coslovent effect of MMA can favor the solubility of PMMA in $scCO_2$, but the operating pressure used in the experiments discussed here ($\leq$ 310 bar) are much below than the required 930 bar to solubilize 5 wt% polymer at 65°C in the presence of 30 wt% monomer.[56] On the other hand, Fehrenbacher *et al.* have reported, in their study of the early stage of dispersion polymerization of MMA in $scCO_2$, that the polymerization proceeds via homogeneous nucleation of particles of polymer which is generated in the continuous phase and precipitates if the

molecular weight exceeds a given value.[95] This means that PMMA oligomers are soluble in carbon dioxide until a certain extent. Johnston *et al.* have reported that PMMA oligomers of 30 monomer units are insoluble in CO_2 at a pressure of 200 bar and a temperature of 35°C.[160] Moreover, Müller *et al.* have shown using their predictive model that in the case of the dispersion polymerization of MMA in $scCO_2$ it can be considered that the macroradicals generated in the continuous phase enter the polymer particles before terminating, and therefore the polymer-rich phase can be considered to be the main reaction locus in this case.[156] It is assumed that these remarks can be neglected, allowing the approximation that the production of polymer in the continuous phase can be neglected.

3.3 Kinetic model

According to the previous assumptions, the kinetic scheme includes the following kinetic steps, typical for the free-radical polymerization of a vinyl monomer.

Initiation:	$I_1 \xrightarrow{k_{d1}} 2I_1^{\bullet}$
	$I_2^{\bullet} + M_2 \xrightarrow{k_{Ij}} R_{1,2}$
Propagation:	$R_{x,2} + M_2 \xrightarrow{k_{p2}} R_{x+1,2}$
Chain transfer to monomer:	$R_{x,2} + M_2 \xrightarrow{k_{fm2}} P_{x,2} + R_{1,2}$
Termination	
by disproportionation:	$R_{x,2} + R_{y,2} \xrightarrow{k_{td2}} P_{x,2} + P_{y,2}$
by combination:	$R_{x,2} + R_{y,2} \xrightarrow{k_{tc2}} P_{x+y,2}$

When two subscripts are given, the first one (denoted x or y) indicates the chain length and the second one the phase (j=1 for the continuous CO_2-rich phase and j=2 for the dispersed polymer-rich phase). R represents the active chains and P the dead chains.

3.3.1 Initiator decomposition rate constant in $scCO_2$

The rate constant of initiator decomposition is estimated using the data of Guan *et al.* in supercritical carbon dioxide: [161]

$$k_{d1} = 4.19 \cdot 10^{15}[1/s] \cdot \exp\left(\frac{\text{-134.6[kJ/mol]}}{RT}\right) \qquad 3.2$$

Guan *et al*. have reported that the decomposition rate of AIBN in $scCO_2$ is approximately 2.5 times lower than that measured in benzene.[161] They attribute this difference to the lower dielectric constant of CO_2 relative to benzene. They have shown that the initiator efficiency of AIBN in $scCO_2$ ($f = 0.83 \pm 0.02$), used in the model, was 1.5 higher than that observed in benzene. Moreover, no significant pressure effect was observed.

According to equation 3.2:

k_{d1} at $65°C = 6.75 \cdot 10^{-6}\,[1/s]$ $\qquad$ k_{d1} at $80°C = 5.16 \cdot 10^{-5}\,[1/s]$

3.3.2 Propagation rate constant in polymer-rich phase

The propagation rate constant in the dispersed polymer-rich phase at zero conversion ($k_{p2,0}$) is estimated using the Arrhenius law established by Mahabadi *et al.*:[162]

$$k_{p2,0}(P_0) = 4.92 \cdot 10^5 [\text{l/mol/s}] \cdot \exp\left(\frac{\text{-18.2 [kJ/mol]}}{RT}\right) \qquad 3.3$$

The pressure dependence of the propagation rate constant can be considered according to the relation found by Beuermann *et al.*:[163]

$$k_{p2,0}(P) = k_{p2,0}(P_0) \cdot \exp\left(\frac{16.7 \cdot 10^{-6} [\text{m}^3/\text{mol}] \cdot (P - P_0)[\text{Pa}]}{RT}\right) \qquad 3.4$$

where P_0 is equal to 0.1 MPa.[162]

Maxwell and Russel have published an exhaustive theoretical development of diffusion-controlled polymerization kinetics.[164] A similar approach can be found in the model developed by Chatzidoukas *et al.*[155] and Müller *et al.*[156, 157].

The fundamental equation used to treat diffusion-limited reactions is based on the resolution of the second Fick's law, which deals with the diffusion of a chemical specie from an area of high concentration to an area of lower concentration:

$$\frac{\partial C(x,t)}{\partial t} = D \frac{\partial^2 C(x,t)}{\partial x^2} \qquad 3.5$$

where D is the diffusion constant of the material that is diffusing in a specific solvent and $\partial C(x,t)/\partial x$ is the gradient concentration.

The Smoluchowski equation is a solution of the second Fick's law:

$$k = 4\pi Dr \qquad 3.6$$

where k is the rate coefficient obtained for the diffusion-limited reactions between two species with mutual diffusion coefficient, D, that need to come within distance r of each other in order for reaction to take place.

The rate coefficient for diffusion-controlled propagation (so-called residual propagation), $k_{p,d}$, can be estimated based on the Smoluchowski expression:[164]

$$k_{p,d} = 4\pi D_{MP} r_{MP} N_A \qquad 3.7$$

The Avogadro's number, N_A, is introduced in equation 3.7 to consider the diffusion limited propagation not only for two reacting species but for one mole of components.

The overall propagation rate coefficient can be obtained considering that the time taken for propagation to occur is approximately the sum of times taken for the encounter, $1/k_{p,d}$, and for the chemical reaction, $1/k_{p,c}$:[164]

$$\frac{1}{k_p} = \frac{1}{k_{p,d}} + \frac{1}{k_{p,c}} \qquad 3.8$$

Considering the previous equations, the diffusion-controlled rate constant of propagation in the dispersed phase, k_{p2}, can be evaluated using the following relationship:

$$k_{p2} = \left(\frac{1}{k_{p2,0}} + \frac{1}{4\pi r_{MP} D_{MP} N_A} \right)^{-1} \qquad 3.9$$

where $k_{p2,0}$ is the value of k_{p2} at zero conversion, D_{MP} is the mutual diffusion coefficient of a polymer chain end and a monomer molecule and r_{MP} the radius of interaction for propagation:

The mutual diffusion coefficient is given by:[164]

$$D_{MP} = D_M + D_P \qquad 3.10$$

where D_M is the diffusion coefficient of the monomer through the polymer/monomer network and D_P the diffusion of the free radical end of a polymeric radical.

It is necessary to point out that the diffusion of the free radical end of a macroradical, D_P, is composed of two contributions, being the center of mass diffusion of the chain as a whole, which is expected to be chain length dependent, and by the so-called reaction diffusion of the chain end itself as a result of the propagation reaction. Generally, in glassy or near glassy conditions, the former of these contributions is negligible in comparison to the latter. Moreover, under diffusion controlled propagation, it can be considered that the diffusion of the monomer is much faster than the diffusion by propagation of the polymer chain end, i.e. $D_M \gg D_P$.[164] The radius of interaction, r_{MP}, can be estimated to be of the size of a monomer molecule, which in turn can be estimated by the Lennard-Jones diameter, σ_M.[164] Taking into account the previous remarks, equation 3.9 is reduced to the expression used in this work:

$$k_{p2} = \left(\frac{1}{k_{p2,0}} + \frac{1}{4\pi\sigma_M D_M N_A} \right)^{-1} \qquad 3.11$$

where the value σ_M for MMA equals to 5.85 $\mathring{A}$.[165]

The monomer diffusion coefficient is calculated from the free volume theory of Vrentas and Duda[166-173] that allows predicting self-diffusion coefficients in ternary systems[174], i.e. *M*onomer / *S*olvent / *P*olymer :

$$D_M = D_0 \cdot \exp\left(-\frac{E}{RT} \right) \cdot \exp\left(-\frac{\gamma\left(\omega_M V_M^* + \omega_S \xi_{MS} V_S^* + \omega_P \xi_{MP} V_P^* \right)}{V_{FH}} \right) \qquad 3.12$$

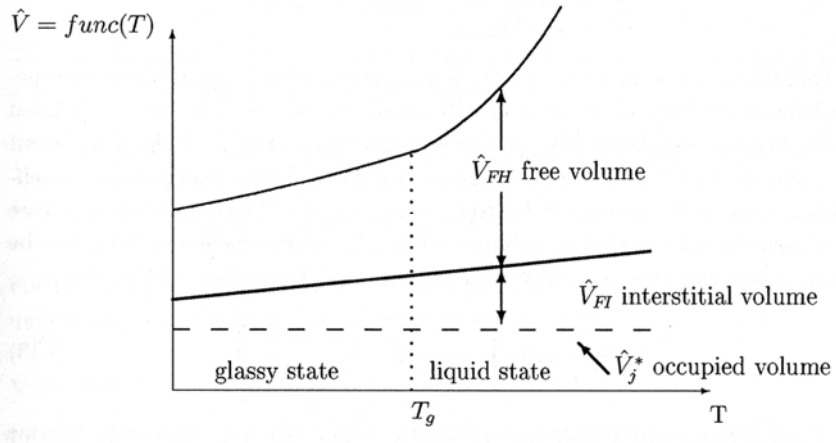

Figure 3.1: Free volume as a function of temperature.[173]

The theory developed by Vrentas, Duda *et al.* [166-173] is the most effective transport theory for concentrated polymer solutions that describes the diffusion of polymer in solvents above and below the glass transition temperature T_g. The theory is based on the idea that all transport processes are governed by the availability of the free volume within a system allowing the molecules to move in the space. As two molecules come to close proximity to one another, their electron clouds overlap and repulsive forces are no longer negligible. As a consequence, not all the free volumes within a system are equally accessible for molecular transport. This means that the total free volume within a mixture is composed by a distribution of attainable free-volume sites throughout the fluid. To account for this distribution, the total volume is divided into different components as shown in Figure 3.1:

- $\hat{V}_{FH}$ or V_{FH} in equation 3.12 corresponds to the available free volume for molecular transport.

- $\hat{V}_j^* + \hat{V}_{FI}$ corresponds to the unavailable volume, which is divided into two contributions. $\hat{V}_j^*$ (or V_j^* in equation 3.12) represents the close packed volume of a component j, defined as the volume occupied at 0 K. The second contribution, $\hat{V}_{FI}$, the so-called interstitial volume is considered to be uniformly distributed among the molecules since the energy for its redistribution is large.

The available volume is referred to as a hole free volume $\hat{V}_{FH}$ reflecting that it is associated with the discontinuous distribution of holes in the liquid or mixture and that no energy changes are required for redistribution of this volume. According to this derivation, the molecules diffuse in space by successive discrete jumps from one hole to another. The requirements for a molecule to take a diffusive step are (1) a vacancy of sufficient size is adjacent to the molecule and (2) the molecule possesses enough energy to break nearest neighbor contacts. Assuming that the vacancy and energy availability can be represented by Boltzmann probability functions,[175] the expression for the self-diffusion coefficient is given by equation 3.12.

In equation 3.12, D_0 represents a pre-exponential factor, $1.61 \cdot 10^{-3}[\mathrm{cm}^3/\mathrm{s}]$.[176] E represents the effective energy per mole that a molecule needs to overcome attractive forces that hold it to its neighbors, $3.26 \cdot 10^3[\mathrm{J/mol}]$.[176] γ is an overlap factor accounting for the fact that the same free volume is available to more than one molecule. ω_i is the weight fraction of component i; $\omega_M = 0.05$, $\omega_S = 0.15$, $\omega_P = 0.80$ [155]. In the calculation of the monomer diffusion in the polymer phase, the composition of the latter is considered to be constant throughout the polymerization ($\omega_i = \text{constant}$). This assumption is based on the fact that the polymer-rich phase

represents physically the polymer-rich particles dispersed in the continuous CO_2 phase. These particles are mainly composed of polymer, up to 80wt%.[155] V_i^* is the specific hole free volume of component i required for a diffusion jump; $V_M^* = 0.870[\mathrm{cm}^3/\mathrm{g}]$[176], $V_S^* = 0.589[\mathrm{cm}^3/\mathrm{g}]$[69, 177], $V_P^* = 0.757[\mathrm{cm}^3/\mathrm{g}]$[176]. ξ_{ij} is the ratio of the critical molar volume of the jumping unit of component i to the critical molar volume jumping unit of component j; $\xi_{MS} = 0.18$[178], $\xi_{MP} = 0.60$[176].

V_{FH} is the average hole free volume per gram of mixture and can be estimated from those of the individual species with the assumption of volume additivity at any concentration and temperature:

$$V_{FH} = \omega_M V_{FH,M} + \omega_S V_{FH,S} + \omega_P V_{FH,P} \qquad 3.13$$

Vrentas and Duda in their original work have given the following expression for the hole free volume of component i:

$$\frac{V_{FH,i}}{\gamma} = \frac{K_{1i}}{\gamma} \cdot \left(K_{2i} + T - T_{g,i} \right) \qquad 3.14$$

where K_{1i} and K_{2i} are the so-called free volume parameters, T_{gi} the glass transition temperature of component i. The values used to evaluate equation 3.14 for the monomer and the polymer are the following:[176]

$K_{1M} / \gamma = 8.15 \cdot 10^{-4}\,[\mathrm{cm}^3/\mathrm{g/K}]$ $\quad K_{2M} = 143\,[\mathrm{K}]$ $\quad \mathrm{T_{g,M}} = 143\,[\mathrm{K}]$

$K_{1P} / \gamma = 4.77 \cdot 10^{-4}\,[\mathrm{cm}^3/\mathrm{g/K}]$ $\quad K_{2P} = 54.4[\mathrm{K}]$ $\quad \mathrm{T_{g,P}} = 392\,[\mathrm{K}]$

The hole free volume of the polymer, $V_{FH,P}$, is calculated using a modified expression of equation 3.14 as introduced by Faldi *et al.*[176] and used by Müller *et al.*[157]:

$$\frac{V_{FH,P}}{\gamma} = \frac{K_{1P}}{\gamma} \cdot \left(K_{2P} + \widetilde{\alpha_P}(T - T_{g,P}) \right) \qquad 3.15$$

where $\widetilde{a_P}$ is the ratio of the coefficients of thermal expansion below and above $T_{g,P}$; $\widetilde{a_P} = 0.44$.[176]

Faldi *et al.* have introduced this parameter in order to avoid negative values of the hole free volume of the polymer.[176] Since the hole free volume parameters, K_{1P} / γ and K_{2P}, are typically obtained from measurement carried out above the glass transition temperature of the

polymer, extrapolation to lower temperatures can lead to negative values of polymer free volume, $V_{FH,P}$.

The hole free volume of the solvent, i.e. carbon dioxide, is estimated by:[177]

$$V_{FH,S} = V_{FH,S}^{ref} + \alpha_S (T - T^{ref}) \qquad 3.16$$

where $V_{FH,S}^{ref} = 0.231[\mathrm{cm}^3/\mathrm{g}]$ is the hole free volume at the reference temperature $T^{ref} = 313\,[\mathrm{K}]$.[69] α_S is the coefficient of thermal expansion, $8.76 \cdot 10^{-4}[1/\mathrm{K}]$. The overlap factor, γ, is assumed to be equal to 1.0.

The rate constant of propagation calculated using the previous equations and parameter values are:

k_{p2} at 65°C and 260 bar $= 891[l/mol/s]$

k_{p2} at 80°C and 302 bar $= 1186\ [l/mol/s]$

3.3.3 Chain transfer to monomer in polymer-rich phase

CO_2 is inert towards polymer-based free radicals, because it does not support chain transfer to solvent during free radically initiated polymerization.[40] Therefore, only the chain transfer to monomer is considered in the discussed model.

The chain transfer to monomer constant, C_{fm}, is usually reported as the ratio of transfer and propagation rate constant:

$$C_{fm} = \frac{k_{fm}}{k_p} \qquad 3.17$$

As reported by Müller *et al.* [157], it is possible to evaluate the constant for the chain transfer to monomer using the value determined by Kukulj *et al.* [179] for bulk polymerization of MMA at 50°C and low pressure.

$$\frac{k_{fm2}}{k_{p2}} = 5.15 \cdot 10^{-5} \qquad 3.18$$

3.3.4 Termination rate constant in polymer-rich phase

Benson and North have developed a three-stage mechanistic picture of the diffusion-controlled nature of the bimolecular termination, occurring during the so-called gel effect:[180]

Step 1: Two polymer coils must first come into contact as a result of center of mass diffusion.

Step 2: Once this contact has been made, a segmental reorientation of the two macroradicals has to occur in order to bring both reactive chain ends in close proximity (i.e. within the so-called capture radius) to form radical-radical encounter pair. The dynamic of entanglement and disentanglement of the polymer coils plays an important role in this segmental diffusion process, as well as the degree of freedom for the motion of the polymer chain ends.

Step 3: The final step comprises the actual termination reaction itself, in which the two functionalities are annihilated.

Mahabadi and O'Driscoll have proposed the following Arrhenius relationship for k_{t2} at low monomer conversion:[162]

$$k_{tc2,0}(P_0) = 9.8 \cdot 10^7 [l / mol / s] \cdot \exp\left(\frac{\text{-2.9 [kJ/mol]}}{RT} \right) \qquad 3.19$$

The pressure dependence is taken into account according to the relation proposed by Buback and Kowollik:[181]

$$k_{tc2,0}(P) = k_{tc2,0}(P_0) \cdot \exp\left(\frac{\text{-15.0} \cdot 10^{-6} [\text{m}^3/\text{mol}] \cdot (P - P_0)[\text{Pa}]}{RT} \right) \qquad 3.20$$

where P_0 is equal to 0.1 MPa.[162]

In almost any polymerization, in which the polymer is present to an extent of more than several percent by mass, a significant proportion of the polymer chains will be entangled in an increasing viscous system and therefore will experience hindered mobility. Under these conditions bimolecular termination can occur only by diffusion of the two free radical chain ends towards each other.

Therefore, in order to account for diffusion-limited termination rate constant, mutual diffusion of the macroradicals chain has to be considered:[165 157]

$$k_{tc2}^{xy} = \left(\frac{1}{k_{tc2,0}} + \frac{1}{4\pi r_{xy} D_{xy} N_A} \right)^{-1} \qquad 3.21$$

where D_{xy} is the mutual diffusion coefficient of the two reacting macroradicals characterized by a degree of polymerization x and y and r_{xy} is the distance at which termination is assumed to take place instantaneously.

Russell *et al.* have pointed out, in their theoretical development of the termination reaction at high conversion, two limiting cases that have to be considered in order to estimate r_{xy}.[164, 165] In the limit, that the chain end is configurationally immobile on the timescale of propagation (the so-called rigid chain limit), the radius of interaction can be estimated to be twice the sum of the radii of the interacting species; a quantity well estimated by the Lennard-Jones diameter of a monomer unit:

$$r_{xy} = \sigma_M \qquad 3.22$$

On the other hand, the maximum value of the termination rate coefficient is given when the chain end is so configurationally flexible on the timescale of propagation that the chain end thoroughly explores all the volume available to it between propagation events. Characterizing a polymer chain by nodes of entanglement every j_c monomer units, which restrict the center of mass motion of the chain as a whole, the radius of interaction for termination is thus given by the distance of the chain end from the node of entanglement closest to it:

$$r_{xy} = 2aj_c^{1/2} \qquad 3.23$$

where a is the root-mean-square end-to-end distance per square root of the number of monomer units, $0.69[\text{nm}]$ for MMA.[165] j_c is the entanglement spacing of pure polymer, 47 monomer units.[165]

Russel *et al.* have demonstrated that the use of the maximal value of the diffusion-controlled rate of termination is consistent with measured termination rate constants in an emulsion polymerization of MMA at 50°C up to a polymer content of 80 %.[165] Therefore, the maximum value of r_{xy} is used in the calculation of equation 3.21.

As defined, the mutual diffusion coefficient D_{xy} is given by the sum of the self-diffusion coefficients of the two species:

$$D_{xy} = D_x + D_y \qquad 3.24$$

where D_x and D_y refers to the diffusion of the free-radical chain end.

As highlighted previously, the diffusion of a free radical end of a macroradical is dependent on two contributions, i.e. the chain length dependent center of mass diffusion ($D_{x,com}$) and the chain length independent diffusion by propagation reaction (D_{PG}):[157, 164]

$$D_x = D_{x,com} + D_{PG} \qquad 3.25$$

where $D_{x,com}$ is the center of mass diffusion coefficient of the radical species as a whole and D_{PG} is the diffusion coefficient for diffusion by propagational growth of a chain end:[164, 182]

$$D_{PG} = \frac{k_{p2}[M_2]a^2}{6} \qquad 3.26$$

where $[M_2]$ is the concentration of monomer in the dispersed phase $[mol/l]$.

As reported by Müller *et al.* [157], it is possible to evaluate the center of mass diffusion as a function of the chain length using in the universal scaling law published by Griffiths *et al.* [183], in the frame of their study on the diffusion of oligomers in polymeric mixtures:

$$D_{x,com} = D_M \cdot x^{-(0.664+2.02\omega_P)} \qquad 3.27$$

where D_M is the self-diffusion coefficient of monomer as given in equation 3.12 and ω_P the weight fraction of polymer (0.80).

As highlighted previously, the diffusion coefficient of the monomer in the polymer-solvent-monomer matrix, D_M, is evaluated considering a constant composition of the polymer-rich phase. This assumption is based on the fact that the particles are mainly composed of polymer. This results to the calculation of a constant diffusion coefficient of the monomer throughout the polymerization. Therefore, the variable parameter in equation 3.27 is the chain length dependent term of the center-of-masse diffusion.

The final general expression for the chain-length dependent termination rate coefficient is given by:

$$k_{tc2}^{xy} = \left(\frac{1}{k_{tc2,0}} + \frac{1}{8\pi a j_c^{1/2} \cdot (D_{x,com} + D_{y,com} + k_{p2}[M_2]a^2/3) \cdot N_A} \right)^{-1} \quad 3.28$$

In summary, in the scheme of the previous equations, the termination rate constant is considered to be chain length dependent. Then, all polymeric radicals have a unique diffusion coefficient, $D_{x,y}$, depending upon their degree of polymerization (x, y). This means that the computation of k_{tc2}^{xy} requires important mathematical treatment. In this study, as first approximation, the diffusion coefficient in equation 3.28 is evaluated considering an average degree of polymerization at each step of time:

$$\bar{x}, \bar{y} = \frac{\overline{M_n}}{M_0} \quad 3.29$$

where $\overline{M_n}$ is the number average molecular weight [g/mol] and M_0 the molecular weight of a monomer unit [g/mol].

Zammit *et al*. have reported a measured ratio of disproportionation and combination, k_{td} / k_{tc}, at 90°C of 4.37 ± 1.1, determined by MALDI-TOF mass sprectrometry.[184] This value is used for the modeling of dispersion polymerization at 80°C and implies that disproportionation is the dominant termination mode. In their paper, they made a summary of investigations of the termination mode for thermal homopolymerization found in the literature. It appears that at 60°C many authors have reported measured ratio of approximately 1:

$$\frac{k_{td2}}{k_{tc2}} \text{ at } 65°\text{C} = 1 \quad 3.30$$

$$\frac{k_{td2}}{k_{tc2}} \text{ at } 80°\text{C} = 4.37 \quad 3.31$$

The values for the bimolecular termination estimated from the number average molecular weight predicted by the model at 50% conversion are:

k_{tc2} at 65°C and 260 bar = 2234[$l / mol / s$]

k_{tc2} at 80°C and 302 bar = 7731[$l / mol / s$]

The value at 65°C can be compared with reported values of termination rate constant predicted by Müller *et al.*[156] calculated in this case as a function of the chain length of the reacting macroradicals; $k_{t2} = 3000[l/mol/s]$ at 50% conversion. This comparison supports the approximation for considering only an average value of the rate constant of termination based on the number average molecular weight.

Even though the model results will be exhaustively discussed in chapter 6.6, it is interesting to point out the main features of the calculated rate constants and hence their influence on the predicted molecular weight distributions.

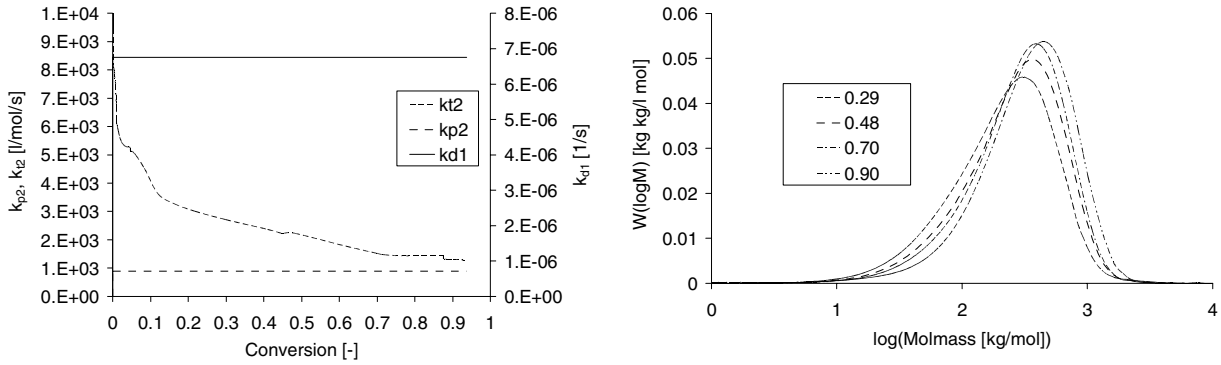

a b

Figure 3.2: a) Calculated rate constant of initiator decomposition in the CO_2-rich phase, rate constant of propagation and termination in the polymer-rich phase as a function of conversion and b) molecular weight distribution obtained at various conversions for a simulated polymerization at 65°C and 260 bar. Recipe: MMA=250g, AIBN=2.5 g, CO_2=810 g.

From the Figures 3.2 and 3.3, it is observed that no glass effect occurs during the dispersion polymerization in the polymer-rich particles (80wt% polymer). This means that the propagation reaction is not diffusion-limited in the range of the operating conditions and k_{p2} is constant. The decreasing value of k_{t2} indicates that a kind of gel effect occurs within the polymer-rich phase leading to a decrease of the rate constant of termination. The presence of this gel effect in the polymer-rich phase is responsible for the slight shift of the maxima of the molecular weight distribution towards higher molecular weight as the conversion increases.

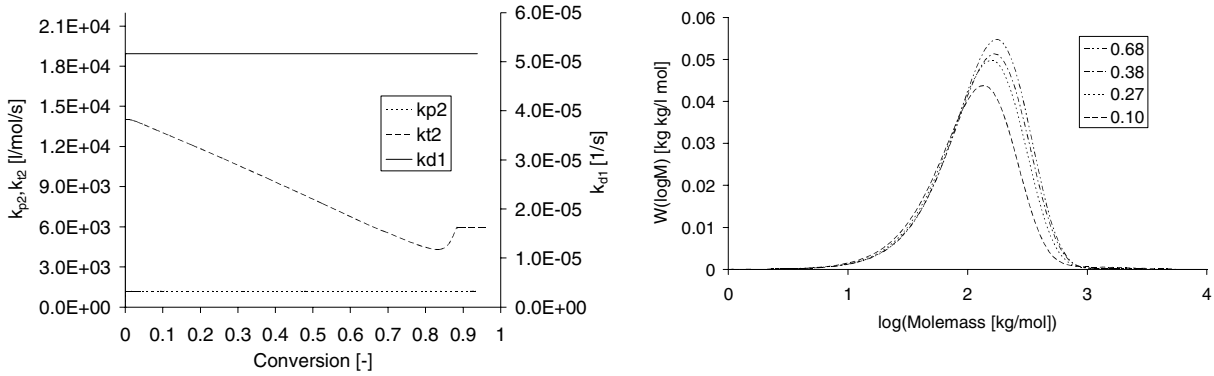

a b

Figure 3.3: a) Calculated rate constant of initiator decomposition in the CO_2-rich phase, rate constant of propagation and termination in the polymer-rich phase as a function of conversion and b) molecular weight distribution obtained at various conversions for a simulated polymerization at 80°C and 302 bar. Recipe: MMA=250g, AIBN=2.5 g, CO_2=810 g.

3.3.5 Phase exchange and calculation of equilibrium concentration

The equilibrium concentrations of the monomer in the polymer-rich phase and in the CO_2-rich phase are calculated using the following differential equations computed by the software Predici®:

$$\frac{d[\mathrm{M}_2]}{dt} = -kla \cdot \left([\mathrm{M}_2] - \frac{[\mathrm{M}_1]}{K_{eq}} \right) \qquad 3.32$$

$$\frac{d[\mathrm{M}_1]}{dt} = kla \cdot \left([\mathrm{M}_2] - \frac{[\mathrm{M}_1]}{K_{eq}} \right) \cdot \frac{V_1}{V_2} \qquad 3.33$$

Where $[\mathrm{M}_1]$ and $[M_2]$ are the concentration of monomer $[mol/l]$ in the continuous and in the dispersed phase, respectively.

The equations 3.32 and 3.33 allow equilibrating the monomer concentration between the phases. The monomer concentration in the dispersed phase is computed from the concentration of the monomer in the continuous phase and a prescribed value given by the equilibrium constant, K_{eq}:

$$K_{eq} = \frac{[\mathrm{M}_1]}{[\mathrm{M}_2]} \qquad 3.34$$

The volume ratio V_1 / V_2 permits to take into account the change in volume of the related phases.

The parameter values of the rate coefficient of mass transport, kla, and the equilibrium constant used in the simulation are:

$$\text{at } 65°\text{C: } kla = 1.2 \cdot 10^{-1} [1/s] \quad K_{eq} = 4.5\ [-]$$
$$\text{at } 80°\text{C: } kla = 1.2 \cdot 10^{-1} [1/s] \quad K_{eq} = 2.1\ [-]$$

For the mass transfer of the initiator from the continuous to the dispersed phase, the values of the rate constant of mass transport, kla, given above are used:

$$\frac{d[I_1^\bullet]}{dt} = -kla \cdot [I_1^\bullet] \qquad 3.35$$

$$\frac{d[I_2^\bullet]}{dt} = kla \cdot [I_1^\bullet] \cdot \frac{V_1}{V_2} \qquad 3.36$$

where $[I_1^\bullet]$ and $[I_2^\bullet]$ are the initiator radical concentration $[mol/l]$ in the continuous and the dispersed phase, respectively. The volume ratio V_1 / V_2 permits to take into account the change in volume of the related phases.

3.3.6 Propagation and termination rate constant in $scCO_2$

In order to compare the kinetic and molecular properties of the dispersion polymerization of MMA and a solution polymerization in $scCO_2$ a simple model considering only the polymerization in $scCO_2$ has been developed.

As reported by Müller *et al.*[156], the propagation rate constant in CO_2 can be estimated using the Arrhenius relationship given by Quadir *et al.*:[185]

$$k_{p1,0}(P_0) = 5.2 \cdot 10^6 [\text{l/mol/s}] \cdot \exp\left(\frac{\text{-25.4 [kJ/mol]}}{RT}\right) \qquad 3.37$$

where P_0 is equal to 18 MPa.[185]

The relation given in equation 3.4 is used to correct the value for the pressure dependence.

$kp1 = 1132\ [l/mol/s]$ at 80°C and 290 bar

In their study of rate coefficients of free radical polymerization determined by pulsed laser experiments, Beuermann *et al.* have shown that in the case of the polymerization of the methyl acrylate (MA) in supercritical carbon dioxide similar values of the rate constant of termination was measured in bulk and in solution polymerization.[186] Therefore, the rate constant of termination in $scCO_2$ is calculated using equation 3.19 and 3.20 and no diffusion-limitation is considered, considering a solution polymerization.

$$k_{tc1} = 3.1 \cdot 10^7\ [l/mol/s] \qquad 3.38$$

The same values used to evaluate the disproportionation termination rate constant and chain transfer to monomer in the dispersed phase constant are used in the CO_2 continuous phase:

$$\frac{k_{td1}}{k_{tc1}} \text{ at } 80°C = 4.37$$

$$\frac{k_{fm1}}{k_{p1}} = 5.15 \cdot 10^{-5}$$

3.3.7 Algorithm used in Predici®

The simulation package Predici® has been developed by Dr. Micheal Wulkow who has developed an algorithm capable to calculate the molecular weight distribution of polymers in complex systems of polyreactions without the need of major assumptions, such as the quasi steady-state approximation (QSSA), and with no restriction on the form of the molecular weight distribution.[187] He has demonstrated that despite the fact that the rate equations describing the molecular weight distributions appear like high dimensional systems of ordinary differential equations (dy/dt = f(y,t)) solved for all the components (initiator, monomer, live and dead polymers), they approach in nature discrete partial differential equations. He has concluded that this hidden structure might be the reason that difficulties for calculating the numerical solutions in complex systems like polymerization have often been encountered.

The algorithm developed in his work is based on the discrete "Galerkin h-p method". In this method, the differential equations describing the variation of the concentration with respect to time are expressed in the form of a countable system of ordinary differential equation:

$$u_S^{'}(t) = f_S(u_1(t),...,u_{S_{tot}}(t)) \qquad s = 1,...,s_{tot} \tag{3.39}$$

where $u_S^{'}(t)$ is a vector composed of all the variables $u_s(t)$ being the concentrations of the macromolecules (live and dead polymers) with chain length i at time t and the concentrations of initiator and monomer. The high dimensional vector u contains all the components of the kinetic equations and their numerical representations at time $t(t+\tau)$. Considering that a molecular weight distribution is composed of numerous chains of different length, this means that the dimension of the complete system can be in practice very large up to 10^3 to 10^6.[187]

In order to find a numerical solution, a time discretization is used to discretize the countable system. In turn, this procedure allows obtaining a linear system of 2 equations for an approximation u_1 of the solution $u_1(t+\tau)$ after a time step from t to $t+\tau$. At this point, an algorithm is used to calculate the correct time step at each step of time by controlling the "deviation" between an approximate solution of $u_1(t)$ and an inexact solution solved for a linear system. This control is made by defining an admissible tolerance that determines the accuracy of the time interval or time step. Once the estimation of the time step is calculated, a second algorithm is used to calculate the chain length distribution in the given interval by varying the number of the expansion coefficients in the algorithm and their order.

The originality of the algorithm is that it gives the possibility to minimize the number of internal variables (degrees of freedom) of the system and is intrinsically composed of an automatic error control mechanism.

4 Equipment, Materials and Methods

Experiments were carried out in the reaction calorimeter, RC1*e*, supplied by Mettler-Toledo GmbH (Switzerland). The reaction calorimeter, prototype for supercritical conditions, is designed to monitor batch dispersion polymerization of MMA in $scCO_2$. The system can be divided in four modules: the high pressure reactor, the thermostat unit, the CO_2 feed line and the reactants feed line.

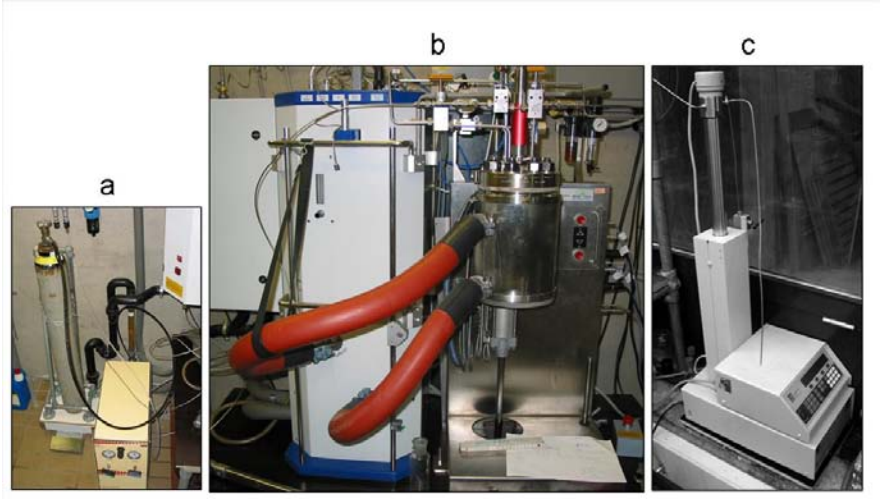

Figure 4.1: Pictures of the supercritical reaction calorimeter showing: the CO_2 feed line (a), the supecritical reaction calorimeter (b) and the reactants feed line (c).

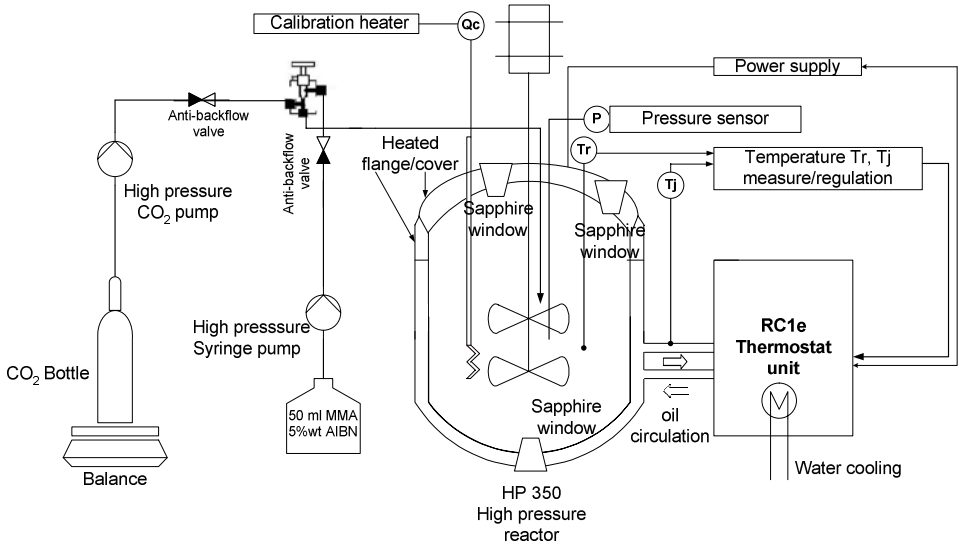

Figure 4.2: Technical scheme of the supercritical reaction calorimeter.

4.1 Equipment

4.1.1 High pressure reactor

The high pressure reactor is composed of:

- An autoclave: model PREMEX HP350, high strength stainless steel No 1.4980, nominal volume 1.2 liters, inner diameter 95 mm, maximum operating temperature and pressure 300°C and 350 bar respectively, 3 fittings composed of high pressure valves from SITEC (Switzerland). The reactor is equipped with a 25 W calibration heater, a PT100 temperature sensor and a pressure unit from KELLER (Switzerland) composed of a pressure gauge, a pressure transducer with an overall linear precision of 0.04% in the range of 200-400 bar.
- A rupture disk connected in line to the pressure transducer with a maximum allowable pressure of 400 bar ± 10%.
- A pneumatic system used to move the double jacket up and down along the axis of the chassis where the reactor is fixed.
- A magneticly coupled stirrer with a maximum stirring speed of 3000 rpm. Two different impeller types with equally spaced blades were used; a two-stage turbine and a three-stage EKATO MIG®(EKATO Rühr-und Mischtechnick, Germany):

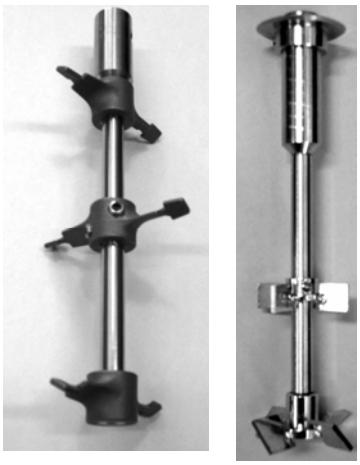

a) d_S = 56 mm b) d_S = 40 mm

Figure 4.3: Pictures of the two impellers used a) three-stage Ekato MIG® b) two-stage turbine.

- A high pressure ultrasonic probe especially designed by Sensotech (Germany) for measurements in supercritical carbon dioxide, made of stainless steel No 1.4571, piloted by a Liquidsonic 20 LCD controller, maximum operating temperature and pressure 120°C and 300 bar respectively. The measuring method is based on the determination of the propagation speed of ultrasonic waves of 1 MHz frequency and 1W/mm^2 maximum power, generated by a piezoelectric transducer (the emitter) and received by an another one (the receiver) separated by a precise distance of 9mm. An offset of 1 m/s is considered to correct the experimental measured values (Annex A.1).[23] When the ultrasonic probe is introduced inside the reactor, the Ekato MIG® impeller cannot be used anymore because of its blades' size.

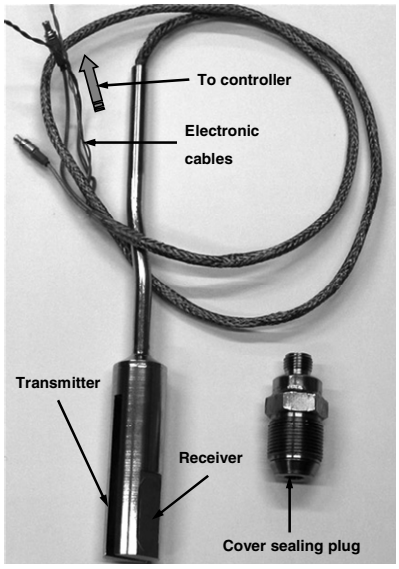

Figure 4.4: Picture of the high pressure ultrasonic probe.

- A readout display and computer acquisition, using two RD10 (electronic interface, Mettler-Toledo) and the software WinRC-NT (Mettler-Toledo), for reactor, jacket, cover and flange temperatures, pressure, stirring speed, calibration power and speed of sound data.
- Two circular electrical heaters that surround the cover and the flange parts of the reactor allowing their temperature control. Temperature measurement is made by PT100 sensors. Cooling is made by air. The electrical heaters are isolated from their environment using a heat transfer cement (Electrolux professional, Switzerland, Thermon T63).

- Three sapphires windows, two placed on the cover and one at the bottom of the reactor. They allow the use of a video imaging system, which is not used in this work. When the nucleation occurs and the particles formed separate from the CO_2 continuous phase, the medium starts to become turbid giving simply "black" pictures.

4.1.2 Thermostat unit - RC1*e* technology

The thermostat unit allows the control of the reactor temperature by adjusting the jacket temperature. The silicon oil used as heating fluid is pumped in a closed loop and circulates at high flow rate of 0.1 l/s. The oil loop is divided in two parts including a cooling system with water and an electrically heated one. The tuning of the jacket temperature is done with a proper mixing between hot and cold oil in order to maintain the desired reactor temperature.

4.1.3 CO_2 and reactants feed line

The carbon dioxide feed line is composed of:

- A 13.4 litres CO_2 bottle (Carbagaz, Zwitzerland) equipped with a dip tube and mounted on a balance (Mettler-Toledo, model SR 64001 delta-range) having a precision of ± 0.1 g over the range of 0-13 kg.
- A high pressure piston pump for liquid CO_2 (New Ways of Analytics, Germany, model PM101), maximum operating pressure 600 bar. The pump is provided with a condenser (-25°C) and compressed air.
- An anti-back pressure valve placed before the reactor charging valve in order to not allow the back flow of CO_2.
- At the end of an experiment, the separation of the CO_2 from the reacting medium is made by venting the CO_2 directly in a fume hood during at least 1 hour in order to avoid as much as possible freezing in.

The reactants feed line is composed of:

- A high pressure syringe pump (Isco Inc, model 100 DX) with a maximum operating pressure of 690 bar, connected to a three ways valve (SITEC AG, Switzerland) and allowing the addition of reactants under pressure. The maximum volume of the piston is 100 ml and the flow rate range is between 0.01 µl/min and 50 ml/min with ±0.3% precision.

- An anti-back pressure valve placed before the reactor charging valve in order to not allow the back flow of reactor content.

4.2 Materials

Methyl methacrylate (MMA) and 2,2'-azobis(isobutyronitrile) (AIBN) were obtained from Fluka and were used as received. Carbon dioxide of 99,9% purity was supplied by Carbagas (Switzerland) and used as received. The stabilizer was the monomethacryloxypropyl terminated poly(dimethylsiloxane) supplied by ABCR (Germany) and was used as received. It has a molecular weight of 5000 g mol^{-1} and a polydispersity of 1.11.

4.3 Methods

4.3.1 Determination of the reactor volume

The total volume of the reactor has been determined using two different methods:

- Filling the reactor with a known amount of nitrogen and using an appropriate equation of state (EOS).[27]
- Filling the reactor with a known amount of carbon dioxide and comparing the isothermal properties as density and pressure given by the EOS of Wagner and Span.[27]

In the isochoric system, the density of pure supercritical carbon dioxide is calculated as:

$$\rho_{CO_2} = \frac{m_{CO_2}}{V_r} \qquad 4.1$$

Table 4.1: Results of the N_2 and CO_2 experiments.[23]

Material	T_r[°C]	P[bar]	Density [kg/m^3]	V [l][a]
N_2	20	133.1	149.2	1.293±0.026
N_2	60	156.3	149.5	1.291±0.026
N_2	80	167.8	149.4	1.292±0.026
CO_2	32	79.3	643.8	1.28±0.0031
CO_2	50	130.8	639.4	1.29±0.0031
CO_2	100	280.0	635.6	1.30±0.0031

[a] V_{tot} uncertainty 2%

The total reactor volume considered in the experiments is of 1.29 ± 0.02 liters including the dead volume as pipes and tubes while taking also into account the standard equipment as the T_r sensor, the calibration probe and the stirrer, which are inserted into the reactor. When the

ultrasonic probe is inserted in the reactor, the considered volume is 1.26 ± 0.02 liters taking into account the 30 ml volume occupied by the probe.

4.3.2 Reaction procedure and thermal analysis

The experimental procedure of the dispersion polymerization is explained in this section. Figure 4.5 and 4.6 show the typical thermograms obtained during the dispersion polymerization of MMA in $scCO_2$.

Step1: Known amounts of the monomer (around 203 g) and of the stabilizer (between 0 and 25g) are directly charged to the reactor at room temperature. The reactor is then sealed and filled with CO_2 (around 800 g). The data acquisition using the WinRC® software is started and the reactor is heated to the set temperature (65°C or 80°C).

Step 2: When the desired reactor temperature is reached, a calibration is run during 1 hour to determine the overall heat transfer coefficient before the start of the polymerization; 20 minutes for the baseline, 20 minutes of calibration and 20 minutes for the baseline (see Figure 4.7 and the related explanations).

Step 3: When the calibration procedure is finished, a 50 ml monomer solution containing 5.1 wt% initiator is added at a flow rate of 50 ml/min using the syringe pump; 2.5 g of AIBN and 46.8 g of MMA are introduced into the reactor. This procedure allows avoiding the polymerization occurring during the heating and the calibration steps.

Step 4: After the dosing, the polymerization occurs and is left running 4 hours or more when required.

Step 5: At the end of the dispersion polymerization, a second calibration is made during 1 hour to determine the final overall heat transfer coefficient; 20 minutes baseline, 20 minutes calibration, 20 minutes baseline.

Step 6: To quench the reaction, the reactor is then rapidly cooled down to room temperature.

Step 7: The CO_2 is slowly vented during 1 hour.

Step 8: The reactor is opened and the polymer is collected. Samples are taken for further analyses (molecular weight distribution, particle size distribution and gravimetric monomer conversion, percent chemically incorporated stabilizer) .

Step 9: The reactor is cleaned with ethyl acetate heated up to its boiling point. Due to the large quantity introduced, the pressure increases inside the reactor allowing, at least by the vapor phase, the cleaning of the tubes and inner part of the cover.

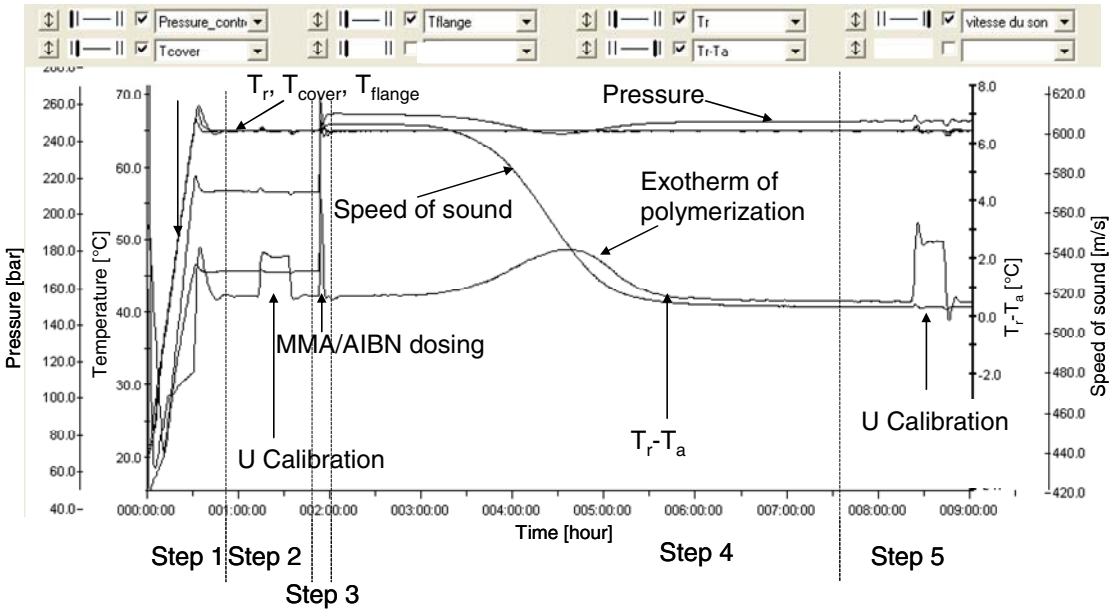

Figure 4.5: Typical thermogram obtained during a dispersion polymerization of methyl methacrylate in $scCO_2$ at 65°C.

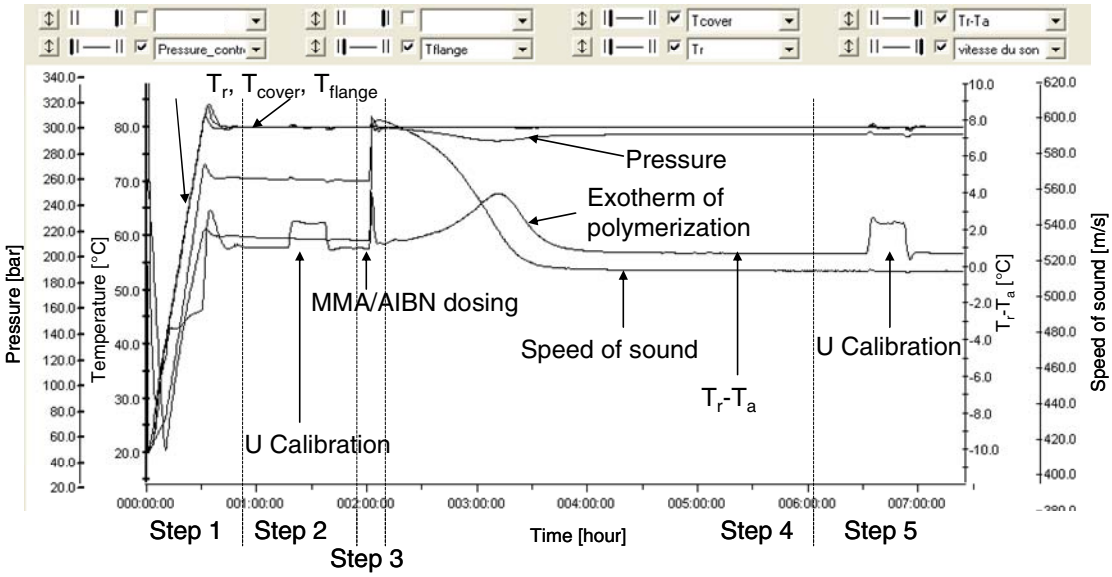

Figure 4.6: Typical thermogram obtained during a dispersion polymerization of methyl methacrylate in $scCO_2$ at 80°C.

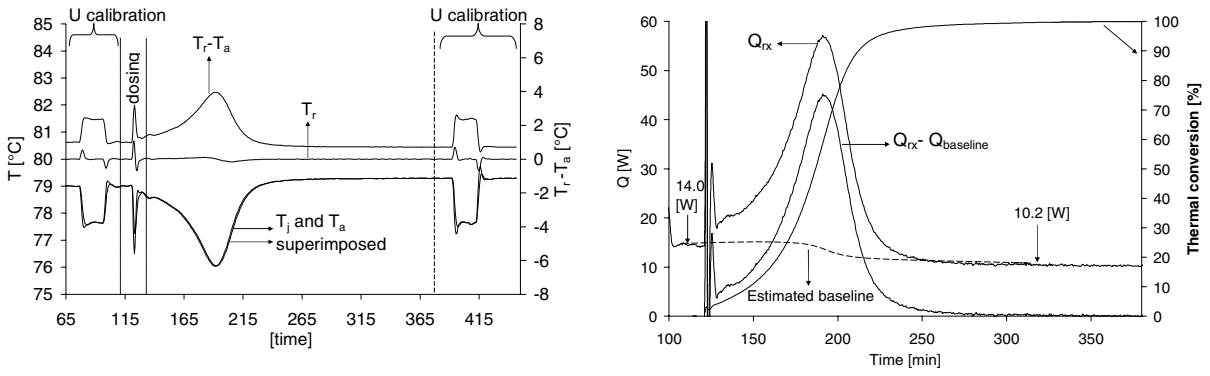

a b

Figure 4.7: a) Data acquisition of T_r, T_j, T_a and T_r-T_a during the course of an experiment and b) evalutaion of the baseline for the calculation of Q_{rx}.

Figure 4.7 a shows the on-line acquisition of the temperature data used in the calorimetric analysis for the calculation of the heat generation, Q_{rx}, and hence of the thermal conversion, X_{th}. In isothermal mode and at steady state, the theoretical value of T_a is very close to the physical jacket temperature value, T_j. The reactor wall is already heated up, and all the heat is transferred from the reaction mass to the jacket without loss in heat accumulation by the reactor wall. The evaluation of Q_{rx} is based on the measurement of the temperature difference, T_r-T_a, and on the evaluation of the overall heat transfer coefficient U (calibration). The evolution of the term T_r-T_a allows determining the start and the end of the polymerization (Figure 4.5, 4.6 and 4.7). Figure 4.7 b shows that the value of the baseline at the end of the polymerization is approximately 4 [W] lower than the one before the start of the reaction. The profile of the baseline is calculated by the software between the start point and the end point of the polymerization exothermic peak. This baseline, proportional to the conversion, allows taking into account non linear changes in the heat transfer coefficient (i.e. the baseline is not linear between the start point and the end point). The calculation of the baseline is iterative assuming a linear connection between the start and the end of the baseline. Figure 4.7 a shows also that the reaction calorimeter is clearly able to maintain a constant reactor temperature throughout the polymerization. This means that the contribution of the accumulation term in equation 4.2 is negligible.

The final equation used to calculate the heat generation rate of the dispersion polymerization of MMA in $scCO_2$ is the following:

$$Q_{rx} = Q_{acc} + Q_{flow} + Q_{loss} - Q_{stir} = Q_{acc} + Q_{flow} - Q_{baseline} \qquad 4.2$$

Figure 4.5 shows that in the case of the experiments realized at 65°C an induction time of 1 hour is present before the start of the polymerization. This incubation period can be the result of the stabilization of the monomer using hydroquinone as inhibitor. Hydroquinone is commonly used as polymerization inhibitor, because it directly reacts with radicals present in the medium allowing tying up the polymerization. Normally, the presence of inhibitor (very small quantity compared to the initiator concentration) does not affect the initiation rate of the dispersion polymerization but only delays the reaction. Once the inhibitor is completely consumed by the initiator radicals, the polymerization starts. The advantage of having a pronounced induction time is that after the perturbation of the initiator dosing (see the corresponding peak in Figure 4.5, 4.6 and 4.7) a well defined baseline is obtained before the start of the polymerization. As shown in Figure 4.5, 4.6 and 4.7, the dosing of the MMA/AIBN solution leads to an increase in pressure of 40 bars inside the reactor due to the pressure required by the pump to introduce the reactants. Respect to the relationship between the pressure and the temperature in a closed system (i.e. $PV = nRT$ for an ideal gas), an increase in pressure leads to an increase in temperature inside the reactor of less than 1 degree. But this is sufficient to perturb the evaluation of the initial baseline in the case of the experiments at 80°C. For these experiments, no induction time is observed before the start of polymerization. This can be explained by the fact that the initiation rate constant at 80°C is one order of magnitude higher than the one at 65°C (see chapter 3). Therefore, for polymerizations at 80°C, the initial baseline is selected before the dosing step. An evaluation of the accumulation peak has shown that its contribution corresponds to 3 % of the total heat delivered by the polymerization. This heat contribution is removed in the final calculation of the enthalpy of polymerization and of the thermal conversion.

When the magnitude of the heat generated by the polymerization and the one of the baseline variation are compared (Figure 4.7 b), it appears that the evaluation described in this section is enough accurate. This is supported by the accuracy of the calorimetric results discussed in chapter 6.

If required, it is possible to find methods allowing the calculation of the changes of the overall heat transfer coefficient during the course of a polymerization reaction and thus allowing the evaluation of the baseline at the same time. The method developed by Reichert *et al.*, the so-called temperature oscillating calorimetry, permits the simultaneous measurement of U and Q_{rx}.[188] A characteristic feature of the temperature oscillation calorimetry is that to the constant set point of the reactor temperature a small sinusoidal temperature oscillation is added. The oscillating setpoint forces an oscillating heat input into the heating device of the thermostat. Therefore, the technique is based on the fact that the energy balance of the oscillating contributions can be separated from the contribution of the reaction and leads to the resolution of a system of 2 equations for 2 unknowns.

4.3.3 Polymer characterization

4.3.3.1 Gravimetric monomer conversion

To evaluate gravimetrically the monomer conversion, the polymer recovered (white powder at conversion higher than 93%) is let the whole night at room temperature. Afterwards, the polymer is dried in a vacuum oven for at least 24 hours at 65°C. When a sticky solid is obtained, the majority of the polymer can only be recovered using dichloromethane. The solution is then let to evaporate first at room temperature for 1 or 2 days and finally dried in a vacuum oven at 65°C for at least 24 hours.

Yields are determined from the ratio of the final mass of polymer collected to the initial monomer charged. In the calculation, the whole amount of the initiator is taken into account, as it is chemically grafted onto the polymer. The stabilizer, only partly grafted into the polymer, is considered to be completely recovered with the polymer.

4.3.3.2 Sampling under pressure for monomer conversion

In order to validate the heat balance model and to measure the polymer molecular weight as a function of time, an on-line sampling under pressure was realized. The evaluation of the monomer content in the polymer sample is made using Headspace Gas Chromatography (HSGC). Because of the reactor size and the corresponding quantity of materials used, like the very expensive stabilizer, sampling is more economical than repeating many times the same experiments quenched at different steps of time.

For quantitative analysis of volatile organic compounds gas chromatography (GC) with liquid injection is the analytical method of choice. However, because polymers have a high vaporization temperature that can lead to undesired degradation reactions of the polymer, the technique cannot be used in its original form. A subtle way to examine the organic volatile content in a non vaporizable substance is the headspace gas chromatography (HSGC). There, the volatile substances (monomer) are evaporated from the non-volatile matrix to the vapour phase. A part of this vapour is then transferred into the capillary of the gas chromatograph. The monomer is thermally desorbed from the matrix using the dynamic headspace desorber (TurboMatrix, PerkinElmer). The solid sample is heated up to 120°C during 1 hour under a constant flow of helium. The extracted volatile compounds are then condensed in a trap at -30°C. When the desorption is finished, the trap is heated in few seconds to a temperature of 130°C. Finally, the volatile compounds are released in a narrow distribution into the chromatographic column. The gas chromatography analysis takes approximately 30 minutes and permits to know

the composition of the volatile phase extracted from the original solid sample, and thus the monomer content in the polymer sample.

The different steps of the sampling procedure are the following:

Step 1: Steel tubes of 10 ml are connected to two ball valves put in series. At a given time, two samples are taken; one for monomer conversion measurement and the other one for molecular weight analysis. The driving force is based on the pressure difference between the reactor under pressure and the tube at ambient pressure. When the pressure equilibration is reached, the tube is removed. To quench the reaction, the tubes are cooled as fast as possible in an ice bath (T=0°C).

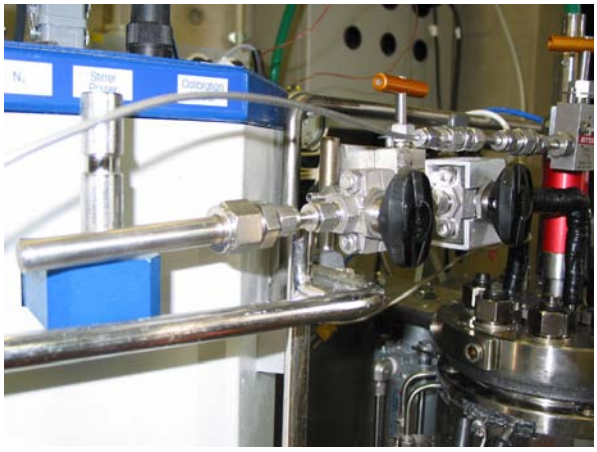

Figure 4.8: Sampling system installed on the reactor composed of two connected valves and a tube for collecting the samples.

Step 2: For the GPC analysis, the tube is simply depressurized and the solid product is recovered and then put in a fridge (T = -25°C).

Step 3: The determination of the monomer content in the polymer sample requires knowing the exact quantity of the second sample taken from the reactor for the HSGC analysis. In order to recover as much as possible the liquid monomer contained in the tube, the latter is depressurized very slowly and the CO_2 is let bubbling through a 10 ml solution of dimethyl formamide (DMF for HPLC analysis, Reactolab S.A. Switzerland) introduced in a closed bottle containing two holes on its cap; one to introduce a degassing pipe and the other one for pressure release and CO_2 evacuation (Figure 4.9).

Figure 4.9: Depressurization system used to separate CO_2 from the sample content (Step3).

Step 4: Once the CO_2 is completely released, the tube is opened and the polymer can be collected. The tube is washed two times with 2 ml of DMF. The DMF volumes used in each step are precisely measured in order to know the exact mass of DMF.

Step 5: The whole solution contained in the bottle (step 3) and the whole polymer collected (step 4) are transferred together into a small bottle, which has been previously precisely weighted. Then, the bottle and its content are weighted. By gravimetric analysis, it is possible to determine the whole sample amount taken from the reactor (around 1g).

Step 6: The bottle is put in a fridge (T = -25°C). The DMF solution containing the solubilised monomer and polymer is used to prepare the sample for the HSGC analysis.

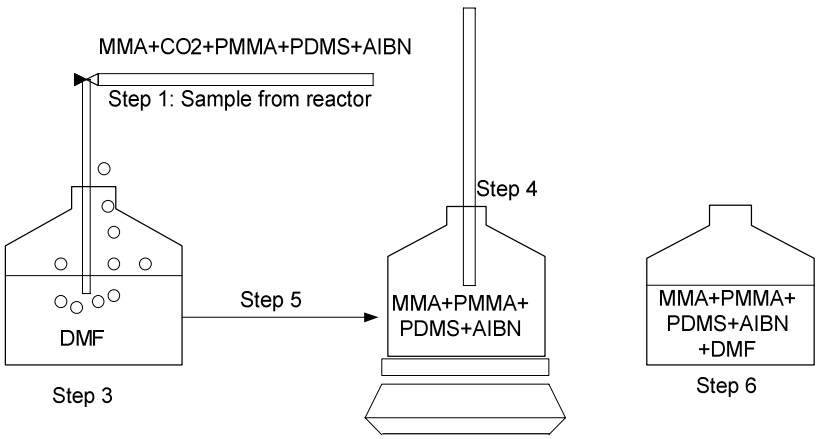

Figure 4.10 : Schematic representation of the products' recovery from the sample tube.

Step 7: HSGC analysis. 1 ml sample solution, which is left previously several hours at ambient temperature, is mixed with 25 µl of butyl acetate (BuAc), used as calibrated reference. A small quantity of silane treated glass wool (Socochime S.A., Switzerland) is introduced in a PTFE tube in order to form a porous cap used to stop the solid particles transported from the carrier gas. Then, 20 µl of the sample-BuAc solution is injected in the PTFE tube. The PTFE tube is then sealed in a metallic tube and introduced in the automatic sampler. Using calibration curves, it is possible to determine the MMA content in the sample-BuAc solution and therefore in the sample extracted from the reactor knowing exactly its mass.

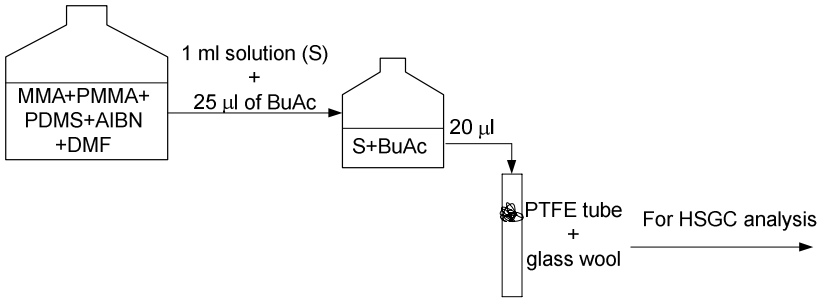

Figure 4.11: Schematic representation of the sample preparation for HSGC analysis

4.3.3.3 Molecular weight distribution

The molecular weight (MW) and the molecular weight distribution (MWD) of polymers are their most important characteristics, governing both physical properties and end-use applications. A very well established method for their determination is the size exclusion chromatography (SEC).[189] The SEC separation method is based on the molecular hydrodynamic volume and hence on the size of the molecules in solution. In fact, the columns contain surface pores of different size. The larger molecules will not fit into the smaller pores and travel faster through the column. Conversely, the smaller molecules will diffuse into most of the pores and be retained longer. This separation method is used to determine the molecular weight distribution of the poly(methyl methacrylate) samples.

The PMMA samples are dissolved in tetrahydrofuran (THF). Once the sample is dissolved, it is injected onto a set of 2 columns in series (diameter x length 8x300 mm) packed with a crosslinked gel (silicon type gel, Polymer standards service) characterized by particle size of 5 µm. Tetrahydrofuran, heated up at 35°C, is used as eluent at a flow rate of 1 ml/min. The MWDs are measured using the Viscotek Triple Detector SEC (TDA model 300) composed of three different detectors:

- The differential refractive index (RI) detector operates by measuring the deflection of a light source caused by a difference in the refractive index between sample –solvent mixture and pure solvent. Different polymer types have different differential RI responses with concentration, $dn/dc = 0.083$ for PMMA. The RI area is proportional to the quantity of the polymer injected and its dn/dc value. Thus, the refractometer provides a signal which is proportional to the concentration of the sample.
- The differential pressure (DP) detector is a molecular-weight sensitive detector and provides a signal proportional to the change in specific viscosity. The MW determination by viscosity is based on the fact that the viscosity of a polymer solution is larger than that of the solvent and depends directly on the molecular weight of the polymer.

  Therefore, the RI and the DP detectors, taken together, permit the calculation of the intrinsic viscosity of the sample at every eluted point, constituting the intrinsic viscosity distribution of the polymer sample.
- The right angle laser light scattering (RALLS) detector is also a molecular-weight sensitive detector that can provide absolute molecular weight (MW) and size (radius of gyration) of macromolecules in solution. When light interacts with a molecule, it induces a temporary dipole moment which oscillates in phase with the incident beam. This scattered light is referred to as Rayleigh scattering and is of the same wavelength of the incident beam. The amount of light scattered is directly proportional to the product of the molar mass and the solute concentration. Due to thermal fluctuation, pure solvent also scatters light, although at a lower degree than the polymer solution. The information about the size and the molecular weight of polymer is experimentally deduced from the excess light scattering intensity above the solvent background. The normalized LS intensity caused by the presence of polymer molecules is proportional to polymer weight distribution and sample concentration.

Figure 4.12 shows the typical signals measured by the detectors for the MWD determination of the PMMA samples.

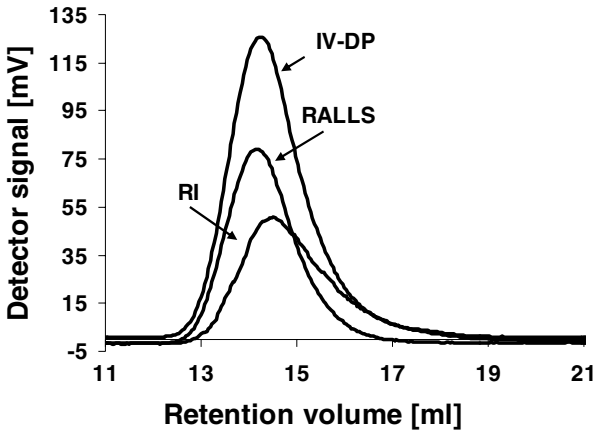

Figure 4.12: Signals measured by the detectors for the MWD determination. IV= intrinsic viscosity, RALLS = right angle laser light scattering, RI = refraction index.

The triple detection allows the determination of the molecular weight distribution without the need of a preconstruction of a calibration curve. Because broadening and peak distortion can occur when eluting the sample through a number of detector cells, it is crucial to determine the dead volumes between detectors. The most commonly used approach is the measurement of the peak maxima (or breakthrough volume) difference of a narrow-MW distribution of a polymer standard. In other words, the difference between the eluted volume and the expected one permits to calculate the dead volume between detectors.[190, 191] Standards of polystyrene having a molecular weight close to the one measured were used (Viscotek) to calibrate the detectors.

4.3.3.4 Product morphology and particles size characterization

Particle morphology and particle size distribution are analyzed by scanning electron microscopy (SEM) (Philips XL30 SFEG) and by laser diffraction (Malvern Mastersizer 2000), respectively. The samples for SEM analysis are redispersed in hexane and dried during one night under vacuum at 60°C. The samples are then mounted on an aluminum stub using a non-conductive adhesive tab to fix them and are gold-coated before the measurement. The aluminum stab and the adhesive material are previously gold-coated before the preparation of the PMMA samples. The samples for the laser diffraction analysis are redispersed in hexane and let 20 minutes in an ultrasonic bath in order to break the agglomerates, the hexane being the solvent used during the measurement.

4.3.3.5 Analysis of the chemically incorporated stabilizer

A gravimetric method was developed in order to evaluate the percent of PDMS macromonomer chemically incorporated in the final product. 4 samples of 0.5 g are prepared from the product recovered from reactor. They are dried in a vacuum oven at 60°C allowing calculating the residual MMA content. Then 4 small tubes containing around 0.2 g of dried product and hexane for PDMS extraction are put under stirring for 2 hours. Then the small samples are put in a centrifuge for 15 min at 9000 min^{-1}. Hexane containing the extracted PDMS is removed with precaution. The solid samples are dried during 24 hours at 65°C in a vacuum oven. The main assumption for the final calculation of PDMS incorporated is that all the compounds are recovered from the reactor at the end of the dispersion polymerization. Hence there is no residual product inside the reactor and no product losses during the venting of carbon dioxide.

4.3.4 Cloud point measurement and high pressure view cell

A high pressure variable volume cell (New Ways of Analytics GmbH, Germany) is used for the study of phase transition and cloud point measurement. The system is composed of:

- A horizontal cylinder with a diameter of 36 mm.
- Two sapphire windows; one inserted in the cover of the cell and the other one at the back part of the cell. The back sapphire window is able to move and is used as a piston allowing a volume variation between 31-62 ml.
- A piston system operated by a pneumatic system working with compressed air (maximum pressure 10 bar). The linear position of the piston is measured using a variable electrical resistance between 0 and 100 kΩ, precision ± 100 Ω. A linear relation permits to determine the volume of the cell from the resistance measurement.
- A light at the back part of the cylinder.
- A magnetic drive propeller with a diameter of 22 mm.
- A heating system composed by two electrical band heaters (Ihne and Tesch, Germany) delivering a maximum power of 600 W and 350 W, respectively. The maximum operating temperature of the cell is 180 ± 0.1°C.
- A pressure sensor (WIKA, Germany) working between 1 and 1000 bars, with a precision of 1 bar, maximum operating pressure of the cell 700 ± 1 bar.

- A HPLC pump (Gilson Inc, USA, model M305) allowing the addition of MMA or stabilizer with a maximum pressure of 600 bar and a maximum volume flow rate of 10ml/min.

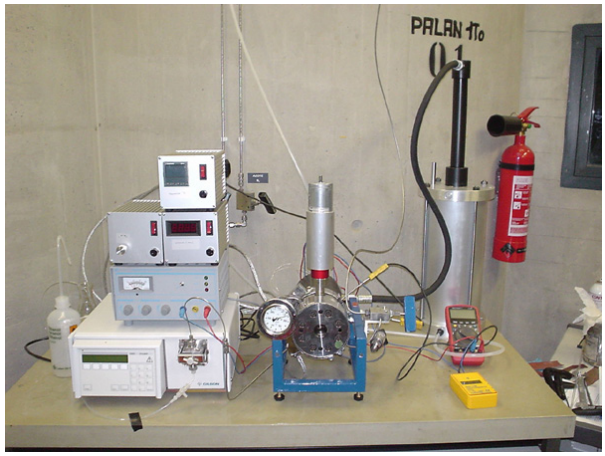

Figure 4.13: Picture of the high pressure variable volume cell.

The measurement procedure is the following:

- The cell is purged three times with an arbitrary amount of CO_2 before the calibration procedure.
- Then, the cell is filled with an approximate mass of CO_2.
- After the introduction of CO_2, the cell is heated up to temperatures far from the critical temperature. For different temperature steps, the corresponding pressure in the supercritical state is noted. A linear regression is fitted from those points and the corresponding slope is characteristic of the CO_2 density

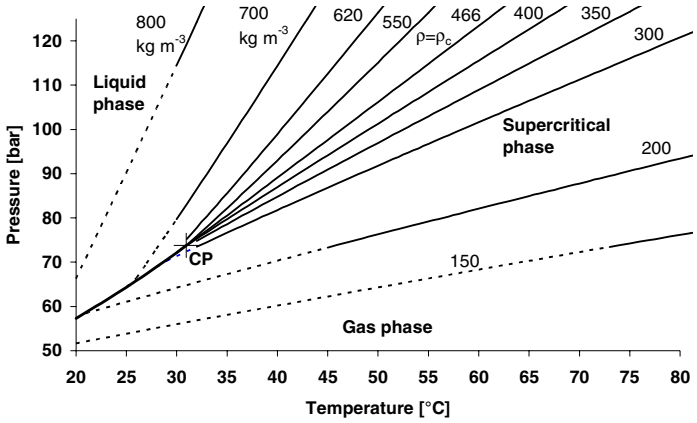

Figure 4.14: Isochors of pure carbon dioxide, values taken from NIST. The behavior of the pressure as a function of temperature is shown for different CO_2's densities in kg/m^3; ρ_c CO_2 = 466 kg/m^3.

- Once the density of CO_2 is determined, it is possible to calculate the introduced mass of CO_2 knowing the volume of the cell.

The disadvantages of using such a technique are that CO_2 has to be introduced first. When the cell is heated up to temperature of 60°C it takes at least several hours to cool down the equipment. Moreover, it is necessary to add a moderate mass because of cell pressure and piston limitations.

- For the study of the isotherms of the binary mixtures MMA-CO_2, the monomer is added in the variable volume cell using the HPLC pump. The component is introduced in steps. Between each addition the small bottle containing the pure MMA is weighted as a complementary measurement of the introduced volume.
- For the cloud point measurement (P-T phase diagram) of the binary mixture PDMS-CO_2 and of the ternary mixture PDMS-MMA-CO_2, a known amount of PDMS and a known amount of solution of precise composition of PDMS-MMA is introduced, respectively, in the variable volume cell using the HPLC pump.

The choice of the technique for the determination of phase transitions is based on the fact that it is easier in the system to manipulate the pressure than the temperature. In other words, to vary the pressure and note the corresponding temperature at a transition point. In the first step, the system is heated to a temperature (increase in pressure at the same time) until the obtaining of a homogeneous mixture or fluid phase. Then, the piston is moved backward slowly in order to increase the volume of the cell and to lower the pressure until a phase transition (cloud point) is observed. A transition point is considered as soon as the second phase starts to appear. For example, a bubble point is noted when the first micro bubbles appear at the top of the stirrer shaft and a dew point when the first manifestation of condensation is observed as a foggy state. Cloud points in polymer-CO_2 system are characterized by a cloudiness appearing in the mixture at the transition point.

5 Phase equilibrium: Results and Discussion

5.1 PDMS mMA-CO_2 phase envelope

A dispersion polymerization is characterized by an initial homogeneous mixture composed of the initiator, the monomer, the stabilizer and the solvent, i.e. 2,2'-azobis(isobutyronitrile), methyl methacrylate, poly(dimethylsiloxane) macromonomer (PDMS-mMA) and carbon dioxide. This means that all the initial compounds have to be soluble in the solvent. Therefore, it is essential to know the phase envelope of the ternary mixture monomer-stabilizer-solvent in order to choose correctly the operating conditions. Due to the small quantity of AIBN present in the mixture (0.24wt%), its influence on the phase behavior of the mixture can be neglected. Using the high pressure view cell, it has been possible to define the P-T phase diagram of the binary mixture PDMSmMA-CO_2 and the ternary mixture MMA-PDMSmMA-CO_2. For simplification reasons, poly(dimethylsiloxane) monomethacrylate will be hence forth referred to as PDMS, while keeping in mind that this polymer has a terminal methacrylate unit.

Polymers exhibit much more complex phase behavior than small molecules with supercritical fluids, because the molecular weight (MW) and the polydispersity (PDI) of the polymer play an important role on the cloud point locations and modify the phase envelope. Figure 5.1 shows the cloud point measurements for the binary mixture stabilizer-carbon dioxide at concentration identical to that used in the dispersion polymerizations.

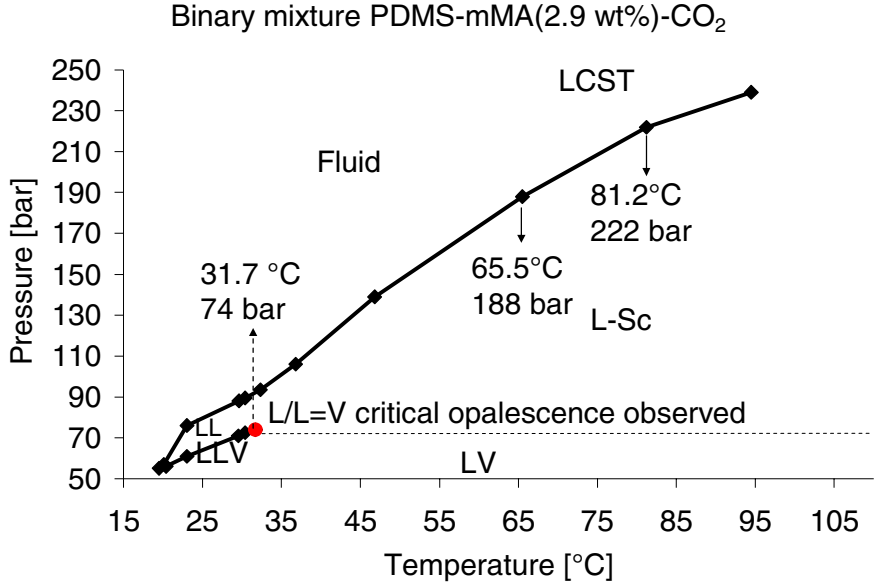

Figure 5.1: Cloud point measurements for the binary mixture CO_2-PDMS (Mw = 5'000 g/mol and polydispersity =1.11).

O'Neill *et al.* have reported that the solubility of the PDMS monomethacrylate in $scCO_2$ is comparable with the one of the PDMS homopolymer (Mw = 13'000 g/mol).[160] They have concluded that the monomer unit does not affect the cloud point locations because it interacts reasonably well with CO_2 and does not affect significantly the solubility. This can be expected because there is only one monomer unit at the end of the polymeric stabilizer. On the other hand, this monomer unit is essential to increase the solubility of the stabilizer in the polymer phase acting as an anchor to the growing polymer either by physical adsorption and chemical grafting, keeping in mind that a certain percentage of the stabilizer will copolymerize with the polymer. Thus, it is possible to compare the results with the literature data for the homopolymer.

Polysiloxanes can be used as stabilizers in dispersion polymerizations in CO_2 because they exhibit a relative good solubility in carbon dioxide allowing working at low pressures; between 300 and 400 bar.[160, 192] Figure 5.2 b shows that to solubilize 2.42wt% PDMS homopolymer having a MW of 13'000 g/mol at least a pressure of 253 bar at 65°C is required. In the case studied, because the PDMS has a lower MW (5'000 g/mol), a pressure of 188 bar is sufficient to solubilize 2.9 wt% polymer in $scCO_2$ at a similar temperature (Figure 5.1).

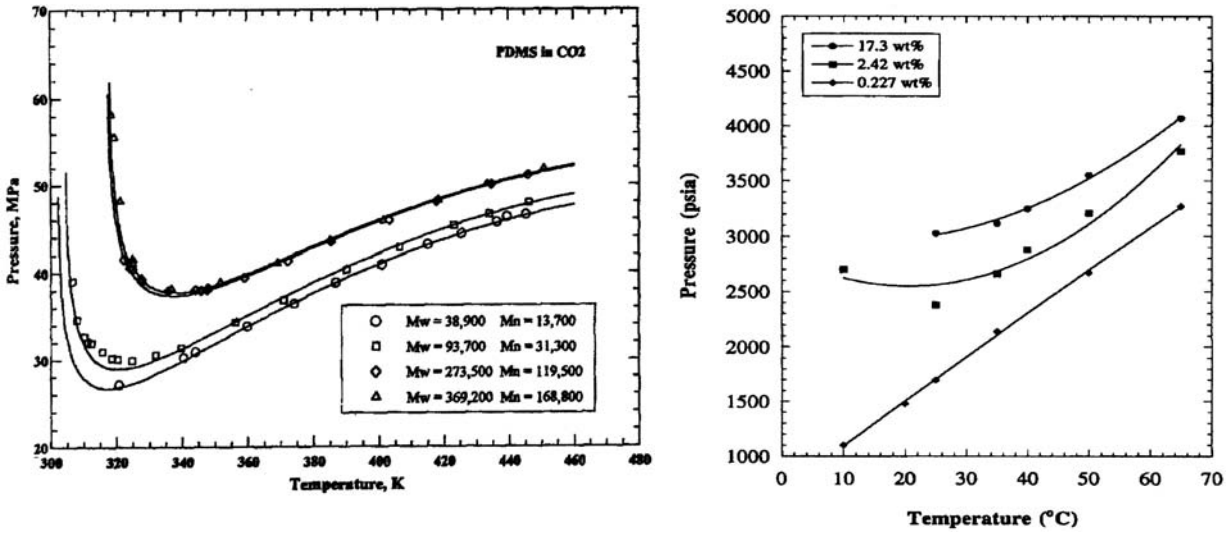

a b

Figure 5.2: Cloud point pressures of the PDMS homopolymer in CO_2 a) for a concentration of 5wt% at different molecular weights (M_w) and polydispersities (M_W/M_n) [192] and b) for a polymer of 13'000 g/mol at various concentrations [160].

From the results given in Figure 5.1, it is observed that the binary mixture PDMS-CO_2 is characterized by a type III phase behavior with respect to the classification given in chapter 1. Literature data of cloud points for similar concentrations and molecular weights as the one studied here are not available. Thus the direct comparison is impossible. Nevertheless, from

Figure 5.1 and 5.2 a, it can be observed that depending on the molecular weight of the PDMS different types of phase behavior are exhibited. The results of the cloud point measurements given in Figure 5.2 a demonstrate that as soon as the difference in molecule size between the PDMS (40'000 g/mol) and the CO_2 increases drastically the phase behavior shift from a type III to a type IV phase behavior, where the upper and lower critical solution temperature curves merge. Hence, this behavior is expected when the properties of the mixture constituents become more and more dissimilar. At low temperature, the system will reach a region where much higher pressures are required to solubilize the PDMS. With a polymer of 5000 g/mol and a narrow molecular weight distribution of 1.11, the molecular asymmetry between the PDMS and CO_2 is decreased. This can explain why a type III phase behavior is observed in Figure 5.1. A lower molecular weight polymer favors greatly the entropic contribution of the Gibbs energy that governs the solubility of a compound in a mixture. When the difference in free volume between the species is lowered, this favors their random rearrangement in space and thus their mixing. Respect to the Gibbs energy law, the entropic contribution is expected to become more and more important at elevated temperature. Moreover, when the chain length of the polymer is smaller, it is expected that the small molecules of carbon dioxide can interact better with the polymer segments leading to an increase of the enthalpic contribution of the solubility.

From the result given in Figure 5.3, it can be observed that the LLV curve of the PDMS-CO_2 mixture is superimposed to the LV curve of the pure CO_2:

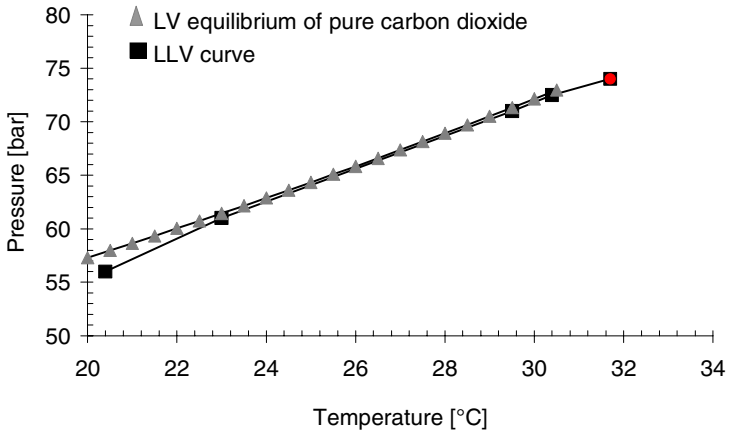

Figure 5.3: Comparison of the LLV measured pressure for the PDMS mMA-CO_2 system and the predicted vapor pressure of pure carbon dioxide [27] at a density of 469 kg/m^3.

Therefore, this means that the presence of the PDMS in the mixture does not really affect the liquid vapor equilibrium of the pure carbon dioxide. Actually, this can be easily explained by the fact that the PDMS, being a polymeric compound, has a negligible vapor pressure. Hence, the LLV curve of a polymer-SCF mixture is expected to essentially superpose onto the vapor pressure of the solvent.[45] Moreover, a reddish orange opalescence typically observed at critical point (last point in the LLV curve in Figure 5.1) has been observed in the binary mixture at 31.7°C and 74 bar. This point corresponds exactly to the location of the critical point expected for pure carbon dioxide. At this point, a liquid and a vapor phase merge critically. This tends to demonstrate that the carbon dioxide forms a supercritical phase (fluid phase) in equilibrium with a liquid phase expected to be composed mainly of the PDMS. An important remark has to be now added. When a fluid phase is reached in a polymer-SCF mixture, this means that the polymer is soluble in the SCF phase, but this does not mean that the polymer itself is in a supercritical state. Obviously, all the previous explanations could be even more supported if analytic phase compositions would be available.

In a sealed system when the temperature is continuously increased close to the critical point of the component or mixture the liquid gradually turns into gas raising the density of the gas phase. At the same time the density of the liquid phase decreases till the critical point is reached where the two phases have exactly the same density. In that critical state, the fluid is continually fluctuating between gas and liquid. Because of the very large compressibility, these density fluctuations are particularly pronounced near the critical point. If the order of magnitude of the fluctuations is the same than that of the wavelength of visible light or higher, scattering of the light leads to critical opalescence, which may be apparent as a clouding or coloration of the system.

5.2 MMA cosolvent effect

In order to analyze the effect of the monomer on the phase envelope of the PDMS-CO_2 system, cloud point measurements have been realized for the ternary mixture MMA-CO_2-PDMS at similar concentrations to those used in the dispersion polymerizations.

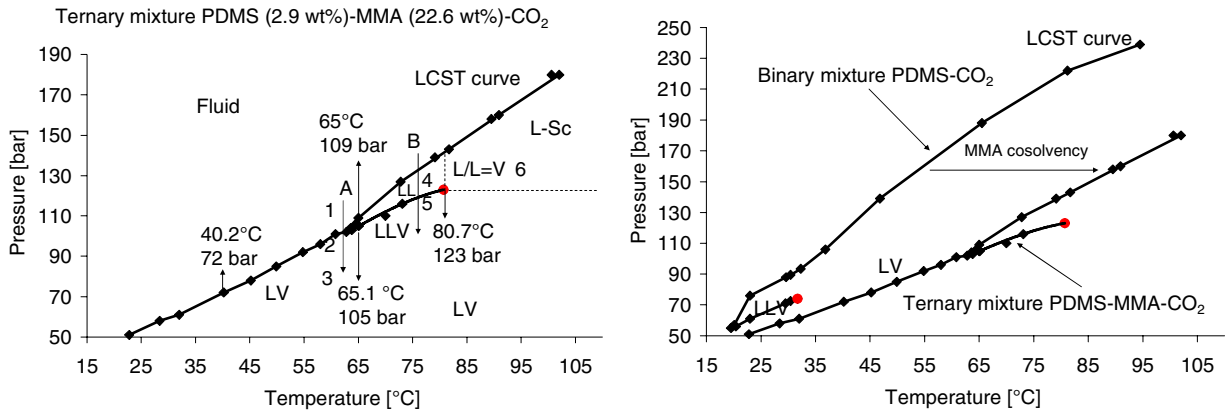

a b

Figure 5.4 : a) Cloud point measurements of the ternary mixture MMA-CO_2-PDMS and b) comparison of the P-T phase diagram between the binary mixture and the ternary mixture.

Figure 5.4 a and b show the effect on the phase diagram of the presence of the monomer in the mixture of PDMS-CO_2. It is observed that the monomer acts as a cosolvent leading to a reduction of the measured cloud point pressures and thus increasing the fluid domain. O'Neill *et al.* have reported that the addition of MMA in a CO_2-PDMS mMA (10'000 g/mol) mixture results in a reduction in the phase separation pressure of ≈ 6 bar/wt% MMA added, indicating that MMA is a cosolvent for the PDMS.[57] They have measured a cloud point for the ternary mixture of composition approximately PDMS-mMA (1.2wt%)-MMA (20wt%)-CO_2 at 65°C and 122 bar. These data can be compared with the measured cloud point at 65°C and 109 bar (Figure 5.4 a). The observed decrease in pressure in the presented results is approximately of 3.5 bar/wt% MMA added. The lower cloud point pressure observed can be explained by the lower MW of the PDMS. Moreover, the lower decrease in pressure with respect to the addition of the MMA can be explained by the fact that initially the CO_2 has shown to be a good solvent for the small chain length polymer. Therefore, the addition of the monomer helps to increase the solubility of the polymer but with a weaker influence than it would have been the case for a higher MW PDMS.

1 2 2 3

*Figure 5.5:*A *transition in Figure 5.4 a observed with the view cell; 1 = fluid phase, 2 = appearance of the vapor phase on the LV curve and 3 = liquid-vapor domain.*

Figure 5.5 shows the typical observations realized when crossing the liquid-vapor equilibrium curve. The presence of the gas phase (upper part of the cell, 2-3) is detected when the foggy or cloudy volutes start to appear.

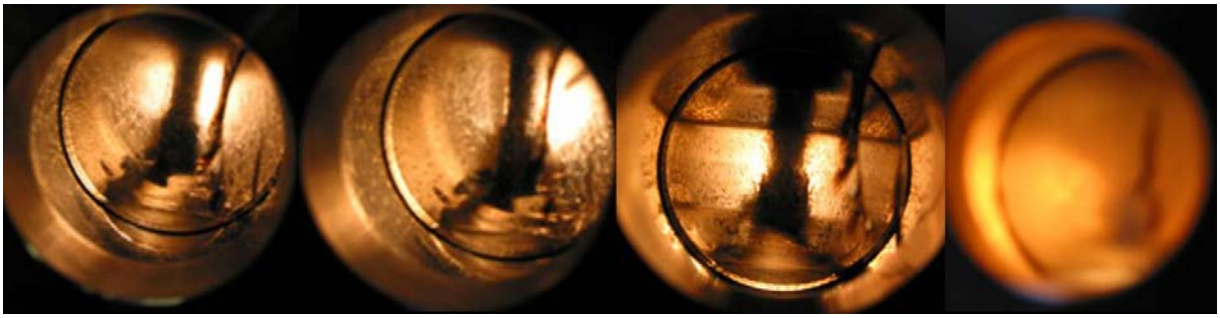

4 4 5 6

*Figure 5.6:*B *transition in Figure 5.4 a observed with the view cell; 4 = LL domain (second small phase at the bottom), 5 = LLV curve. 6 = L/(L=V) transition characterized by the critical opalescence.*

Figure 5.6 4 shows the precipitation of the PDMS at the bottom of the cell forming the second phase in the LL domain. The volume fraction is small due to the very small amount of stabilizer in the system. Figure 5.6 5 shows the observed transition on the LLV curve where three phases can be easily distinguished. Figure 5.6 6 shows the critical opalescence observed at 80.7°C and 123 bar (Figure 5.4 a) in the ternary system MMA-CO_2-PDMS.

The use of free monomer as a cosolvent in CO_2 is particularly interesting when working with vinyl polymer as the poly(methylmethacrylate) (PMMA); these polymers showing very poor solubility in CO_2. For example, PMMA does not dissolve in pure CO_2 at temperatures less than 250°C and pressures below 2500 bar. Byun *et al.* [193] have demonstrated that it is possible to dissolve polar acrylate polymers in supercritical CO_2 over a large temperature range at modest

pressures if the acrylate monomer is used as a cosolvent. They have observed (Figure 5.7 b) a similar phase behavior as the one shown in Figure 5.4 a in the case of the ternary mixture of poly(buthylmethacrylate) (PBMA)-CO_2-butyl methacrylate (BMA).

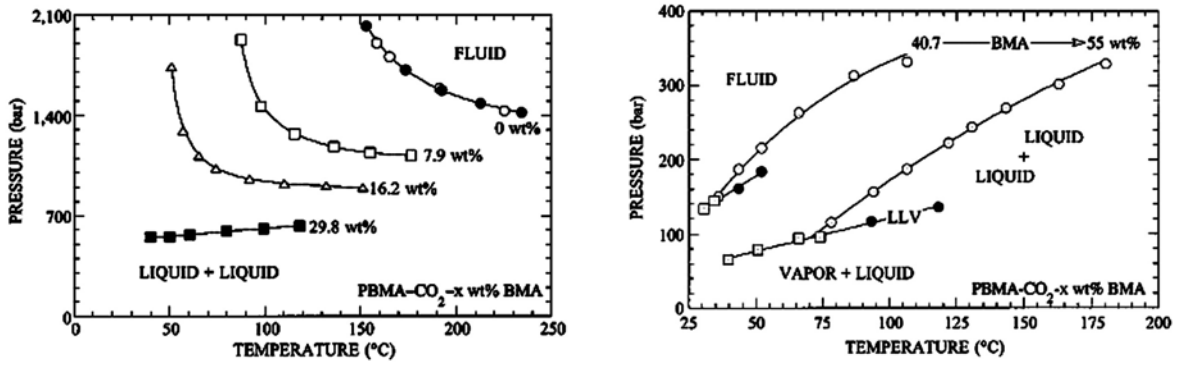

a B

Figure 5.7: Phase behavior of the PBMA-CO_2-BMA mixture at different concentrations of monomer and with a polymer of 320'000 g/mol and a polydispersity of 4.35.[193]

Figure 5.7 a shows that adding 16.2 wt% butyl methacrylate in a binary PBMA-CO_2 mixture can reduce the pressure from 2'100 bar up to 900 bar. In Figure 5.7 b, both 40.7wt% and 55.0%wt monomer curves exhibit a typical LCST type III phase behavior, as the one observed in the case of PDMS-CO_2-MMA ternary mixture. The comparison between Figure 5.7 a and b demonstrate that the addition of the monomer in the polymer-CO_2 mixture allows to shift the phase behavior from a type IV (0, 7.9 and 16.2 wt% monomer) to a type III (40.7 and 55 wt% monomer) phase behavior when enough monomer is added to the system.

Monomer can enhance the polymer solubility due to several factors. If the solvent is highly expanded, the addition of a dense, liquid cosolvent reduces the free volume difference between the polymer and the solvent. Interpreting the effect of a cosolvent added to a SCF solvent is slightly more complicated since increasing the system pressure reduces the free volume difference between the solvent and the polymer and it also modulates the probability of interactions between the polymer segments, the solvent and the cosolvent in solution. Studies reported in the literature have shown that cloud points monotonically decrease with pressure and temperature during the addition of polar solvent as long as the cosolvent does not form complexes with the polar repeat units of the polymer.[194-196] In these cases the cosolvency effect is directly related to the polar forces of attraction contributed by the cosolvent and the increase in solvent density. These explanations can be directly applied to the studied case. MMA increases the solubility of the PDMS because of the global increase of the density of the system. Moreover, the polarity of the MMA improves the solvent properties of the CO_2 for the PDMS. The last remark is clearly proved by the fact that at low temperatures (Figure 5.4 b), the transition from a LLV equilibrium in the binary mixture to a LV equilibrium in the ternary mixture is observed

when the MMA is added in the system. In other words, the presence of the monomer allows the complete solubility of the PDMS in the liquid CO_2 leading to the formation of a unique homogeneous liquid phase.

5.3 Isotherms of the binary mixture MMA-CO_2

It is interesting to compare the ternary mixture behavior with the P-x binary phase diagram of MMA in CO_2 as shown in Figure 5.8. For a MMA composition similar to the one of the ternary mixture (Figure 5.8 dotted line), the pressures corresponding to the isotherms of 65°C and 80°C are 105 and 120 bar, respectively. At 65.1°C and 105 bar and at 80.7°C and 123 bar, the ternary system is at both extremities of the LLV curve (Figure 5.4 a). Considering that the temperature and pressure deviations are included in the experimental error (visual observation of the transition), this again demonstrates that the presence of the PDMS in the liquid phase does not affect the vapor pressure of the system. But in the ternary system, the "solvent" is composed of CO_2 and MMA, the latter being volatile. Thus it is expected that the gas phase in the ternary system is mainly composed of MMA and CO_2. This means also that the vapor phase present on the LLV curve is in equilibrium with one liquid phase composed mainly by the MMA and the CO_2 and with another liquid phase composed mainly by the precipitated PDMS. The last remark is supported by the fact that the critical opalescence observed in the ternary system at 80.7 °C and 123 bar is very close the critical point observed in the binary system of MMA-CO_2 at 80°C and 118 bar. Again, considering that the temperature and pressure deviations are included in the experimental error (visual observation of the transition), the critical opalescence observed in the ternary mixture might be characterized by a critical transition of the liquid and vapor phases composed mainly by the MMA-CO_2 components. The PDMS becomes soluble in the supercritical phase only when the system reaches the cloud point pressure on the LCST curve.

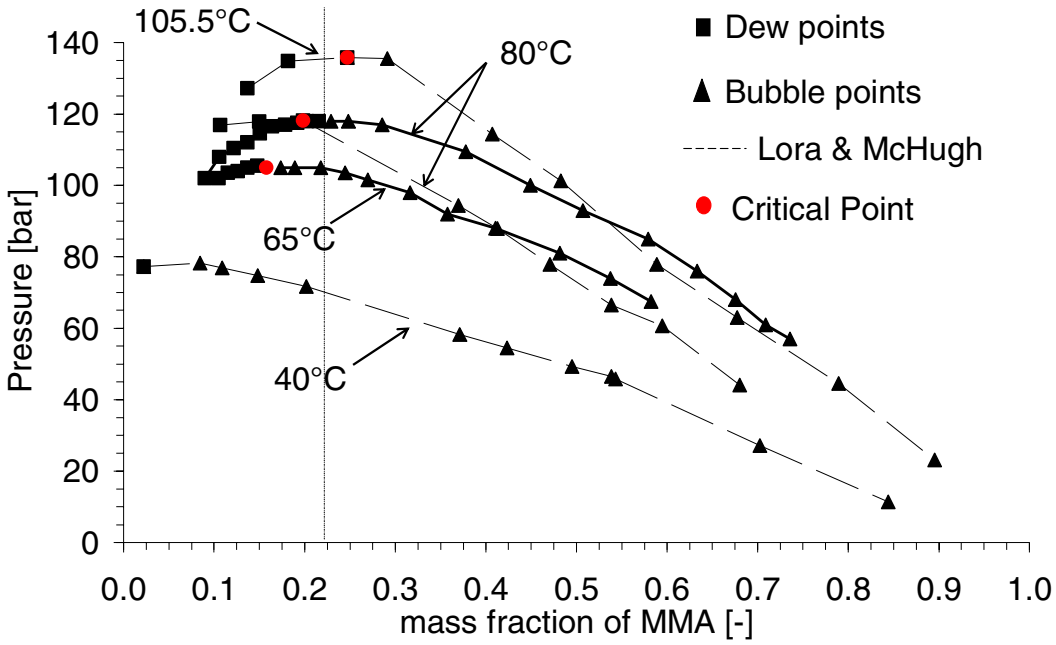

Figure 5.8 : P-x phase diagram of the binary mixture MMA-CO_2 for two different isotherms at 65°C and 80°C compared to the data obtained by Lora et al.[56] at 40, 80 and 105.5°C.

The shape of the isotherms in Figure 5.8 confirms that the MMA-CO_2 binary mixture has a type I phase behavior, characterized by the absence of demixing domains. Moreover, the measurements corroborate the results obtained by Lora *et al.*[56] But significant experimental deviations, even more pronounced at high MMA mass fraction, are observed between both data for the isotherm at 80°C. Lora *et al.* have estimated the following experimental inaccuracies for their measurements: ± 0.7 bar and ± 0.4°C and 1wt% for the mass fraction of MMA.

With the set up used in the discussed study, the experimental errors are estimated to be ± 1 bar for the pressure determined by the precision of the pressure transducer and ± 0.5°C for the temperature. The temperature deviation to its set point is related to the small cooling occurring during the decompression, required to observe the phase transitions. The inaccuracy in the composition of the mixture comes principally from the evaluation of the introduced amount of CO_2 and is estimated to be 2%, mainly due to the determination of the volume of the cell. The inaccuracy of the introduced amount of MMA can be neglected with respect to the error of the amount of CO_2. Therefore, the experimental error of the weight fraction of MMA can be estimated to be approximately 2%.

Despite the presence of experimental errors, even more pronounced in visual and subjective observation, this cannot explain the deviation of the data between both analyses. To understand the complexity of cloud point and phase transition measurements, it is very interesting to understand the phenomenon of phase separation:

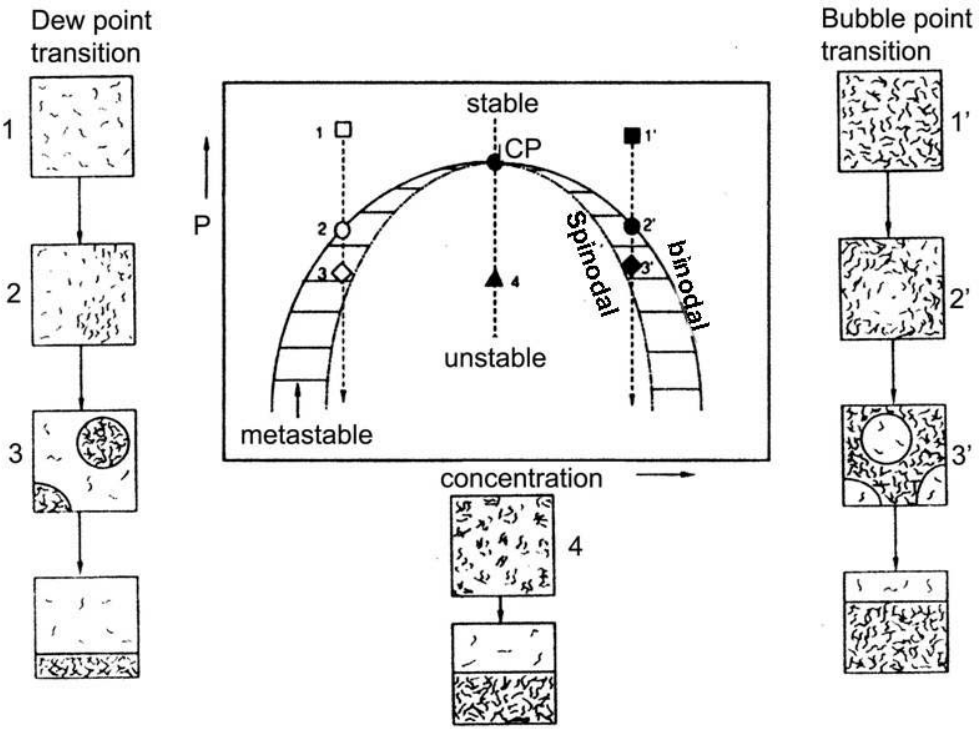

Figure 5.9: Schematic representation of a P-x binary phase diagram showing the mechanisms of spinodal separation and progressive nucleation.[197]

At critical points as well as at cloud points on the UCST and LCST curves for polymer-solvent systems, the phase separation is spontaneous and complete when coming from the homogeneous state (decrease in pressure). In Figure 5.9, the so-called binodal and spinodal curves define the envelopes that allow identifying the boundaries of three distinct domains, i.e. the one-phase, the metastable and the unstable regions. The region above the binodal is the stable one-phase region. The binodal curve gives the exact composition of the phases in equilibrium for small molecules. The region between the binodal and the spinodal envelopes represents the metastable region where the solution is stable to small fluctuations, but for large fluctuations undergoes demixing. Inside the spinodal envelope, all fluctuations result in a decrease of free energy and as a result, the solution is unstable and demixing is spontaneous. In the metastable region, nuclei of the new phase are formed and grow into dispersed droplets in the continuous

matrix of the other phase. This energy intensive demixing mechanism is known as the nucleation and growth mechanism. In general, crossing the binodal from a one to a two phase system is a necessary condition for demixing to occur, whereas crossing the spinodal is a sufficient condition for a spontaneous and irreversible demixing. At critical concentration, all fluctuations result in a decrease of free energy and as a result, the solution is unstable and demixing is spontaneous.[197, 198]

Lora and McHugh, as most of the scientists, define the transition points as the points where the mixture becomes so opaque that it is no longer possible to see the stir bar in the solution.[56] They have compared results obtained using this definition with results using laser light turbidity measurements where the cloud point is defined as the condition where a 90% decrease in the light transmitted through the solution occurs. They have concluded that the measurements obtained by both methods are identical within the reproducibility of the data. In this study, transition points are considered as soon as the second phase starts to appear. Taking into account the theoretical mechanism of phase separation, it is possible to understand the deviation between both measurements. At identical composition and temperature, Lora *et al.* have observed lower pressures than the one observed in this work for the points measured away from the critical point.[56] On the contrary, the measured critical point at 80°C in the binary mixture MMA-CO_2 exactly superposes with their result. At the critical point the transition is fast and can be determined without ambiguity. For the points measured far away from the critical point, the metastable region increases more and more. As explained previously, this means that the second phase can appear progressively over a certain pressure range when the perturbations (increased volume cell) is enough smooth. Moreover, in this domain the phase separation is not complete and only small manifestations of the second phase can be observed, as the cloudy volutes observed in Figure 5.5 2 for example.

Kuijpers *et al.*[199] has also noted that the P-x MMA-CO_2 data measured using two different apparatuses appear to be systematically at higher pressures than the one obtained by Lora *et al.*[56] and particularly for the points at high MMA concentration. An explanation for this difference is related to the construction of the view cell used by Lora *et al.* where the pressure transducer is mounted at the back side of the view cell.[56] Kuijpers has concluded that the deviation at low pressures could probably originate from the plunger apparatus being less accurate at low pressures due to friction during the pressure equilibration procedure.

All these remarks show that phase equilibrium measurements are complex and difficult. It is obvious that visual methods are interpreted subjectively by the observer. Nevertheless, it has to be noted that, despite the deviations observed, the trend stays the same on an acceptable range to define experimental conditions. This highlights the crucial purpose of having more complete

data banks on the phase equilibria of SCF mixtures in order to promote supercritical fluid processes and determine the most efficient operating conditions. Moreover, it should be always kept in mind that it is not trivial to develop apparatuses for high pressure analysis.

The results presented in this chapter have shown that the low MW PDMS macromonomer, used as stabilizer in the dispersion polymerization of MMA in $scCO_2$, exhibits a relatively good solubility in carbon dioxide due to its small chain length. It has been demonstrated that the molecular weight of the stabilizer can greatly influence the phase envelopes of the polymer-CO_2 mixture. Decreasing the MW leads to an increase in solubility of the stabilizer or more generally of the polymeric compound. On the other hand, this advantage has to be balanced with the fact that the chain length of the stabilizer is a key parameter that controls the sterical stabilization mechanism of the growing particles in a dispersion polymerization. This means that a compromise between the solubility of the dispersant and the efficiency of the stabilization has to be found.

The results have shown that the presence of the monomer influences significantly the solubility of the stabilizer in the CO_2 mixture. If it is considered that during a dispersion polymerization the composition of each phase changes as a function of the monomer conversion, it is therefore expected that the solubility of the stabilizer in the mixture will also change. This means that it might be insufficient to know the phase envelope given by the cloud point locations for the initial composition, because the phase behavior will change as the polymerization proceeds. This last remark will be supported by the results of the stability of the dispersion polymerization of MMA in $scCO_2$ realized with different monomer concentrations (see subchapter 6.4).

6 Polymerization of MMA in $scCO_2$: Results and Modeling

6.1 Calorimetric monitoring of dispersion polymerizations in $scCO_2$

Continuous process monitoring is a fundamental requirement for process control. The conversion, corresponding in a batch process as the weight of polymer produced respect to the initial monomer feed, is a key variable to follow the evolution of the reacting system. The conversion monitoring permits to control the reproducibility of the reaction conditions and to have direct information of the effect of experimental variables (concentration, pressure, temperature) on the course of the reactions. Monomer conversion is often determined by sampling and by quantitatively analyzing the monomer content in the polymer sample. Such methods are invasive method, tedious and time consuming.

Thanks to an adapted heat balance around the reaction calorimeter, the monomer conversion profile and the global rate of polymerization can be determined using thermal data, without perturbing the system. The heat generation rate, measured on-line, allows the reaction monitoring in real time. In this chapter, the accuracy and the reproducibility of the results obtained by the use of the reaction calorimeter especially developed for supercritical fluid applications are discussed.

The effects on the dispersion polymerization of MMA in $scCO_2$ of the operating parameters, such as temperature, impeller type, stirring speed and stabilizer concentration, are investigated. Results comparison is based on the measurements of molecular weight (MW), molecular weight distribution (MWD), particle size (PS), particle size distribution (PSD), and product morphology of the produced polymer. Using the on-line calorimetric monitoring, the influence of experimental variables on the global rate of the dispersion polymerization can be evaluated.

6.1.1 Temperature effect

In order to use reaction calorimetry and heat flow measurements to study and control the dispersion polymerization of MMA in $scCO_2$, it is necessary to satisfy two limiting conditions. A thermal and concentration homogeneity is required and is satisfied by the use of an efficient mixing. Moreover, the reactant concentrations and the rate of reaction have to be sufficiently high and fast, respectively, in order to obtain a detectable and analyzable thermal signal.

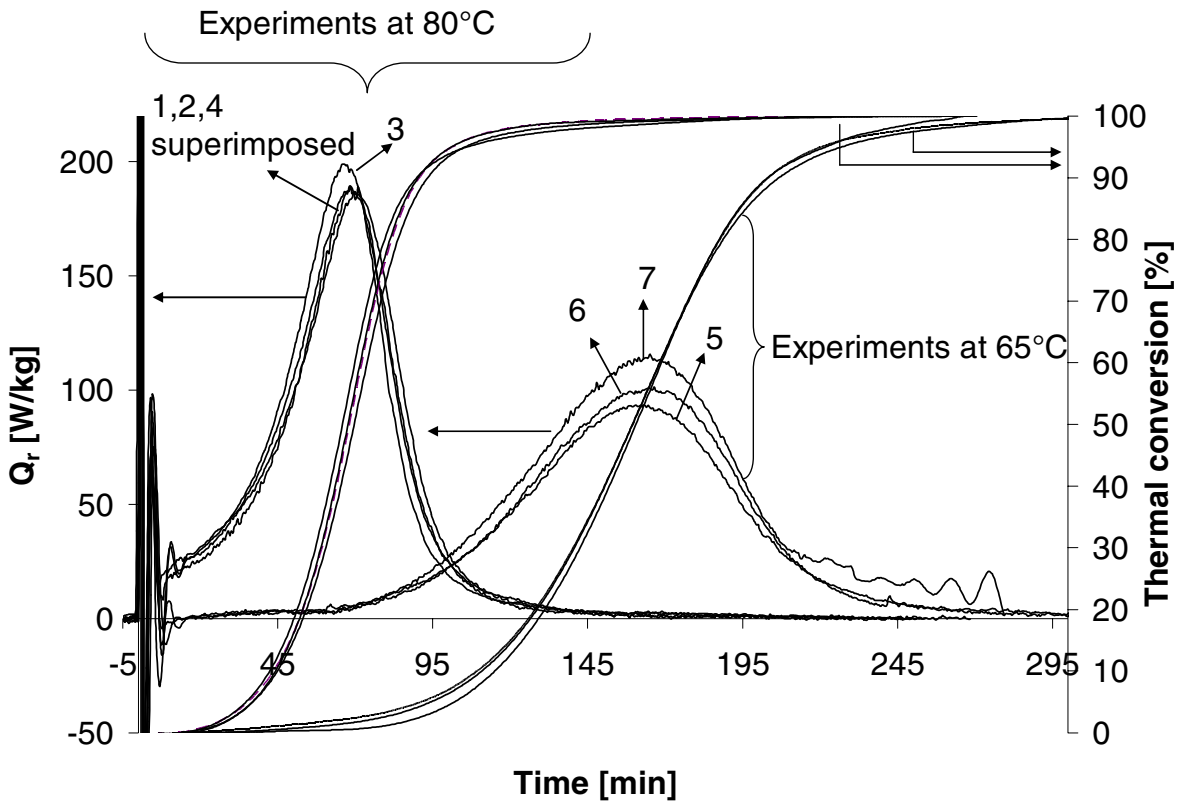

Figure 6.1: Heat generation rate, Q_r, and thermal conversion measured for dispersion polymerizations of MMA in $scCO_2$ at 65°C and 80°C, using the two-stage turbine and the Ekato MIG® impellers at 400 rpm.

Figure 6.1 shows the thermograms obtained for dispersion polymerizations of MMA in $scCO_2$ realized at 65°C and 80°C with 10wt% PDMS macromonomer/MMA, 30wt% MMA/CO_2 and 1wt% AIBN/MMA.

The initial peak observed in the thermal curve at $t = 0$ is due to the dosing of the 50 ml monomer-initiator solution. The pressure required by the syringe pump to introduce the reactant under pressure leads to an increase in pressure inside the reactor of 40 bar. When the pressure is increased in a closed system the temperature increases at the same time. This corresponds to the observed exothermic peak. The temperature in the reactor increases approximately of less than a tenth of degree as shown in Figure 6.2 a. Preliminary experiments realized to control the temperature of the dosed reactants by the use of a micro heat exchanger (Annex 3) are shown in Figure 6.2 b. The results show that neither the cooling (5°C) nor the heating (65°C) of the reactants leads to a better temperature control at the dosing step (Figure 6.2 b). This confirms that in the high pressure closed vessel the temperature increases due to the increase in pressure during the dosing step.

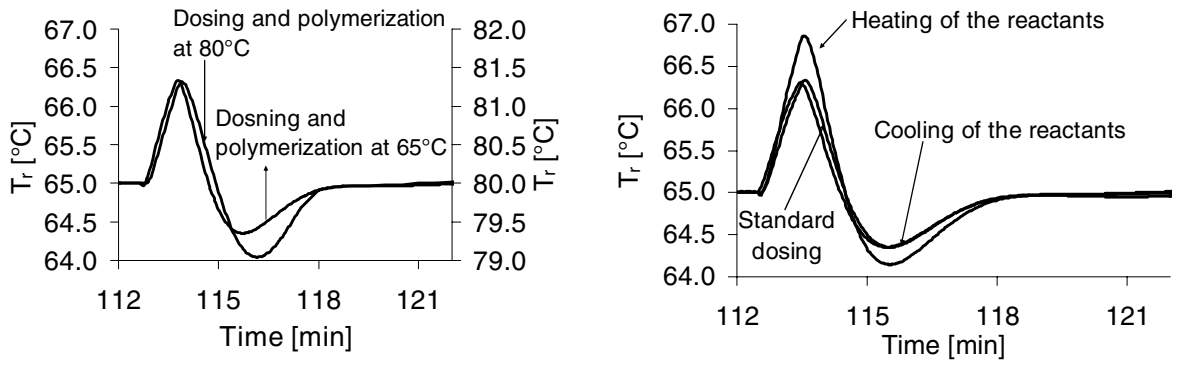

a b

Figure 6.2 a) Dosing effect on the reactor temperature for experiments realized at 65°C and 80°C, b) Effect of the dosing on the reactor temperature using a micro heat exchanger (Annex 3) to control the temperature of the added reactants.

In Figure 6.1, the measured thermal conversions show that the shape of the time-conversion curve is sigmoid as expected for dispersion polymerizations.[200] Fehrenbacher *et al.* have studied the behavior of the dispersion polymerization of MMA in $scCO_2$ for a conversion below than 0.1%.[95, 111] They have shown that, in the early stage of the polymerization, the polymerization takes place in the homogeneous phase (CO_2-rich phase) and polymerization within the particles does not play any significant role, explaining the initial low rate of polymerization. The polymer generated in the homogeneous phase precipitates when the molecular weight exceeds a given value. In a later stage, when larger particles are present and when the monomer concentration in the homogeneous phase has decreased considerably, the polymerization takes place within the polymer-rich particles. The fact that the conversion reveals an auto-acceleration of the polymerization rate at increasing conversion indicates that diffusion limitations are operative in the system. It is therefore expected to observe a gel effect (Trommsdorf or Norrish-Smith effect) occurring during the polymerization. Many authors have already studied this effect some decades ago.[201-204] This effect corresponds to an auto-acceleration of the global rate of polymerization and is particularly marked in bulk polymerization of MMA or can be pronounced in solution polymerization with an initial high monomer concentration. The gel effect has been shown to be the result of a decrease in the termination rate as the viscosity of the polymerization medium increases. Although the diffusion of monomer is still possible within the increasingly viscous medium, the diffusion of the much larger growing polymer radicals is considerably retarded and makes them much less likely to terminate with each other. Therefore, although the propagation of polymer is largely unhindered under these conditions, the termination rate is considerably reduced. The quantity $k_p/k_t^{0.5}$ (see equation 6.1), thus increases with a resulting increase of the overall rate of polymerization. The tailing-off of the conversion observed in Figure 6.1 corresponds to a gradual diminution in the residual monomer concentration.

$$R_p = k_p \cdot \left[2f \cdot \frac{k_d}{k_t} \right]^{0.5} \cdot [I]^{0.5} \cdot [M] \qquad 6.1$$

The observed increase in the molecular weight (Figure 6.3 b) confirms that a kind of gel effect is present during the polymerization, as shown by many authors for dispersion polymerizations in $scCO_2$.[94, 99] This situation is similar to what is typically observed in dispersion polymerization in common organic solvents where a gel effect occurs for a conversion between 20 and 80%.[93]

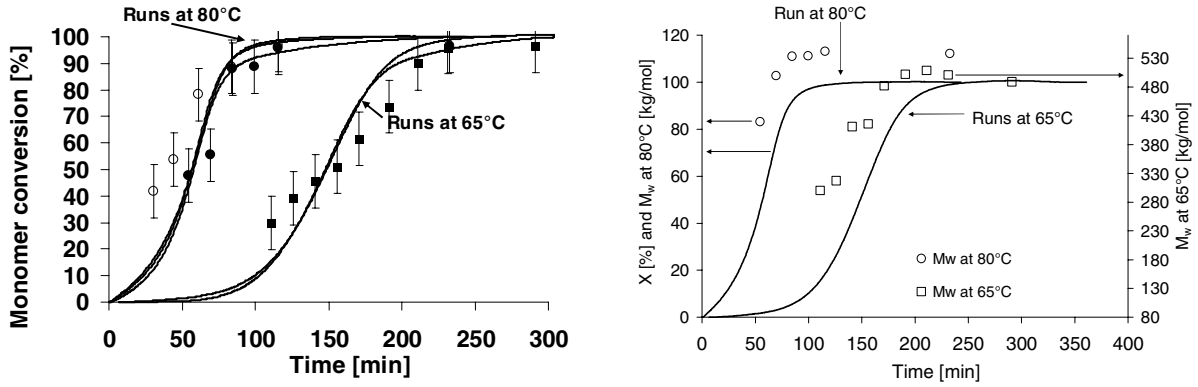

a b

Figure 6.3: a) Comparison between thermal conversion and off-line gravimetric monomer conversion and b) evolution of the molecular weight versus time.

In order to validate the heat balance model established for the SC reaction calorimeter, off-line gravimetric monomer conversion analyses were realized using the sampling method described in chapter 4. The analytical method of head space gas chromatography (HSGC) is an accurate technique for the evaluation of the monomer content in polymer samples. Nevertheless, important sources of experimental errors are related to the difficulty to recover the whole monomer content within a sample during the depressurization step. Some MMA can be lost during the CO_2 venting and bubbling in the DMF solvent. Moreover, the final MMA evaluation is dependent on the precision of the solvent (DMF) amount used in each step for the sample treatment (1-1.5g) and recovery. Therefore, it appears that at low monomer conversion (below 30%) the HSGC measurements are not representative of the collected samples. As the total sample amount required for complete analysis is around 10 grams (respect to 278 g without the CO_2 content), it can be considered that the composition of the reacting medium is maintained constant throughout the reaction. Despite the previous remarks, the sampling under pressure clearly corroborates the profile of the measured thermal conversion. Respect to the experimental errors, the thermal conversion should be obviously preferred to the off-line sampling method.

The advantage of the off-line sampling is related to the possibility to measure the molecular weight evolution as a function of conversion (Figure 6.3 b).

Based on the thermal conversion and on the knowledge of the total amount of polymer produced, it is possible to calculate the global rate of the polymerization defined as the average weight of polymer produced per minute in one liter vessel:

$R_p = 0.92$[g/l/min] at 65°C
$R_p = 1.27$ [g/l/min] at 80°C

Barrett *et al.* have reported kinetic results obtained by differential scanning calorimetry of the dispersion polymerization of methyl methacrylate in n-dodecane.[200] They have measured the thermal conversion for a mixture composed of 0.5wt% AIBN, 2.5wt% stabilizer and 20wt % MMA. In Figure 6.1, the composition of the dispersion polymerization with respect to the total weight is 0.23wt% AIBN, 2.3wt% stabilizer and 23wt% monomer. In the organic medium, it takes approximately 110 minutes at 80°C to reach a conversion as high as the one obtained in the presented study after 153 minutes. It can be expected that chemically controlled reactions are only moderately affected by the presence of CO_2, whereas CO_2 might have an impact on the diffusion-limited reactions.[205] However, the comparison tends to demonstrate that the use of CO_2 does not influence significantly the reaction in term of global kinetics.

Table 6.1: Summary of the data of the experiments shown in Figure 6.1.

No	T [°C]	P [bar]	Stirrer	X [c] [%]	$\Delta_r H$ [kJ/mol]	MW[d] [kg/mol]	PDI[e] [-]	D(v,0.9)[f] [μm]
1	80	302	DT[a]	95	-56.3	109	2.3	1.98
2	80	301	DT	94	-57.2	104	2.3	-
3	80	273	MIG[b]	93	-56.7	118	2.3	2.06
4	80	283	MIG	93	-56.0	115	2.4	-
5	65	260	DT	94	-55.0	428	2.9	-
6	65	281	DT	95	-55.8	465	2.2	-
7	65	220	MIG	94	-	495	2.9	-

a = two-stage turbine, b = three-stage Ekato MIG®, c = gravimetric monomer conversion after 5 hours experiment, d = weight molecular weight, e = polydispersity, f = 90% of particles have a size below the D(v,0.9) value, stirring speed = 400 rpm.

Figure 6.1 shows that the reaction calorimeter gives very reproducible results and no significant difference is observed between the two impellers used, i.e. the two-stage turbine and the three-stage Ekato MIG®. The average enthalpy of polymerization calculated is -55.5 kJ/mol with a standard deviation of ± 1.4 kJ/mol and an average relative error of 4%. Therefore, the calculated values are in very good agreement with the literature data of -57.8 kJ/mol.[206]

These results contribute to prove the accuracy of the heat balance and the potential of the developed reaction calorimeter for supercritical fluid applications. Moreover, the results confirm the pertinence of the assumption that the propagation step is the main source of heat production. It is observed that for the polymerization realized with the three-stage Ekato MIG® at 65°C, the measurement of Q_r starts to be less accurate at high monomer conversion. In fact the control of the reactor temperature is very sensitive to small variation in temperature inside the reactor. If temperature instabilities are present in the system, the jacket tries to compensate the effect as much as possible. In terms of absolute values, the reactor temperature is maintained between 64.7 and 65.2°C, but the temperature instability is enough to perturb the jacket temperature control. Although the polymer quantity formed at 65°C and 80°C is identical, the volume fraction occupied by the polymer produced at 65°C is higher than the one at 80°C. Therefore, the filling of the reactor is not the same during the polymerization. This indicates that the apparent density of the powder produced at 65°C is lower than the one produced at 80°C. At 65 °C, more efficient stirring is required and the two-stage turbine appears to be more adapted in this case.

Optimal operating conditions are a compromise between calorimetric and synthetic requirements for the production of a high quality polymer. At 400 rpm, with both types of impellers and 10 wt% stabilizer respect to monomer, a white powder is produced at high monomer conversion, between 93 and 95%. The polymer has a high molecular weight of approximately 450 kg/mol and 100 kg/mol at 65°C and 80°C, respectively. The molecular weight (MW) obtained at 80°C is lower than the one obtained at 65°C, as expected, due to the higher rate of the initiator decomposition leading to a higher concentration of radicals and thus lower MW. Figure 6.4 shows the SEM images of the produced PMMA. The products exhibit a well defined particulate morphology with a particles diameter between 1-2 μm. The global rate of polymerization and product characteristics are corroborated by results reported in the literature for similar systems at 65°C.[57] The achievement of stability in sterically-stabilized colloidal dispersions depends, among others, on maintaining the particles at a sufficient distance from each other so they are beyond the effective range of their mutual attraction.[93] This means that the stabilizer should have at least a sufficient chain length to avoid the contact between particles. Hence, the results show that the molecular weight (chain length) of the 5'000 g/mol PDMS is sufficient to sterically stabilize the growing particles. Additionally, the concentration of the stabilizer adsorbed at the surface (surface coverage) is also a key parameter. In these experiments, the relatively important amount of stabilizer (10wt% with respect to monomer) contributes also in the stability of the dispersion.

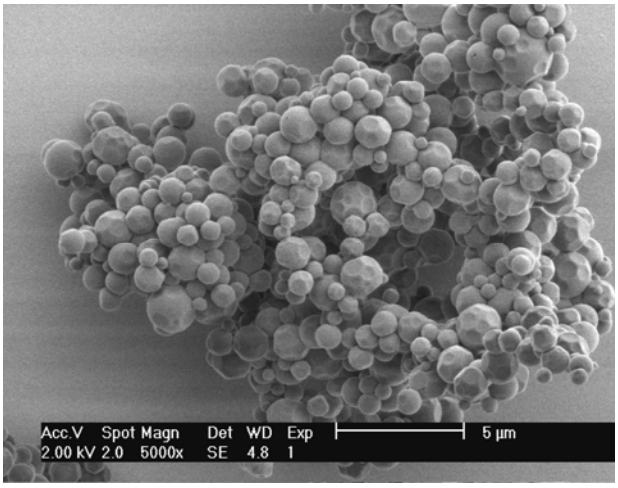

No 1. DT, 80°C

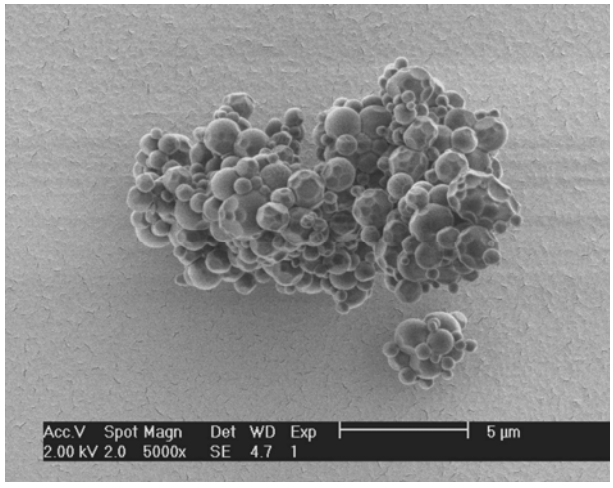

No 2. DT, 80°

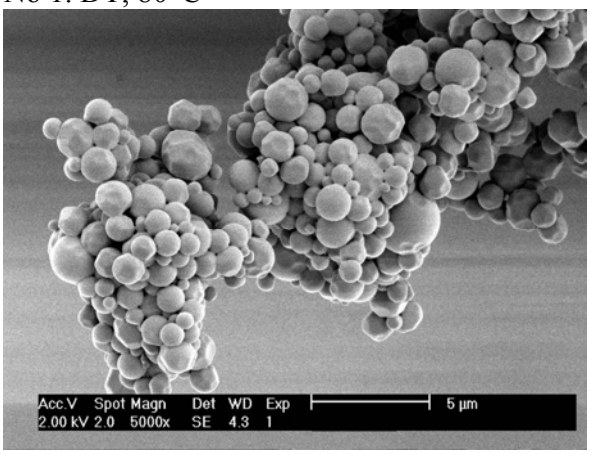

No 3. MIG, 80°C

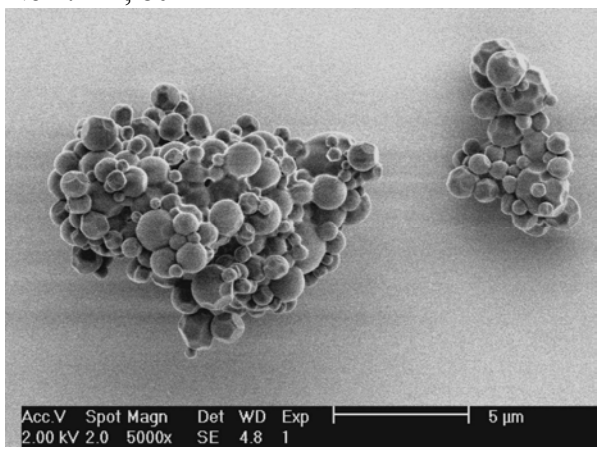

No 4. MIG, 80°C

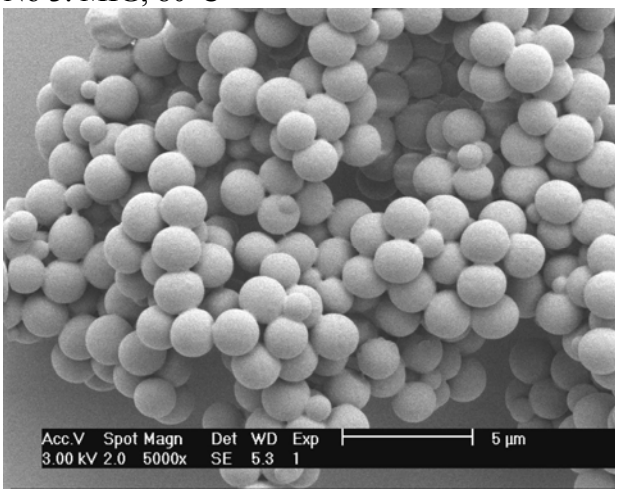

No 6. DT, 65°C

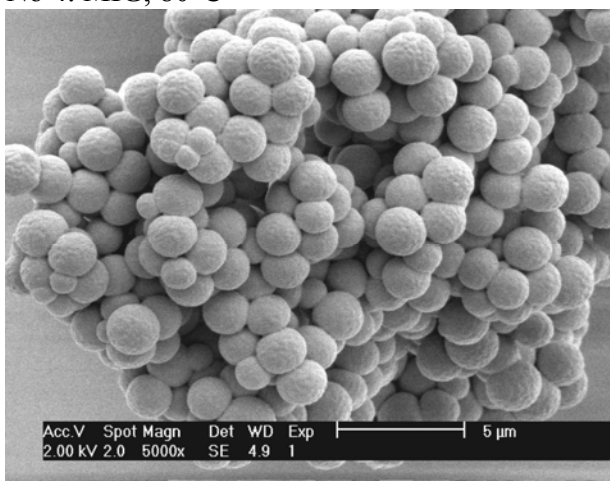

No 7. MIG, 65°C

Figure 6.4: SEM images for experiments summarized in Table 6.1.

Fehrenbacher *et al.*[95, 111] and O'Neill *et al.*[57, 94] have studied the particle formation and the particles growth regime at 65°C for the dispersion polymerization of MMA using a PDMS macromonomer (10'000 g/mol) as stabilizer using turbidity measurements. Experimental results and theoretical calculations tend to prove that the nucleation stage occurs at the very early stage of the polymerization leading to rather monodisperse particle size distribution (PSD). Hence, the particles are formed during a very short time and their number remains constant throughout the polymerization process. The growth then occurs for a much longer period. The steric stabilization by the macromonomer is the decisive factor that determines the critical diameter of the particles and hence their size. O'Neill *et al.* have concluded that the primary particles coagulate during the early stage of polymerization until a size is reached at which the stabilization of the particles is achieved through a sufficient coverage of the particles by macromonomer.[57, 94] After this period the number of the particles remains constant and further growth takes place by the controlled coagulation with smaller aggregates as well as by the polymerization within the stable particles. Fehrenbacher *et al.*, in their mechanism, have considered that the particles grow principally through precipitation of polymer onto their surface.[95, 111]

It can be observed in Figure 6.4 and 6.5 that the temperature has an effect on the particle size distribution (PSD) of the produced PMMA. At 65°C, a rather monodispersed PSD is observed. As discussed above, this indicates that the particles are formed within a short period of time and subsequent growth takes place without the formation of further particles and in the absence of agglomeration processes. At 80°C, a rather polydispersed PSD is observed with a fraction of particles having a diameter below 1 μm. Therefore, it seems that at 80°C the nucleation step is less uniform than at 65°C. Furthermore, it can be observed that, at the surface of the particles produced at 80°C, facets like golf balls are present. These facets appear to be the fingerprints of smaller particles (Figure 6.4 No 1). This tends to indicate that at 80°C the steric stabilization is such that contact between particles cannot be completely avoided. In dispersions, particle collisions can be either due to Brownian collisions or to collisions induced by large shear fields. In order to avoid particles collision and attraction, it is essential that the repulsive forces generated by the adsorbed stabilizer at the surface of the particles are not dissipated by other stress effects (thermal energy among others) that could lead to the desorption of the stabilizer chains from the particles surface. One has to consider that in certain cases the lateral chain mobility of the stabilizer is possible on the surface of particles. If this is combined with an incomplete adsorbed layer of polymer chains, the chains can be displaced sideways without generating any significant mutual lateral repulsion. Under these circumstances, particles can approach each other with negligible repulsive work and be in close contact. An explanation can also be found in the fact that at 80°C higher pressure can lead to an increase compression of the stabilizer chains at the particles surface and can force the contact between particles.

On the other hand, these explanations are in contradiction with the less uniform nucleation observed for the dispersions realized at 80°C (polydispersed particles). In fact, in many cases, the production of polydispersed powder can be due to an excess of stabilizer in the medium. If the stabilizer is present in excess at any stage of the polymerization, it can cause further nucleation to occur additionally to the initial crop of the particles produced at the beginning.

The understanding of the fundamental reasons for the differences observed between experiments at 65°C and 80°C would have required a thesis completely devoted to this subject. Nevertheless, as all the experiments discussed in this section were made at identical composition, the particle morphology and particle size distribution demonstrate clearly an effect of the temperature on the numerous parameters controlling the stability of dispersions and the particles formation.

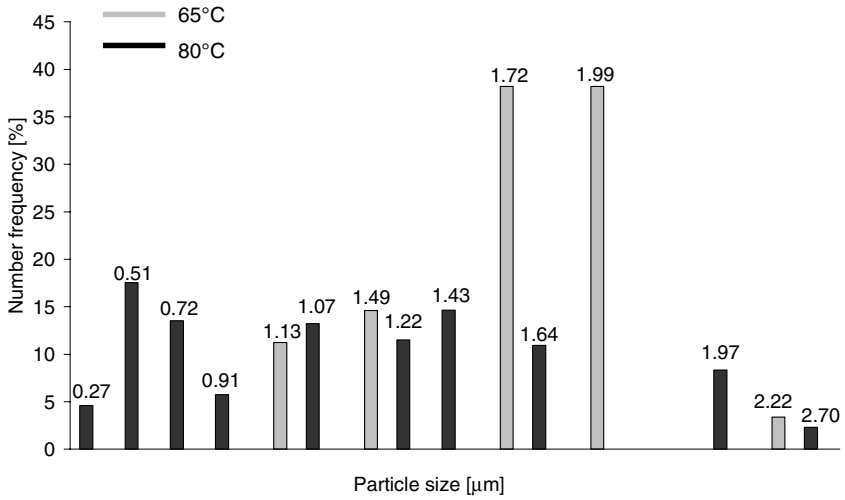

Figure 6.5: Particle size distribution of PMMA particles produced at 65°C (No 6, 100 particles counted) and at 80°C (No 1, 400 particles counted) obtained from SEM image analyses.

In Table 6.1, the results of PSD measurements by laser diffraction are shown in the last column. The parameter D(v,0.9) means that 90% of the particles have a diameter below the given value. Figure 6.6 shows the PSD measured for experiments at 65°C and 80°C. Generally, the typical accuracy of laser diffraction measurement for PSD determination is between 5%. By comparing Figure 6.4 (SEM images) and 6.6, one can conclude that the PSD measured by laser diffraction for experiments at 65°C are not representative of the analyzed powders. In fact, the most important factor for accurate PSD measurement by laser diffraction technique is the quality

of particles redispersion. All samples were redispersed in hexane and left 20 minutes in an ultrasonic bath. It appears that this treatment is not enough efficient to redisperse the powder produced at 65°C. The second mode presents in the measured PSD at 65°C (Figure 6.6 b) is of the typical size of agglomerates. For the powder produced at 80°C, the SEM micrographs corroborate the results obtained by laser diffraction. This tends to show that the particles produced at 65°C are more stacked together than the one produced at 80°C. Figure 6.5 shows the PSD distribution obtained from the SEM images for experiments at 80°C and 65°C. As discussed previously, the PSD measured by this method demonstrate that the PSD is narrower at 65°C and larger particles are formed.

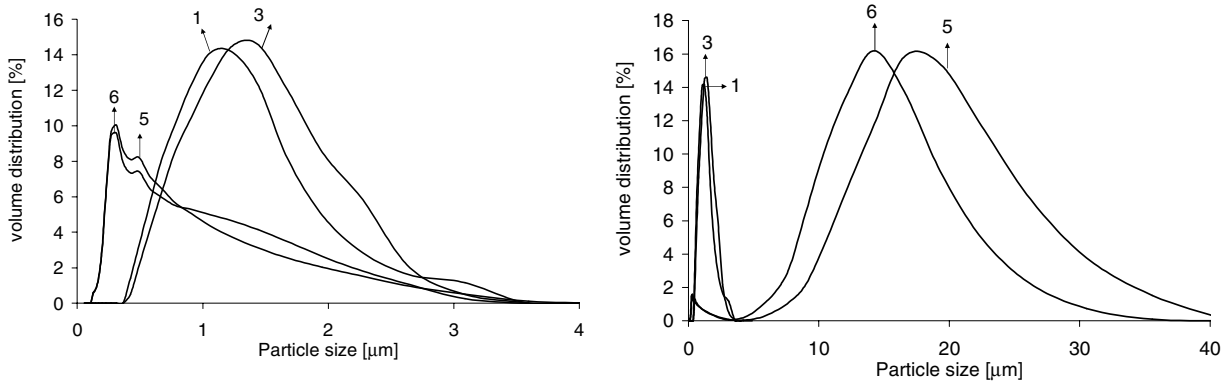

a b

Figure 6.6: a) Particle size distribution obtained by laser diffraction for dispersion polymerizations realized at 65°C (first mode) (No 5 and 6) and at 80°C (No 1 and 3) and b) particle size distribution showing the second mode measured at 65°C.

6.2 Pressure behavior and pressure effect

Figure 6.7 shows the pressure profile observed during the dispersion polymerization of MMA in $scCO_2$ at 65°C and 80°C.

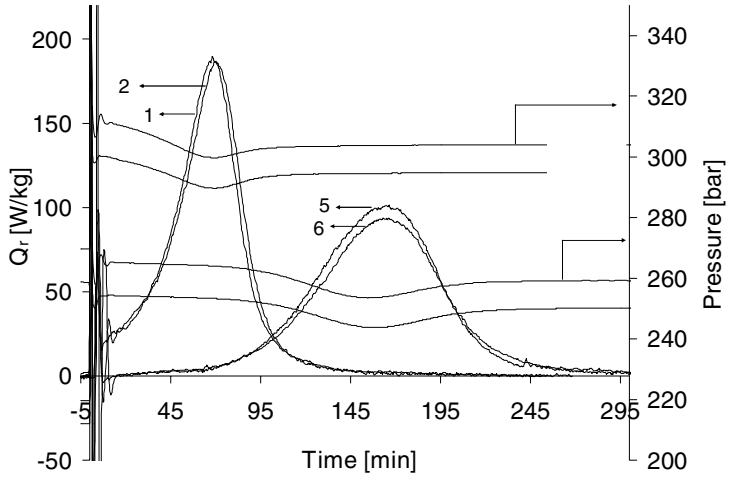

Figure 6.7: Typical pressure behavior observed during the dispersion polymerization of MMA in $scCO_2$ for experiments realized at 65°C and 80°C (Table 6.1).

As noted by Howdle *et al.*,[117] Figure 6.7 shows that the pressure can also be used to follow the course of the polymerization. When conversions are higher than 90%, the pressure reaches a plateau.

It is reported in the literature that either a decrease or an increase in pressure can be observed during a vinyl monomer polymerization in supercritical fluid. Hsiao *et al.,* in their study of the dispersion polymerizations of MMA in $scCO_2$ using the poly(FOA) as stabilizer, have observed a pressure drop for polymerizations conducted between 269 and 331 bar and an increase in pressure for polymerizations conducted at 145 and 193 bar.[99] The pressure drop can be easily explained by the fact that the molar volume of a vinyl monomer is expected to be higher than that of the unit in the subsequent polymer, thus leading to a volume contraction. Therefore, one might expect that the pressure should always decrease upon polymerization. This volume change is the basis for the use of dilatometry in the determination of polymerization rates in conventional liquid systems.[207] Lepilleur and Beckman have evaluated in their study the rate of the dispersion polymerization of MMA in $scCO_2$ directly from the change in pressure with time.[100] In their work, they have assumed that the pressure change can be also affected by the volume change upon mixing when considering in a non-ideal system. Hence, the non-ideal

behavior of the MMA-CO_2 mixture could lead to pressure increase. They have pointed out that at high pressure these non-ideal contributions are expected to become less important due to the decrease of CO_2 compressibility exhibiting therefore a liquid-like behavior.

In Figure 6.7, it is observed that the pressure starts to decrease and reaches a minimum 10 bar lower than the initial pressure. At 55% conversion, the pressure increases up to a value slightly lower than the initial one. As expected, the mixture behavior changes not only with respect to pressure but also with respect to composition. To understand the pressure behavior observed in Figure 6.7, the start point is to consider that the volume of mixing, ΔV_m, of a MMA-CO_2 mixture is expected to be negative.[100] Therefore, the initial high concentration of MMA in the mixture can lead to volume contraction as well as the polymerization itself, as discussed previously. As the concentration of MMA in the mixture decreases, it can be assumed that ΔV_m increases (move towards zero). This means that this contribution to the volume contraction decreases in the same way. This could explain why the pressure starts to increase when a certain conversion is reached. Furthermore, the quantity of the insoluble PMMA in the mixture increases and the particles produced start to occupy a non negligible volume fraction of the reactor.

It has to be kept in mind that the pressure is a very important operating parameter affecting phase equilibrium, solubility, carbon dioxide density and solvent power, and as a final consequence the stability of the dispersion, the polymerization loci and hence the product properties. As an example, Howdle *et al.* have reported that a decrease in pressure leads to a decrease in the molecular weight and in polymerization rate in the case of the precipitation polymerization of the vinylidene fluoride in $scCO_2$, attributed to the lower solubility of the PVDF in the monomer-CO_2 mixtures.[118]

6.3 Stirring effect

On commercial scale, stirring is essential to ensure thermal homogeneity and to avoid thermal runaway. Many authors have reported that the dispersion polymerization of MMA in $scCO_2$ can be destabilized under efficient stirring. Christian *et al.* have reported that, in the case of the dispersion polymerization of MMA using 10wt% of PDMS-mMA (10'000 g/mol), a low molecular weight (MW) tacky solid at low yield (31%) was obtained under stirring at 400 rpm in their 60 ml autoclave.[105] In the absence of any stirring, a white powder composed of spherical particles of PMMA of high MW at high monomer conversion (84%) was obtained. They have concluded that in the absence of stirring a passivating film of PMMA is formed on the inner surface of the autoclave inhibiting the contact of the growing radicals with the metal wall that can lead to premature termination. Rosell *et al.*, in their study of the free radical polymerization of MMA in $scCO_2$ using 1wt% Krytox^{TM} 157 FSL as stabilizer, have reported that an oily

product with low molecular weight at low monomer conversion was obtained at stirring speed of 400 rpm in their 500 ml autoclave.[103] In their system, the stirring speed has to be lowered up to 25 rpm in order to obtain a fluffy powder composed of PMMA with high MW at high monomer conversion. They have demonstrated that the mechanism responsible for the dispersion destabilization was a shear induced coagulation due to the weak interaction between the terminal acid functionality of the stabilizer and the ester group of the poly-MMA by hydrogen bond. In agreement with their remarks, most of the literature on dispersion polymerization report experiments realized in small autoclaves or view cells (2ml-60ml) with small magnetic stirring bar inducing a relatively low level of shear. Therefore, efficiency of stirring cannot be proved in these systems because when enough polymer is produced the stir bar is certainly not visible anymore.[103]

With respect to these observations, a study of the effect of impeller types and stirring speed was realized in the frame of the presented work. Firstly, it is interesting to understand from a theoretical point of view how stirrer type and stirring speed can affect dispersed systems.

The heat dissipated by mixing in a medium is given by the power equation:

$$P = Ne \cdot \rho_M \cdot n^3 \cdot {d_S}^5 \qquad 6.2$$

where Ne is the Newton number, ρ_M the density of the mixture, n the revolution frequency of the agitator and d_S the diameter of the agitator.

Newton number can be estimated using plots of the Newton number as a function of the Reynolds number, Re, available in the literature for common media and established for a variety of different types of stirrer operating with Newtonian fluids.[153, 154]

$$\mathrm{Re} = \frac{\rho_M \cdot n \cdot {d_S}^2}{\eta_M} \qquad 6.3$$

where η_M is the dynamic viscosity of the medium.

The first question is to define whether or not a dispersion polymerization can be treated as a Newtonian fluid, i.e. a fluid that has a constant viscosity at all shear rates at constant temperature and pressure. Barrett, in his book treating the dispersion polymerization in organic media, has demonstrated that dispersions of intermediate range of particle concentrations, between 4 to 40% phase volume can still be treated as Newtonian fluid under normal shear

rates.[93] In the typical experiments presented, the volume percent of polymer is around 20 V/V%. Hence, Newtonian behavior can be considered.

Because Newton plots are not available for supercritical media characterized by low viscosity and elevated Re, the values of the Newton number given by the supplier are used in the calculation of equation 6.2, i.e.4.6 and 0.55 for the two-stage turbine and the Ekato MIG, respectively.[208] The estimated dissipated energies at 400 rpm are 0.14 W and 0.09 W for the two-stage turbine and the Ekato MIG, respectively, using an average density of 1000 kg/m^3. The values calculated using equation 6.2 are one order of magnitude lower than the values measured by isothermal calorimetry, i.e. 3.2 W and 2.2 W respectively for the two-stage turbine and the Ekato MIG, respectively.[23] Nevertehless, both evaluations indicate that the turbine disperses higher mechanical energy (higher shear forces) to the medium than the Ekato MIG. Taking into account a representative viscosity of supercritical fluid of $5.2 \cdot 10^{-5}$ kg/m/s , typical values of the Reynolds number at 400 rpm are higher than 10^5, corresponding to a turbulent regime.

From the power transferred into the dispersed medium, the average energy dissipation per unit of mass, ε_{av}, can be estimated by:

$$\varepsilon_{av} = \frac{P}{m} \qquad 6.4$$

This parameter allows evaluating the Kolmogorov microscale of turbulence, L :[209]

$$L = \left(\frac{\eta^3}{\varepsilon_{av}} \right)^{1/4} \qquad 6.5$$

Taking into account the power calculated using equation 6.2 and 1 kg product, the Kolmogorov microscale is equal to 1000 µm. The Kolmogorov theory denotes the eddies microscale where viscous forces begin to have a noticeable effect on the motion of a fluid. The calculation shows that the particles (1-2 µm) have a diameter smaller than the Kolmogorov microscale. In this theory, if the particles are smaller than this microscale, then they are not susceptible to shear forces that could be the source of agglomeration and coagulation processes as for particles break up.

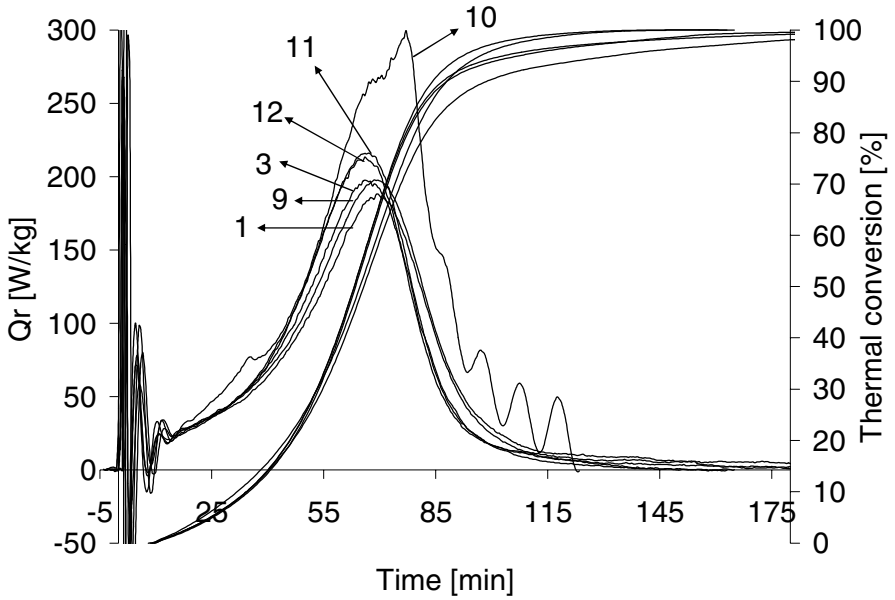

Figure 6.8: Heat generation rate, Q_r, and thermal conversion for dispersion polymerizations at 80°C realized for different stirring speed (200, 400, 600 rpm), data given in Table 6.2.

Figure 6.8 shows the thermograms obtained for dispersion polymerizations realized at 80°C with the same recipe at different stirring speed with both studied impellers. The data of the experiments are given in Table 6.2. In terms of calorimetric signals, no significant effects are observed between measurements at 400 and 600 rpm. It is difficult to explain why the measurements at 600 rpm with the Ekato MIG show higher reproducible maxima. On the other hand, it is observed that at 200 rpm for both stirrers (curve shown only for an experiment realized with the MIG), the mixing is too weak leading to thermal inhomogeneity and inefficient reactor temperature control. In this case, the evaluation of the overall heat transfer coefficient, U, at the end of the polymerization, used to evaluate the heat generation rate and the baseline, becomes inaccurate. With respect to the observation highlighted in subchapter 6.1, the experiment No 13 in Table 6.2 has been made to evaluate the possibility to maintain the thermal control of the dispersion polymerization at 65°C with the Ekato MIG at 600 rpm (curve not shown). The results have shown that with this stirrer it is not possible to obtain a perfect thermal control of the polymerization at 65°C neither at 400 rpm nor at 600 rpm. In fact, the Ekato MIG® is an impeller developed for the mixing of heterogeneous systems when minimized shear forces are required and it was especially used for that purpose. In counter part, in chapter 6.1 Figure 6.1, we have seen that at 400 rpm and 65°C the use of the two-stage turbine leads to a perfect reactor control, meaning that the latter has a better capability to homogenize the reactor content because it provides a more efficient mixing (higher dissipated energy).

Table 6.2: Summary of the experiments shown in Figure 6.8.

No	T [°C]	P [bar]	Stirrer	[rpm]	X [c] [%]	$\Delta_r H$ [kJ/mol]	MW[d]/PDI[e] [kg/mol]/[-]	D(v,0.9)[f]	PDMS[g] [%]
8	80	277	DT[a]	200	90	-	110 / 2.3	1.83	4.4
1	80	302	DT	400	93	-56.3	109 / 2.3	1.98	5.1
9	80	294	DT	600	93	-58.6	112 / 2.2	2.14	5.5
10	80	260	MIG[b]	200	95	-	114 / 2.5	1.40	3.7
3	80	273	MIG	400	93	-56.1	118 / 2.3	2.06	4.3
11	80	265	MIG	600	94	-57.6	116 / 2.2	-	4.8
12	80	265	MIG	600	95	-57.5	124 / 2.3	2.10	4.3
13	65	230	MIG	600	94	-	482 / 2.3	-	-

Composition: **10wt% PDMS/MMA, 30wt% MMA/CO_2 and 1 wt% AIBN/MMA**, a = two-stage turbine, b = three-stage Ekato MIG®, c = gravimetric monomer conversion after 5 hours experiment, d =molecular weight, e = polydispersity, f = 90% of particles have a size below the D(v,0.9) value, g= percentage of the PDMS incorporated with respect with the total weight of polymer collected.

The measured MW and the observed PSD (Figure 6.9 and 6.10) show that neither the stirring speed nor the impeller type affects significantly the product quality of the PMMA produced, despite the fact that the PSD measured by laser diffraction tend to show a slight increase in particle size as a function of stirring speed. In summary, the dispersion polymerizations characterized by a compositions of 10 wt% PDMS/MMA, 30 wt% MMA/CO_2 and 1wt% AIBN/MMA are insensitive to shear forces and the stabilization is maintained on the range of the studied operating conditions. As demonstrated by Barrett, from practical experience and theoretical point of view, when an entire and complete barrier of soluble chains of sufficient dimensions can be irreversibly maintained at the surface of the particles, steric stabilization produces an unconditionally stable dispersed systems whatever the magnitude of the shear forces present in the system.[93] This is confirmed by the results presented in this part of the work.

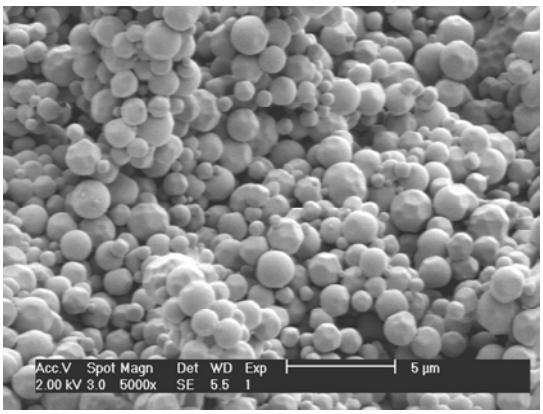

No 8. DT, 80°C, 200 rpm

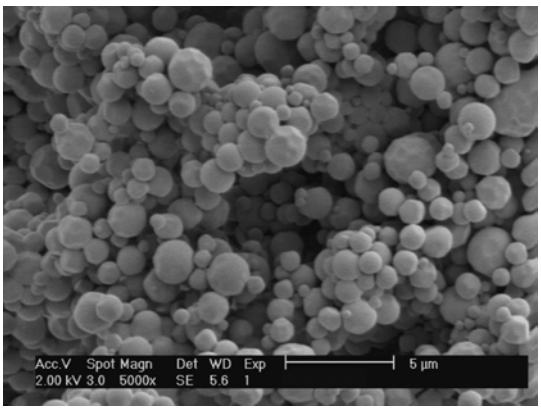

No 10. MIG, 80°C, 200 rpm

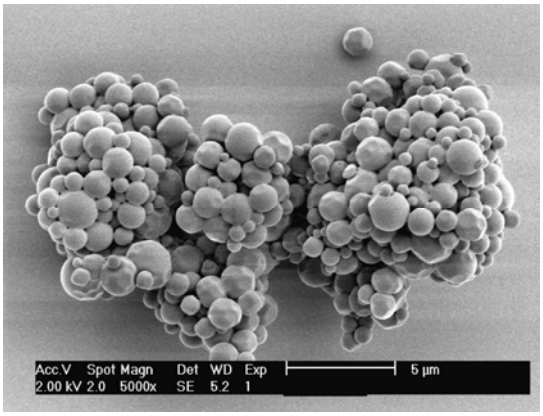

No 9. DT, 80°C, 600rpm

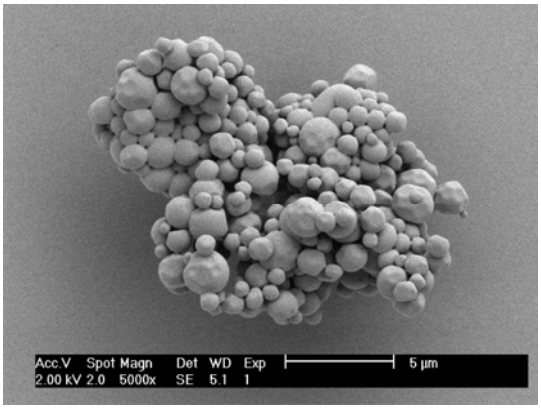

No 11. MIG, 80°C, 600rpm

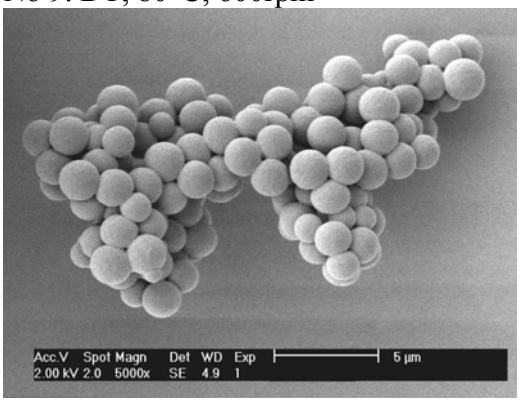

No 13. MIG, 65°C, 600 rpm

Figure 6.9: SEM images for experiments summarized in Table 6.2.

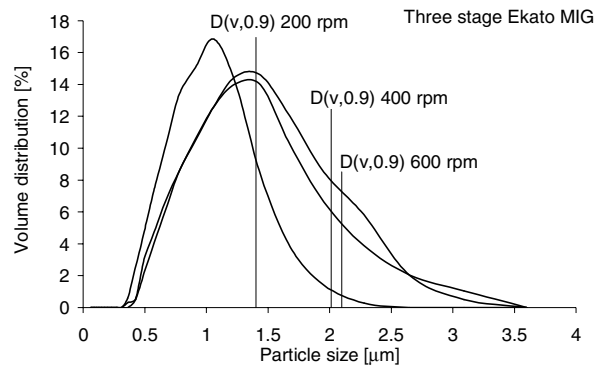

a

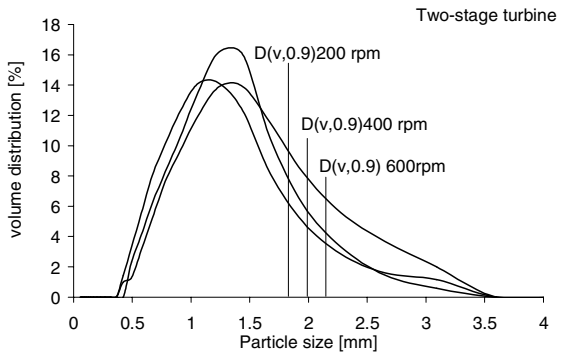

b

Figure 6.10: Particle size distribution obtained by laser diffraction for dispersion polymerizations realized at 80°C at different stirring speed a) for the three-stage Ekato MIG® impeller and b) for the two-stage turbine impeller.

Stirring effect

The interesting thing is to understand the difference between the experiments discussed in this work and the one where destabilization of the dispersions are observed under efficient stirring. In the case of the Krytox^{TM}, only 1wt% of stabilizer is used with respect to monomer. One has to consider that the surface coverage of the particles by the stabilizer is a key parameter to prevent particles collisions, contact and hence coagulation or agglomeration. In this study 10wt% stabilizer is used with respect to monomer. Another important difference between both systems is related to the size of the stabilizer chain and its anchorage to the polymer matrix of the particles. The commercially available Krytox has a molecular weight of 2'500 g/mol and the PDMS has a molecular weight of 5'000 g/mol. The size of the stabilizer chain is a crucial parameter in the case of sterically stabilized dispersion. [210-212] The longer the chain length the longer the distance maintained between particles. A longer chain helps to increases the efficiency of the steric barrier. With respect to the important destabilization of the dispersion under shear stress for experiments realized with the Krytox, the anchorage or interaction of the stabilizer with the polymer particles is another key parameter. The stronger the chemical interaction the higher the anchorage of the stabilizer. As highlighted by the authors, the shear induced coagulation can be attributed to the weak interaction between the terminal acid functionality of the stabilizer and the ester group of the poly-MMA by hydrogen bond.[103] In the case of the PDMS-mMA, a certain amount of the stabilizer can be grafted to the growing poly-MMA leading to a strong interaction. Moreover, because the chemical identity of the terminal unit of the PDMS-mMA is identical to the polymer chemical backbone, it can be expected that the attraction of the stabilizer in the polymer matrix is high. In this case, higher shear forces are required to desorb the stabilizer from the particles surface.

In the case reported by Christian *et al.*, the results are surprising because they use a higher MW PDMS macromonomer (10'000g/mol) than the one used in this study.[105] Furthermore, the concentration of the stabilizer and the stirring speed are identical, i.e. 10wt% PDMS and 400 rpm, respectively. In this study, the reactor is always washed carefully with ethyl acetate heated up to its boiling point during 5 hours. Thus, it is not expected that a passivating film of PMMA is maintained at the reactor wall between two consecutive experiments. Moreover, no fouling is observed at the reactor wall at the end of the experiments. It seems that the difference comes from the operating conditions. They do not give the exact composition (concentration) of their mixture. In this case, it is difficult to estimate the carbon dioxide density from the pressure, as all the components present in the system affect the measured pressure. It appears that they work at least at 50 bar (178 bar) below the pressure used in the experiment No 13 at 65°C in Table 6.2. This can be surprising if it is considered that they use a higher MW stabilizer and hence less soluble in the CO_2. As it will be shown in the next section the solvent power of the mixture to solubilize the stabilizer efficiently in the reacting mixture is a key factor to maintain a stable dispersion. As highlighted by Barrett,[93] studies have demonstrated that to

achieve indefinite stability of a dispersion, the dispersion medium must be "better than a theta solvent" for the stabilizing soluble part of the polymeric dispersant.

The results discussed in this section have shown that with a composition of 10wt% PDMS/MMA, 30wt% MMA/CO_2 and 1wt% AIBN/MMA at pressure higher than 200 bar, the dispersion polymerization of MMA in scCO_2 is stable over a wide range of operating conditions.

Based on a gravimetric analysis, the amount of PDMS monomethacrylate chemically incorporated in the final PMMA produced, is determined to be approximately 4% respect to the total collected polymer. This corresponds to approximately 40% of the total PDMS feed. Studies of dispersion polymerizations of MMA in scCO_2 with a 10'000 g/mol PDMS-mMA realized by Shaffer *et al.* have shown that only a small fraction of stabilizer is incorporated in the final product, i.e. 0.25 wt% respect to the total amount of polymer collected and corresponding to approximately 4% of total PDMS feed. The analyses were realized by ^{1}H NMR.[104] The difference between both analyses is surprising and no obvious theoretical argument can be given. Respect to the method used here, a systematic experimental error can weaken the accuracy of measurements. The analysis is based on the assumption that the total amount of PDMS is recovered when the polymer is collected. It appears to be probable that a fraction of PDMS is systematically lost when the CO_2 is vented at the end of the polymerization. This could lead to important experimental errors in the final evaluation. The lack of experiments dealing with this subject does not permit to really discriminate one method. But obviously, the nuclear magnetic resonance is a fundamental method at atomic scale free of experimental manipulation steps.

6.4 Effect of monomer and carbon dioxide concentration

Experiments have been made with reduced content of monomer, i.e. 20wt% MMA/CO_2. The idea is to decrease the final amount of polymer produced and avoid the difficulty to control the reactor, especially with the three-stage Ekato MIG® at 65°C. Moreover, in order to work at lower pressure at 80°C, experiments with reduced amount of CO_2 have been realized.

In Table 6.3, it is observed that for experiments realized with 20wt% MMA (No 14, 15, 16 and 17), sticky solids with lower molecular weight and broader molecular weight distribution are produced. Moreover, decreasing the introduced mass of CO_2 from 800 g to 700 g in the 1.29 liter autoclave (No 18 and 19) leads to the production of a PMMA characterized also with lower MW and broader MWD.

Table 6.3: Operating conditions for standard dispersion polymerizations and experiments realized with lower concentrations of MMA and CO_2.

No	T [°C]	P[a] [bar]	MMA[b] [wt %]	PDMS[c] [wt %]	AIBN[d] [wt %]	CO_2[e] [wt %]	Time[f] [hour]	X[g] [%]	MW/PDI[e] [kg/mol]/[-]	Product
5	65	259	30	10	1	75	5	94	428/2.9	Fluffy powder
14	65	189	20	10	1	82	17	89	181/4.4	Sticky solid /coagulated powder
15	65	166	21	16	1.6	81	8	28	125/10	Sticky solid /coagulated powder
1	80	305	30	10	1	75	5	95	109/2.3	Fluffy powder
16	80	248	20	10	1	82	10	87	37/3.0	Sticky solid /coagulated powder
17	80	215	20	16	1.4	81	12	90	23/4.4	Sticky solid /coagulated powder
18	80	211	36	10	1	72	4	36	14/2.8	Sticky solid
19	80	211	36	10	1	72	5.5	44	19/4.1	Sticky solid

a = average pressure, b = MMA/CO_2, c = PDMS/MMA, d = AIBN/MMA, e = CO_2/total feed, f = duration of the measurement, g = gravimetric conversion, e = mean molecular weight /polydispersity .

As shown in Figure 6.11, the polymer morphology changes also significantly. In the micrographs, it can be observed that the products are characterized by a large extent of coagulation, where the coagulated particles are embedded in a bulky matrix. Additionally, residual monomer in the samples, the former being a good solvent for the PMMA, can also affects the morphology, sticking the particles together. The collected polymer in this case is a block of sticky solid containing a fraction of free particles or powder-like product.

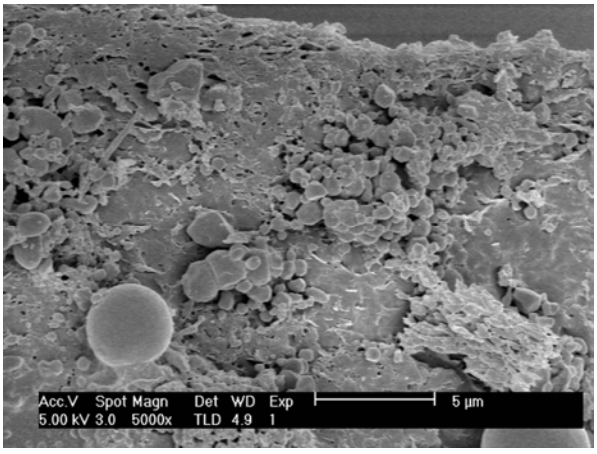

No 15.

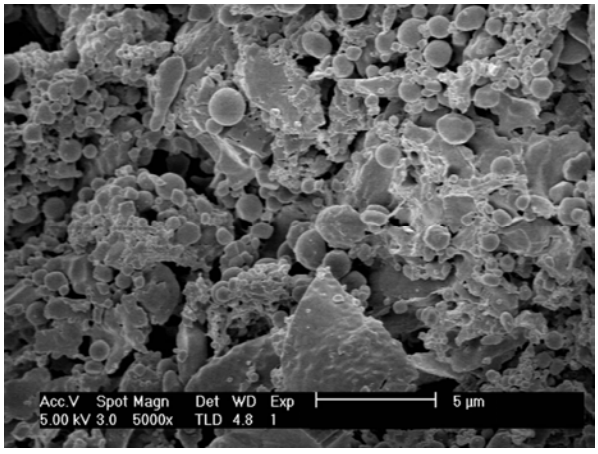

No 15.

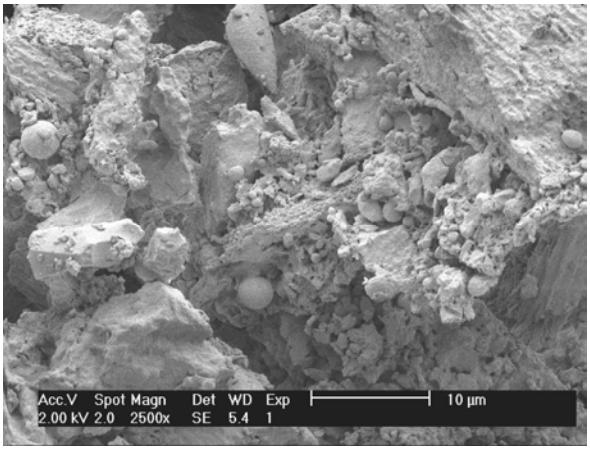

No 16.

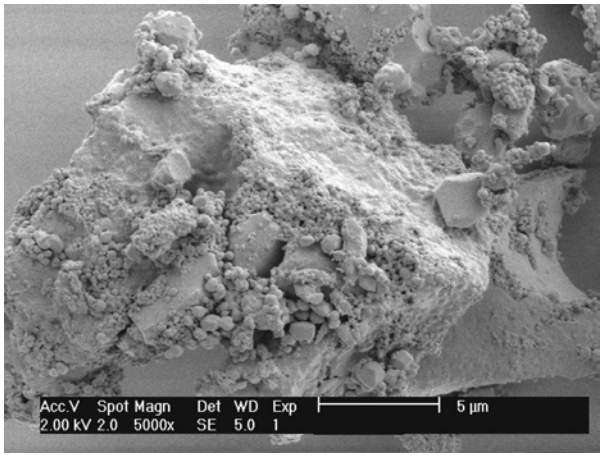

No 17.

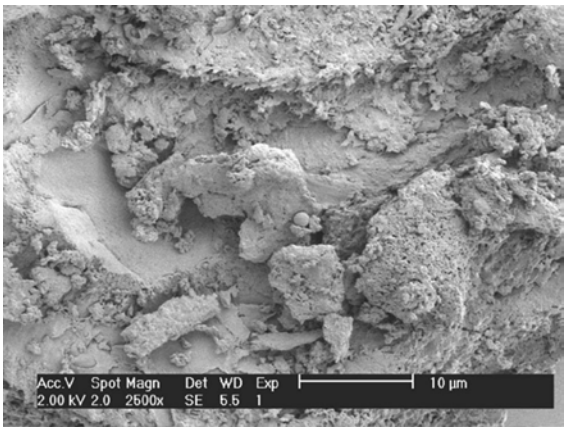

No 19.

Figure 6.11: SEM images of PMMA produced during destabilized dispersion polymerizations.

The results demonstrate that decreasing the monomer amount reduces the stabilizer efficiency, even if the total amount of stabilizer is increased with respect to monomer content (No 15 and 17). As observed experimentally in chapter 5, O'Neill *et al.* have studied the particle growth regime and have shown the role of the monomer acting as a cosolvent for PDMS in $scCO_2$.[57] They have observed that upon extraction of monomer the collected latexes (yield < 34%) flocculate and sediment. This clearly indicates that the removal of MMA results in a reduction of the solvency of the continuous phase for the PDMS tail and in a concomitant lost of stabilization. This demonstrates that the PDMS-mMA macromonomer requires the presence of monomer during the course of the polymerization to stabilize the growing polymer particles. With 20 wt% MMA/CO_2, the experimental pressure and temperature are sufficient to ensure initial homogeneity of the medium and solubility of the PDMS (see chapter 5).[57] Therefore, this indicates that the destabilization of the system occurs during the polymerization process itself. Lower initial concentration of monomer reduces the solvent properties of the medium and depletion of monomer is faster. In summary, it is necessary but not sufficient to know the initial

phase envelope of the mixture to ensure effective dispersion polymerization. One has to consider the phase equilibrium at each step of time or conversion leading to change in compositions. For experiment No 18 and 19, the lack of stability can be attributed to the lower density of carbon dioxide and a related lower solvent power.

Many authors have reported that in the absence of stabilizer, i.e. synthesis of the PMMA in CO_2 solution, low MW polymer is produced at very low rate of polymerization.[103 99-101, 104, 213] The same observation is made in the case of the experiments discussed in this section (see Table 6.3 columns time/conversion). Figure 6.12 shows that in the case of the experiments with lower monomer content (No 14 and 16) a second mode at low MW is observed in the measured molecular weight distribution. For the experiment with lower carbon dioxide content (No 19), a broad monomodal MWD is observed. Furthermore, the low MW shoulder observed for experiments No 14 and 16 (lower monomer content) is exactly located at chain lengths similar to the one produced in the experiments No 19 (lower CO_2 content). It is important to note that the MW measured in the experiment at lower CO_2 content is located precisely at the MW measured in the case of an experiment realized in absence of stabilizer (Figure 6.15 p. 133). This tends to demonstrate in this case the polymer is produced mainly in the CO_2 continuous phase at low rate of polymerization as given in Table 6.3. In the case of the experiments with reduced MMA content, bimodal distributions are obtained with a main mode at higher MW. This tends to demonstrate that the main locus of the polymerization remains the polymer-rich particles but polymerization in the CO_2-rich phase is present at the same time.

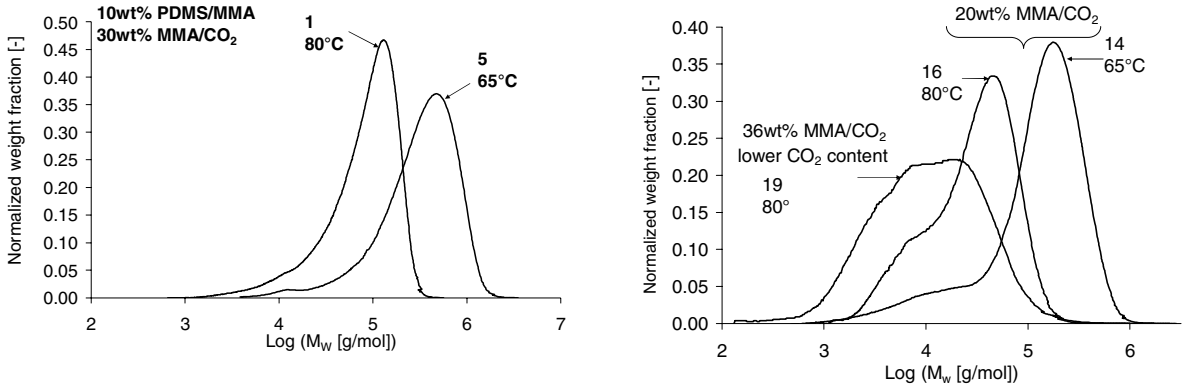

a b

Figure 6.12: Molecular weight distribution for a) standard dispersion polymerizations at 65°C and 80°C and b) unstable dispersion polymerization at 65°C and 80°C.

The combination of these results show unambiguously that the decrease in solvent power of the medium for the PDMS due to a decrease of monomer content in the mixture or carbon dioxide density leads to the production of polymers in both phases, i.e. the polymer-rich particles

and the CO_2 continuous phase. If the solubility of the stabilizer is not sufficient, it will precipitate from the continuous phase. In turn, only the residual fraction of the stabilizer still soluble can be active for the steric stabilization. Here, the explanation of the stability of the dispersion is understood in terms of activity and concentration of the dispersant. In the next subchapter, it will be demonstrated that other parameters can affect the polymerization loci.

6.5 Effect of stabilizer concentration and polymerization loci

Müller *et al.* in their predictive model for the dispersion polymerization of MMA in $scCO_2$ have demonstrated that a key parameter in determining the reaction loci is the rate of interphase mass transport.[157 156] They have analyzed the role of mass transport using a parameter, Ω, defined as the ratio between the characteristic time of termination within one phase and the characteristic time of diffusion of the macroradicals out of that phase:

$$\Omega_{1,2} = \frac{K_{1,2}(x) \cdot A_p}{k_{t,1,2} \cdot \lambda_{0,1,2}} \qquad 6.6$$

where 1,2 refer to the continuous and dispersed phase, respectively; K is the overall mass transfer coefficient [m/s]; A_p is the overall particle surface [m^2]; x corresponds to the chain length of the macroradicals; k_t is the termination rate constant [l/mol/s]; $\lambda_{k,j}$ is the k_{th} order moment of active chain distribution in phase j [mol].

Fehrenbacher *et al.* have demonstrated that in the case of the dispersion polymerization of methyl methacryalte in carbon dioxide, the polymerization starts in the homogeneous CO_2 continuous phase.[95, 111] Therefore, at the early stage of the polymerization, the polymer is exclusively produced in the homogeneous CO_2 phase. Once the polymer has reached a critical chain length, it becomes not soluble anymore in the CO_2 phase and starts to nucleate. This nucleation step leads to the production of the primary polymer-rich particles. Only once the particles are formed, the polymerization can take place inside the particles. The goal now is to try to understand how the phases are connected to each other in the later stage of the polymerization. As the dispersion polymerization is a heterogeneous system, this means that the diffusion between both phases of the different species (initiator, monomer, polymeric radicals) that intervene in the polymerization has to be considered. If the diffusion of all the species is fast in the timescale of the different kinetics step, the components can be considered to be at interphase equilibrium at each time during the polymerization process. The opposite situation is observed in a complete segregated system where the different species do not have the time to diffuse from one phase to another and no exchange between the phases occurs. Müller *et al.* have

considered that that key parameter that governs the polymerization loci is the timescale of the diffusion and termination of the macroradicals, as the macroradicals termination leads to the production of dead polymer chains.[157 156]

Therefore, the parameter Ω, estimated for the continuous and the dispersed phase, gives an evaluation of the segregation state of the dispersion polymerization. Highly segregated systems correspond to systems where the active chains terminate in the same phase where they have been initiated. This is the case when in each phase the characteristic time for radical termination is much shorter than that for interphase mass transport. In their model, they also consider that the driving forces are such that the polymeric radicals are preferentially transported from the continuous to the dispersed phase, because PMMA is not soluble in $scCO_2$. In this scheme, the polymerization loci are governed fundamentally by the mass transport limitation of the macroradicals.

In this subchapter, experiments realized with different concentration of stabilizers are discussed. The kinetic results and the MWD measured are analyzed in the light of the theoretical considerations considered in the previous paragraph.

Table 6.4: Data and operating conditions for dispersion polymerizations realized at 80°C with different concentrations of stabilizer.

No	P [bar]	Stirrer[a]	PDMS-mMA[c] [wt %]	Time[d] [hour]	X[e] [%]	M_W[f] [kg/mol]	PDI[h] [-]	D(v,0.9)[i] [µm]	Product
1	302	DT[a]	10	2.42	95	109	2.3	1.98	Fluffy powder
4	283	MIG[b]	10	2.42	93	115	2.4	2.06	Fluffy powder
20	290	DT	5	2.42	95	84	3.1	6.76	Fluffy powder
21	302	MIG	5	2.42	95	96	3.5	6.35	Fluffy powder
22	270	DT	2	3.25	91	74	2.4	53.85	Agglomerated powder
23	310	MIG	2	3.25	92	73	2.3	43.46	Agglomerated powder
24	292	DT	1	5.00	92	64	3.0	-	Agglomerated powder
25	260	DT	0.76	4.00	71	45	4.7	-	Sticky solid
26	230	DT	0.54	4.00	60	29	2.3	-	Sticky solid
27	259	DT	0.24	4.00	52	28	2.4	-	Sticly solid
28	292	DT	0	13.00	87	22	2.2	-	Oily/viscous solid

composition: 30wt% MMA/CO_2 and 1wt% AIBN/MMA, stirring speed = 400 rpm, a = two-stage turbine, b = three-stage Ekato MIG, c = PDMS/MMA , d = characteristic time of the dispersion polymerization, e = gravimetric conversion, f = mean molecular weight, h = polydispersity, i = 90% of particles have a size below the D(v,0.9) value.

Figure 6.13 shows the thermal conversions measured for dispersion polymerization realized with 10, 5, 2 and 1wt% stabilizer. It can be observed that the use of 5wt% stabilizer does not affect the global rate of polymerization if compared with experiments with 10wt% stabilizer. On the contrary, when the stabilizer content is lowered up to 2 and 1wt% PDMS, the global rate starts to decrease.

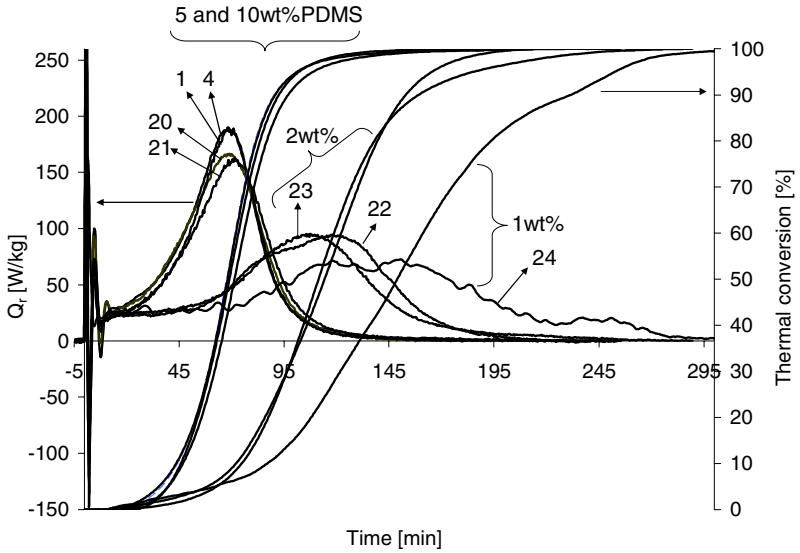

Figure 6.13: Heat generation rate, Qr, and thermal conversion for experiments realized with 10, 5, 2, 1 wt% PDMS-mMA.

Figure 6.14 a shows the micrographs of the PMMA produced with 5, 2 and 1 wt% PDMS. With those ratios of stabilizer, the product obtained is still a white powder, but being particularly agglomerated at 1 and 2 wt% stabilizer. The SEM images show that with 1 and 2 wt% stabilizer not only much bigger particles are obtained but also string elements. With 5wt% PDMS, the product has still a particulate morphology. When the concentration of stabilizer adsorbed onto the surface of the particles is too low to avoid particles collision, transient contact between unprotected areas occurs. This is clearly observed looking at the holes left on the larger particles and corresponding to the fingerprints of smaller one (experiments No 20 and 21). Moreover, collisions between particles can lead to coalescence between particles forming bigger one (experiments No 22, 23 and 24 with 2 and 1 wt% PDMS). As observed in dispersion polymerizations in conventional solvents[93]and in $scCO_2$[96], the lower the concentration of stabilizer the larger the particles diameter. The influence of the stabilizer concentration on the size of the particles can be interpreted in the following way. The number of particles formed will depend on the rate at which the stabilizer adsorbs at the surface of the particles. In turn, the rate of adsorption depends directly on the concentration of the stabilizer. In other words, the number of particles formed will depend on the probability of a nucleated polymer to encounter stabilizer

molecules in the mixture. Particles size distributions measured by laser diffraction are shown in Figure 6.14 b and are representative of the samples when compared to the SEM images. The particle size increases and particle size distribution broadens as the content of stabilizer decreases. As soon as string or cylinders–like elements are present in the samples, the measurement of PSD by laser diffraction has to be treated carefully. In fact, the analysis by laser diffraction is based on the assumption of spherical particles. When cylinder elements are present, their real total surface is underestimated in the analysis. Because the final PSD evaluation is based on volume percentage of the detected elements, only a small fraction of these elements is finally included in the calculated PSD.

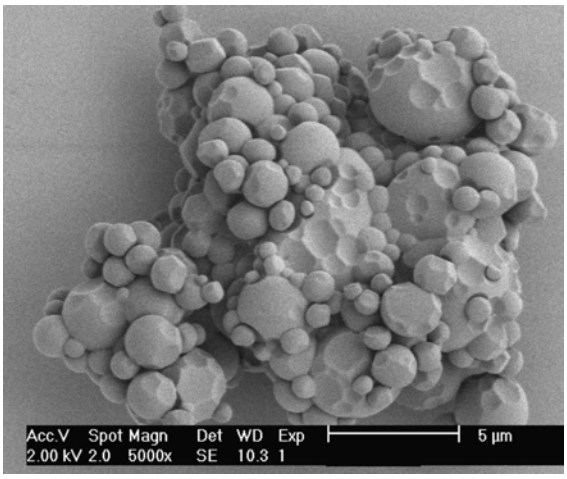

a No 20. DT, 5wt% PDMS-mMA

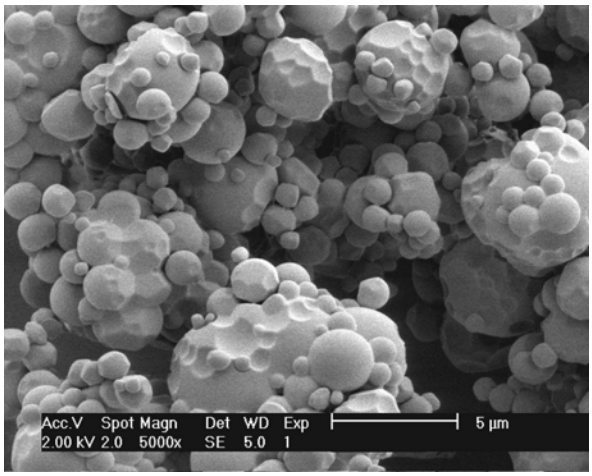

a No 21. MIG, 5wt% PDMS-mMA

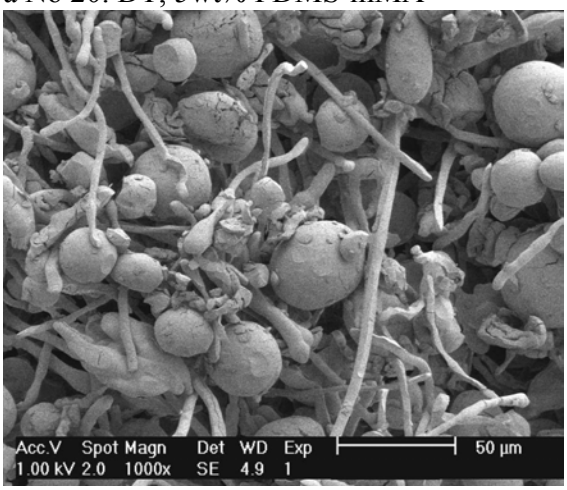

a No 22. DT, 2wt% PDMS-mMA

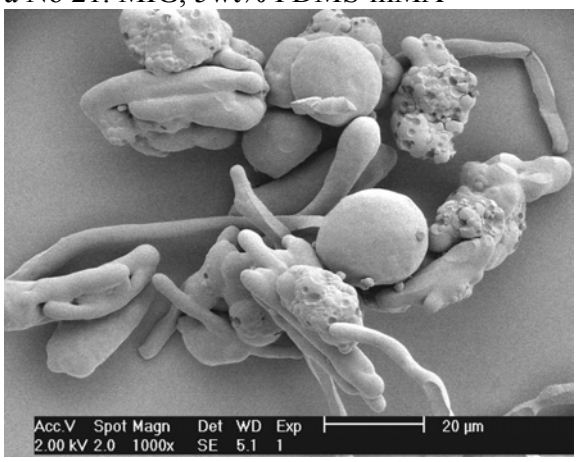

a No 23. MIG, 2wt% PDMS-mMA

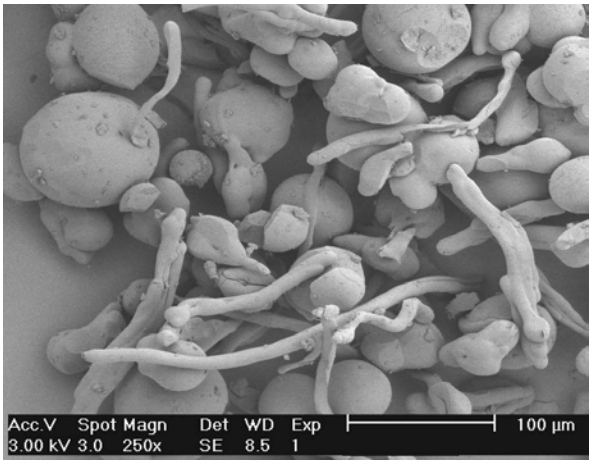

a No 24. DT, 1wt% PDMS-mMA

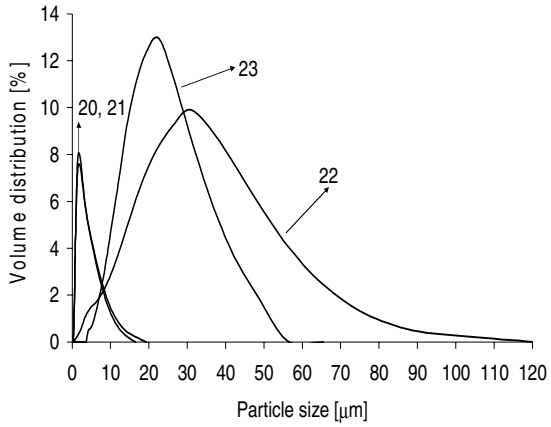

b

Figure 6.14 : a) SEM images of PMMA produced with 5, 2 and 1 wt% PDMS-mMA and b) particle size distribution obtained by laser diffraction.

Figure 6.15 a and b shows the comparison of the MWD obtained for dispersion polymerizations realized without stabilizer and with concentration of stabilizer of 1, 2, 5 and 10 wt%. Figure 6.15 b shows MWD measurements realized with a size exclusion chromatograph (Hewlett Packard-1100 series) mounted with special columns (Polymer Laboratories OligoPore) more sensitive to low molecular weight chains. These measurements were realized in the Morbidelli group (ETHZ) in the frame of our collaboration. With 0wt% stabilizer, a monomodal MWD at low molecular weight is observed. With 1, 2, 5 and 10 wt% stabilizer, the MWDs exhibit a main mode at high MW. But with 1 and 2 wt% stabilizer (Figure 6.15 b) small shoulders at low chain length start to appear in the MWDs. Moreover, their location corresponds exactly to the location of the chain length of polymer produced in the absence of stabilizer. This indicates that a small fraction of polymer starts to be produced in the CO_2-rich phase.

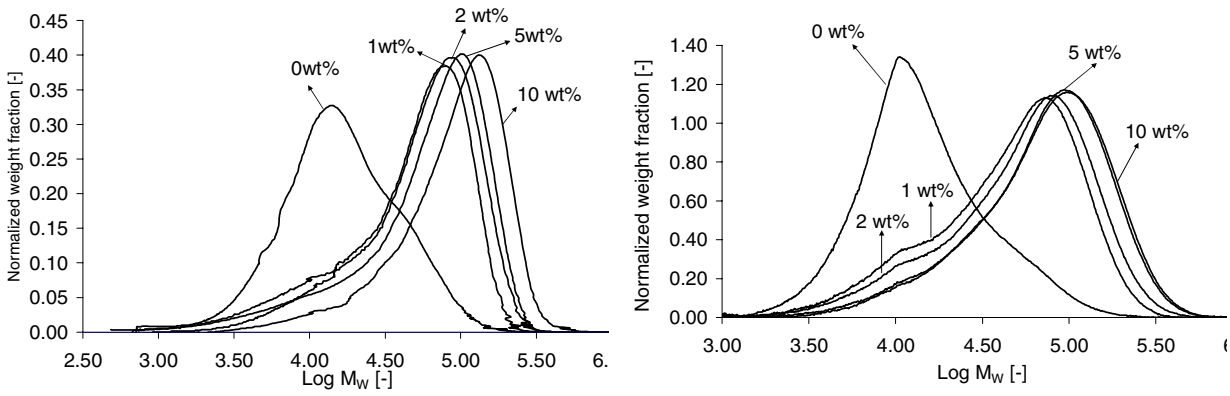

a b

Figure 6.15: Molecular weight distribution of PMMA produced with 0, 1, 2, 5 and 10 wt% PDMS-mMA respect to monomer.

Figure 6.13 shows that the rate of polymerization decreases as the stabilizer concentration decreases (1 and 2 wt%). The SEM images, the product quality, and the measured MWD indicate that for experiments realized with 2 and 1 wt% PDMS, the main locus of the polymerization is still the polymer-rich phase. Moreover, the global profile of the time-conversion curve indicates that the kinetics mechanisms are identical among all experiments. Therefore, the observed decrease in the polymerization rate can be explained by the fact that the diffusion of the species (monomer, initiator, macroradicals) from the continuous to the dispersed phase, where the polymerization occurs, is hindered by the size and shape of the polymeric elements (lower surface for mass transport). In fact, it appears that the polymerization starts to be mass transfer limited. This is typical for reactions taking place in heterogeneous systems.

Figure 6.16 shows the calorimetric results obtained for the experiments realized with 0wt% and 0.54wt% PDMS. It can be observed that the reaction calorimeter is very sensitive and gives an analyzable thermal signal even in the case of the polymerization at 0wt% PDMS, which has lasted more than 13 hours. It is important to note that the thermal conversion profiles are not similar between the experiment realized at 0wt% and the experiment realized with 0.54wt% PDMS. The profile of the conversion measured for the experiment at 0wt% PDMS is typical of solution polymerization (drastic decrease of the polymerization rate). The global rate of polymerization is constant at the beginning (constant slope) and decreases at higher conversion as the monomer concentration in the medium decreases. The conversion profile measured for the experiment realized with 0.54wt% looks like the one measured previously. From Figure 6.17, it can be observed that the on-line measurement of the pressure can also give some indications of the course of the polymerization, as the pressure increases during the polymerization (PDMS < 1wt%).

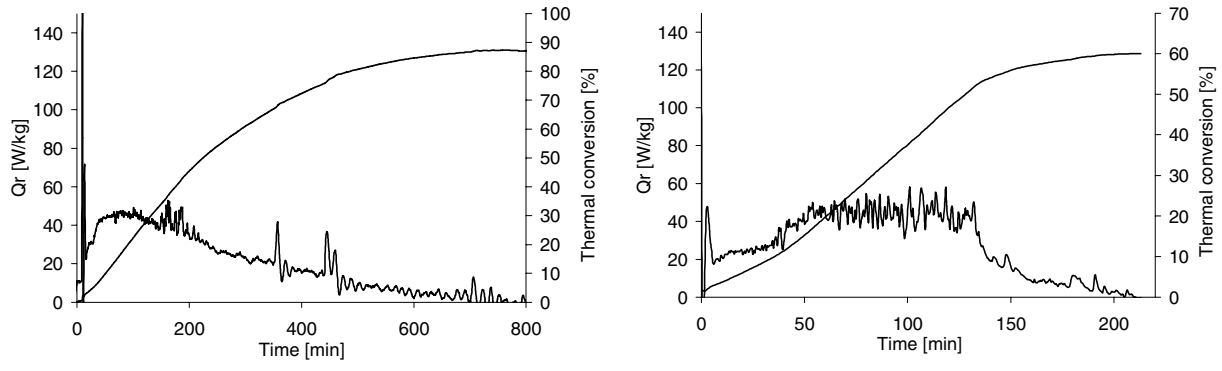

a b

Figure 6.16: Calorimetric signal for dispersion polymerizations with a) 0wt% PDMS-mMA and b) 0.54wt% PDMS-mMA.

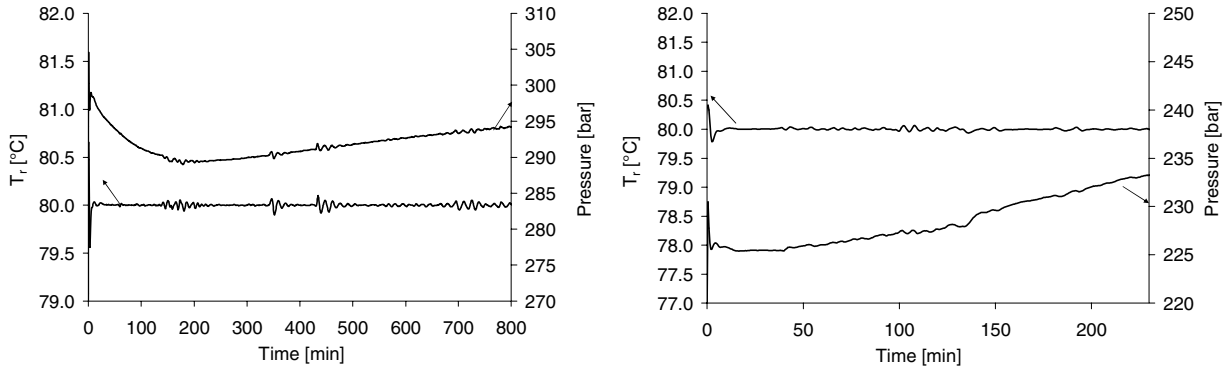

a b

Figure 6.17: Reactor temperature and pressure profiles for dispersion polymerizations a) 0wt% PDMS-mMA and b) 0.54wt% PDMS-mMA.

Figure 6.18 shows the micrographs of the PMMA produced with 0, 0.24, 0.54 and 0.76wt% PDMS. The product collected in these experiments is not anymore a white powder but a sticky solid. In the presence of stabilizer, the SEM images show that a small fraction of free particles of different size can be observed embedded in the bulky amorphous matrix, but also big unstructured elements (big blocks of polymer) are present. In absence of stabilizer, an unstructured bulky morphology is observed.

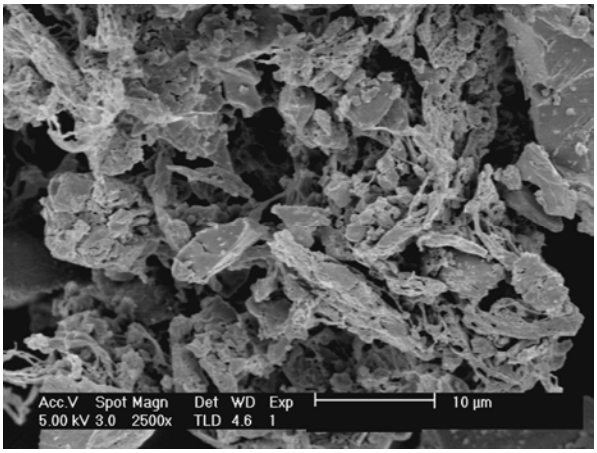

No 25. 0.76wt% PDMS-mMA

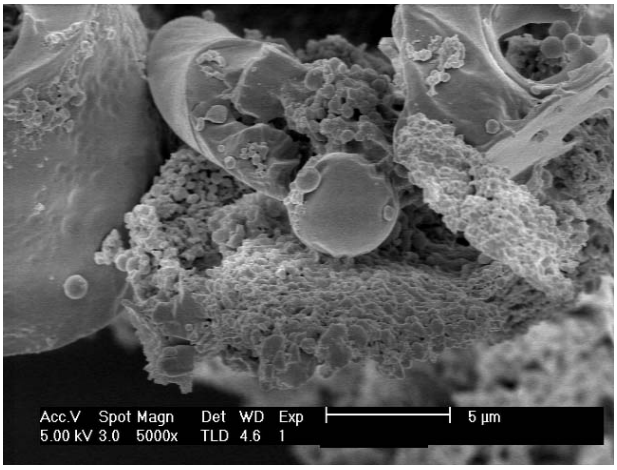

No 25. 0.76wt% PDMS-mMA

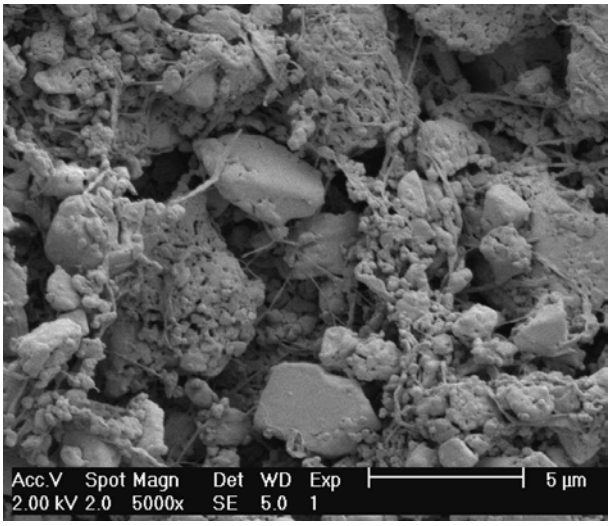

No 26. DT, 0.54 wt% PDMS-mMA

No 26. DT, 0.54 wt%PDMS-mMA

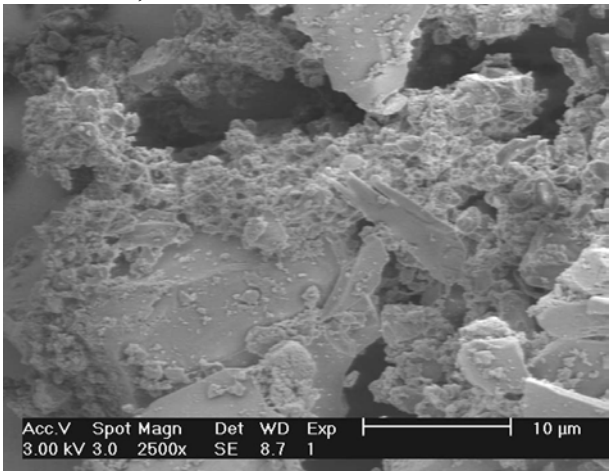

No 28. DT , 0 wt %PDMS-mMA

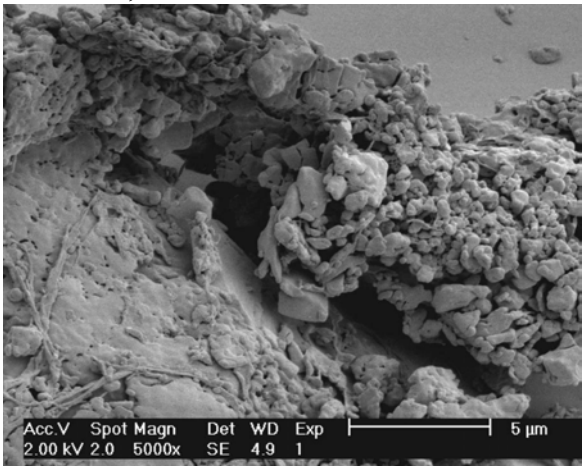

No 27. DT, 0.24 wt%PDMS-mMA

Figure 6.18: SEM images of dispersion polymerizations realized with 0.76, 0.54 and 0.24 and 0 wt% PDMS-mMA, experiments data available in Table 6.4.

Figure 6.19 a and b shows that with stabilizer concentration between 0.24 and 0.76 the polymer produced is characterized by strong bimodal MWDs exhibiting two modes easily identified. The bimodal MWDs indicate that the polymerization takes place in the particles as well as in the continuous CO_2 phase. At 0.54wt% PDMS the main reaction locus is the continuous phase. Only a small variation in concentration of the PDMS (0.76wt%) leads to the shift of the polymerization locus into the particles.

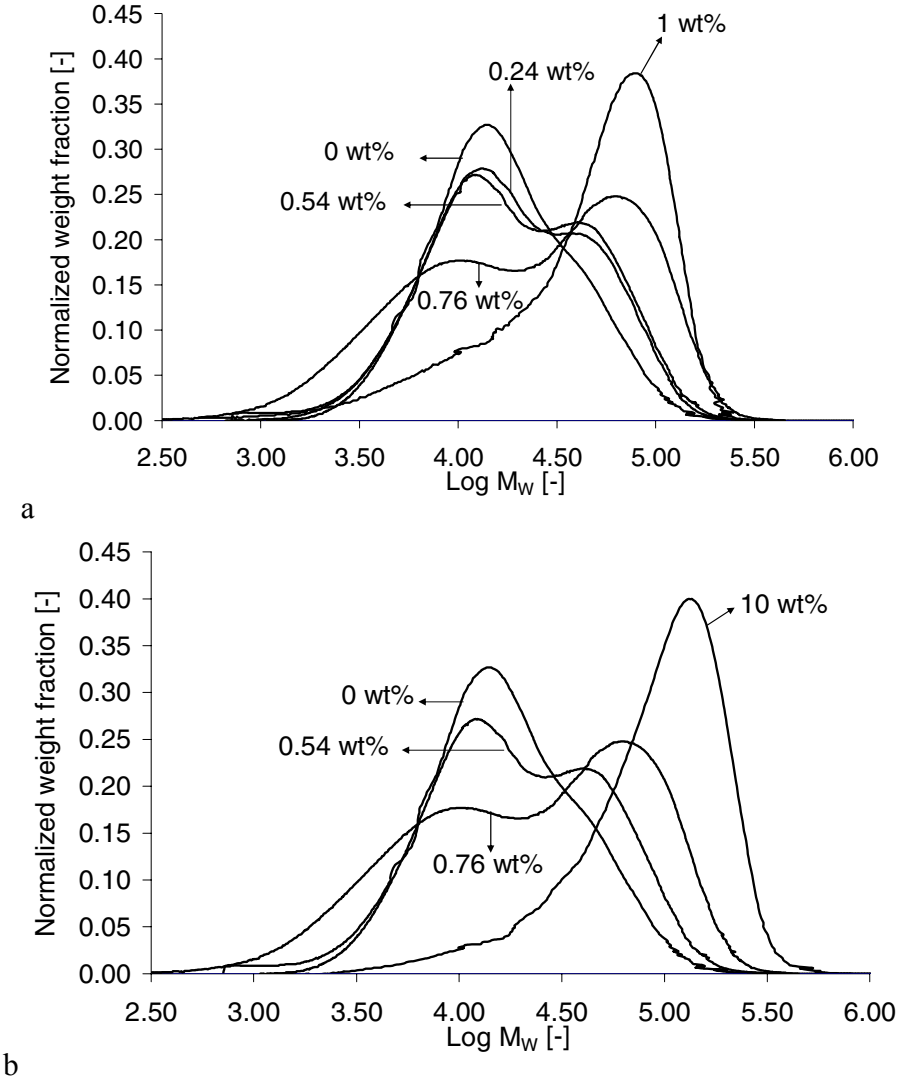

Figure 6.19: Molecular weight distribution of PMMA produced with 0, 0.24, 0.54, 0.76, 1 and 10wt% PDMS-mMA/MMA.

The combination of all these results allows constructing the complete picture of the dispersion polymerization of MMA in $scCO_2$. As soon as the stabilizer concentration decreases, the number of particles in the system decreases and their size increases. This hinders the mass transport of the different species from the continuous to the dispersed phase. If the concentration of stabilizer is between 1 and 2 wt%, the main polymerization locus is still the particles. The macroradicals have the time to diffuse before they terminate. But, mass transfer limitations are operative because a decrease of the polymerization rate is observed, despite the fact the global shape of the time-conversion curve is typical for polymerization in the particles (diffusion limited). Below 1wt% stabilizer, the diffusion is highly hindered by the poor specific interfacial area available for mass transport. The system starts to be highly segregated. The macroradicals

can only terminate where they have been initiated (bimodal MWD). Because the polymerization in the CO_2-rich phase is very slow, the global polymerization rate decreases even more. In the case of high stabilizer concentration, the polymerization occurs mainly in the particles because the driving force for the polymeric molecules is in the direction of the particles as PMMA is not soluble in CO_2.

In summary this chapter has treated the various operating parameters that govern:

- The stability of the dispersion polymerization of methyl methcrylate in $scCO_2$
- The rate of polymerization
- The molecular weight distribution
- The polymerization loci
- The particle size and the particle size distribution

The stability of the dispersion polymerization

The results have shown that in order to produce spherical particles with narrow PSD under a wide range of operating conditions the solubility of the stabilizer (PDMS) in the continuous $scCO_2$ phase is a fundamental requirement. The results have demonstrated that in order to maintain a good solubility of the stabilizer throughout the polymerization, the concentration of the monomer in the mixture is important as well as the density of carbon dioxide. Once this requirement is satisfied, the concentration of the stabilizer, its sterical activity and its anchorage to the polymer particles determine the stability of the dispersion polymerization. The concentration of the stabilizer determines the surface coverage of the particles necessary to avoid transient contact between particles. The size of its chain length is fundamental to maintain the particles at a certain distance from each other in order to decrease their force of attraction. The strength of interaction between the stabilizer and the particles governs the strength of adsorption of the stabilizer at the particles' surface. This, in turn, governs the stability of the dispersion against shear forces that could make it to desorb from the surface of the particles.

The rate of polymerization

The results have shown that the polymerization kinetics in the case of an effective dispersion, where the main reaction locus is the polymer-rich particles, is typical of a bulk polymerization. This means that diffusion limitations are operative in the particles leading to the observed auto-acceleration of the rate of polymerization. On the contrary, the results have shown that when the polymerization takes place in the continuous $scCO_2$ (absence of stabilizer), the polymerization rate decreases drastically. The time-conversion profile observed in this case is

typical of solution polymerization. If the polymerization can take place in both phases in parallel, the measured rate of polymerization is intermediate between these two extremes situations. More fundamentally, the polymerization rate is greatly affected by mass transfer limitations. If the specific interfacial area for mass transport is low, this hinders the diffusion of the species from the continuous to the dispersed phase.

The molecular weight distribution

In the case of an effective dispersion polymerization, high molecular weight polymer and monomodal MWDs are measured. The observed increase of the molecular weight as a function of conversion demonstrates that a kind of gel effect occurs inside the polymer-rich particles. When the PMMA is produced in the continuous $scCO_2$ phase, low molecular weight polymer and monomodal MWDs are observed. If the polymerization can take place in both polymerization loci at the same time, the combination leads to the production of PMMA exhibiting bimodal MWDs.

The polymerization loci

The results have shown that depending on the operating conditions the polymerization can take place in both phases, i.e. in the CO_2-rich continuous phase and in the polymer-rich particles. The fundamental parameter that governs the polymerization loci is the stabilizer concentration (also controlled by its solubility). The concentration of stabilizer in the mixture determines the particles diameter and number. In turn, this controls the specific interfacial area for mass transport from the continuous to the dispersed phase. If the concentration of stabilizer is low, the particles diameter increases and their number decreases. This leads to a reduction of the total surface available for mass transfer. Then the diffusion of the species from the continuous to the dispersed phase is hindered leading to a highly segregated system. In this case, both polymerization loci are active, because the macroradicals can only terminate where they have been initiated. Only a very small quantity of PDMS (0.76wt%) is required to shift the polymerization locus from the continuous to the dispersed phase, because the natural driving force is in the direction of the particles, as PMMA is not soluble in CO_2.

The particle size and particle size distribution

The particle size and particle size distribution are controlled mainly by the stabilizer concentration in the medium. A decrease in stabilizer concentration leads to an increase of the particles diameter and a decrease in particles number. And broader particle size distributions are observed (5, 2, 1 wt% PDMS). Moreover, if the stabilizer concentration is very low (1 and 2 wt%), a powder can still be obtained but string-like elements are produced. Furthermore, the results have shown that the temperature can affect the nucleation step and in turn, the polydispersity of the particles produced.

6.6 Model results: reaction kinetic and molecular properties

In this subchapter, the results of the reaction kinetic and molecular weight distribution simulations are discussed. Model simulations were carried out using the parameter values given in chapter 3. The objective is the prediction of the conversion and molecular weight distribution for dispersion polymerizations at 65°C and 80°C. Previously, the experimental results have shown that depending on the concentration of the monomer, the CO_2 and the stabilizer, bimodal molecular weight distributions of the produced PMMA can be observed with, in many cases, a subsequent decrease of the global rate of polymerization. As it has been demonstrated, this indicates that under specific conditions the polymerization can take place in parallel in both phases, i.e. in the CO_2-rich continuous phase and the polymer-rich particles. The kinetic models proposed for the solution polymerization in $scCO_2$ and the diffusion-limited polymerization in the polymer-rich phase help to have a better understanding of the experimental observations. The fundamental assumptions of the model for the dispersion polymerization are that propagation and termination reactions occur only in the polymer-rich phase while the initiator decomposes in the continuous phase before diffusion of the radicals in the polymer phase. The model results will show if these assumptions are correct in order to predict the experimental molecular weight distributions and rate of polymerization observed in the case of stable and effective dispersion polymerizations of MMA in $scCO_2$ (i.e. 10wt% PDMS/MMA, 30wt% MMA/CO_2 and 1wt% AIBN/MMA).

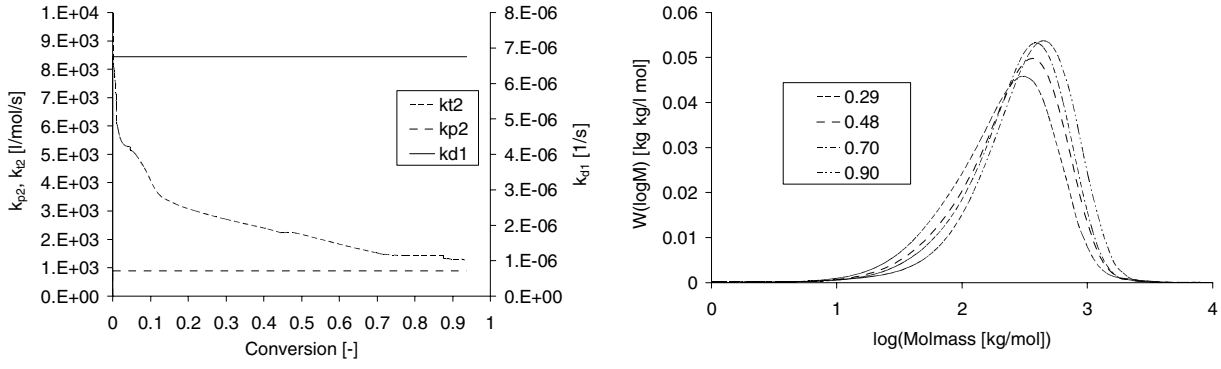

a b

Figure 6.20: a) Calculated rate constant of initiator decomposition in the continuous phase, rate constant of propagation and termination in the dispersed phase versus conversion and b) molecular weight distribution obtained at various conversions for a simulated polymerization at 65°C and 260 bar. Recipe: MMA=250g, AIBN=2.5 g, CO_2=810 g.

As briefly discussed in chapter 3 and shown in Figure 6.20 a, the model does not predict that the propagation reaction is diffusion-limited under the operating conditions, i.e. no glass effect is observed and thus the rate constant of propagation is constant throughout the reaction. On the other hand, the model predicts that the termination rate constant is diffusion-limited and hence decreases with increasing conversion, meaning that a kind of gel effect occurs in the polymer-rich phase. In reality the particles are composed mainly of polymer. Hence, for the calculation of the diffusion coefficient of the monomer in the particles, it is possible to make the assumption of a constant polymer-rich phase composition, i.e. 80wt% polymer, 5wt% monomer, 15wt% CO_2. Therefore, during the polymerization process, the main contribution of the diffusion-limited termination is due to the increasing chain length of the macromolecules. It is important to remember that the model does not consider the chain length of the colliding macroradicals, but the average number molecular weight of the dead chains produced at each step of time. It has been shown in chapter 3 that the value calculated for k_{t2} at 65°C and 50% conversion (i.e. 2234 l/mol/s) is very similar to the value reported by Müller *et al.* (i.e. 3000 l/mol/s) who consider in their evaluation of the diffusion coefficient the chain length of each macroradical present at time t in the polymer phase.[156] In the latter case the computation time and the effort for computation are much higher. The presence of a gel effect explains why the maxima of the molecular weight distributions (Figure 6.20 b) move towards higher MW values at increasing conversion, as it has been observed experimentally (Figure 6.3).

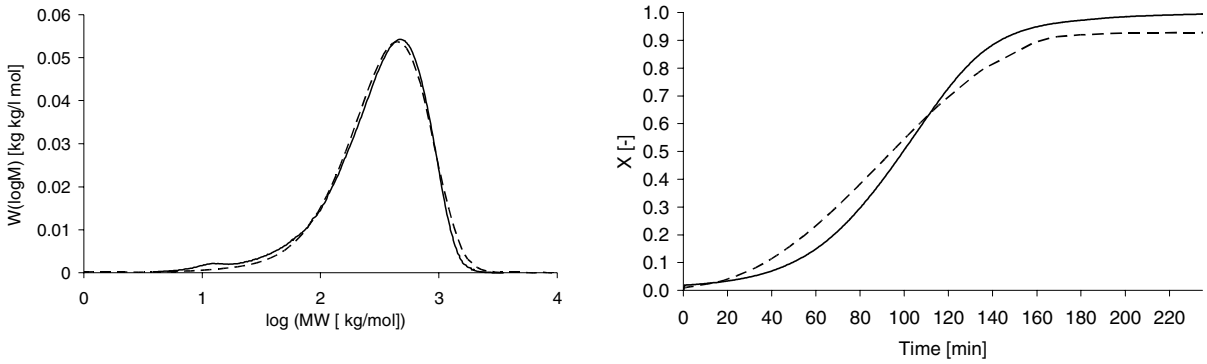

a b

Figure 6.21: a) Molecular weight distribution and b) conversion versus reaction time obtained by the model (dashed line) and comparison with experimental results at 65°C and 260 bar of polymerization No 5 in Table 6.1 (solid line). Recipe: 25 g stabilizer, 250 g MMA, 2.5 g AIBN and 810 g CO_2.

Figure 6.21 shows that the model developed in chapter 3 can describe with very good agreement the experimental MWD obtained during an effective dispersion polymerization at 65°C. This means that in the case of a dispersion polymerization of MMA in $scCO_2$ under effective conditions (optimized concentration and solubility of the stabilizer in the medium), the

polymer-rich particles are the main loci of the polymerization.[156] The small shoulder observed in the experimental MWDs for polymer produced at effective conditions can be either due to the presence of residual PDMS (5'000 g/mol) in the sample or to a very small fraction of polymer produced in the continuous phase.

The agreement between the time-conversion profiles shown in Figure 6.21 b demonstrates that diffusion limitations are operative during the polymerization process inside the particles leading to the observed auto-acceleration of the rate of polymerization. In fact, the increase in the simulated conversion can be attributed to both the increase of the polymer mass (i.e. increase of polymer reaction volume) and the presence of the gel effect (diffusion-limited termination). At high conversion, the polymerization rate decreases as the monomer in the dispersed phase is consumed. Based on the integration of the heat generation rate, the thermal conversion gives always ending value of 100% conversion. When the chemical conversion is sufficiently high, as in this experiment, the correction of the curve with respect to the off-line conversion measurement can be neglected. The final conversion calculated by the model is 93% and corresponds perfectly to the one obtained by gravimetric conversion, i.e. 94% for the polymerization No 5 in Table 6.1.

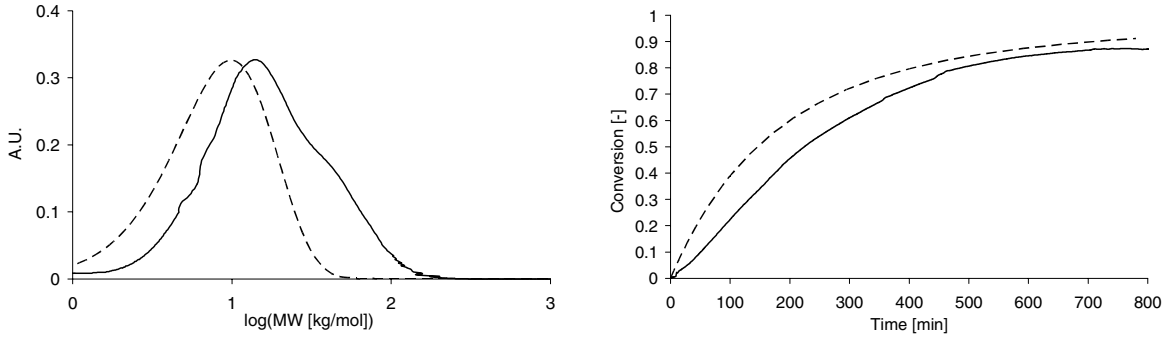

a b

Figure 6.22: a) Molecular weight distribution and b) conversion versus reaction time obtained by the model (dashed line) and comparison with experimental results at 80°C and 290 bar for a solution polymerization in $scCO_2$ No 28 in Table 6.4 (solid line). Recipe: 0 g stabilizer, 250 g MMA, 2.5 g AIBN and 810 g CO_2.

Figure 6.22 shows the comparison between model prediction and experimental results for a solution polymerization realized in $scCO_2$ using the kinetic equations and parameters given in chapter 3. The model demonstrates that when the polymerization occurs in the CO_2-rich phase the behavior is typical of a solution polymerization leading to the obtaining of a low molecular weight polymer at low rate. This is mainly due to the very high termination rate constant in the CO_2 phase, at least 10^4 higher than that in the polymer-rich phase. In the CO_2-rich phase, the mobility of the macroradicals is enhanced leading to the enhancement of the termination

reaction. This leads to a decrease of the global rate of polymerization (see equation 6.9 p.145) and the production of low MW polymer (see equation 6.8 p. 144).

Therefore, the combination of both models explains the results obtained at low stabilizer concentration. When the polymerization can take place in both reaction loci (CO_2-rich continuous phase and polymer-rich dispersed phase), the combination of the production of low MW polymer in the CO_2 continuous phase and high MW polymer in the particles leads to the observed bimodal MWDs. Furthermore, as the polymerization in the CO_2 proceeds at low rate, this explains why a decrease in the global rate of polymerization is observed in this case.

The main weakness of the model developed for the dispersion polymerization is related to the fact that no equation of state has been implemented in order to predict the partitioning of the monomer between the CO_2-rich phase and the polymer-rich phase. Moreover, the same remark can be made for the evaluation of the rate constant of mass transport because no physical equation has been used to evaluate this parameter. At this point, a possibility is to fit those parameters from experimental data. This procedure has been avoided in the case of the predictions for the polymerization at 65°C. In the frame of our collaboration with the Morbidelli group (ETHZ), they have kindly accepted to give us the parameter values of the equilibrium constant and rate constant of mass transport based on the treatment of the Sanchez–Lacombe equation of state and the two-film theory, respectively [156, 157]. As the partitioning of the monomer between the phases changes as a function of the phase compositions, the equilibrium constant introduced in our model should change as a function of conversion. In order to simplify the computation and as a first approximation, an average value has been introduced in our model, i.e. $K_{eq} = 4.5$. Figure 6.23 shows the comparison of the MMA concentration profile in both phases calculated by our model considering an average value of the equilibrium constant (Figure 6.23 a) and calculated by the Morbidelli group solving the Sanchez-Lacombe EOS (Figure 6.23 b), which has been taken as a reference to evaluate K_{eq}. This comparison demonstrates that at a first approximation it is sufficient to consider a constant partitioning of the monomer between the polymer-rich phase and the CO_2-rich phase, if the value is accurately estimated.

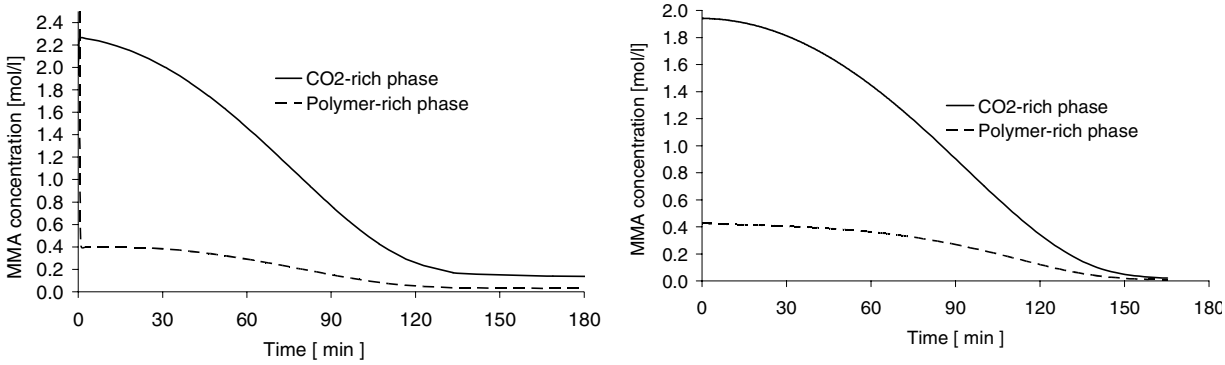

a b

Figure 6.23: Variation of the monomer concentration in the polymer-rich phase and in the CO_2-rich phase at 65°C a) calculated by the model considering an average value of K_{eq} and b) predicted by the Sanchez-Lacombe EOS.

Figure 6.24 shows the comparison between the simulated and experimental MWD and time-conversion curve for a polymerization at 80°C and 302 bar. As expected and observed experimentally, the model predicts that at increasing temperature a lower molecular weight polymer is produced.

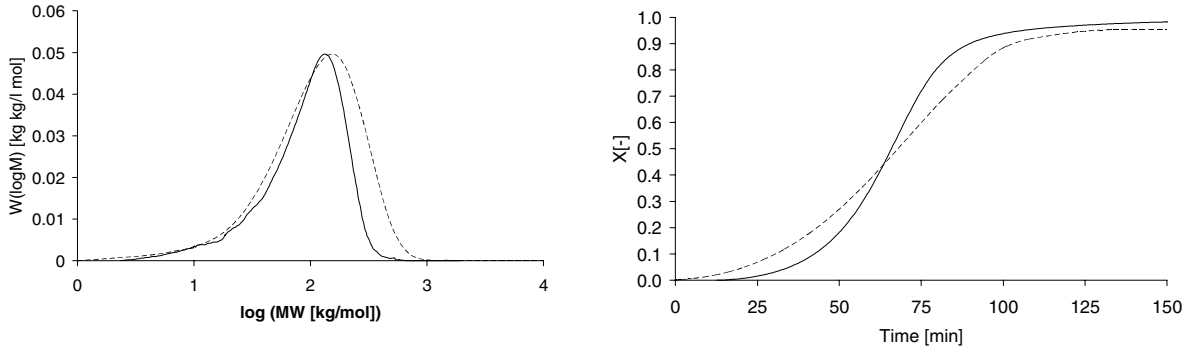

a b

Figure 6.24: : a) Molecular weight distribution and b) conversion versus reaction time obtained by the model (dashed line) and comparison with experimental results at 80°C and 302 bar of polymerization No 3 in Table 6.1 (solid line). Recipe: 25 g stabilizer, 250 g MMA, 2.5 g AIBN and 810 g CO_2.

The instantaneous chain length, CL, can be evaluated as the ratio between the frequencies of propagation and termination:

$$CL = \frac{r_P}{r_t} = \frac{k_p[R][M]}{2k_t[R]^2} = \frac{k_p[M]}{2k_t[R]} \qquad 6.7$$

In order to determine the radical concentration, $[R]$, the quasi-steady-state assumption (QSSA) for the concentration of the active centers can be applied, i.e. the concentration of the different active intermediate species remains quasi stationary throughout the polymerization. In a quasi-steady state, the rate of the variation of the concentration of the active species, R, is much smaller than the rate at which they appear or disappear leading to $r_i = r_t$. In this case, the instantaneous chain length is given by:

$$CL = \frac{k_p[M]}{2\sqrt{2fk_dk_t[I]}} \qquad 6.8$$

At 80°C the rate constant of initiator decomposition, k_d, is much higher than the one at 65°C leading to a higher concentration of initiator radicals and a lower molecular weight of the produced polymer. The concentration of initiator radicals in the dispersed phase calculated by the model are 10^{-10} and 10^{-9} [mol/l] at 65°C and 80°C, respectively. The comparison between the values of the propagation and termination rate constant at 65°C (k_{p2} =891 l/mol/s, k_{t2} = 2234 l/mol/s) and at 80°C (k_{p2} =1186 l/mol/s, k_{t2} = 7731 l/mol/s) shows that the decrease in MW is mainly due to a pronounced increase of the termination rate with respect to temperature. The equations 3.4 and 3.20 in chapter 3 show that the rate of propagation increases with increasing pressure while the rate of termination decreases with increasing pressure. The comparison between the calculated constant at 65°C (260 bar) and 80°C (302 bar) demonstrate that the temperature effect is more important and leads to the increase of both rate constants.

When the Arrhenius relation is applied to the apparent rate constant of radical polymerization initiated by initiator thermal decomposition, expression 6.10 can be obtained in the case of the ideal kinetics scheme (QSSA):

$$R_p = k_p \cdot \left[2f \cdot \frac{k_d}{k_t} \right]^{0.5} \cdot [I]^{0.5} \cdot [M] \qquad 6.9$$

$$k = (2 \cdot f)^{0.5} \cdot \frac{k_p \cdot k_d^{\,0.5}}{k_t^{\,0.5}} = A \cdot \exp\left(-\frac{E_p + 0.5E_d - 0.5E_t}{RT} \right) \qquad 6.10$$

Considering the values given in chapter 3, the decomposition activation energy, $0.5\,E_d$, account for 67 kJ/mol and the term $E_p - 0.5E_t$ for 17 kJ/mol. This means that the main contribution for the increase of the global rate of polymerization as a function of temperature is due to a faster thermal decomposition of the initiator.

As it can be expected the partitioning of the MMA between the phases will be strongly dependent on the temperature. The average value of the equilibrium constant calculated from the results obtained by the Morbidelli group solving the Sanchez-Lacombe EOS at 80°C is K_{eq} =13. This high value indicates that the Sanchez-Lacombe EOS predicts that the partitioning of MMA at 80°C is greatly in favor of the CO_2-rich phase as shown in Figure 6.25 b.

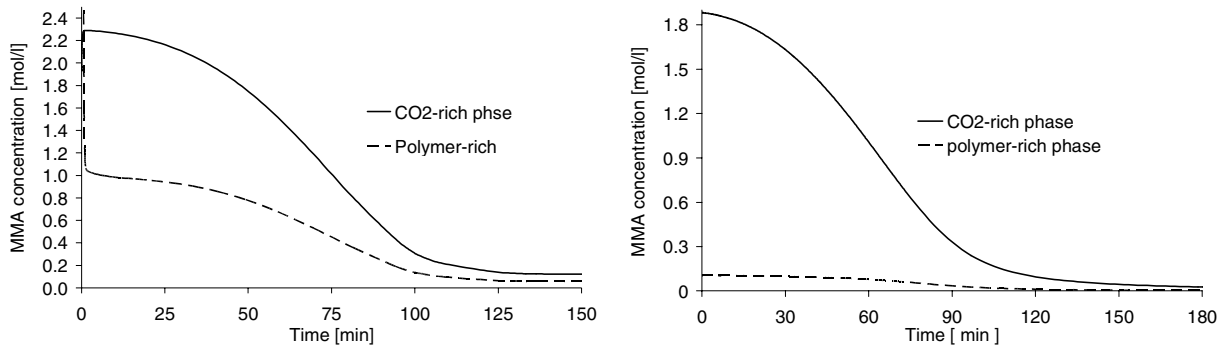

a b

Figure 6.25: Variation of the monomer concentration in the polymer-rich phase and in the CO_2-rich phase at 65°C a) calculated by the model considering a value of K_{eq} = 2.1 and b) predicted by the Sanchez-Lacombe EOS.

The use of this parameter value in the model at 80°C has led to some difficulties during the computation. In fact, once the equilibrium concentration is reached the monomer is consumed in the polymer phase but no monomer is transferred from the continuous phase. The diffusion of the monomer from the continuous to the polymer phase is calculated from the expected equilibrium concentration (K_{eq}) and the rate depends on the value of the rate constant of mass transport, $kla = 1.2 \cdot 10^{-1}\,1/\mathrm{s}$. In order to compensate the poor dynamic of monomer transfer, this rate constant of mass transport has to be increased up to a value of 10^{12} [1/s] but still leading to unexploitable results. Finally, the equilibrium constant at 80°C has been fitted to obtain a rate of mass transport in agreement with the fast kinetic of the polymerization at 80°C leading to K_{eq} = 2.1. Figure 6.25 shows the comparison between the MMA concentration profile in the two phases calculated by the model using a fitted value (K_{eq}) and the profile obtained from the Sanchez-Lacombe EOS. Despite this weakness of the simulation at 80°C, the results allows pointing out the same conclusions as previously. Only the rate constant of termination is diffusion-limited, as shown in Figure 6.26 a, leading to an increase of the molecular weight versus conversion and the obtaining of high MW product at high rate.

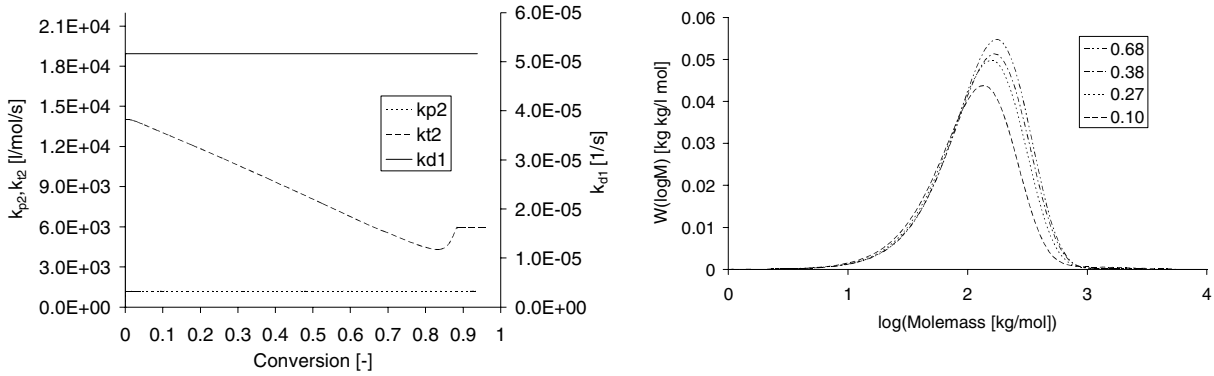

a b

Figure 6.26: a) Calculated rate constant of initiator decomposition in the continuous phase, rate constant of propagation and termination in the dispersed phase as a function of conversion and b) molecular weight distribution obtained at various conversions for a simulated polymerization at 80°C and 302 bar. Recipe: MMA=250g, AIBN=2.5 g, CO_2=810 g.

The models developed in this work can describe the difference between polymerization occurring in the CO_2 phase and the polymerization occurring in the particles. Because no connection or relation is included to couple both reaction loci, the model cannot explain the fundamental mechanism that governs the polymerization loci, i.e. mass transport phenomenon. Therefore, the model cannot predict the strong bimodal molecular weight distributions observed in the previous subchapter at stabilizer concentration below 1wt%.

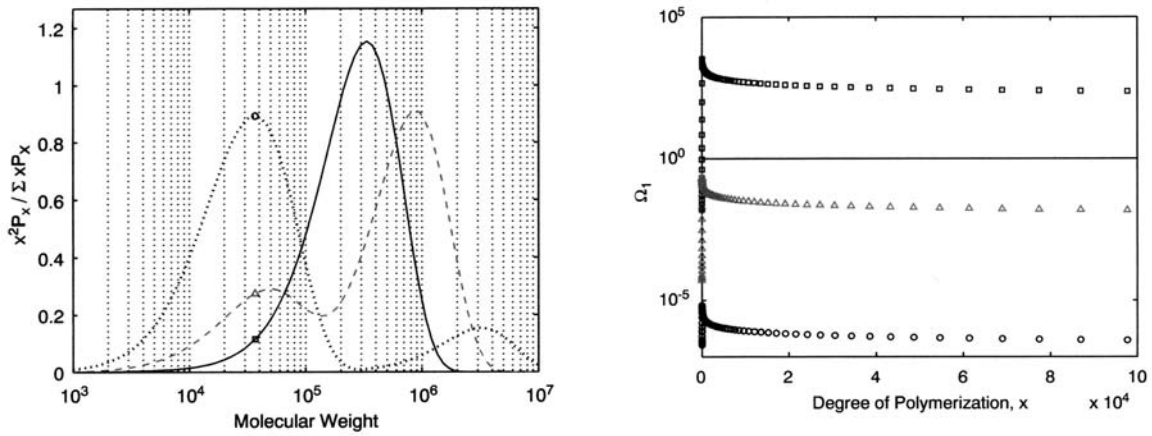

a b

Figure 6.27: a) MWDs predicted by the model of Müller et al. for b) different omega parameter calculated for a diffusion coefficient estimated $D_{x,j}$ estimated for the case of MMA polymerization (□), $D_{x,j}$ divided by 50 (Δ) and $D_{x,j}$ divided by 10^4 (○) as a function of the chain length of the macroradicals. [157]

Figure 6.27 a shows the results predicted by the model developed in the Morbidelli group.[156, 157] In their model, the polymerization is considered to take place in the polymer-rich phase as well as in the CO_2-rich phase. The phases are connected to each other by equilibrium

concentration for the small species (initiator, monomer and solvent). The key of their model is to consider the rate of diffusion of the macroradicals out of a phase as a function of their chain length. Ω decreases as a function of the chain length of the macroradicals. Ω_1 in Figure 6.27 b describes the ratio between the rate of diffusion of the macroradicals out of the CO_2 phase and their rate of termination in that phase. If this parameter is much higher than one (□), the chain initiated in the CO_2 phase have the time to diffuse into the polymer phase where they terminate leading to monomodal MWD at high MW. If omega is slightly lower than one (Δ), the rate of diffusion and the rate of termination of the macroradicals start to be comparable and some macroradicals can terminate in the CO_2 phase leading to a bimodal MWD. If the omega value is much lower than one (○), the diffusion of the macroradicals from the continuous to the dispersed phase is highly hindered; this means that most of the macroradicals terminate in the CO_2 before they have the time to diffuse (monomodal MWD at low MW). As the PMMA has a very small solubility in the CO_2, the omega value is very small for this phase. One has to consider that the driving force in a dispersion polymerization of MMA in $scCO_2$ favors the diffusion of the PMMA species in the direction of the polymer phase due to its small solubility in CO_2. The MWDs predicted by their model corresponds perfectly to the results obtained in this work for dispersion polymerization realized with stabilizer concentration between 0.24, 0.54, 0.76 wt%. The experimental reason to observe such a behavior was highlighted previously. The concentration of stabilizer controls the size and the number of particles present in the system. The latter determine the surface available for mass transport and thus the transport efficiency or rate of diffusion of the species from the continuous phase to the dispersed phase.

The models developed in this work have demonstrated that when the polymerization takes place in the polymer-rich particles high molecular weight polymer can be obtained because diffusion limitations are operative in the particles. The decrease in the rate constant of termination demonstrates that a kind of gel effect occurs in the particles explaining the observed high MW polymer produced in the case of an effective dispersion. In terms of kinetics, this explains the auto-acceleration of the global rate of polymerization observed experimentally. When the polymerization occurs only in the continuous carbon dioxide phase, the behaviour is typical of a solution polymerization. The global kinetics, particularly the high rate of termination, leads to the formation of low molecular weight polymer at low rate, because no diffusion limitations are operative in this case. The combination of these results allows the understanding of the bimodal MWDs and low rate of polymerization observed experimentally at low stabilizer concentrations.

7 Speed of sound and reaction monitoring: Results and Discussion

7.1 Monitoring dispersion polymerizations in $scCO_2$

Sound can be compared to electro-magnetic radiations because it includes mechanical vibrations of sound waves or pressure pulses. In order to transport the sound from a vibrating body to a receiver at a distant point, it is necessary that the intervening medium is capable of transmitting the vibration. Thus, it appears to be obvious that the rate (speed) at which the vibrating wave is transmitted will depend on the physical properties of the medium. The main thermo-physical properties that influence the speed of sound in a medium are the density and the isentropic compressibility. Therefore, the basic condition for monitoring chemical processes using ultrasound propagation velocity measurements is that the physico-chemical properties change significantly during the course of the reaction. Polymer processes can be characterized by drastic changes of the medium properties such as density, viscosity and compressibility explaining why those processes are ideal for the application of ultrasound techniques to detect the reaction extent.

In the previous chapter, the use and the efficiency of reaction calorimetry to monitor dispersion polymerizations in $scCO_2$ have been exhaustively discussed. In this chapter, the coupling between the calorimetric and the speed of sound measurements will show that the latter can also be applied for the on-line monitoring of polymerization processes in SCFs.

Many authors have described the use of ultrasonic sensors to monitor polymerization reactions conducted in homogeneous (bulk and solution polymerizations) or in heterogeneous systems (emulsion polymerizations).[113-116, 214] This means that such sensors could be applied to monitor heterogeneous processes like dispersion polymerizations in $scCO_2$. Moreover, sensors allowing the calculation of monomer conversion through measurement of the ultrasound propagation velocity are cheap, highly reproducible and non-invasive. Hence, they have real advantages and attract interest for industrial applications. The fact that they are cheap, if compared to FT-IR sensors for example, is even more important when working with SCFs, because the investment costs of high pressure reactor and processes are already considerable.

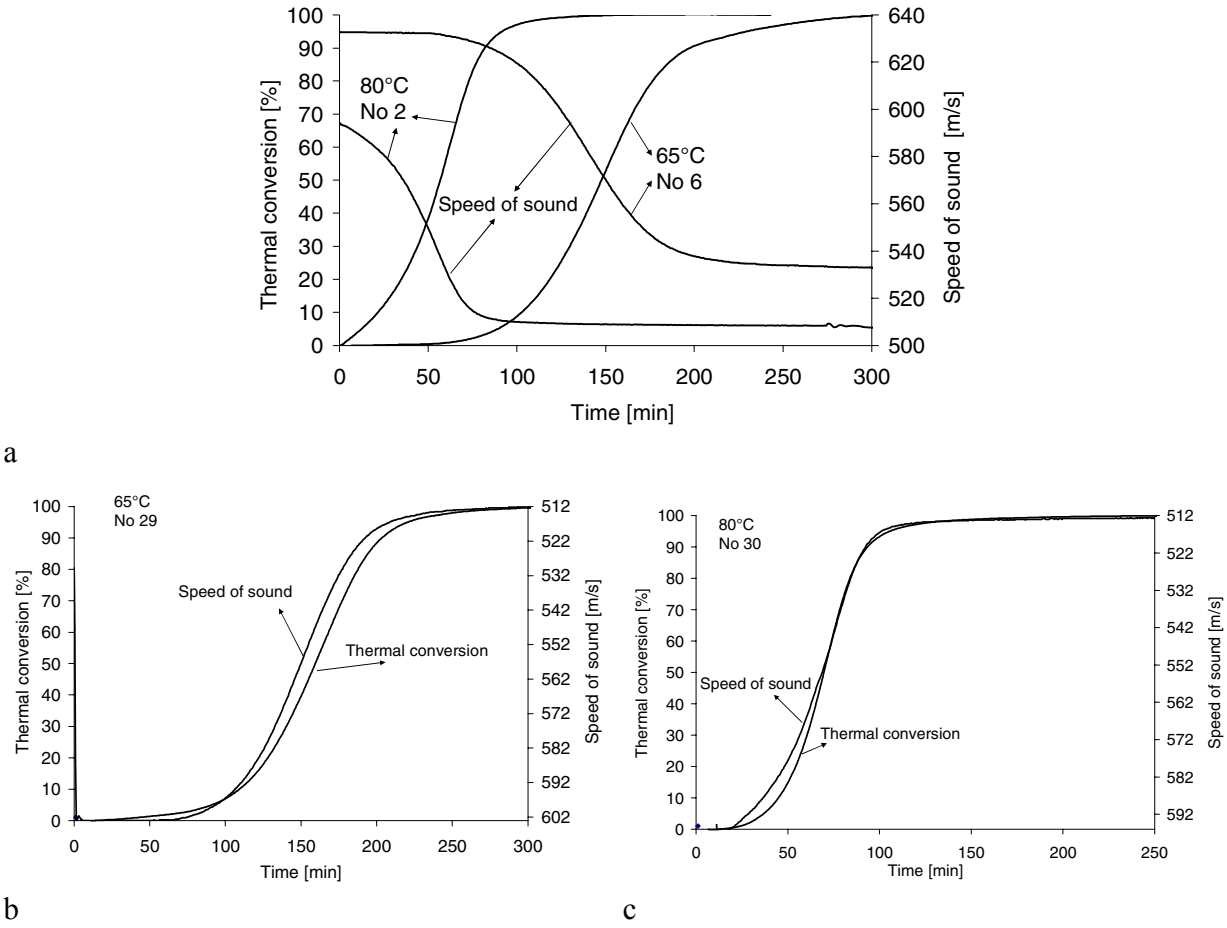

Figure 7.1: Evolution of the speed of sound during the dispersion polymerization of MMA in $scCO_2$ at 65 and 80°C and comparison with the thermal conversion.

Figure 7.1 shows the profile of the speed of sound measured during the dispersion polymerization of MMA in $scCO_2$. It is observed that the profile of the speed of sound during the course of the polymerization has exactly the same shape like the thermal conversion. This direct comparison demonstrates that ultrasound propagation velocity measurements can be applied for the monitoring of dispersion polymerizations in supercritical media with high sensitivity. One has to consider that at least 20% V/V is occupied by the solid polymer (particles). The presence of the particles does not perturb the measurement of the probe clogging the zone between the emitter and the receiver. Furthermore, calibration experiments (annex A.1) have shown that the ultrasonic probe gives very accurate measurements as shown for the case of pure carbon dioxide (1 m/s offset is required to correct the measured value).

Table 7.1: Experimental data of dispersion polymerizations realized at 65°C and 80°C with typical composition of 10wt% PDMS/MMA, 30wt% MMA/CO_2 and 1wt% AIBN/MMA.

No	T [°C]	P[a] [bar]	Conversion[b] [%]	M_W[c] [kg/mol]	PDI[d] [-]
6	65	281	95	465	2.2
29	65	250	95	458	2.2
2	80	301	94	104	2.3
30	80	294	94	105	2.1

a = average pressure, b = gravimetric conversion, c = average weight molecular weight, d = polydispersity.

Table 7.1 summarizes the experimental data of the different experiments studied in this section. Only few experiments are available, because the development of the ultrasonic probe is recent. Therefore, the results are mainly devoted to demonstrate the feasibility of the technique and to point out the possible improvements for its future application.

Experiments No 29 (T=65°C) and 30 (T=80°C) have been realized exactly with the same recipe. The monomer and CO_2 concentrations inside the reactor are slightly higher in reactions No 6 and 2. From Figure 7.1 b and c, it is observed that at identical recipes the difference in temperature (15°C) and in pressure (44 bar) does not affect significantly the absolute value of the speed of sound measured. The initial difference in the measured value is of 7 m/s. Furthermore, the speed of sound reaches the same value at the end of both polymerizations (512 m/s). This indicates the very good reproducibility of the measurement. In other words, for these experiments only the composition of the mixture determines the value of the speed of sound measured.

The goal is to correlate the ultrasound propagation velocity to the monomer conversion and thus, calculate from speed of sound measurements the composition of the medium. For this purpose, a model is required to understand how the properties of the medium are related to the measured speed of sound.

The velocity of sound, c, in a pure liquid is given by: [215]

$$c = \frac{1}{\sqrt{\rho \cdot \beta}} \qquad 7.1$$

where ρ is the density of the component and β the isentropic compressibility.

When treating dispersed systems, such as dispersion, emulsion or suspension polymerizations, a multiphase system has to be considered. The theoretical treatment of the sound propagation in dispersed systems has been widely discussed in the literature and the most fundamental contribution is probably the one of Ahuja.[216, 217 216, 218-222] Following his theoretical analysis, it appears that the crucial parameter to characterized dispersed systems is the ratio between the size of the dispersed particles and the wavelength of the sound wave. In our case, the typical particle size is between 1-2 µm. The value of the wavelength in $scCO_2$ corresponding to a frequency of 1 MHz is approximately 460 µm. Considering an edge size ranging from 1/15 of the wavelength in water to 1/10 of the wavelength for dispersed systems, a cubical volume element of 97'336 μm^3 (46^3) contains approximately 10^5 polymer particles. Ahuja has demonstrated that when the size of the dispersed particles is so small compared to the characteristic wavelength of the oscillating wave, the dispersion can be treated as an ideal homogeneous system.[216] Therefore, it is possible to conclude that the CO_2-polymer particles system can be considered to compose a single phase. But this does not mean that the presence of the particles does not affect the measured speed of sound.

The first theoretical treatment for the velocity of sound waves in dispersions has been given by Wood.[215] The values of density and compressibility are simply considered as the volume average of the components. This means that the density and the isentropic compressibility in equation 7.1 can be replaced by average values, $\overline{\rho}$ and $\overline{\beta}$, characteristic of the mixture, considering a volume additivity rule:

$$\overline{\rho} = \sum_i \phi_i \rho_i \qquad 7.2$$

$$\overline{\beta} = \sum_i \phi_i \beta_i \qquad 7.3$$

where ϕ_i, ρ_i, β_i are the volume fraction, the density and the isentropic compressibility of component i in the medium, respectively.

The volume fraction of component i can be expressed in term of the mass fraction, w_i:

$$\phi_i = \frac{\frac{w_i}{\rho_i}}{\sum_i \frac{w_i}{\rho_i}} \qquad 7.4$$

Combining equations 7.1, 7.2, 7.3 and 7.4, it is possible to obtain a relationship between the composition of the medium and the measured speed of sound:

$$\left(\frac{w_P}{\rho_P}+\frac{w_M}{\rho_M}+\frac{w_S}{\rho_S}\right)=c\cdot\sqrt{\left(\frac{w_P\cdot\beta_P}{\rho_P}+\frac{w_M\cdot\beta_M}{\rho_M}+\frac{w_S\cdot\beta_S}{\rho_S}\right)} \qquad 7.5$$

where P, M and S are the subscripts for the polymer, the monomer and the solvent, respectively.

Following the same approach as Wood,[215] it is possible to have a better estimate of the isentropic compressibility of the polymer particles using equation 7.6:[220]

$$\beta_{Particle}=\phi_P\beta_P+\phi_M\beta_M+\phi_S\beta_S \qquad 7.6$$

The isentropic compressibility of the polymer particles calculated by equation 7.6 allows taking into account the fact that the particles are swollen by the monomer and the carbon dioxide. The typical weight fraction of the particles composition in dispersion polymerization of MMA in $scCO_2$ can be estimated to be 5wt% MMA, 15 wt% CO_2 and 80 wt% PMMA. The value obtained for the compressibility of the particles is introduced in the calculation of equation 7.5 (i.e. β_P is replaced by $\beta_{Particle}$). The data used for all the components are summarized in Table 7.2. It has to be highlighted that it is difficult to find data in the literature for the isentropic compressibility corresponding to the operating conditions used in the experiments. For this, the estimation of the parameter values from literature data was difficult. The value of the compressibility of carbon dioxide has been estimated from the value of the speed of sound corresponding to the pressure and temperature of the system:

$$\beta=\frac{1}{c^2\cdot\rho} \qquad 7.7$$

where the speed of sound of carbon dioxide is equal to 467 m/s at 65°C and 250 bar and 466 m/s at 80°C and 290 bar.[27]

Table 7.2: Literature data and values of the parameters fitted from experimental results.

	T [°C]	ρ CO_2 [kg/m^3]	β CO_2 [1/Pa] $\cdot 10^9$	ρ MMA [kg/m^3]	β MMA [1/Pa] $\cdot 10^9$	ρ polymer [kg/m^3]	β Particle [1/Pa] $\cdot 10^9$
Literature data	65	620[a]	7.4	897[b]	1.011[b]	1188[c]	1.8[d]
Fitted data	65	-	5.3	-	0.5	1500	1.4
Literature data	80	620[a]	7.4	897[b]	1.011[b]	1188[c]	1.8[d]

ρ = density, β = isentropic compressibility, a = calculated from the introduced mass and the reactor volume, b = [223], c = [206], d = calculated from equation 7.6 and using β_{PMMA}=2.9 $\cdot$ 10^{-10} Pa^{-1} [206].

As a first attempt, the model described in the previous equations has been used to evaluate the possibility to predict the trend of the experimental speed of sound measured during the dispersion polymerization. The thermal conversion has been used to calculate the mass fraction of the components in the medium as a function of time (w_{CO_2}=constant). The resolution of equation 7.5 for c gives the results shown in Figure 7.2. The model can predict the correct trend of the speed of sound as a function time (decrease). But the parameter values taken as found in the literature and given in Table 7.2 lead to an underestimation of the absolute value of the speed of sound. Furthermore, the model predicts only a decrease of 33 m/s compared to the observed 91 m/s. Because at the beginning no polymer is present in the system, this indicates that the literature data of the monomer and the carbon dioxide are not consistent with the experimental measured value of the speed of sound. For example, the isentropic compressibility found in the literature for MMA was measured at ambient pressure and at 60°C.[223] Another important approximation in the model is that the mixture behaves like an ideal mixture because this assumption is behind the use of the volume additivity rule. This is not expected to be the case for the monomer-CO_2 mixture as characterized by a negative volume of mixing.

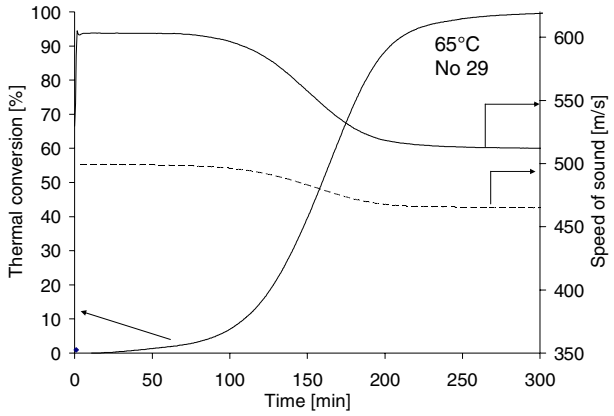

Figure 7.2: Comparison between the calculated speed of sound by the model (dashed line) and the experimental measurement (solid line).

Taking into account the previous remarks, it becomes necessary to fit the model parameters (Figure 7.3 and Table 7.2) from the experiments. The calibration procedure has been made only for the experiment No 29 at 65°C, as the temperature and pressure do not affect significantly the speed of sound measured, within the range of the experimental conditions. The literature values of the speed of sound used to evaluate the isentropic compressibility of carbon dioxide are exactly the same at 65°C and 250 bar and at 80°C and 290 bar. In fact, the speed of sound increases with increasing pressure and decreases with increasing temperature. This explains why globally no effect is observed between experiments No 29 and 30. The fitting of the model parameters has demonstrated that the magnitude of the decrease of the speed of sound is not correctly predicted mainly because the volume additivity rule does not account for the real change in density during the dispersion polymerization. This is shown by the high value of the density fitted for the polymer (1'500 kg/m^3). This value has not a real physical meaning, because most of the PMMA formulations have a density approximately of 1'200 kg/m^3. During the treatment, it appears unambiguously that the correct evaluation of the density change during the polymerization is crucial to predict the correct magnitude of the decrease of the speed of sound.

More complex models are available in the literature to predict the evolution of the speed of sound in dispersed media. The model developed by Canegallo *et al.* for the emulsion polymerization of MMA is a good example.[214] The model is also based on the fact that at least the water-polymer particles mixture can be considered as a single phase. Based on the work of Ahuja,[216] the speed of sound in the water-polymer particles mixture is considered to be equal to the speed of sound in pure water times a complex function including the density and the compressibility of the water and of the polymer particles. In their model, the compressibility of the different components is determined by the value of speed of sound of the pure component using equation 7.1. As highlighted by the author, in order to obtain an accurate estimation of the compressibility, it is necessary to determine the speed of sound of the pure monomer and polymer by fitting from independent experimental measurements. An attempt has been made to apply the model developed by Canegallo *et al.* for the case of an emulsion polymerization in our system.[214] The model results have given the opposite trend as the one observed in this work. The model predicted for our conditions an increase of the speed of sound during the course of the polymerization, as it is observed experimentally in the emulsion polymerization by Canegallo *et al.* [214] This tends to demonstrate that the simple model developed in this work is adapted to the studied system. The main weakness is the evaluation of the model parameters.

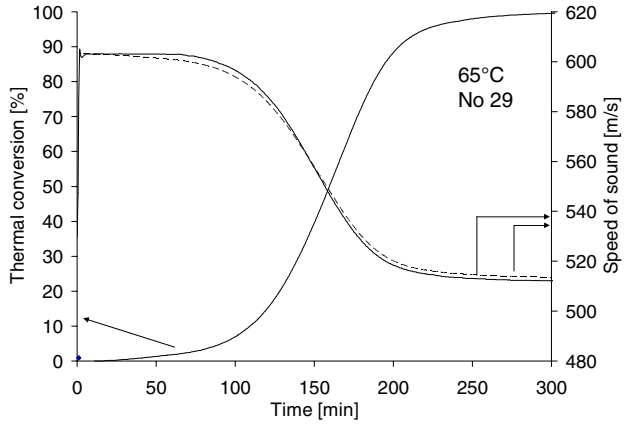

Figure 7.3: Experimental measurement of the speed of sound (solid line) and calculated speed of sound (dashed line) for the calibration procedure used to fit the model parameters given in Table 7.2.

Figure 7.4 shows the comparison between the thermal conversion for dispersion polymerizations realized at 65°C and 80°C and the conversion calculated from the on-line measurement of the speed of sound solving the linear algebraic equation 7.5. Figure 7.4 shows that if the model parameters estimation is improved, it is possible from the speed of sound measurements to calculate the mixture composition and hence the monomer conversion. This can lead to a very good estimation of the monomer conversion, because this method is highly sensitive to the change of properties of the reacting medium as shown by the experimental results.

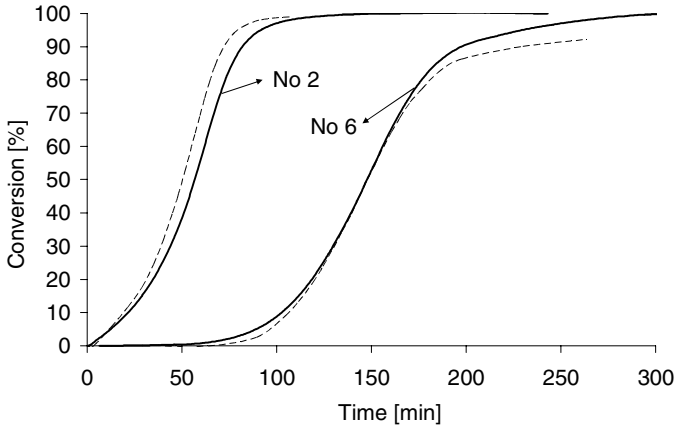

Figure 7.4: Comparison between thermal conversion (solid line) and monomer conversion calculated from experimental speed of sound measurements (dashed line) using a model-based calibration procedure.

The results discussed in this chapter show the first application of the use of an ultrasonic sensor for the on-line monitoring of dispersion polymerizations in supercritical media. The results are very promising and show the potential of ultrasound techniques for the control of polymerizations in SCFs. The direct comparison between the profile of the thermal conversion and the trend of the speed of sound demonstrates unambiguously that this method is highly sensitive to the mixture composition and hence to the conversion. The simple model developed to correlate the speed of sound to monomer conversion allows predicting the correct profile but an important discrepancy is observed in the determination of the absolute value. The speed of sound values are underestimated as well as the magnitude of its drop during the polymerization (Figure 7.2). The main weakness is related to the estimation of the model parameters. In many cases, it is rather impossible to find literature data measured at the operating conditions of the experiments. But principally, the volume additivity rule is based on the assumption that the mixture behaves like an ideal mixture. It can be easily realized that it is not the case in a complex system behavior like monomer-scCO_2-polymer mixture. In order to improve the model prediction and avoid a calibration procedure, independent measurements are required to evaluate the parameters values at the operating conditions. Furthermore, the density of the polymer-CO_2 mixture has to be evaluated. If enough experimental data are available they could lead to the estimation of a factor to correct the volume fraction used in the determination of the density and compressibility of the mixture. If this procedure appears to be insufficient, this means that a more complex model is required.

7.2 Speed of sound, critical point and phase transition

Poliakoff and his coworkers have reported in many studies the possibility to use acoustic measurements for the location of the critical points of pure components and mixtures.[37, 38, 224-226]

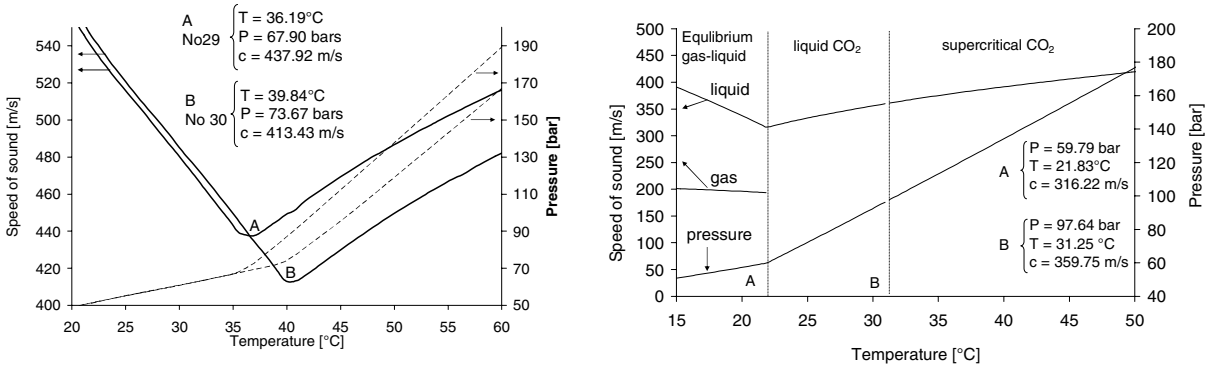

a b

Figure 7.5 : Evolution of the speed of sound and pressure as a function of temperature a) for the ternary mixture PDMS-MMA-CO_2 and b) for pure carbon dioxide at a density of 752 kg/m^3. [27]

Figure 7.5 b shows the behavior of the speed of sound and pressure for pure carbon dioxide as a function of temperature. It appears that in an isochoric system the speed of sound reaches a minimum when a transition from the LV equilibrium to pure liquid occurs (point A in Figure 7.5 b). At increasing pressure, the gas is compressed leading to its liquefaction. Moreover, an inflexion point of the pressure curve is also clearly observed. The transition to supercritical phase corresponds therefore to a liquid – supercritical transition (point B in Figure 7.5 b). It is observed that the values of temperature and pressure where both transitions occur (point A and B in Figure 7.5 b) do not correspond to the one expected for the critical temperature (31.1°C) and critical pressure (73.8 bar) for pure carbon dioxide. From Figure 7.6, it is observed that phase transitions occur exactly at the critical point of a substance or mixture only when the density of the system corresponds to the critical density, being 466 kg/m^3 for pure carbon dioxide. This indicates that the use of acoustic methods to determine critical points has to be treated carefully. The measured phase transition can correspond to a transition close to the critical one but not exactly at the critical point as shown here.

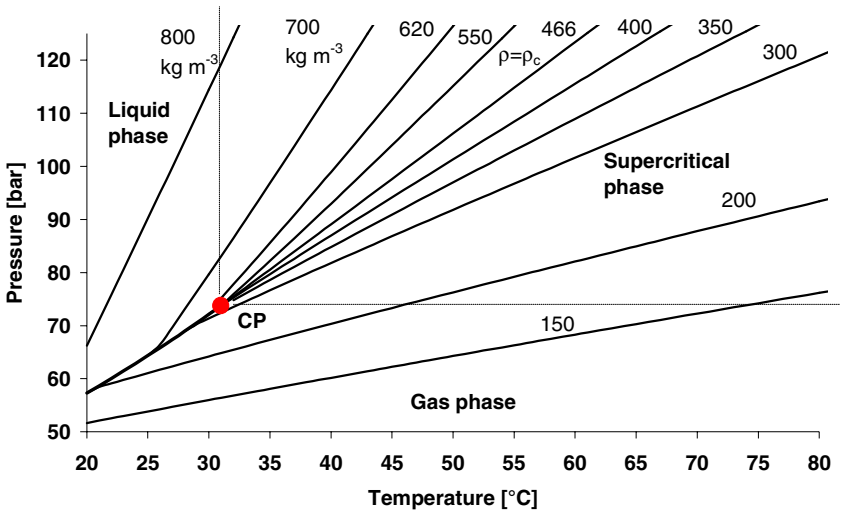

Figure 7.6: Isochors of pure carbon dioxide, values taken from NIST. The behavior of the pressure as a function of temperature is shown for different CO_2's densities in kg/m^3; ρ_c CO_2 = 466 kg/m^3.

Figure 7.5 a shows the behavior of the speed of sound and pressure observed during the heating step of the polymerization experiments No 29 and 30. A similar trend to the one predicted for pure carbon dioxide is observed for the ternary mixture PDMS-MMA-CO_2. Because the discussed experiments have exactly the same recipe, it could be expected that the minimum of the speed of sound would have occured exactly at the same position. The deviation can be explained by the fact that the heating rate (°C/minute) was not exactly the same for both

experiments. This can largely influence the accuracy of the measured minimum. From a practical point of view, in the presence of the gas-liquid equilibrium inside the reactor, the sensor is immersed in the liquid phase and measured the speed of sound in this phase. It is very interesting to note that the measured transition for the experiment No 30 is very close to the cloud point measured in the view cell for the ternary mixture PDMS-MMA-CO_2 at 40.2 °C and 72 bar (Figure 5.4 a) at similar compositions. With the view cell, a transition from the equilibrium liquid-gas to the fluid phase is observed. This direct comparison tends to demonstrate the accuracy of both measurements within the reproducibility of the data. Thus, the presence of the ultrasonic probe inside the reactor allows to a certain extent controlling the initial medium homogeneity.

It has to be noted that ultrasound technology is not only a tool for monitoring chemical reactions and study phase transitions but can also be applied to initiate chemical reactions (sonochemistry). Sonochemistry comprises all the chemical effects that are induced by ultrasound, including the formation of radicals and the enhancement of reaction rates at ambient temperatures.[227-229] The chemical effects of ultrasound are caused by cavitation: the collapse of microscopic bubbles in a liquid. The implosions of the generated cavities can generate temperatures up to 5'000 K and pressure up to 200 bar, because of the compression of the gas phase inside the cavity.[230] Kuijpers *et al.* have demonstrated the feasibility of using ultrasonic waves of 20 kHz to induce in situ radical formation in liquid carbon dioxide.[231-234] Cavitation-induced radical production has been used for the polymerization of MMA in CO_2, yielding high molecular weight polymers. However, it should be noted that this technique will only be successful in liquid-CO_2, not in supercritical regime.

8 Conclusions

8.1 General conclusions

As environmental issues attract more and more the attention of the authorities and consumers, engineers and chemists are directly involved in the development of more sustainable technologies. The increasing pressure of the authorities on the chemical industry, such as the important taxes put into effect for the use of organic volatile compounds (VOCs), leads the scientists to imagine alternatives like the use of supercritical fluids as solvents in chemical synthesis and polymer processing. The best candidate for the development of the so-called "green chemistry" is carbon dioxide (CO_2), because it is an inexpensive natural abundant material exhibiting low toxicity. Furthermore, CO_2 is a non-flammable compound leading to the possibility to increase chemical process safety.

The polymer industry spends a lot of money in the use of huge volumes of organic solvents and separation units for product purification. Thus, the development of polymer synthesis and processing using $scCO_2$ as solvent finds there one of its main interest. The unique properties of supercritical fluids that can behave like gases and/or liquids depending on the operating conditions can increase the flexibility of a process and decrease the cost of separation units. Despite the numerous advantageous properties of $scCO_2$, one is constrained to take note of the limited number of industrial processes applying the supercritical fluid technologies. The main reason is that CO_2 is a poor solvent for many high molecular weight components and polymers. Therefore, the main application for polymer production is the dispersion polymerization which requires the use of an additional polymeric compound, i.e. a stabilizer. Moreover, mixtures behavior starts to be complex because one has to consider the phase behavior in ternary and higher order systems. This study has shown that the poly(dimethylsiloxane) macromonomer (PDMS macromonomer) with a molecular weight of 5'000 g/mol is an effective stabilizer for the dispersion polymerization of the methyl methacrylate (MMA) in $scCO_2$. A comparison between the phase behavior of the binary mixture stabilizer-CO_2 and ternary mixture MMA-CO_2-stabilizer has shown that MMA acts as a cosolvent increasing the solubility of the stabilizer in CO_2. Furthermore, the results demonstrate that the concentration of the monomer in the reacting mixture is a key parameter to control the stabilizer solubility throughout the polymerization and hence, the stability of the dispersion. This positive monomer effect gives the possibility to tune the properties of polymer-CO_2 mixtures. This means that the addition of free monomer in a dispersion polymerization can increase the extent of the initial homogeneous domain and hence decrease the cloud point pressure. This last remark is very important, as lower pressure means lower processing costs.

The improvement of polymer processing and the control of product properties depend on the knowledge of the kinetic mechanism. In this context, the development of apparatuses capable to measure in real time the conversion of the reactants into products is crucial. This work has demonstrated the potential of reaction calorimetry for the on-line monitoring of polymerization reactions in $scCO_2$. The adaptation of this technology to supercritical fluid applications allows the chemist to have an engineering approach of the polymerizations in $scCO_2$, as reactor temperature control, heat transfer analysis, stirring effect, with also the possibility to insert different impellers or sensors inside the reactor. The development of an ultrasonic sensor has shown the possibility to use the on-line measurement of the speed of sound in the reacting medium to follow the monomer conversion. A simple model has proved that it is possible from the measurement of the speed of sound to calculate the mixture composition and hence, the monomer conversion.

The kinetic analysis combined with the measurements of the polymer properties such as the molecular weight distribution, the product morphology and the particle size distribution have allowed underlining some fundamental aspects of the dispersion polymerization of MMA in $scCO_2$. It is important to understand that a dispersion polymerization is composed of two main phases, the polymer-rich particles dispersed in the CO_2-rich continuous phase. The results have shown unambiguously that the polymerization can take place in both phases in parallel depending on the stabilizer solubility and concentration. When enough stabilizer is soluble in the mixture, the main polymerization locus is the polymer-rich particles. Because diffusion limitations are operative (gel effect) in the particles, high molecular weight polymer is produced with a concomitant auto-acceleration of the global rate of polymerization. When the stabilizer concentration is lowered down to a certain quantity, net bimodal molecular weight distributions are observed. Furthermore, these polymerizations are characterized by a decrease in the global polymerization rate. This corresponds to the case where the polymerization occurs in both phases at the same time. At low stabilizer concentration the specific interfacial area available for the mass transport of the species from the continuous to the particle phase decreases leading to the decrease of diffusion rate and the increase of the state of segregation in the system. The correct tuning of the operating conditions can lead to the control of the polymerization loci and hence, to the control of the polymer properties.

8.2 Perspectives

This work has shown the potential of reaction calorimetry to monitor polymerization reactions in supercritical carbon dioxide. This field is at its start and improvements are still possible. In the experimental section, it has been explained that the overall heat transfer coefficient, a crucial parameter to evaluate with accuracy the calorimetric information, cannot be measured during the polymerization itself. As this parameter is a function of the physico-chemical properties of the mixture, it can give a direct insight of their evolution during the polymerization. Therefore, it is important to develop a method allowing its evaluation during the course of the polymerization. This will lead to a better estimation of the heat contributions that are not directly measurable (heat input by the stirrer, heat losses) and hence, of the baseline. Another possible improvement is the control of the dosing temperature of the reactants added before the start of the polymerization. The combination of both improvements will lead to the control of all the heat terms included in the calorimetric analysis. This work has opened a door to study other types of polymerization reactions in supercritical conditions in a system similar to industrial reactor.

In order to "exploit" the whole potential of the developed ultrasonic probe for the monitoring of polymerization in $scCO_2$, it is necessary to improve the knowledge of the properties of the monomer-CO_2-polymer mixture. An accurate estimation of the relationship between the composition of the polymer-CO_2 mixture and the related density is probably the key to explain and predict the observed speed of sound drop during the polymerization. The results have shown that the probe is very sensitive to monomer conversion. But it is required to investigate more deeply the mixture properties (density, compressibility) in order to understand the fundamental parameters that govern the evolution of the speed of sound as a function of mixture composition.

In order to understand the effects that govern the polymerization loci and hence, the polymer properties, it is necessary to complete the model with some fundamental aspects. These aspects are mainly related to the partitioning of the species between the continuous and the dispersed phase and to the physical effects that control the state of segregation of the polymerization (mass transport limitation). This would give a direct link to the experimental results and would allow predicting the polymer properties.

9 Bibliography

[1] K. Zosel, *Angewandte Chemie-International Edition in English*, **1978,** *17*, 702.

[2] G. S. You *et al*., *Journal of the Chinese Institute of Chemical Engineers*, **2002,** *33*, 233.

[3] S. Okuno *et al.*, *Food Science and Technology Research*, **2002,** *8*, 154.

[4] E. Boselli, M. Bonoli, M. F. Caboni, G. Lercker, *European Food Research and Technology*, **2002,** *215*, 72.

[5] J. C. Liu, W. Wang, Z. W. Wang, G. Z. Li, B. X. Han, *Separation Science and Technology*, **2002,** *37*, 2691.

[6] C. Y. W. Ang, *Abstracts of Papers of the American Chemical Society*, **2002,** *223*, 272.

[7] J. J. Yu, K. H. Chiu, *Abstracts of Papers of the American Chemical Society*, **2002,** *223*, 273.

[8] H. G. Daood *et al.*, *Journal of Supercritical Fluids*, **2002,** *23*, 143.

[9] K. Thurbide, M. Al-Jabari, M. Kowalchuk, *Chemical Engineering Communications*, **2002,** *189*, 675.

[10] C. Erkey, *Journal of Supercritical Fluids*, **2000,** *17*, 259.

[11] E. Anklam, A. Muller, *Pharmazie*, **1995,** *50*, 364.

[12] A. Laitinen, A. Michaux, O. Aaltonen, *Environmental Technology*, **1994,** *15*, 715.

[13] M. J. Cocero, J. L. Martinez, *Journal of Supercritical Fluids*, **2004,** *31*, 41.

[14] P. G. Jessop, W. Leitner, in *Chemical Synthesis using Supercritical Fluids*, Jessop, P. G.; Leitner, W., Eds. Wiley-VCH: Weinheim, 1999; pp 1.

[15] Y. Arai, T. Sako, Y. Takebayashi, *Supercritical Fluids : Molecular Interactions, Physical Properties and New Applications*, Warlimont, H.; Weber, E.; Michaeli, W., Material Processing, Springer, 2002; p 446.

[16] D. T. Chen, C. A. Perman, M. E. Riechert, J. Hoven, *Journal of Hazardous Materials*, **1995,** *44*, 53.

[17] F. Cansell, S. Rey, *Revue de l' Institut Français du Petrole*, **1998,** *53*, 71.

[18] J. Sherman, B. Chin, P. D. T. Huibers, R. Garcia-Valls, T. A. Hatton, *Environmental Health Perspectives*, **1998,** *106*, 253.

[19] S. A. Montzka *et al.*, *Science*, **1996,** *272*, 1318.

[20] E. J. Beckman, *Journal of Supercritical Fluids*, **2004,** *28*, 121.

[21] R. Steiner, *Chemical Engineering*, **1993,** *100*, 114.

[22] M. Poliakoff, J. M. Fitzpatrick, T. R. Farren, P. T. Anastas, *Science*, **2002,** *297*, 807.

[23] F. Lavanchy, Ecole Polytechnique Fédérale, Lausanne, 2005, PhD Thesis.

[24] J. M. Prausnitz, R. N. Lichtenthaler, E. Gomez de Azevedo, *Molecular thermodynamics of fluid-phase equilibria*, 2nd edition ed, Prentice-Hall Inc., Engelwood cliffs New Jersey, 1986.

[25] M. A. McHugh, V. Krukonis, *Supercritical Fluid Extraction: Principles and Practice*, 2 ed, Chemical Engineering, Butterworth-Heinemann, Stoneham (MA), 1994.

[26] F. Lavanchy, S. Fortini, T. Meyer, *Chimia*, **2002,** *56*, 126.

[27] http://webbook.nist.gov/chemistry

[28] J. R. Hyde, P. Licence, D. Carter, M. Poliakoff, *Applied Catalysis a-General*, **2001,** *222*, 119.

[29] P. E. Savage, S. Gopalan, T. I. Mizan, C. J. Martino, E. E. Brock, *AIChE Journal*, **1995,** *41*, 1723.

[30] R. Span, W. Wagner, *Journal of Physical and Chemical Reference Data*, **1996,** *25*, 1509.

[31] S. Angus, B. Armstrong, K. d. Reuck, *International Thermodynamic Tables of the Fluid State*, Butterworths, London, 1972; Vol. 1.

[32] M. Kemmere, in *Supercritical carbon dioxide in polymer reaction engineering*, Kemmere, M.; Meyer, T., Eds. Wiley-VCH, Weinheim, 2005.

[33] Y.-P. Sun, *Supercritical fluid technology in materials science and engineering: syntheses, properties, and applications*, Marcel Dekker, Inc., Clemson, 2002; p 582.

[34] N. Ajzenberg, F. Trabelsi, F. Recasens, *Chemical Engineering & Technology*, **2000,** *23*, 829.

[35] R. M. Oag *et al.*, *Journal of Supercritical Fluids*, **2004,** *30*, 259.

[36] R. M. Oag *et al.*, *Analytical Chemistry*, **2003,** *75*, 479.

[37] A. Kordikowski, M. Poliakoff, *Fluid Phase Equilibria*, **1998,** *151*, 493.

[38] V. K. Popov, J. A. Banister, V. N. Bagratashvili, S. M. Howdle, M. Poliakoff, *Journal of Supercritical Fluids*, **1994,** *7*, 69.

[39] D. Hancu, E. J. Beckman, *Green Chemistry*, **2001,** *3*, 80.

[40] J. L. Kendall, D. A. Canelas, J. L. Young, J. M. DeSimone, *Chemical Reviews*, **1999,** *99*, 543.

[41] C. Y. Tsang, W. B. Streett, *Chemical Engineering Science*, **1981,** *36*, 993.

[42] K. N. West *et al.*, *Journal of Physical Chemistry A*, **2001,** *105*, 3947.

[43] Y. Wu 4,483,888, Nov. 20, 1984.

[44] D. Patterson, *Polymer Engineering and Science*, **1982,** *22*, 64.

[45] C. F. Kirby, M. A. McHugh, *Chemical Reviews*, **1999,** *99*, 565.

[46] P. Ehrlich, G. A. Mortimer, *Advances in Polymer Science*, **1970,** *7*, 386.

[47] A. K. McClellan, M. A. McHugh, *Polym. Eng. Sci.*, **1985,** *25*, 1088.

[48] M. A. McHugh, T. L. Guckes, *Macromolecules*, **1985,** *18*, 674.

[49] J. M. Bardin, Patterso.D, *Polymer*, **1969,** *10*, 247.

[50] T. W. de Loos, R. N. Lichtenthaler, G. A. M. Diepen, *Macromolecules*, **1983,** *16*, 117.

[51] T. W. de Loos, W. Poot, G. A. M. Diepen, *Macromolecules*, **1983,** *16*, 111.

[52] R. Koningsv, A. J. Staverma, *Journal of Polymer Science Part a-2-Polymer Physics*, **1968,** *6*, 305.

[53] R. Koningsv, A. J. Staverma, *Journal of Polymer Science Part a-2-Polymer Physics*, **1968,** *6*, 325.

[54] R. Koningsv, A. J. Staverma, *Journal of Polymer Science Part a-2-Polymer Physics*, **1968,** *6*, 349.

[55] V. Wiesmet, E. Weidner, S. Behme, G. Sadowski, W. Arlt, *Journal of Supercritical Fluids*, **2000,** *17*, 1.

[56] M. Lora, M. A. McHugh, *Fluid Phase Equilibria*, **1999,** *157*, 285.

[57] M. L. O'Neill, M. Z. Yates, K. P. Johnston, C. D. Smith, S. P. Wilkinson, *Macromolecules*, **1998,** *31*, 2838.

[58] W. H. Hauthal, *Chemosphere*, **2001,** *43*, 123.

[59] R. Gani, G. Hytoft, C. Jaksland, *Applied Thermal Engineering*, **1997,** *17*, 889.

[60] M. Perrut, *Industrial & Engineering Chemistry Research*, **2000,** *39*, 4531.

[61] M. Kemmere, M. Cleven, M. van Schilt, J. Keurentjes, *Chemical Engineering Science*, **2002,** *57*, 3929.

[62] S. D. Yeo, E. Kiran, *Journal of Supercritical Fluids*, **2005,** *34*, 287.

[63] J. W. Tom, P. G. Debenedetti, *Journal of Aerosol Science*, **1991,** *22*, 555.

[64] E. Reverchon, *Journal of Supercritical Fluids*, **1999,** *15*, 1.

[65] H. S. Tan, S. Borsadia, *Expert Opinion on Therapeutic Patents*, **2001,** *11*, 861.

[66] L. A. Stanton, F. B. Dehghani, N. R. Foster, *Australian Journal of Chemistry*, **2002,** *55*, 443.

[67] B. Subramaniam, R. A. Rajewski, K. Snavely, *Journal of Pharmaceutical Sciences*, **1997,** *86*, 885.

[68] C. M. Wai, F. Hunt, M. Ji, X. Chen, *Journal of Chemical Education*, **1998,** *75*, 1641.

[69] S. Alsoy, J. L. Duda, *Aiche Journal*, **1998,** *44*, 582.

[70] M. W. Park, H. K. Bae, *Journal of Supercritical Fluids*, **2002,** *22*, 65.

[71] M. R. De Giorgi, E. Cadoni, D. Maricca, A. Piras, *Dyes and Pigments*, **2000,** *45*, 75.

[72] A. Schmidt, E. Bach, E. Schollmeyer, *Coloration Technology*, **2003,** *119*, 31.

[73] S. M. Howdle *et al*., *Chemical Communications*, **2001**, 109.

[74] M. A. Jacobs, M. F. Kemmere, J. T. F. Keurentjes, *Polymer*, **2004,** *45*, 7539.

[75] J. McHardy, S. P. Sawan, *Supercritical fluid cleaning*, Noyes Publications, New Jersey, 1998.

[76] Y. T. Shieh *et al.*, *Journal of Applied Polymer Science*, **1996,** *59*, 695.

[77] D. A. Canelas, J. M. DeSimone, in *Metal Complex Catalysts Supercritical Fluid Polymerization Supramolecular Architecture*, SPRINGER-VERLAG BERLIN: Berlin 33, 1997; Vol. 133, pp 103.

[78] A. I. Cooper, *Journal of Materials Chemistry*, **2000,** *10*, 207.

[79] K. M. Scholsky, *Journal of Supercritical Fluids*, **1993,** *6*, 103.

[80] K. A. Shaffer, J. M. Desimone, *Trends in Polymer Science*, **1995,** *3*, 146.

[81] A. I. Cooper, J. M. DeSimone, *Current Opinion in Solid State and Materials Science*, **1996,** *1*, 761.

[82] J. M. DeSimone, Z. Guan, C. S. Elsbernd, *Science*, **1992,** *257*, 945.

[83] J. B. McClain *et al.*, *Journal of the American Chemical Society*, **1996,** *118*, 917.

[84] G. Luna-Barcenas *et al.*, *Fluid Phase Equilibria*, **1998,** *146*, 325.

[85] S. Beuermann, M. Buback, C. Isemer, A. Wahl, *Macromolecular Rapid Communications*, **1999,** *20*, 26.

[86] M. R. Clark, J. M. Desimone, *Macromolecules*, **1995,** *28*, 3002.

[87] M. A. McHugh *et al*., *Macromolecules*, **2002,** *35*, 4653.

[88] T. J. Romack, E. E. Maury, J. M. Desimone, *Macromolecules*, **1995,** *28*, 912.

[89] M. K. Saraf *et al.*, *Macromolecules*, **2002,** *35*, 7976.

[90] T. J. Romack, J. M. Desimone, T. A. Treat, *Macromolecules*, **1995,** *28*, 8429.

[91] A. I. Cooper, J. M. DeSimone, *Abstracts of Papers of the American Chemical Society*, **1996,** *211*, 159.

[92] F. A. Adamsky, E. J. Beckman, *Macromolecules*, **1994,** *27*, 312.

[93] K. E. J. Barrett, *Dispersion Polymerization in Organic Media*, John Wiley & Sons, London, 1975.

[94] M. L. O'Neill, M. Z. Yates, K. P. Johnston, C. D. Smith, S. P. Wilkinson, *Macromolecules*, **1998,** *31*, 2848.

[95] U. Fehrenbacher, O. Muth, T. Hirth, M. Ballauff, *Macromolecular Chemistry and Physics*, **2000,** *201*, 1532.

[96] J. M. DeSimone *et al.*, *Science*, **1994,** *265*, 356.

[97] M. L. O'Neill *et al.*, *Macromolecules*, **1997,** *30*, 5050.

[98] M. Z. Yates *et al.*, *Macromolecules*, **1997,** *30*, 5060.

[99] Y. L. Hsiao, E. E. Maury, J. M. Desimone, S. Mawson, K. P. Johnston, *Macromolecules*, **1995,** *28*, 8159.

[100] C. Lepilleur, E. J. Beckman, *Macromolecules*, **1997,** *30*, 745.

[101] P. Christian *et al.*, *Macromolecules*, **2000,** *33*, 9222.

[102] P. Christian, S. M. Howdle, D. J. Irvine, *Macromolecules*, **2000,** *33*, 237.

[103] A. Rosell, G. Storti, M. Morbidelli, D. Bratton, S. M. Howdle, *Macromolecules*, **2004,** *37*, 2996.

[104] K. A. Shaffer, T. A. Jones, D. A. Canelas, J. M. DeSimone, S. P. Wilkinson, *Macromolecules*, **1996,** *29*, 2704.

[105] P. Christian, M. R. Giles, S. M. Howdle, R. C. Major, J. N. Hay, *Polymer*, **2000,** *41*, 1251.

[106] M. Z. Yates *et al.*, *Macromolecules*, **1999,** *32*, 1018.

[107] T. Meyer, S. Fortini, C. Mantelis, in *Supercritical Carbon Dioxide in Polymer Reaction Engineering*, Kemmere, M. F.; Meyer, T., Eds. WILEY-VCH: Weinheim Germany, 2005; pp 81.

[108] S. V. Olesik, S. B. French, M. Novotny, *Analytical Chemistry*, **1986,** *58*, 2256.

[109] M. Poliakoff, S. M. Howdle, S. G. Kazarian, *Angewandte Chemie-International Edition in English*, **1995,** *34*, 1275.

[110] W. Kessler, G. Luft, W. Zeiss, *Berichte Der Bunsen-Gesellschaft-Physical Chemistry Chemical Physics*, **1997,** *101*, 698.

[111] U. Fehrenbacher, M. Ballauff, *Macromolecules*, **2002,** *35*, 3653.

[112] P. Hauptmann, N. Hoppe, A. Puttmer, *Measurement Science & Technology*, **2002,** *13*, R73.

[113] M. Morbidelli, G. Storti, A. Siani, *J. M. Asua, NATO ASI Series, Series E: Applied Sciences*, **1997,** *335*, 257.

[114] L. Cavin, T. Meyer, A. Renken, *Polymer Reaction Engineering*, **2000,** *8*, 201.

[115] L. Cavin, A. Renken, T. Meyer, *Polymer Reaction Engineering*, **2000,** *8*, 225.

[116] T. Zeilmann, F. Lavanchy, T. Meyer, *Chimia*, **2001,** *55*, 249.

[117] W. X. Wang, R. M. T. Griffiths, M. R. Giles, P. Williams, S. M. Howdle, *European Polymer Journal*, **2003,** *39*, 423.

[118] J. Liu, H. Y. Tai, S. M. Howdle, *Polymer*, **2005,** *46*, 1467.

[119] F. Stoessel, in *Handbook of Polymer Reaction Engineering*, Meyer, T.; Keurentjes, J., Eds. WILEY-VCH, Weinheim, 2005, Vol. 2, pp 553.

[120] F. Stoessel, *La Sécurité des Procédés Chimiques*, Collection d'Enseignement de l'EPFL, Département de Chimie, Institut de Génie Chimique, Swiss Federal Institute of Technology, Lausanne, 2000.

[121] F. Stoessel, *Journal of Thermal Analysis*, **1997,** *49*, 1677.

[122] M. Vicente, S. BenAmor, L. M. Gugliotta, J. R. Leiza, J. M. Asua, *Industrial & Engineering Chemistry Research*, **2001,** *40*, 218.

[123] K. Tauer, H. Muller, C. Schellenberg, L. Rosengarten, *Colloids and Surfaces a-Physicochemical and Engineering Aspects*, **1999,** *153*, 143.

[124] L. L. de Arbina, L. M. Gugliotta, M. J. Barandiaran, J. M. Asua, *Polymer*, **1998,** *39*, 4047.

[125] M. Mosebach, K. H. Reichert, *Journal of Applied Polymer Science*, **1997,** *66*, 673.

[126] M. Lahti, *Acta Polytechnica Scandinavica-Chemical Technology Series*, **1996**, 1.

[127] M. Mosebach, K. H. Reichert, *Chemie Ingenieur Technik*, **1994,** *66*, 1058.

[128] M. Lahti, J. Seppala, A. Avela, *Acta Polytechnica Scandinavica-Chemical Technology Series*, **1993**, 1.

[129] M. Chen, K. H. Reichert, *Chemie Ingenieur Technik*, **1993,** *65*, 78.

[130] C. U. Schmidt, K. H. Reichert, *Chemie Ingenieur Technik*, **1988,** *60*, 233.

[131] S. BenAmor, D. Colombie, T. McKenna, *Industrial & Engineering Chemistry Research*, **2002,** *41*, 4233.

[132] S. Cavallaro, *Journal of Thermal Analysis and Calorimetry*, **1999,** *58*, 3.

[133] H.-U. Moritz, in *Polymer Reaction Engineering*, Reichert, K.-H.; Geiseler, W., Eds. VCH Verlagsgesellschaft: Weinheim, 1989.

[134] T. F. McKenna, S. Othman, G. Fevotte, A. M. Santos, H. Hammouri, *Polymer Reaction Engineering*, **2000,** *8*, 1.

[135] L. V. De la Rosa, E. D. Sudol, M. S. ElAasser, A. Klein, *Journal of Polymer Science Part a-Polymer Chemistry*, **1996,** *34*, 461.

[136] L. V. De la Rosa, E. D. Sudol, M. S. El-Aasser, A. Klein, *Journal of Polymer Science Part a-Polymer Chemistry*, **1999,** *37*, 4054.

[137] L. V. De la Rosa, E. D. Sudol, M. S. El-Aasser, A. Klein, *Journal of Polymer Science Part a-Polymer Chemistry*, **1999,** *37*, 4073.

[138] O. Elizalde, M. Azpeitia, M. M. Reis, J. M. Asua, J. R. Leiza, *Industrial & Engineering Chemistry Research*, **2005,** *44*, 7200.

[139] R. Gesthuisen, S. Kramer, G. Niggemann, J. R. Leiza, J. M. Asua, *Computers & Chemical Engineering*, **2005,** *29*, 349.

[140] M. Vicente, J. R. Leiza, J. M. Asua, *Chemical Engineering Science*, **2003,** *58*, 215.

[141] A. S. de Buruaga, J. C. de la Cal, J. M. Asua, *Polymer*, **2000,** *41*, 1269.

[142] A. Zogg, F. Stoessel, U. Fischer, K. Hungerbuhler, *Thermochimica Acta*, **2004,** *419*, 1.

[143] W. Regenass, *Chimia*, **1971,** *25*, 154.

[144] W. Regenass, *Thermochimica Acta*, **1977,** *20*, 65.

[145] W. Regenass, *Chimia*, **1983,** *37*, 430.

[146] W. Regenass, *Thermochimica Acta*, **1985,** *95*, 351.

[147] W. Regenass, *Journal of Thermal Analysis*, **1997,** *49*, 1661.

[148] W. Regenass, *Journal of Thermal Analysis*, **1997,** *49*, 1661.

[149] W. Regenass, *Chimia*, **1997,** *51*, 189.

[150] S. Fortini, F. Lavanchy, P. Nising, T. Meyer, *Macromolecular Symposia*, **2004,** *206*, 79.

[151] S. Fortini, F. Lavanchy, T. Meyer, *Macromolecular Materials and Engineering*, **2004,** *289*, 757.

[152] F. Lavanchy, S. Fortini, T. Meyer, *Organic Process Research & Development*, **2004,** *8*, 504.

[153] J. H. Rushton, E. W. Costich, H. J. Everett, *Chemical Engineering Progress*, **1950,** *46*, 467.

[154] R. L. Bates, P. L. Fondy, Corpstei.Rr, *Industrial & Engineering Chemistry Process Design and Development*, **1963,** *2*, 310.

[155] C. Chatzidoukas, P. Pladis, C. Kiparissides, *Industrial & Engineering Chemistry Research*, **2003,** *42*, 743.

[156] P. A. Mueller, G. Storti, M. Morbidelli, *Chemical Engineering Science*, **2005,** *60*, 1911.

[157] P. A. Mueller, G. Storti, M. Morbidelli, *Chemical Engineering Science*, **2005,** *60*, 377.

[158] I. C. Sanchez, R. H. Lacombe, *Macromolecules*, **1978,** *11*, 1145.

[159] F. Rindfleisch, T. P. DiNoia, M. A. McHugh, *Journal of Physical Chemistry*, **1996,** *100*, 15581.

[160] M. L. O'Neill *et al.*, *Industrial & Engineering Chemistry Research*, **1998,** *37*, 3067.

[161] Z. B. Guan, J. R. Combes, Y. Z. Menceloglu, J. M. Desimone, *Macromolecules*, **1993,** *26*, 2663.

[162] H. K. Mahabadi, K. F. Odriscoll, *Journal of Macromolecular Science-Chemistry*, **1977,** *A11*, 967.

[163] S. Beuermann, M. Buback, G. T. Russell, *Macromolecular Rapid Communications*, **1994,** *15*, 351.

[164] I. A. Maxwell, G. T. Russell, *Makromolekulare Chemie-Theory and Simulations*, **1993,** *2*, 95.

[165] G. T. Russell, D. H. Napper, R. G. Gilbert, *Macromolecules*, **1988,** *21*, 2133.

[166] J. S. Vrentas, J. L. Duda, *Journal of Polymer Science Part B-Polymer Physics*, **1977,** *15*, 403.

[167] J. S. Vrentas, J. L. Duda, *Journal of Applied Polymer Science*, **1977,** *21*, 1715.

[168] J. S. Vrentas, J. L. Duda, *Journal of Polymer Science Part B-Polymer Physics*, **1977,** *15*, 417.

[169] J. S. Vrentas, J. L. Duda, H. C. Ling, *Journal of Polymer Science Part B-Polymer Physics*, **1985,** *23*, 275.

[170] J. S. Vrentas, C. M. Vrentas, *Journal of Polymer Science Part B-Polymer Physics*, **1993,** *31*, 69.

[171] J. S. Vrentas, C. M. Vrentas, *Journal of Polymer Science Part B-Polymer Physics*, **2003,** *41*, 501.

[172] J. S. Vrentas, J. L. Duda, H. C. Ling, A. C. Hou, *Journal of Polymer Science Part B-Polymer Physics*, **1985,** *23*, 289.

[173] J. S. Vrentas, J. L. Duda, *Aiche Journal*, **1979,** *25*, 1.

[174] J. S. Vrentas, J. L. Duda, H. C. Ling, *Journal of Polymer Science Part B-Polymer Physics*, **1984,** *22*, 459.

[175] P. W. Atkins, *Physical Chemistry*, 5th edition ed, Oxford University Press, Oxford, 1994.

[176] A. Faldi, M. Tirrell, T. P. Lodge, E. Vonmeerwall, *Macromolecules*, **1994,** *27*, 4184.

[177] R. R. Gupta et al., *Macromolecules*, **2003,** *36*, 346.

[178] J. M. Zielinski, J. L. Duda, *Aiche Journal*, **1992,** *38*, 405.

[179] D. Kukulj, T. P. Davis, R. G. Gilbert, *Macromolecules*, **1998,** *31*, 994.

[180] S. W. Benson, A. M. North, *Journal of the American Chemical Society*, **1962,** *84*, 935.

[181] M. Buback, C. Kowollik, *Macromolecules*, **1998,** *31*, 3211.

[182] S. K. Soh, D. C. Sundberg, *Journal of Polymer Science Part a-Polymer Chemistry*, **1982,** *20*, 1315.

[183] M. C. Griffiths, J. Strauch, M. J. Monteiro, R. G. Gilbert, *Macromolecules*, **1998,** *31*, 7835.

[184] M. D. Zammit, T. P. Davis, D. M. Haddleton, K. G. Suddaby, *Macromolecules*, **1997,** *30*, 1915.

[185] M. A. Quadir, J. M. DeSimone, A. M. van Herk, A. L. German, *Macromolecules*, **1998,** *31*, 6481.

[186] S. Beuermann, M. Buback, *Progress in Polymer Science*, **2002,** *27*, 191.

[187] M. Wulkow, *Macromolecular Theory and Simulations*, **1996,** *5*, 393.

[188] A. Tietze, I. Ludke, K. H. Reichert, *Chemical Engineering Science*, **1996,** *51*, 3131.

[189] S. Mori, H. G. Barth, *Size Exclusion Chromatography*, Springer-Verlag Berlin Heidelberg, Germany, 1999.

[190] T. H. Mourey, S. M. Miller, *Journal of Liquid Chromatography*, **1990,** *13*, 693.

[191] T. H. Mourey, S. M. Miller, S. T. Balke, *Journal of Liquid Chromatography*, **1990,** *13*, 435.

[192] Y. Xiong, E. Kiran, *Polymer*, **1995,** *36*, 4817.

[193] H. S. Byun, M. A. McHugh, *Industrial & Engineering Chemistry Research*, **2000,** *39*, 4658.

[194] B. M. Hasch, M. A. Meilchen, S. H. Lee, M. A. McHugh, *Journal of Polymer Science Part B-Polymer Physics*, **1993,** *31*, 429.

[195] B. M. Hasch, M. A. Meilchen, S. H. Lee, M. A. McHugh, *Journal of Polymer Science Part B-Polymer Physics*, **1992,** *30*, 1365.

[196] M. A. Meilchen, B. M. Hasch, S. H. Lee, M. A. McHugh, *Polymer*, **1992,** *33*, 1922.

[197] B. Folie, M. Radosz, *Ind. Eng. Chem. Res.*, **1995,** *34*, 1501.

[198] K. Liu, E. Kiran, *Journal of Supercritical Fluids*, **1999,** *16*, 59.

[199] M. W. A. Kuijpers, Technische Universiteit Eindhoven, Eindhoven, 2004, PhD Thesis.

[200] K. E. J. Barrett, H. R. Thomas, *Journal of Polymer Science Part a-1-Polymer Chemistry*, **1969,** *7*, 2621.

[201] G. M. Burnett, G. L. Duncan, *Makromolekulare Chemie*, **1962,** *51*, 154.

[202] G. M. Burnett, G. L. Duncan, *Makromolekulare Chemie*, **1962,** *51*, 171.

[203] G. M. Burnett, G. L. Duncan, *Makromolekulare Chemie*, **1962,** *51*, 177.

[204] P. Hayden, H. Melville, *Journal of Polymer Science*, **1960,** *43*, 201.

[205] S. Beuermann, M. Buback, in *Supercritical Carbon Dioxide in polymer reaction engineering*, Kemmere, M. F.; Meyer, T., Eds. WILEY-VCH: Weinheim Germany, 2005.

[206] J. Brandrup, E. H. Immergut, *Polymer Handbook*, Third ed, Wiley-Interscience, 1989.

[207] G. Odian, *Principles of polymerization*, John Wiley and Sons, I., 2nd edition ed, New York, 1970.

[208] Schneider Labor AG, Switzerland

[209] K. A. Kusters, J. G. Wijers, D. Thoenes, *Chemical Engineering Science*, **1997,** *52*, 107.

[210] G. J. Fleer, M. A. Cohen-Stuart, J.M.H.M. Scheutjens, T. Cosgrove, B. Vincent, *Polymer at interfaces*, Chapman & Hall, London, 1993.

[211] P. C. Hiemenz, R. Rajagoplan, *Principles of colloid and surface chemistry*, Marcel Dekker, New york, 1997.

[212] D. H. Napper, *Polymeric stabilization of colloidal dispersions*, Academic Press., London, 1983.

[213] Y. L. Hsiao, E. E. Maury, J. M. Desimone, *Abstracts of Papers of the American Chemical Society*, **1995,** *210*, 191.

[214] S. Canegallo, M. Apostolo, G. Storti, M. Morbidelli, *Journal of Applied Polymer Science*, **1995,** *57*, 1333.

[215] A. Wood, *A Text-Book of Sound*, 1st Edition ed, G. BELL and SONS LTD, London, 1932.

[216] A. S. Ahuja, *Journal of the Acoustical Society of America*, **1972,** *51*, 916.

[217] A. S. Ahuja, *Journal of Applied Physics*, **1973,** *44*, 4863.

[218] J. R. Allegra, S. A. Hawley, *Journal of the Acoustical Society of America*, **1972,** *51*, 1545.

[219] P. S. Epstein, R. R. Carhart, *Journal of the Acoustical Society of America*, **1953,** *25*, 553.

[220] M. A. Barrettgultepe, M. E. Gultepe, E. B. Yeager, *Journal of Physical Chemistry*, **1983,** *87*, 1039.

[221] W. S. Ament, *Journal of the Acoustical Society of America*, **1953,** *25*, 638.

[222] A. H. Harker, J. A. G. Temple, *Journal of Physics D-Applied Physics*, **1988,** *21*, 1576.

[223] S. L. Oswal, B. M. Patel, A. M. Patel, N. Y. Ghael, *Fluid Phase Equilibria*, **2003,** *206*, 313.

[224] J. Ke, B. X. Han, M. W. George, H. K. Yan, M. Poliakoff, *Fluid Phase Equilibria*, **2001,** *185*, 327.

[225] A. Kordikowski *et al.*, *Journal of Physical Chemistry*, **1996,** *100*, 9522.

[226] A. Kordikowski *et al.*, *Journal of Physical Chemistry B*, **1997,** *101*, 5853.

[227] G. J. Price, A. A. Clifton, F. Keen, *Polymer*, **1996,** *37*, 5825.

[228] G. J. Price, M. McCollom, *Ultrasonics Sonochemistry*, **1995,** *2*, S67.

[229] G. J. Price, A. M. Patel, *European Polymer Journal*, **1996,** *32*, 1289.

[230] K. S. Suslick, *Scientific American*, **1989,** *260*, 80.

[231] M. W. A. Kuijpers, P. D. Iedema, M. F. Kemmere, J. T. F. Keurentjes, *Polymer*, **2004,** *45*, 6461.

[232] M. W. A. Kuijpers, M. F. Kemmere, J. T. F. Keurentjes, *Ultrasonics*, **2002,** *40*, 675.

[233] M. W. A. Kuijpers, R. M. H. Prickaerts, M. F. Kemmere, J. T. F. Keurentjes, *Macromolecules*, **2005,** *38*, 1493.

[234] M. W. A. Kuijpers, D. van Eck, M. F. Kemmere, J. T. F. Keurentjes, *Science*, **2002,** *298*, 1969.

A Annexes

A.1 Calibration of the ultrasonic probe

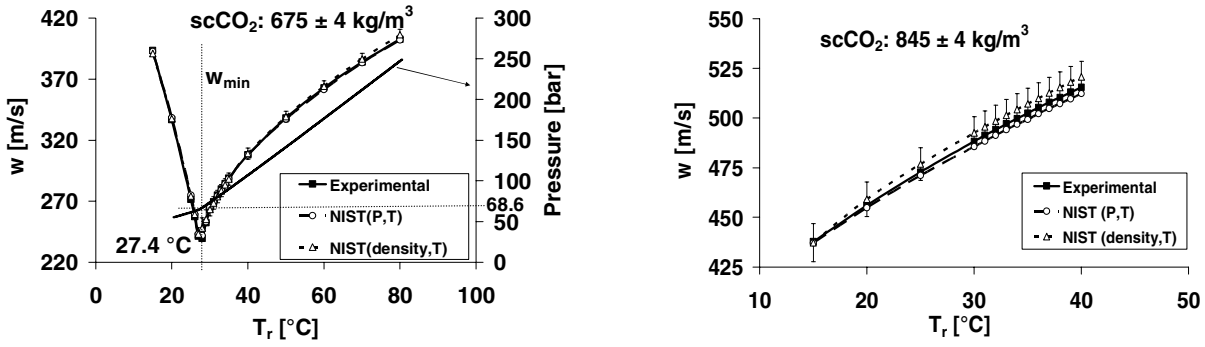

a b

Figure A.1: a) and b) Comparison of the experimental speed of sound values as a function of temperature for two different densities of pure CO_2 and the corresponding predicted values from NIST, comparison based either on pressure-temperature or on density-temperature.[23]

A.2 Micro heat exchanger

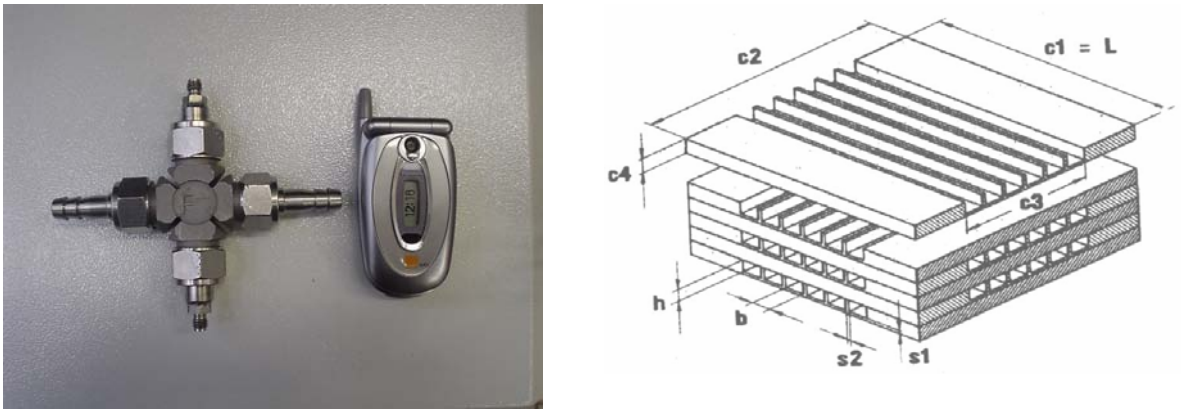

a b

FigureA.3: a) Picture and b) structure scheme of the micro cross flow heat exchanger developed in the Forshungszentrum in Karlsruhe, composed of channel diameter and length of 50-500 μm and 20-100 mm respectively, channel number 200-1000, specific surface 10^4-10^5 m^2/m^3. The heat exchanger was connected to a cryothermostat (IG Instrmenten-Gesellschaft AG).

A.3 Overall Heat transfer coefficient

T=80°C

Exp	**1**	**2**	**3**	**4**	**8**	**9**	**10**	**11**	**12**	**16**	**17**	**18**	**19**
Uinitial [W/m^2/K]	366	335	349	290	250	405	285	394	387	320	321	323	324
Ufinal [W/m^2/K]	302	271	289	210	NA	337	NA	307	300	NA	NA	NA	300

T=80°C

Exp	**20**	**21**	**22**	**23**	**24**	**25**	**26**	**27**	**28**	**30**
Uinitial [W/m^2/K]	327	293	328	303	323	333	316	394	271	335
Ufinal [W/m^2/K]	289	244	296	279	307	235	NA	307	NA	271

T=65°C

Exp	**5**	**6**	**7**	**13**	**14**	**15**	**29**
Uinitial [W/m^2/K]	313	325	296	326	320	319	329
Ufinal [W/m^2/K]	220	216	NA	NA	NA	NA	211

A.4 Predici® computation

Phase exchange for monomer transport

```
Arguments 4
Mc value
Mp value
R1:Vol value
R1:latex value
//
mc= arg1
mp= arg2
vol= arg3
phasevol= arg4
//computation of conversion
contivol=vol-phasevol
mole=phasevol*mp+contivol*mc
input=getcin("Mc")+getcin("Mp")
x=1-mole/input
K=4.5
result1=getkp("kla_pol")*(mp-(mc/K))
```

Propagation rate constant

```
T=gettemp("R1")
P=getpressure("R1")
DV=16.7
R=8.314
P0=1
sigma=5.85/(10^8)
D=(1.61/10^3)*exp((-3.26*10^3)/(R*(T+273.15)))
Vc=0.589
Vm=0.870
Vp=0.757
imp=0.6
imc=0.18
oc=0.15
om=0.05
op=0.8
Vhfm=(8.15/(10^4))*(143+(T+273.15)-143)
Vhfp=(4.77/10^4)*(52.4+0.44*((T+273.15)-392))
Vhfc=0.231+((8.76/10^4)*((T+273.15)-313.15))
B=getkp("kp20")*exp(((DV/10^6)*((P-P0)*10^5))/(R*(T+273.15)))
A=((om*Vm)+(Vc*imc*oc)+(op*imp*Vp))/(om*Vhfm+op*Vhfp+oc*Vhfc)
Y=D*exp(-A)
expr=1/((1/B)+(1/((4*3.14*sigma*Y*6.022*10^23)/1000)))
result1=setkp("kp2",expr)
result2=getkp("kp20")
```

Termination rate constant

```
T=gettemp("R1")
P=getpressure("R1")
DV=-15
P0=1
R=8.314
a=0.69/(10^7)
jc=47
D=(1.61/10^3)*exp((-3.26*10^3)/(R*(T+273.15)))
Vc=0.589
Vm=0.870
Vp=0.757
imp=0.6
imc=0.18
oc=0.15
om=0.05
op=0.8
Vhfm=(8.15/(10^4))*(143+(T+273.15)-143)
Vhfp=(4.77/10^4)*(52.4+0.44*((T+273.15)-392))
Vhfc=0.231+((8.76/10^4)*((T+273.15)-313.15))
```

```
A=((om*Vm)+(Vc*imc*oc)+(op*imp*Vp))/(om*Vhfm+op*Vhfp+oc*Vhfc)
DM=D*exp(-A)
B=8*3.14*a*(jc^0.5)
C=(getco("Mp")*getkp("kp2")*(a^2))/3
kt=getkp("ktc20")*exp(((DV/10^6)*((P-P0)*10^5))/(8.314*(T+273.15)))
x = getmn("P")
y = getmn("P")
d = 0.1
Dx=DM*(x/d)^(-0.664-(2.02*op))
Dy=DM*(y/d)^(-0.664-(2.02*op))
expr=1/((1/kt)+(1/((B*6.022*10^23*(Dx+Dy+C))/1000)))
result1=setkp("ktc2",expr)
ktd2=expr*1.0
result2=setkp("ktd2",ktd2)
```

CURRICULUM VITAE

Sophie FORTINI
Chemical Engineer
Nationalities: Swiss and Italian
Born December 12th 1976
Monthey (VS)
Single

EDUCATION

2002-2005	Swiss Federal Institute of Technology, Lausanne (Switzerland) PhD thesis in polymer reaction engineering (Supervisor: MER. Dr. Th. Meyer)
1997 - 2002	Swiss Federal Institute of Technology, Lausanne (Switzerland) Diploma of chemical engineer
1991 - 1996	Collège de l'Abbaye, Saint-Maurice (Switzerland, Valais) High school degree of type C (Modern Languages)

PROFESSIONAL EXPERIENCE

2002-2005 — Swiss Federal Institute of Technology, Lausanne (Switzerland), Section of Chemistry and Chemical Engineering

Research thesis:"supercritical reaction calorimetry- A study of the dispersion polymerization of methyl methcracrylate in supercritical carbon dioxide"

- Work awarded in the 11th RXE User Forum Europe
- Development, in collaboration with Mettler-Toldeo (GmbH, Switzerland), of a reaction calorimeter for the on-line monitoring of polymerization reactions in supercritical carbon dioxide
- Experience in polymer analyses and powder technologies
- Simulation of polymerization reactions
- Formation of students and scientific co-workers, Formation on scientific working for diploma students

2001-2002 — Swiss Federal Institute of Technology, Lausanne (Switzerland), Section of Chemistry and Chemical Engineering

Diploma work: "Characterization of a high pressure reaction calorimeter for the study of the supercritical carbon dioxide"

- Work awarded (Ciba Specialty Chemicals SA Monthey)

CONTINUOUS FORMATION

- Management of co-workers: the role of the leadership in team performance
- Management of conflicts: the assertiveness as an important tool to manage conflicts and maintain the team cohesion

LANGUAGE SKILLS

- French – Italian – English - German

PUBLICATIONS

1. Thierry Meyer, Sophie Fortini, Charalampos Mantelis, "*Monitoring Reactions in Supercritical Media*", in Kemmere M. and Meyer Th., Supercritical Carbon Dioxide in polymer reaction engineering, **2005**, Wiley VCH, Weinheim, Germany, 81-103.

2. Sophie Fortini, Frédéric Lavanchy, Thierry Meyer, "*Reaction Calorimetry in Supercritical Carbon Dioxide - Methodology Development*", Macromolecular Materials and Engineering, **2004**, *289*, 757-762.

3. Frédéric Lavanchy, Sophie Fortini, Thierry Meyer, "*Reaction Calorimetry as a New Tool for Supercritical Fluids*", Organic Process Research & Development, **2004**, *8*, 504-510.

4. Sophie Fortini, Frédéric Lavanchy, Thierry Meyer, "*A New Tool for the Study of Polymerization under Supercritical Conditions- Preliminary Results*"- Macromolecular Symposia, **2004**, *206*, 79-92.

5. Frédéric Lavanchy, Sophie Fortini, Thierry Meyer, "*Supercritical Calorimetry: An Emerging Field*", Chimia, **2004**, *56*, 126-131.

CONFERENCES-PROCEEDINGS

ORAL COMMUNICATIONS

1. *Monitoring Reactions in Supercritical Carbon Dioxide Using Heat Flow Calorimetry*
   Sophie Fortini, Charalampos Mantelis, Thierry Meyer
   7th World Congress of Chemical Engineering
   Glasgow, Scotland, 10-14 July 2005

2. *Reaction Calorimetry Applied to the Dispersion Polymerization of Methyl Methacrylate in $scCO_2$*
   Sophie Fortini, Frédéric Lavanchy, Thierry Meyer
   7th International Conference on Supercritical Fluids and Their Applications
   Trieste, Italy, 13-16 June 2004

3. *Polymerization in Supercritical Reaction Calorimeter – Method Evaluation*
   Sophie Fortini, Frédéric Lavanchy, Thierry Meyer
   4th European Congress of Chemical Engineering
   Granada, Spain, 21-25 September 2003

4. *Reaction Calorimetry in Supercritical Fluids – A Novel Tool*
   Frédéric Lavanchy, Sophie Fortini, Thierry Meyer
   11th RXE User Forum Europe, Pontresina, Switzerland, 28 September - 2 October 2003

Posters

1. Monitoring Chemical Reactions in Supercritical Fluids
Sophie Fortini, Thierry Meyer
7th International Symposium on Supercritical Fluids
Orlando, USA, 1-4 May 2005

2. *Monitoring Polymerizations in Supercritical Carbon Dioxide by Reaction Calorimetry*
Sophie Fortini, Thierry Meyer
8th International Workshop on Polymer Reaction Engineering
Hamburg, Germany, 3-6 October 2004

3. *Development of the Reaction Calorimetry Field with Supercritical Carbon Dioxide*
Sophie Fortini, Frédéric Lavanchy, Thierry Meyer
18th International Symposium on Chemical Reaction Engineering
Chicago, USA, 6-9 June 2004

4. *A New Tool for the Study of Polymerization under Supercritical Conditions*
-Preliminary Results-
Sophie Fortini, Frédéric Lavanchy, Philip Nising, Thierry Meyer
5th Polymer Reaction Engineering Working Party
Quebec City, Canada, 18-24 May 2003

5. *Reaction Calorimetry in Supercritical Fluids – A Novel Tool*
Thierry Meyer, Frédéric Lavanchy, Sophie Fortini
6th International Symposium on Supercritical Fluids
Versailles, France, 28-30 April 2003

6. *Supercritical Calorimetry : A Novel Tool*
Frédéric Lavanchy, Sophie Fortini, Bernard Kloetzli, Thierry Meyer
4th International Symposium on High Pressure Technology
Venice, Italy, 22-25 September 2002